UNIVERSITY OF LIVERPOOL

Characterisation of the Parkinson's disease related protein LRRK2 in melanoma cells and melanocytes

Hannah Elcocks

Thesis submitted in accordance with the requirements of the University of Liverpool for the degree of doctor in philosophy.

July 2021

Characterisation of LRRK2 function in melanocytes and melanoma

Hannah Elcocks

Abstract

Parkinson's disease (PD) is the second most common neurodegenerative disease with ≈ 145,000 people in the UK living with the disease. Most cases are idiopathic, with only 10-15% of cases having a known familial cause. PD patients are more likely to get melanoma compared to the general population. The mechanisms linking these diseases are not understood. LRRK2 is a serine/threonine kinase and is the most commonly mutated gene in familial PD. Hyperactivating mutations in LRRK2 cause defects in a number of pathways including the endolysosomal system and mitophagy. In this body of work, I aimed to investigate the cell biology of LRRK2 in the context of melanocytes and melanoma cells which express high levels of LRRK2. I have shown that LRRK2 is inversely related to pigmentation markers in melanoma cells and is upregulated in cell lines with high invasive potential. MLi-2 is a highly specific, commercially available inhibitor for LRRK2 kinase activity. I found that LRRK2 inhibition increases pigmentation in melanocytes and melanoma cells, suggesting that LRRK2 functions to negatively regulate melanogenesis. I present data showing acute LRRK2 inhibition induces rapid acidification of organelles in melanocytes and pigmented melanoma cells. This was coupled with a change in the morphology of melanosomes which is resolved after 24 hours of LRRK2 inhibition, at which point an increase in late stage pigmented melanosomes was observed. Collectively the data indicate that LRRK2 acts at early acidic melanosomes and late stage pigmented melanosomes. In addition to effects on pigmentation, I have shown LRRK2 inhibition decreases cell mobility of non-pigmented, invasive melanoma cells. I also found by EM that LRRK2 inhibition increases ER-mitochondrial contact sites in melanocytes.

Mutations in the retromer component VPS35 cause an autosomal dominant form of PD. The [D620N] mutation in VPS35 has been shown to hyperactivate LRRK2, indicating they operate in the same pathway. LRRK2 hyperactivation has been shown by others to induce a disrupted trans-golgi network (TGN). I have shown that the VPS35 [D620N] mutation also induces a dispersed TGN, further supporting a role for LRRK2 and VPS35 in common pathways. Both VPS35 and LRRK2 have been shown to negatively regulate Rab7, however, it is not known if these effects are through a common pathway or two separate pathways. I have generated inducible VPS35 WT and [D620N] RPE1 Flp-In cells, as well as pools of these Flp-In cells transduced with lentiviral constructs expressing wild type, hyperactive and kinase dead forms of LRRK2. I also set up an already established assay to measure Rab7 activity. I have generated and characterised these tools in detail, which provide a platform to answer questions about the intersection of VPS35 and LRRK2 cell biology.

Table of Contents

Table of Figures

List of tables

Abbreviations

AMBRA1	Autophagy and beclin 1 regulator 1
AMPK	5'-AMP activating protein kinase
ApoE	Apolipoprotein E
APs	Adaptor proteins
AR	Autosomal recessive
ARF-1	ADP ribosylation factor-1
ARH	autosomal recessive hypercholesterolemia
ATG	Autophagy related gene
ATP13A2	Probable cation-transporting ATPase 13A2
BBB	Blood brain barrier
bHLH-Zip	Basic helix/loop/helix zipper
BLOC	biogenesis of lysosome-related organelle complex
CCV	Clathrin coated vesicles
CD63	Cluster of differentiation 63
CDK2A	Cyclin dependent kinase inhibitor 2A
CIMPR	Cation-independent mannose-6-phosphate receptor
CK1α	Casein Kinase 1 isoform alpha
CLEAR	Coordinated Lysosomal Expression and Recognition
CMA	Chaperone mediated autophagy
DA	Dopamine
DAPI	4',6-diamidino-2-phenylindole
DEPTOR	DEP domain-containing mTOR-interacting protein
DFCP1	Double FYVE domain containing protein 1
DHI	Dihydroxindole
DHICA	DHI carboxylic acid
DLP1	Dynamin-Like Protein 1
DNAJC6	DnaJ Heat shock protein family (HSP40) member C6
EEA1	Early endosome antigen 1
EGFR	Epidermal growth factor receptor
EMT	Epithelial-mesenchymal transition
ER	Endoplasmic reticulum
ERK2	Extracellular-signal related kinase 2
ESCRT	Endosomal sorting complexes required for transport
FACS	Fluorescence activated cell sorting
FBXO7	F-box only protein 1
FRT	Flippase recognition target
GAP	GTPase activating protein
GARP	Golgi Associated Retrograde Protein
GCase	Glucocerebrosidase
GDIs	GDP dissociation inhibitors
GDP	Guanosine diphosphate

GEF	Guanine nucleotide exchange factor
GFP	Green fluorescent protein
GGA	Golgi-localising, Gamma-adaptin ear homology, ARF-binding proteins
GOI	Gene of interest
GTP	Guanosine triphosphate
GWAS	Genome wide association study
HA	Hemagglutinin
HOPS	Homotypic fusion and vacuole protein sorting
HRS	Hepatocyte growth factor-regulated tyrosine kinase substrate
Hsp40	Heat shock protein 40
ILVs	Intraluminal vesicles
iNPCs	Induced neural progenitor cells
iPSCs	Induced pluripotent stem cells
KO	Knockout
L-DOPA	Levodopa
LAMP2A	Lysosome-associated protein 2A
LBs	Lewy Bodies
LC3	Microtubule-associated proteins 1A/1B light chain 3B
LIR	LC3 interacting region
LKB1	Liver kinase B1
LLMOE	$_{L}$-leucyl-$_{L}$-leucine methyl ester
LROs	Lysosome related organelles
LRRK2	Leucine rich repeat kinase 2
M6P	Mannose-6-phosphate
MAPK	Mitogen-activating protein kinase
MART-1	Melanoma antigen recognized by T cells 1
MCOLN1	Mucolipin 1
MiT	Microphthalmia/TFE
MITF	Microphthalmia transcription factor
mLST8	mammalian lethal with SEC13 protein 8
MOI	Multiplicity of infection
MTOC	Microtubule organising centre
mTOR	Mammalian target of rapamycin
mTORC1	mTOR complex 1
mTORC1	mTOR complex 2
MVBs	Multi-vesicular bodies
Myrip	Myosin and Rab interacting protein
NLS	Nuclear localisation signal
NSF	N-ethylmaleimide-sensitive fusion protein
OPTN	Optineurin
PARL	Presenilins-associated rhomboid-like protein
PD	Parkinson's disease

PDK1	Phosphoinositide-dependent kinase 1
PE	Phosphatidylethanolamine
PH	Pleckstrin homology
PI	Phosphoinositide
PI3K	Phosphoinositide 3-kinase
PINK-1	PTEN Induced kinase 1
PKA	Protein kinase A
PKB	Protein kinase B
PM	Plasma membrane
PMEL	Pre-melanosomal protein
PNS	Post nuclear supernatant
RAPTOR	Regulatory associated protein of mTOR
REPs	Rab escort complex proteins
RHEB	Ras homolog enriched in brain
RICTOR	Rapamycin-independent companion of mTOR
RILP	Rab interacting lysosomal protein
ROC-COR	Ras of complex-C-terminal of ROC
ROS	Reactive oxidative species
SH3	SRC Homology 3
SNARE	SNAP Receptor
SNCA	Alpha-synuclein
SNpc	Substantia nigra pars compacta
SNpr	Substantia nigra pars reticular
SVs	Synaptic vesicles
SYNJ1	Synaptojanin 1
TFEB	Transcription factor EB
TGN	Trans-Golgi network
TIMM	Trans-inner mitochondrial membrane
TM	Trans-membrane
TOMM	Trans-outer mitochondrial membrane
TSC	Tuberous sclerosis complex
TYRP1	Tyrosinase related protein 1
TYRP2	Tyrosinase related protein 2
UBL	Ubiquitin like
ULK1/2	Unc-51 like autophagy activating kinase 1/2
UPS	Ubiquitin proteasome system
UV	Ultraviolet
UVRAG	UV radiation resistance-associated gene
v-ATPase	Vaculoar ATPase
VAMP7	Vesicle associated membrane protein 7
VARP	VPS9-ankyrin-repeat protein
VPS	Vaculoar protein sorting

WIP1	Wild-type p53-induced phosphatase 1
WT	Wild type

Acknowledgements

The years completing my PhD have been some of the most challenging of my life and I could not have completed them without the huge amount of support and guidance I was lucky enough to receive.

I would like to thank my supervisors Professor Michael Clague and Professor Sylvie Urbé for all their time, support and guidance and for giving me the opportunity to do a PhD when no-one else would. I would also like to thank Dr Heather Mortiboys for hosting me for my placement at SITraN and for all her input throughout our collaboration. I would also like to express my gratitude to the MRC DiMeN DTP for funding my project and awarding the money that allowed me to complete my placement in Sheffield.

I was very lucky to land in such a great working environment for my PhD. Thank you to all the 5th floor for making that happen. In particular I would like to thank Katy McCarron for all of her help on the LRRK2-VPS35 project. A special thank you must go to Andreas Kallinos and Anne Clancy for their endless patience with all my questions and without whom the lab would have fallen apart (several times). A special shoutout to my best biscuit Yasmina Sahraoui for all the emotional and moral support. Thanks for all the time listening to me having a screm and for spending all of your cash on cappuccinos. Thank you to Joana Gomes Neto for coming back and brightening up the lab. The last year of my PhD was better because of you!

I would not have made it through the last four years without my wonderful friends. Thanks to Kate, Yasmin, Lewis and Henry for the endless support and subbing me while I've been a broke bitch.

Last but not least, I'm incredibly blessed to have such a loving and supportive family. To my parents, I am so thankful for your unwavering support and belief in me. To my sister Ruth, thank you for never failing to make me laugh even on my worst days.

To all the people mentioned above and any that I have accidentally missed out, I appreciate you!

I worked hard and sacrificed to get what I get. Ladies it ain't easy being independent- Destiny's Child, Chapter 3, Verse 2.

1. Chapter 1 Introduction

1.1. Membrane Trafficking

Membrane traffic is the complex set of processes which establish the dynamic membrane bound subcellular compartments which are required for normal cell maintenance and homeostasis. Compartmentalisation within the cell allows separation of various cellular activities which can be controlled by a web of signals and pathways. This network requires cross talk and the ability to confer identity to and recognise specific compartments. These trafficking events can facilitate the general maintenance of the cell, or drive cell type specific functions. Examples of the latter include the generation of melanosomes in melanocytes or the transport of synaptic vesicles in neuronal cells. Specific pathways are also integral to the cell's ability to respond to and adapt to changes in the environment such as nutrient availability (e.g. GLUT4 trafficking).

One of the key principles of membrane traffic is the budding or formation of vesicles to transport cargos from one compartment to another, and the subsequent fusion with the target membrane. This requires a number of processes such as inducing membrane curvature to form the vesicle bud from the donor membrane, organisation of correct cargo to be transported, scission of the bud membrane to release the vesicle from the donor membrane and recognition of the donor membrane by the target membrane. This process is tightly controlled by a number of sequential events which ensures correct and effective trafficking of cargos (Chiang et al., 1989; Kaushik and Cuervo, 2012; Rothman, 1994).

1.1.1. Vesicle Coat formation

The formation of a vesicle bud requires the manipulation of the lipid bilayers that make up eukaryotic cell membranes. The forces acting on these membranes make them resistant to bending, and therefore proteins which sense, recognise, induce and stabilise membrane curvature are required

(McMahon and Boucrot, 2015). It is usually a combined effort of multiple proteins and interactions that results in successful bud formation. Transmembrane proteins with a conical structure can induce curvature by clustering together at one site. Some proteins (e.g. Arf proteins and Sar1) can also insert a hydrophobic motif into the lipid bilayer between lipid head groups, creating a wedge which induces bending. If multiple insertions are made in close proximity, this can induce membrane curvature (Pucadyil and Schmid, 2009).

Coat proteins such as clathrin or coatomer components polymerise to form a coat around an emerging bud to induce and stabilise membrane curvature. Different coat proteins are associated with different trafficking routes. COPI coated vesicles transport cargo from the cis-Golgi to the endoplasmic reticulum (ER) and retrograde transport from Golgi cisternae. COPII coated vesicles shuttle between the ER and the Golgi. Finally, clathrin coated vesicles mediate endocytosis from the plasma membrane to the endosomal network and from the trans-Golgi network (TGN) to endosomes. Coat proteins cannot directly interact with the membrane but instead bind via adaptor proteins (Kirchhausen, 2000; Pucadyil and Schmid, 2009; McMahon and Boucrot, 2015).

1.1.2. Vesicle release and coat disassembly

Once formed the bud must separate itself from the donor organelle, and the coat must be lost from the resulting vesicle. This process differs between vesicle types. In the case of CCVs this process requires the protein Dynamin (Lafer, 2002). Dynamin is a GTPase associated with CCVs. Dynamin can bind to membranes via a PH domain and binds to the SH3 domain of accessory proteins at the membrane (Pucadyil and Schmid, 2009). Dynamin GTPase polymerises around the neck of the vesicle before hydrolysing GTP. This hydrolysis drives the scission of the vesicle from the parent membrane (Takei et al., 1995; Marks et al., 2001; Schmid et al., 1998). Once pinched off, the vesicle loses it's coat following ATP hydrolysis by Hsp70 which drives the

disassembly of the clathrin coat (Ungewickell et al., 1995). Dynamin is not required for the scission of COPI or COPII coated vesicles. The release of the bud and the energy required for scission is provided by the coat polymer itself (Bonifacino and Glick, 2004; Kirchhausen, 2000).

1.1.3. Vesicle Fusion and SNARE proteins

SNARE [soluble NSF (*N*-ethylmaleimide-sensitive fusion protein) attachment protein receptor] proteins are a family of receptor proteins involved in vesicle fusion events. Originally SNARE proteins were subdivided into v-SNAREs, which are present on the trafficking vesicle, and t-SNAREs present on the target membrane. In the original model, recognition of a v-SNARE and t-SNARE on two cognate membranes brings them within close enough proximity to fuse by forming a trans-SNARE complex with a 1:3 ratio of helices. (Fasshauer et al., 2002; Hanson et al., 1997; Lin and Scheller, 1997; Söllner et al., 1993). We now have better understanding of SNARE proteins and their interactions, and they are now divided into the subcategories Qa-, Qb-, Qc- and R-SNAREs. Classification is based on the residue at the position of the zero ionic layer of the 4-helical bundle. R-SNAREs have an Arg/R residue, whilst Q-SNAREs have a Gln/Q residue. The Q-SNAREs are further subdivided based on the amino acid sequence of their SNARE motif (Clague and Urbé, 2020; Jahn and Scheller, 2006; Fasshauer et al., 1998).

SNARE proteins are first trafficked to the relevant compartments. Most SNARE proteins have a C-terminal transmembrane domain, a SNARE motif, and a N-terminal domain which varies between the subsets of SNARE proteins (Hong, 2005; Jahn and Scheller, 2006). In many (but not all) cases, when not in complex, SNARE motifs are unstructured. The two membranes to be fused are first brought together by tethering complexes. These proteins, or multi-subunit complexes, can provide some specificity to membrane trafficking. Early endosome antigen 1 (EEA1) acts as a tethering complex for the homotypic fusion of early endosomes. It binds to Rab5 and PI3P present on each endosome to dock the two vesicles together prior to their fusion (Mills et

al., 2001; Christoforidis et al., 1999). Similarly, in the fusion of endosomes with lysosomes, the homotypic fusion and vacuole protein sorting (HOPS) tethering complex binds Rab7 on late endosomes and Arl8b on lysosomes to bring the two membranes into close proximity (Balderhaar and Ungermann, 2013; Khatter et al., 2015). Finally, the exocyst complex tethers secretory vesicles to the plasma membrane prior to fusion (Mei and Guo, 2018) and has also been linked to melanosome secretion (Moreiras et al., 2020).

SNARE proteins mediate membrane fusion by forming a spontaneous complex. The SNARE motifs associate in a four-helical bundle which is highly stable and formed from one of each of the subcategories of SNAREs (Yoon and Munson, 2018; Chen and Scheller, 2001; Hong, 2005; Jahn and Scheller, 2006; Bonifacino and Glick, 2004). The highly stable tetra-helical complex helps overcome the energy barrier created by the hydrophobic forces of the opposing membranes. Thus, the formation of this complex may be sufficient to drive vesicle fusion (Yoon and Munson, 2018). Following fusion, the SNARE complex remains intact in the target compartment. This then disassembles by the combined action of NSF and SNAP proteins, which free the v-SNARE to recycle back for future rounds of fusion, whilst the t-SNARE remains in the target membrane (Bonifacino and Glick, 2004; Jahn and Scheller, 2006; Hong, 2005; Chen and Scheller, 2001; Yoon and Munson, 2018; Morgan and Burgoyne, 1995). SNARE proteins belong to one of two major families which account for specificity in trafficking and the fusion of vesicles. For example, SNAP-25, synaptobrevin and syntaxin-1 form the SNARE complex involved in fusion of synaptic vesicles with the plasma membrane in neurons. The other family are the Rab proteins. Additionally, tethering complexes dock specific organelles to their target membranes to add additional control to trafficking pathways.

1.1.4. Rab proteins

Rab GTPases are a family of proteins integral to membrane trafficking. They belong to the Ras superfamily of GTPases and act in conjunction with a

number of interactors to mediate trafficking events (Zerial and McBride, 2001). They facilitate vesicle motility, docking and fusion with the appropriate membrane compartment. They were first discovered in yeast, with a major finding coming when Novick and Schekman identified the SEC genes responsible for progression through the secretory pathway in the 1980s (Novick et al., 1980). They discovered that Sec4 protein was a Ras like GTPase protein which was essential for secretion (Salminen and Novick, 1987). This marked the identification of the first Rab protein. Following this discovery, Tavitian and Zerial started cloning the mammalian homologues (Zahraouis et al., 1989; Chavrier et al., 1990) which were numbered in the order they were sequenced. Zerial later showed that different Rab proteins localised to different membrane compartments (Chavrier et al., 1990) (**Figure 1.1**). Their discovery provided the first set of organelle specific membrane markers. There are 11 Rab proteins expressed in yeast and over 60 Rab family members identified in mammalian cells (Bock et al., 2001). This increase in family members is reflective of the increase in complexity, and need for more organised vesicular traffic in mammalian cells (Zerial and McBride, 2001).

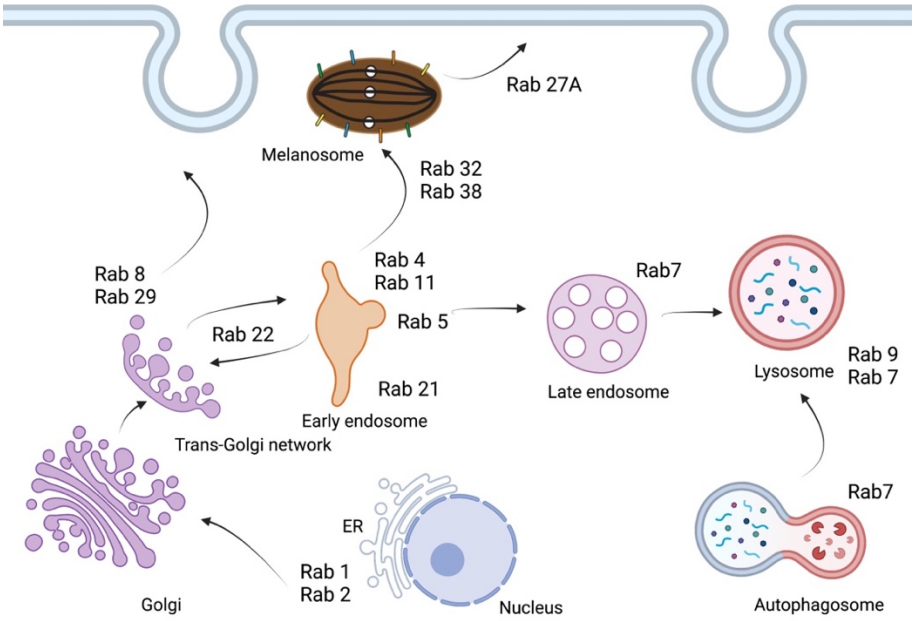

Figure 1.1 Localisation of Rab proteins across the endolysosomal system
Rab proteins localise to distinct subcellular compartments and can act as organelle markers. Created with BioRender.com.

1.1.5. The Rab cycle

Like other GTPases, Rab proteins (Rabs) cycle between their active (GTP bound) and inactive (GDP bound) forms through cycles of GTP binding and hydrolysis (**Figure 1.2A**). A variety of proteins interact with Rabs as they go through this cycle. A general schematic of the Rab cycle is depicted in **Figure 1.2B**. Newly formed Rabs are geranylgeranylated at their C-terminus- a process carried out by the Rab escort complex proteins (REPs) together with a geranylgeranyltransferase (GGTase). They interact non-specifically to modify Rab proteins, allowing their insertion into their target membrane in their GDP bound form (Desnoyers et al., 1996; Wu et al., 2007; Alexandrov et al., 1994; Seabra, 1996). Once within their target membrane, Rabs can interact with their specific guanine nucleotide exchange factor (GEF). Rab proteins bind GTP and GDP with similar high affinity. Consequently, there is a low basal rate of dissociation. GEFs accelerate this process by changing the nucleotide binding site leading to dissociation of the bound GDP and the rebinding of a new nucleotide. Although Rab proteins have similar affinities for GDP and GTP, there is approximately ten times higher concentration of GTP in the cell

meaning GDP is replaced with GTP. (Bos et al., 2007). The binding of GTP causes a conformational change in the Rab protein which enables interaction with effector proteins to carry out downstream functions (Zerial and McBride, 2001).

Effector protein interactions are tailored to individual Rabs based on the functional needs of the associated organelle and trafficking events. For example, EEA1 is an effector for early endosome associated Rab5 (Simonsen et al., 1998). Inactivation of a Rab protein requires the hydrolysis of the bound GTP to GDP. The basal rate of GTP hydrolysis by Rab proteins is very slow. Therefore, hydrolysis requires interaction of Rab proteins with their respective GTPase activating proteins (GAPs). These can catalyse conversion of GTP to GDP returning the Rab to its inactive conformation (**Figure 1.2A**) (Bos et al., 2007). Chaperone proteins known as GDP dissociation inhibitors (GDIs) can then extract the inactive membrane bound Rab protein which can then re-enter the cycle for further rounds of GTP binding and hydrolysis (**Figure 1.2B**) (Araki et al., 1990; Pfeffer et al., 1995). The presence of Rab proteins on distinct membranes allows for specificity in trafficking of cargos from one compartment to another. Rabs can bind to effector proteins which act to relocate vesicles to new parts of the cell by binding to microtubules (e.g. Rab7 effector RILP in the positioning of late endosomes to lysosomes). Other effectors such as tethering factors, bring two membranes into close proximity (e.g. the Rab7 effector HOPS complex in the fusion of late endosomes to lysosomes, Rab11 and the exocyst in the docking of secretory vesicles at the plasma membrane, or the Rab5 effector EEA1 in the homotypic fusion of early endosomes) (Rubino et al., 2000; Lin et al., 2014; Jordens et al., 2001; Van Der Kant et al., 2013). Once Rab proteins have docked a vesicle to its appropriate target membrane (acceptor membrane) SNARE proteins facilitate vesicle fusion with the acceptor membrane (Yoon and Munson, 2018; Chen and Scheller, 2001; Jahn and Scheller, 2006).

1.1.6. Rab cascades

Rab proteins can act in cascades, which coordinate trafficking events, organelle maturation and give some pathways (like the endolysosomal pathway) directionality. One well studied example is the progression of early to late endosomes in the endolysosomal system. Rab5 is a well-established marker for early endosomes, whereas Rab7 is localised to the late endosome. (Chavrier et al., 1990; Poteryaev et al., 2010). This indicates that there must be a so called “Rab conversion”, where the Rab identity of an organelle is changed during the maturation process. Two possible mechanisms were considered. In the first, cargos destined for lysosomal degradation were trafficked from a Rab5 positive compartment to a Rab7 positive compartment. In the second model, early endosomes exchange their Rab5 molecules for Rab7 in an organelle maturation step. It is now widely believed that Rab5 and Rab7 operate in a cascade reaction where Rab7 is recruited by active Rab5 and activated Rab7 can switch off Rab5 activity (Rink et al., 2005). This cascade ensures the polarity of the endolysosomal system.

1.1.7. Recruitment and activation of Rab7 in the endolysosomal system

Rab7 is one of the best studied Rab proteins and is well known to localise to the late endosomal compartment (Bucci et al., 2000). Research has found that Rab7 has key roles in late endosome maturation, late endosome-lysosome fusion events as well as lysosome positioning through a number of effector proteins (Bucci et al., 2000; Guerra and Bucci, 2016). On early endosomes Rab5 is activated by its GEF Rabex-5. Activation of Rab5 recruits the phosphoinositide 3-kinase (PI3 kinase) VPS34, which exclusively generates PI3*P.* This increases the recruitment of Rab5 effector proteins such as EEA1, which can recruit further Rab5 molecules, generating a positive feedback mechanism (Mills et al., 1999; Poteryaev et al., 2010; Rojas et al., 2008; Rubino et al., 2000). This positive feedback loop can be interrupted by recruitment of another Rab5 effector, the Mon1/CCZ1 complex (Rink et al., 2005). Binding of Mon1/CCZ1 can displace Rabex-5, preventing further

activation of Rab5. Rab7 is recruited to the endosomal compartment by Mon1 complex which also acts as a Rab7 GEF (Balderhaar and Ungermann, 2013; Poteryaev et al., 2010). Activated Rab7 can now bind to its effectors which include the HOPS complex, VPS35 and Rab interacting lysosomal protein (RILP) (Balderhaar and Ungermann, 2013; Rojas et al., 2008; Cantalupo et al., 2001; Jordens et al., 2001; Stenmark, 2009). Rab7 can also recruit RabGAP-5 which inactivates Rab5 by activating GTP hydrolysis to GDP. This targets Rab5 for extraction by GDI proteins, thus leaving active Rab7 alone at the late endosomal membrane (Del Conte-Zerial et al., 2008; Haas et al., 2005). This concomitant inactivation of Rab5 and activation of Rab7 ensures the polarity of the endosomal pathway and is one example of how Rab proteins act in unidirectional cascades.

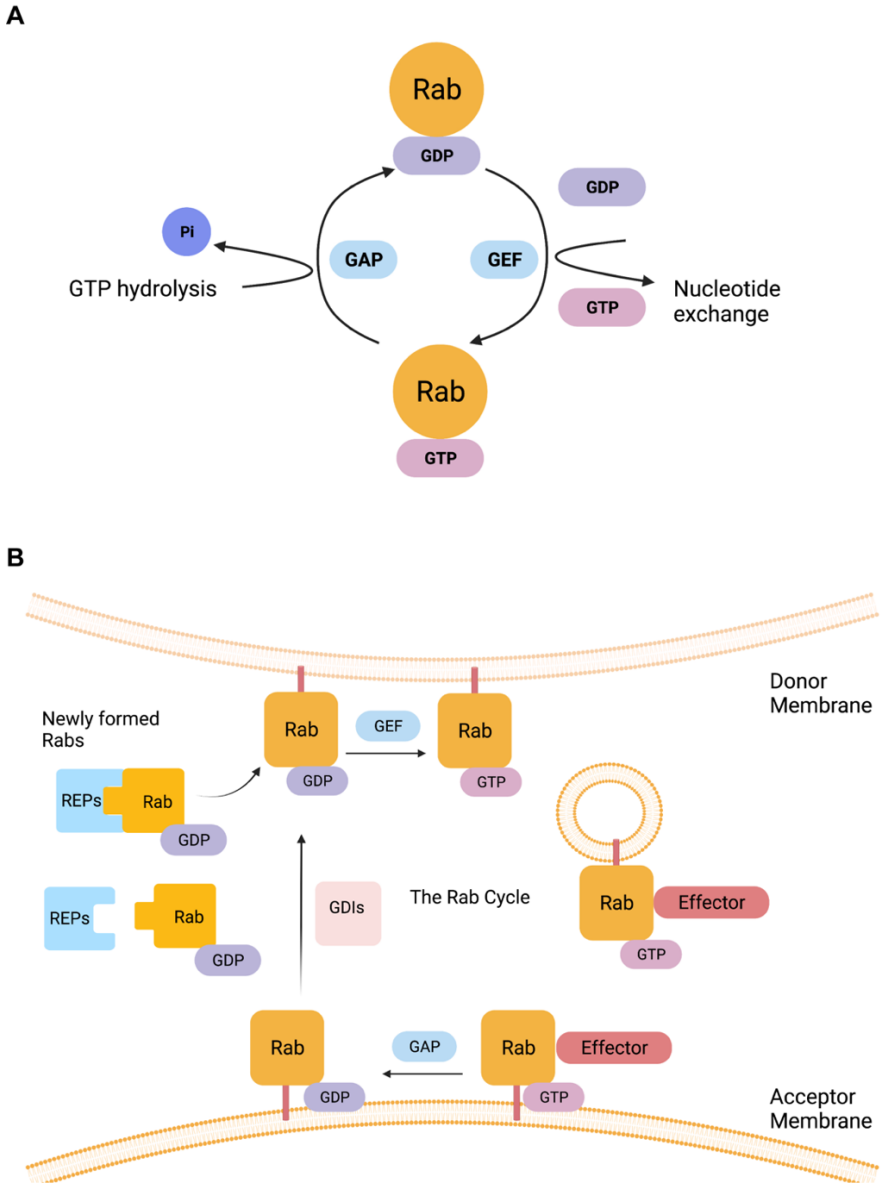

Figure 1.2 Rab GTPases are molecular switches which undergo a tightly controlled cycle of nucleotide exchange and hydrolysis.
A Rab proteins cycle between their inactive GDP-bound form and active GTP-bound form in a cycle which requires the action of GEFs for exchange of GDP to GTP and GAPs for the hydrolysis of GTP to GDP. **B** Newly synthesised GDP bound Rab proteins are geranylgeranylated by the Rab escort complex and geranylgeranyl transferase before being inserted into their target membrane. Here they interact with a GEF which promotes nucleotide exchange for GTP leading to Rab activation. Active Rab proteins interact with effector proteins to carry out their roles in membrane traffic. Rab GAPs catalyse the hydrolysis of GTP to GDP leaving Rabs in an inactive state. Rab GDIs can extract inactive membrane bound Rabs for further cycles. Created with BioRender.com.

1.2. The Endolysosomal system

The endolysosomal system is a dynamic tubulo-vesicular network which participates in a wide array of cell functions including signalling, cell homeostasis, protein degradation and recycling, nutrient uptake and endocytic cargo control. The success of such a network is dependent on the coordinated action of proteins and signals which overlap and maintain distinct organelles and their subdomains.

The pathway begins with early endosomes- membrane bound organelles which undergo a maturation process which is defined by distinct stages. Early endosomes can be operationally defined using pulse chase experiments, or as organelles which are slightly acidic and enriched in Rab5, Rab11 and EEA1 (Clague, 1998). The maturation of endosomes is characterised by the number of intraluminal vesicles, the intraluminal pH, the transport from the cell periphery to the microtubule organising centre (MTOC) and the Rab proteins present (Hu et al., 2015; Huotari and Helenius, 2011; Helenius et al., 1983; Hopkins et al., 1990; Futter et al., 1996). Early endosomes gradually undergo maturation to late endosomes before finally fusing with the lysosome (Hu et al., 2015; Jovic et al., 2010; Futter et al., 1996).

1.2.1. Endocytosis

Endocytosis is the internalisation of cargo or cargoes from outside of the cell in vesicles which enter into the endosomal system (Roth and Porter, 1964). Endocytosis can largely be split into four categories- phagocytosis, pinocytosis, caveolae and receptor mediated endocytosis. Internalisation typically occurs by an invagination of the plasma membrane which contains the desired cargo. This forms the beginning of a vesicle which eventually is pinched off into the cell's cytoplasm (Schmid et al., 2014). The resulting endocytic vesicle can then join the endolysosomal system by fusion with an early endosome (Jovic et al., 2010; Hu et al., 2015).

1.2.2. Early endosomes

Early endosomes provide a sorting hub for the cell, determining the fate of proteins targeted to the endolysosomal system. Proteins within this pathway are either delivered to the lysosome for degradation, or can be recycled back to the plasma membrane or the TGN by retrograde transport (Jovic et al., 2010; Hu et al., 2015). Early endosomes have a different morphology compared with the later compartments of the pathway. They have tubular structures which extend out from the vacuolar body of the vesicle which form the basis of the recycling elements. These can bud off from early endosomes and traffic back to the TGN or the plasma membrane (Jovic et al., 2010; Naslavsky and Caplan, 2018; Zerial and McBride, 2001; Mukherjee et al., 1997). Over time early endosomes increase in size as they undergo homotypic fusion and fusion events with endocytic vesicles. Rab proteins on early endosomes such as Rab5, Rab4, Rab21 and Rab11 localise to distinct microdomains which govern the sorting of cargos for different fates (Naslavsky and Caplan, 2018). As early endosomes mature, invaginations of the membrane occur which bud off into the lumen to form internal vesicles. Increasing numbers of these luminal vesicles marks the formation of multivesicular bodies (MVBs) or late endosomes (Futter et al., 1996; Hopkins et al., 1990)

1.2.3. Late endosomes

As early endosomes mature into late endosomes, the complex sorting-events that maintain this pathway continue recycling proteins through retrograde transport, whilst proteins that remain in late endosomes will be degraded after fusion with the lysosome (Huotari and Helenius, 2011; Mukherjee et al., 1997; Helenius et al., 1983). The transition from early to late endosome is marked by a Rab switch from Rab5 to Rab7 (see **section 1.1.7**). Additionally, as vesicles progress through the endosomal pathway, they become progressively more acidic due to the action of vacuolar ATPase (v-ATPase), which establishes an acidic environment in late endosomes (Maxfield and McGraw, 2004; Mukherjee et al., 1997)(**Section 1.2.7**). This reduction is integral to the recycling of the cation independent mannose-6-phosphate receptor (CIMPR-

see section 1.2.5) (Brown et al., 1986). The CIMPR is able to bind mannose-6-phosphate (M6P) residues at the more neutral pH of the TGN and early endosomes (approx. 6.5). As the endosomal pathway becomes more acidic, the binding affinity decreases and CIMPR releases the M6P residue at pH <6. Therefore, by the time these vesicles arrive at late endosomes the lysosomal proteins are released and will continue along the endosomal pathway to the lysosome. Meanwhile, the CIMPR is recycled back from the late endosomal compartment to the TGN where it can bind another round of lysosomal proteins (Brown et al., 1986; Kornfeld and Mellman, 1989; Hirst et al., 1998). Lysosomal membrane proteins remain in the membrane of late endosomes, whereas trans-membrane (TM) cargos for degradation are sorted into internal vesicles. Late endosomes progress through the endosomal pathway until they reach and fuse with the lysosomal compartment. Fusion of a late endosome with a lysosome leads to lysosomal membrane proteins being integrated into the lysosome membrane, whilst vesicles and their contents to be degraded are released into the lysosome lumen (De Duve and Wattiaux, 1966; De Duve et al., 1955; Ciechanover, 2005; Futter et al., 1996).

1.2.4. Lysosomes

Lysosomes are the terminal compartment of the endolysosomal system, as well as the autophagy pathway. The lysosome was first discovered by Christian De Duve using centrifugation techniques separating a granule organelle containing hydrolase enzymes from mitochondria and microsomes (De Duve et al., 1953, 1955). The lysosome acts as the mammalian equivalent of the vacuole in yeast. The lysosomal system represents one of two major pathways by which proteins are degraded and cell homeostasis is maintained- the other being the ubiquitin-proteasome system (UPS) (Tanaka et al., 1983; Hough et al., 1986; Ciechanover, 2005; Clague and Urbé, 2020).

Lysosomes are classically regarded as acidic organelles which contain a variety of proteolytic enzymes, including hydrolases, which non-selectively degrade proteins and organelles (Haider and Segal, 1972; De Duve et al., 1955). More recent studies have found that the pH of lysosomes is variable

and that not all lysosomes are acidic (Bright et al., 2016; Johnson et al., 2016). The acidic environment of the lysosome is established and maintained by the v-ATPase proton pump which maintains a pH of around 4 (Schneider, 1981) (**Section 1.2.7**). Cargos destined for degradation are delivered to the lumen of the lysosome by the endosomal or autophagy pathways where they are digested by resident acid-dependent proteases. This pathway processes a range of cargos and serves a variety of functions to maintain the homeostasis of the cell and adaptation to the cellular environment. This includes degrading receptors taken up by endocytosis (such as epidermal growth factor receptor (EGFR)), misfolded or unwanted proteins within the cell, and damaged organelles (Futter et al., 1996; Maxfield and McGraw, 2004). Damaged organelles can be taken up by selective autophagy (e.g. in the case of damaged mitochondria-mitophagy) and the subsequent autophagosome fuses with the lysosome for degradation (Xie and Klionsky, 2007).

In the case of cellular stress (e.g. nutrient deprivation) the lysosome can be used in conjunction with autophagy to ensure cell survival (Martina et al., 2012; Settembre and Ballabio, 2011). Organelles and proteins are enveloped non-selectively by the autophagy machinery into autophagosomes which are then delivered to and fuse with the lysosome. The cargo are then degraded and amino acid permeases in the lysosomal membrane transfer free amino acids back to the cytoplasm for use in synthesis of new proteins (Yorimitsu and Klionsky, 2005; Xie and Klionsky, 2007). The lysosome is also a hub for mTOR signalling which will be discussed in more detail in **section 1.2.15.**

1.2.5. Selective activity and delivery of lysosomal enzymes

Because the role of lysosomal enzymes is to degrade proteins non-specifically, it is of great importance that they are selectively delivered to the lysosome and only become activated once they reach the lysosome lumen. Therefore, these proteins are not released into the cytoplasm but are instead trafficked in vesicles which join the endolysosomal system. Lysosomal hydrolases exist in a pro-precursor form during trafficking. Upon delivery to the lysosome, the pro-

sequence is removed and the enzymes become activated (Cooper and Stevens, 1996). Soluble lysosomal proteins are targeted to the lysosome by the CIMPR and sorting receptor sortilin (Petersen et al., 1997; Seaman, 2004). In the case of CIMPR, the relevant proteins are modified in the cis-Golgi network leaving the carbohydrate molecule mannose-6-phosphate (M6P) attached. In the TGN these modifications can bind the CIMPR tightly and specifically (Cooper and Stevens, 1996). This interaction is maintained as these proteins bud off into vesicles from the TGN which eventually fuse with endosomal compartments. The CIMPR interaction is lost in the acidic environment of the MVBs and is recycled back to the TGN for further rounds of traffic (Hirst et al., 1998). Once delivered to the lysosome the hydrolases are converted to their active form following a cleavage event (Gieselmann et al., 1985). This protects the endosomal pathway machinery as well as other proteins in the late endosomal compartments from being degraded until they have reached the lumen of the lysosome.

1.2.6. The retromer complex

The retromer complex was first discovered in yeast and was found to be integral to the retrograde traffic of the yeast CIMPR homolog-Vps10. Three members of the VPS proteins form a heterotrimeric complex which forms the scaffold for a number of accessory factors (Seaman et al., 1997, 1998). The retromer is highly conserved in higher eukaryotes and in mammalian cells the heterotrimeric core is made up of: VPS35, VPS26 and VPS29 (Swarbrick et al., 2011; Seaman, 2012). A number of other accessory proteins form transient interactions with the core of the retromer complex, including SNX-BAR proteins which are integral for the correct sorting of cargos (Seaman, 2012). One major function of the retromer complex is retrograde sorting and transport of proteins from the late endosome back to the TGN or the plasma membrane. As we have seen above, the recycling of the CIMPR is integral to the homeostasis of the lysosome in ensuring continual delivery of its functional enzymes. Similarly, receptors and their ligands internalised by endocytosis reach the endosomal compartment (Seaman, 2004; Braulke and Bonifacino,

2009). Receptors are sorted for either degradation, or recycled back to the plasma membrane, depending on the signalling needs of the cell. The retromer complex is recruited to the endosomal network by Rab7 and acts as a Rab7 effector (Rojas et al., 2008; Seaman, 2012). The core retromer complex is key to sorting cargos via its interaction with the SNX proteins and helps to deform the endosomal membranes in the initiation and formation of carriers (Temkin et al., 2011; Harterink et al., 2011; Wassmer et al., 2009, 2007). The retromer can also recruit the WASH complex. WASH is an actin polymerising complex which drives the formation of subdomains at early endosomes, important for sorting of cargos for different fates (Gomez and Billadeau, 2009; Derivery et al., 2009). The core retromer complex also interacts with TBC1D5, a Rab7 GAP (Seaman et al., 2009). Furthermore, as well as being a Rab7 effector, the retromer can also act as a Rab7 regulator. Retromer associated TBC1D5 can catalyse the hydrolysis of GTP to GDP, switching off Rab7. This is supported by data which shows knockout of VPS35 and VPS29 core subunits results in hyperactive Rab7 (Jimenez-Orgaz et al., 2018).

1.2.7. v-ATPase

Acidification is integral to certain membrane trafficking events and organelle functions. The process of acidification is carried out by the v-ATPase (Maxson and Grinstein, 2014). The v-ATPases are multi-subunit complexes which can be split into two domains, the V_0 and V_1 domains. In all isoforms the V_0 domain is made up of 6 subunits and functions to translocate protons across the membrane. The V_1 domain is composed of 8 subunits which are able to hydrolyse ATP (Toei et al., 2010). The energy harnessed from ATP hydrolysis is used to drive protons across the membrane against the proton gradient. The different isoforms are targeted to different organelles. The a1 subunit has been implicated in the endolysosomal pathway. This is perhaps the best characterised acidification pathway with pH being important for both effective retrograde transport and lysosomal hydrolase activity (discussed in **section 1.2.5**) (Toei et al., 2010). Melanosomes are a specialised organelle which

undergo acidification. Melanosomes are lysosome related organelles which undergo a 4-stage maturation process. (**Section 1.3.2**). Early-stage melanosomes are acidified by a v-ATPase isoform containing the a3 subunit, however, the later stages require a neutral pH consequent to loss of the v-ATPase (Toei et al., 2010; Tabata et al., 2008; Ancans et al., 2001).

Control of the v-ATPase is central in regulating the luminal pH of organelles and is thought to occur at multiple levels. Dissociation of the V_0 and V_1 subunits has been reported in some organelles, which is a rapid way of regulating v-ATPase function (Kane, 2006; Forgac, 2007). The efficiency of the v-ATPase at pumping protons across the membrane has been reported to vary between organelles and is likely isoform specific (Toei et al., 2010; Maxson and Grinstein, 2014). Finally, transcriptional and protein stability control of v-ATPase can regulate the levels present in the cell and therefore its activity. v-ATPase is under the transcriptional control of TFEB (**Section 1.2.13**) and is up regulated in response to cellular stress. The levels of RILP protein within the cell has also been reported to affect the recruitment and stability of the v-ATPase (Maxson and Grinstein, 2014).

Counterion channels are essential to the effective acidification. The pumping of protons across the membrane by the v-ATPase will increase the positive charge within the organelle, creating an electrochemical gradient as well as a pH gradient (Mills et al., 2001; Paroutis et al., 2004a; Forgac, 1998a). This accumulation impedes the further flux of protons and increases the leak of protons back across the membrane. Therefore, chloride channels are used to give counterions which balance out this electrochemical gradient and allow for further transport of protons across the membrane by the v-ATPase (Mills et al., 2001; Paroutis et al., 2004b; Forgac, 1998b).

Lysosomal acidification is essential to effective lysosomal function (**Section 1.2.5**). There is a growing body of evidence implicating function of the v-ATPase in neurodegenerative disease. Neurons are more sensitive to defects in the lysosomal pathway as they are post mitotic. As such defects in v-

ATPase function have been linked to Alzheimer's, PD and lysosomal storage diseases (Song et al., 2020). In particular, PD related protein LRRK2 (**Section 1.4.7**) has been shown to directly interact with the a1 subunit of the v-ATPase. Pathogenic mutation in LRRK2 has been shown to induce a decrease in protein levels of the a1 subunit as well as mis-localisation (Wallings et al., 2019a).

1.2.8. Rab7 and lysosome fusion

One of Rab7's key functions is to mediate the fusion of late endosomes with the lysosome. This is a function actioned by the HOPS complex which acts as a downstream Rab7 effector through its associated proteins. The HOPS machinery and its function was first identified in yeast as a multimeric protein complex which acts as a tethering factor (Balderhaar and Ungermann, 2013). In yeast the HOPS complex binds to two Rab7 molecules (Ypt7 in yeast)- one on the late endosome and one on the vacuole (the yeast equivalent of the lysosome). In this model, Rab7 and the HOPS complex together tether the late endosome and lysosome (Bröcker et al., 2012)- a precursor step required for fusion. In yeast the HOPS complex also recruits the relevant SNARE proteins responsible for the actual fusion event (Lürick et al., 2015; Behrmann et al., 2014). Although this process is still being defined in mammalian cells, there are some key differences from the process in yeast. The HOPS complex binds to a Rab7-RILP complex on late endosomes (Lin et al., 2014; Van Der Kant et al., 2015, 2013). RILP is a Rab7 effector, crucial for Rab7's role in lysosome positioning, discussed in more detail below (Sun et al., 2009; Guerra and Bucci, 2016; Cantalupo et al., 2001; Jordens et al., 2001). HOPS binds Arl8b GTPase on the lysosome to bring these two compartments into close proximity (Khatter et al., 2015) and allows for their subsequent fusion.

1.2.9. Rab7 and lysosomal positioning

Typically, most lysosomes are localised primarily to the microtubule organising centre (MTOC), although lysosomes can be found dispersed through the cytoplasm and in the cell periphery. Rab7 has a role in lysosome positioning

through interaction with its effector RILP. RILP can interact with the dynein-dynactin complex (Van Der Kant et al., 2013, 2015). Cytoplasmic dynein (from here referred to as Dynein) is a cytoskeletal motor protein that moves along the microtubules. It is responsible for the retrograde transport of lysosomes from the cell periphery towards the cell centre (from plus to minus end of microtubules). Dynein interacts with dynactin, a multimeric protein complex made up of more than 20 components (Pu et al., 2016). Activated Rab7 on late endosomes and lysosomes recruits dynein-dynactin via RILP, to tether organelles to the cytoskeleton for their transport. (Van Der Kant et al., 2013; Pu et al., 2016; Jordens et al., 2001).

1.2.10. Activation of Lysosome biogenesis

The formation of lysosomes is a tightly controlled process which can be upregulated depending on the degradative needs of the cell. For example, in cellular stress, the pathway is activated to increase the degradative capacity of the cell to produce more amino acids for synthesis of new proteins. This controlled activation requires selective transcription of lysosomal genes. Many of these genes are under the transcriptional control of transcription factor EB (TFEB) (Napolitano and Ballabio, 2016).

1.2.11. Autophagy

Autophagy is a recycling pathway where cells digest their own proteins and organelles to generate building blocks for further protein synthesis and organelle biogenesis. Autophagy can be subdivided into macro-autophagy, micro-autophagy and chaperone mediated autophagy (CMA). In addition to these broad non-specific forms of autophagy there are also organelle specific forms of autophagy such as mitophagy. The terminal compartment for all forms of autophagy is the degradative lysosomal compartment (Klionsky, 2005; Wang and Klionsky, 2003; Glick et al., 2010; Dikic and Elazar, 2018).

Originally, autophagy was defined by De Duve when double membrane structures were identified by electron microscopy (De Duve and Wattiaux,

1966; De Duve et al., 1953). It was subsequently shown that the degradation of cargo by the autophagy pathway was distinct from the endocytosis pathway for degradation (Essner and Novikoff, 1961; Klionsky, 2008; Kanki and Klionsky, 2008). At steady state, a baseline of autophagy is required to maintain protein and organelle homeostasis. In times of cellular stress and nutrient deprivation the cell responds by increasing this catabolic activity, non-specifically digesting portions of itself. In macro-autophagy, this is done by the engulfment of part of the cytosol by a double membrane forming a vesicle called an autophagosome. Autophagosomes are trafficked to the lysosomal compartment where fusion of an autophagosome with a lysosome generates an autolysosome. Cargo delivered here is degraded by the hydrolase enzymes in the lysosome. In micro-autophagy, the lysosomal membrane generates invaginations which directly take up cytosol for degradation (Yim and Mizushima, 2020) (**Figure 1.3**).

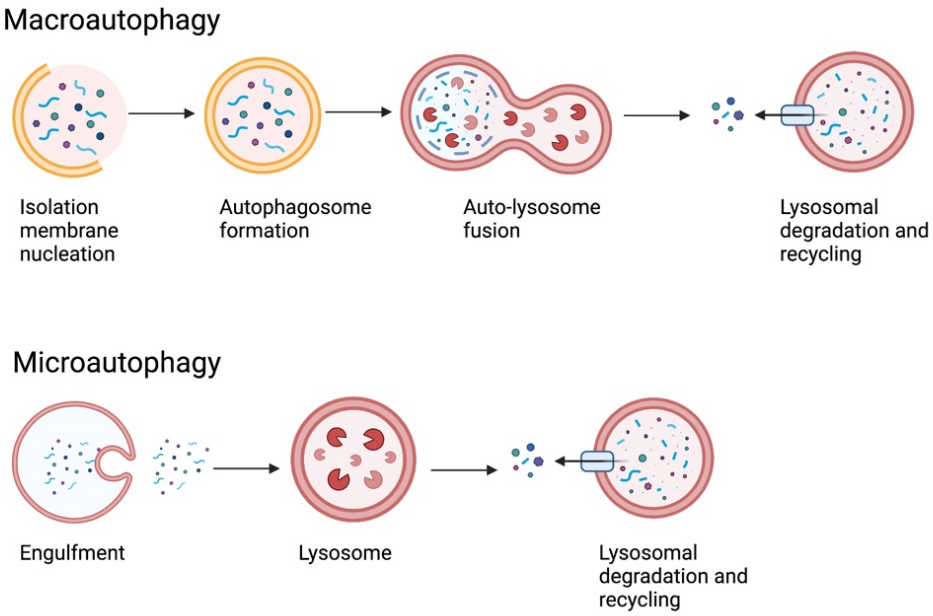

Figure 1.3 Macro and micro-autophagy pathways
Macro-autophagy: the non-selective engulfment of cell contents within an isolation membrane which are delivered to the lysosome for degradation. Micro-autophagy: The direct engulfment of cellular contents by the lysosome for degradation. Created with BioRender.com.

In macro-autophagy the initiating steps require the nucleation of the engulfing curved membrane known as a phagophore (also known as an isolation membrane) (Essner and Novikoff, 1961; Réz G; Meldolesi, 1980). The elongation of this membrane results in the formation of a spherical vesicle- the final step of formation being the fusion of either end of the membrane. Any cytosolic proteins or other materials which are captured within the autophagosome are trafficked along the microtubules to the lysosome (Seglen and Bohley, 1992). Fusion with the lysosomal membrane releases these components into the lysosomal lumen where degradative enzymes break them down (Lamb et al., 2013; Stolz et al., 2014; Mizushima et al., 2011). Lysosomal permeases and other transporters export amino acids and other degradation products out of the lysosome into the cytoplasm, where they can be used as building blocks for new macromolecules or for metabolism (Glick et al., 2010; Dikic and Elazar, 2018).

An advancement in our understanding of autophagy came when work from Ohsumi's group discovered the autophagy related genes (ATG) proteins in yeast (Tsukada and Ohsumi, 1993). These were determined to be the key proteins required for autophagy. Importantly, many of the ATG genes discovered in yeast are highly conserved in humans. There is significant interest in understanding this pathway, as dysfunction in autophagy genes and autophagic flux have been linked to diseases including cancer and neurodegenerative diseases (Nixon, 2013; Jiang et al., 2019; Mizushima and Levine, 2010; Liang et al., 1999; Kuma et al., 2004).

1.2.12. Regulation of autophagy

As mentioned above, autophagy is always operating in some capacity within the cell. The level of autophagic flux is linked to several factors, especially the availability of nutrients within the cell. Therefore, there must be a system which activates the autophagic pathway when nutrients are depleted and stems autophagy when the cell is fed. A major player in this regulatory pathway is the mammalian target of rapamycin (mTOR). mTOR can form 2 complexes-

mTORC1 and mTORC2 which play 2 different roles (Figure 1.4). Components common to both complexes are mammalian lethal with SEC13 protein 8 (mLST8) and DEP domain-containing mTOR-interacting protein (DEPTOR) which act as positive and negative regulators of the complexes respectively. In addition to these common components there are also subunits which are unique to each complex. mTORC1 also contains the scaffold protein, regulatory associated protein of mTOR (RAPTOR) and negative regulator, PRAS40/AKTIS1. mTORC2 contains a different scaffold protein called rapamycin-independent companion of mTOR (RICTOR) and regulator subunits PROTOR1/2 and mSIN1/MAPKAP1 (Loewith et al., 2002; Zoncu et al., 2011b).

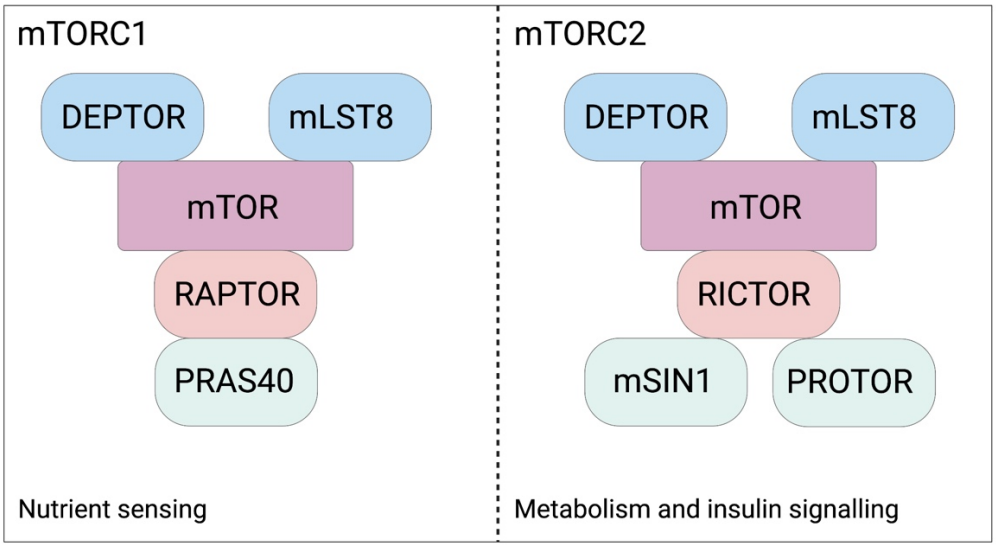

Figure 1.4 Components of the mTORC1 and mTORC2 complexes
mTORC1 and mTORC2 complexes share some core components but have different effector proteins which give rise to distinct functions. Created with BioRender.com.

When nutrients in the cell are in good supply, mTORC1 is recruited to the lysosome membrane (Rogala et al., 2019; Condon and Sabatini, 2019; Wyant et al., 2017). In a fed state the cell activates the PI3K pathway via growth factor and insulin receptors (White, 1998). This generates PtdIns3,4,5-P_3 which in turn activates the phosphoinositide-dependent kinase 1 (PDK1) kinase and mTORC2 complex. Both are able to phosphorylate and activate protein kinase B (AKT/PKB) (Liao and Hung, 2010; Moore et al., 2011; Datta et al., 1999).

Activated AKT/PKB can then phosphorylate tuberous sclerosis (TSC1/2) complex which acts as a GAP protein for Ras homolog enriched in brain (RHEB) GTPase (Yang et al., 2006; Zoncu et al., 2011b). Phosphorylation of TSC1/2 inhibits its GAP activity preventing the hydrolysis of GTP by RHEB. Active RHEB promotes the activity of mTOR in a nutrient fed state. In addition to RHEB GTPase the Rag GTPases also play a role in the regulation of autophagy. Rag GTPases form heterodimers of either RagA or RagB with RagC or RagD. When the cell is fed, RagA or RagB in the heterodimer is GTP bound, whilst the RagC or RagD component is GDP bound. In this conformation the heterodimer interacts with RAPTOR and recruits the mTORC1 complex to the lysosome or late endosome where RHEB can promote mTOR activity (Sancak et al., 2008, 2010; Sancak and Sabatini, 2009; Liu and Sabatini, 2020; Shen et al., 2017). The effect of mTORC1 on regulating autophagy is through the hyperphosphorylation of Unc-51 like autophagy activating kinase (ULK)1/2 and ATG13 which prevents the formation of a complex between the two (Kim et al., 2011b; Kamada et al., 2010).

When nutrients are depleted, and the cell no longer activates the PI3K pathway, this results in the inactivation of AKT/PKB. This subsequently leads to the activation of 5'-AMP activating protein kinase (AMPK) by liver kinase B1 (LKB1) leading to the activation of the TSC1/2 complex and the hydrolysis of GTP to GDP by RHEB (Sancak et al., 2008). Additionally, the Rag GTPases switch to their inactive conformation where the composite GTPases switch their nucleotide binding state (Sancak and Sabatini, 2009). The combined results of the changes to these 2 GTPase cycles results in the inactivation of mTORC1 which results in the formation of a complex between ULK1/2 and ATG13, ATG101 and FIP100 which promotes the nucleation of autophagic membranes (Ganley et al., 2009; Chan and Tooze, 2009) (**Figure 1.5**).

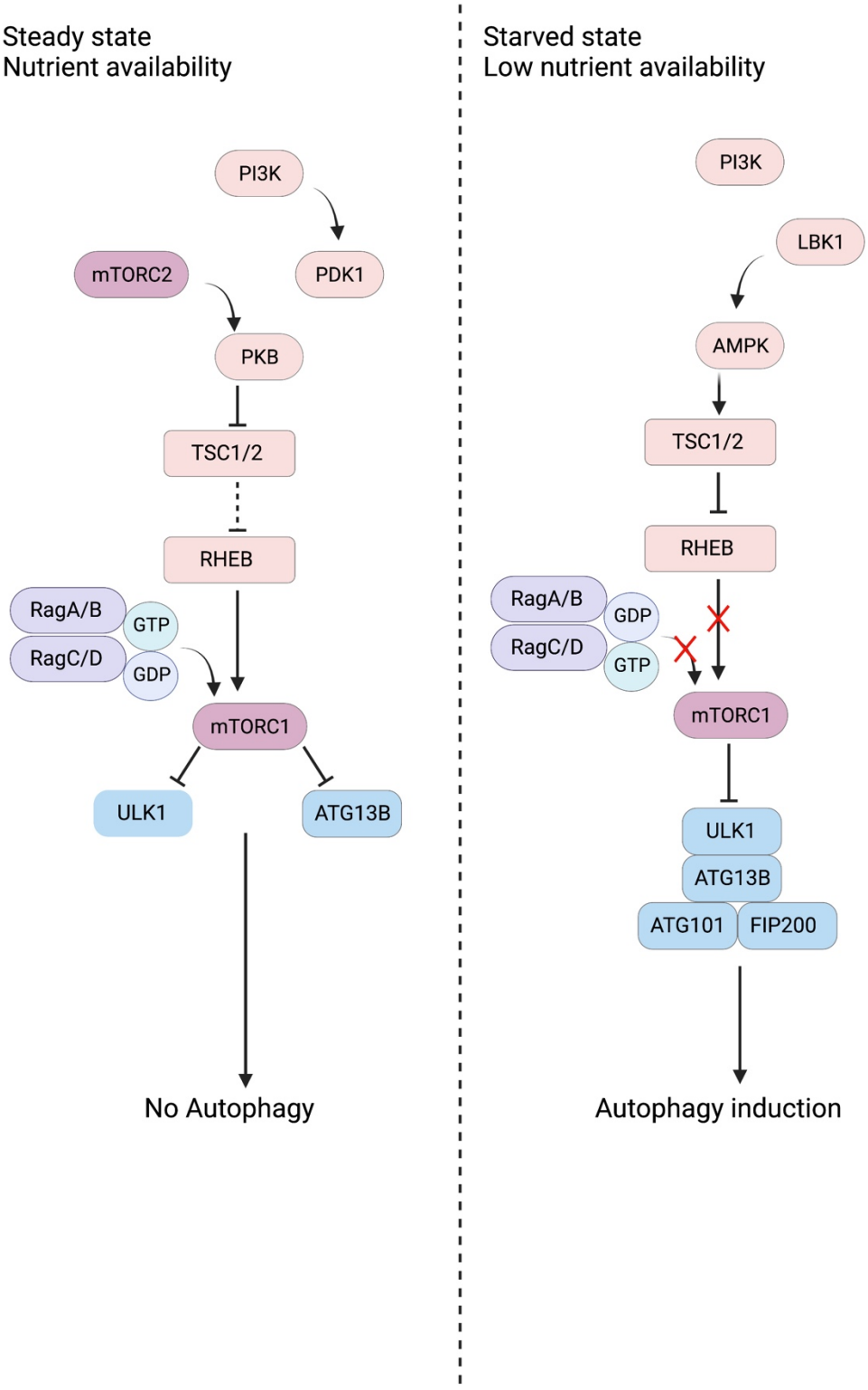

Figure 1.5 Nutrient availability regulates the activation of the mTORC1 pathway
At steady state mTORC1 is active and inhibits the activation of autophagy via Rag GTPases. In starved conditions, mTORC1 is no longer active and autophagy is induced. Created with BioRender.com.

1.2.13. TFEB

TFEB is a member of the Microphthalmia/TFE (MiT) family of transcription factors- a distinct set of bHLH-Zip transcriptions factors. The family also contains MITF (**section 1.3.15**) as well as TFEC and TFE3 (**Figure 1.6**). TFEB activates the transcription of lysosomal genes by binding to a recognition sequence in their promotor known as a Coordinated Lysosomal Expression and Recognition (CLEAR) element. TFEB binding to the promoter activates transcription and therefore upregulation of these lysosomal proteins to drive lysosomal biogenesis (Sardiello et al., 2009). TFEB is known to regulate the expression of a variety of lysosomal proteins including hydrolase enzymes for degradation, lysosomal membrane proteins, and components of the v-ATPase acidification pump. Overexpression of TFEB results in an increase in the number of lysosomes in cells (Palmieri et al., 2011; Sardiello et al., 2009). As well as being a regulator of lysosomal genes, TFEB has also been found to regulate genes which are key to related processes, such as autophagy and lysosome exocytosis (Palmieri et al., 2011; Napolitano and Ballabio, 2016).

1.2.14. Post-translational control of TFEB

Under steady state, nutrient rich conditions, TFEB is inactive and maintains a diffuse localisation throughout the cytoplasm. Translocation to the nucleus is prevented by phosphorylation of two serine residues, Ser142 and Ser211 (Martina et al., 2012; Roczniak-Ferguson et al., 2012; Settembre et al., 2012; Settembre and Ballabio, 2011). Phosphorylation of TFEB at Ser211 promotes its binding to 14-3-3 chaperone protein which sequesters TFEB in the cytosol- likely through masking its nuclear localisation signal (NLS) (Martina et al., 2012; Roczniak-Ferguson et al., 2012). There has been some debate about the kinases which phosphorylate TFEB, however, mTORC1 and extracellular-signal related kinase 2 (ERK2) have been reported to phosphorylate TFEB at the significant sites for its regulation (Martina et al., 2012; Roczniak-Ferguson et al., 2012; Settembre and Ballabio, 2011; Settembre et al., 2012).

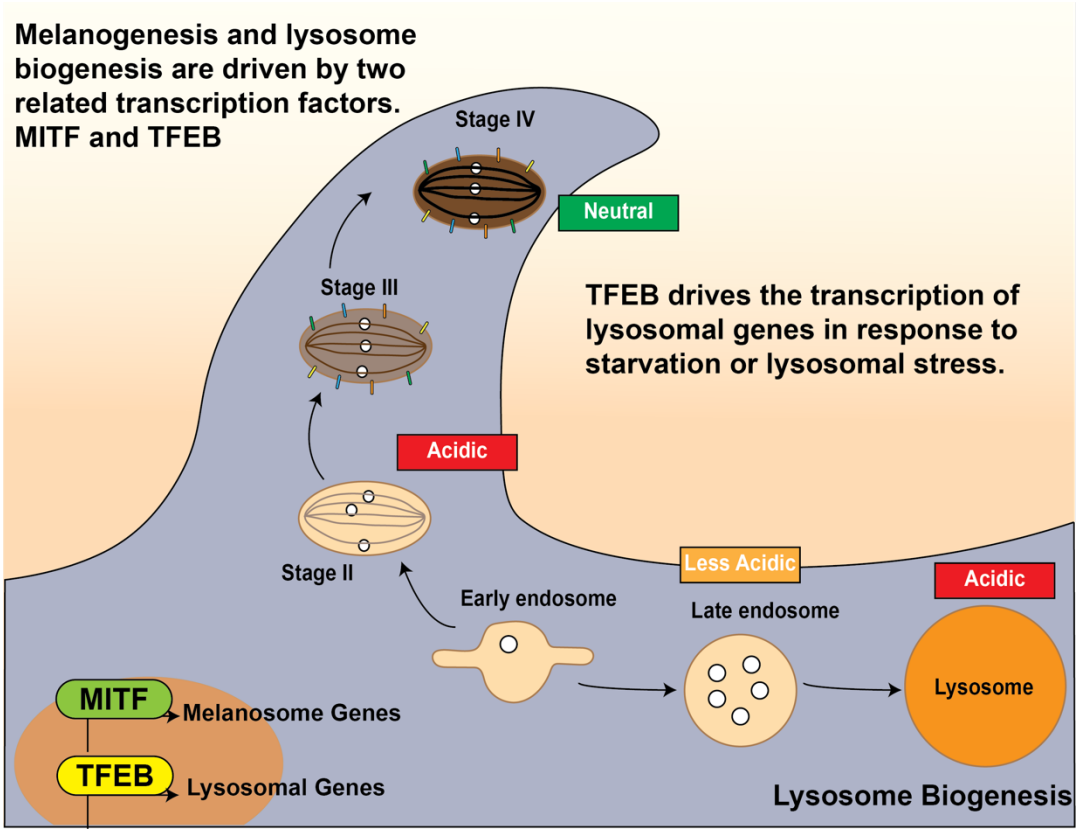

Figure 1.6 MITF and TFEB drive the biogenesis of two related organelles
MITF and TFEB are two transcription factors from the MiT transcription factor family. They drive the biogenesis of melanosomes and lysosomes respectively. Both organelles originate from the early endosome compartment. They are also both acidified via the action of the v-ATPase throughout their maturation, although melanosomes are neutralised at their later stages.

1.2.15. mTORC1 nutrient sensing and regulation of TFEB

At steady state, in nutrient rich conditions, TFEB is phosphorylated by mTORC1 and is retained in the cytosol (Martina et al., 2012; Roczniak-Ferguson et al., 2012; Settembre and Ballabio, 2011; Settembre et al., 2012). Under starvation conditions this modification must be reversed to allow TFEB to translocate to the nucleus (Palmieri et al., 2011; Sardiello et al., 2009). Regulation of TFEB by mTORC1 occurs at the lysosomal membrane (Jimenez‐Orgaz et al., 2018). The lysosomal v-ATPase is key for the maintenance of the low pH of the lysosome but also participates in nutrient

driven signalling. Where nutrients are rich, v-ATPase recruits the Rag-GTPase proteins to the cytoplasmic surface of the lysosome via interactions with the scaffolding complex Ragulator. Active Rag-GTPases recruit mTORC1 to the lysosomal surface where it can phosphorylate TFEB (Sancak et al., 2010; Settembre et al., 2012; Zoncu et al., 2011a).

Under conditions of cellular stress or starvation, v-ATPase no longer interacts with Ragulator and the Rag-GTPases are inactivated. This results in mTORC1 complex being released into the cytosol preventing further phosphorylation of TFEB (Zoncu et al., 2011a; Sancak et al., 2010). In addition to this, cell starvation also results in calcium efflux from the lysosome through Ca^{2+} channel mucolipin 1 (MCOLN1). This flux activates phosphatase calcineurin, which can dephosphorylate TFEB, allowing it to translocate to the nucleus and activate transcription of autophagy/lysosome genes (Medina et al., 2015) (**Figure 1.7**).

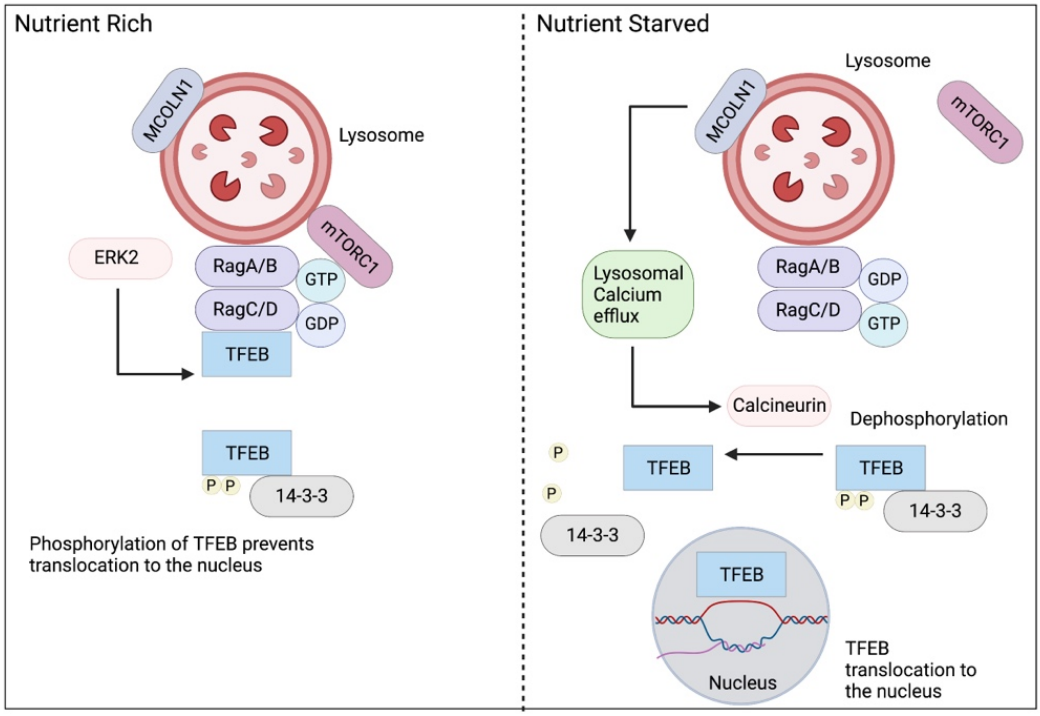

Figure 1.7 mTORC1 regulation of TFEB
TFEB is a transcription factor under the control of mTORC1. At steady state, TFEB is phosphorylated by mTORC1 and bound by the 14-3-3 chaperone protein. This sequesters TFEB in the cytoplasm and prevents transcription of its target genes. In nutrient starvation, TFEB is dephosphorylated by calcineurin which releases TFEB from the 14-3-3 chaperone and TFEB translocates to the nucleus. TFEB activates transcription of a number of lysosome and autophagy related genes by binding to CLEAR elements in their promoters. Created with BioRender.com.

1.3. Melanoma

According to Cancer Research UK, melanoma is the 5th most common type of cancer in the UK with 16,200 people being diagnosed per year in 2020 (www.cancerresearchuk.org). Melanoma is a form of skin cancer which results from the transformation of melanocytes- cells located between the dermis and the skin epidermis. The main environmental risk factor for melanoma is UV radiation from the sun or the use of sunbeds. Other factors which affect the risk of developing melanoma include hair colour, skin type, some genetic risk factors and the number of melanocytic nevi (BERAL et al., 1983). The rising number of melanoma cases could be attributed to the increase in awareness, surveillance and detection of cases, alongside the increased trend in sun tanning and the use of sunbeds. According to the American cancer society, the key to a good melanoma prognosis is early detection, with the most significant factor in outcome prediction being Breslow's tumour thickness. Later metastatic forms of melanoma are generally associated with a poor prognosis (www.cancer.org).

1.3.1. Melanocytes

Melanocytes are skin cells which are located at the base of the skin epidermis where it meets the dermis (**Figure 1.8**). They produce the pigment melanin which is packaged into pigment granules called melanosomes through a process termed melanogenesis. Melanosomes, once formed, are transferred to neighbouring cells where they form a nuclear protective cap which serves to protect nuclear DNA from UV damage. The number of melanocytes does not vary between skin types, but rather the amount of UV-protective melanin pigments produced, which accounts for the increased risk of melanoma in white fair-skinned populations.

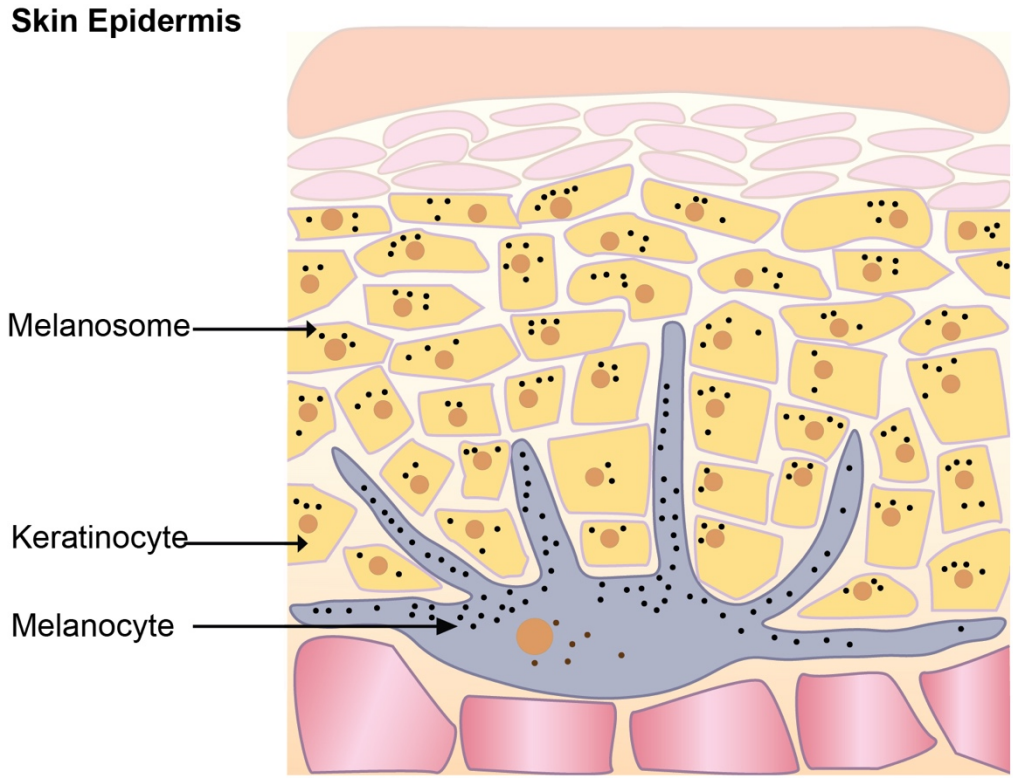

Figure 1.8 Localisation of Melanocytes
Melanocytes are pigment granule producing cells which lie in the base of the skin epidermis. They are in contact with around 40 keratinocytes. Once pigment granules (melanosomes) are formed they are transferred to the neighbouring keratinocytes where they form a nuclear protective cap.

1.3.2. Melanogenesis

Melanosomes are specialised lysosome related organelles. They derive from early endosomes and go through a 4-stage maturation process termed melanogenesis resulting in pigmented, mature melanosomes (Raposo and Marks, 2007). This process is termed melanogenesis (**Figure 1.10**). Melanosomes appear as round or ovoid organelles with a diameter of approximately 500 nm (Birbeck et al., 1956; Raposo and Marks, 2007; SEIJI et al., 1961). The 4-stage development can be defined by distinct markers at each stage (SEIJI et al., 1963). Stage I melanosomes are derived from early endosomes and resemble multi-vesicular bodies (MVBs) containing intra-luminal vesicles (Raposo et al., 2001). Stage II melanosomes contain a fibril network which distorts the shape of melanosomes to an ellipsoid. A melanosome is considered stage III following melanin synthesis which is

deposited onto the fibril network. Stage IV melanosomes are fully pigmented, mature melanosomes which are ready for transport onto neighbouring keratinocytes (SEIJI et al., 1963).

1.3.3. Stage I melanosomes

Stage I and II melanosomes are defined by a fibril network which is made up of pre-melanosomal protein (PMEL, also known as Pmel17). PMEL is an amyloid protein which is different to other pathogenic amyloids in that it serves a known biological function (Hurbain et al., 2008). Stage I melanosomes can be characterised by the presence of a clathrin coat as well as pools of PMEL protein localised to the limiting melanosome membrane and intra-luminal vesicles (Hurbain et al., 2008; Raposo and Marks, 2007). PMEL is trafficked to the early melanosomes following synthesis in the ER, after which it is further modified in the Golgi apparatus to target it to the plasma membrane (PM). PMEL is then internalised and transported to early-stage melanosomes. PMEL has two functional roles in early melanosomes. It forms the fibril network onto which melanin is deposited (Berson et al., 2001; McGlinchey et al., 2009), and it sequesters reactive oxidative species (ROS) generated during melanin synthesis (Watt et al., 2013). The latter function is essential in protecting melanocytes from toxic by-products of melanosome formation.

1.3.4. Stage II melanosomes

Once at the early melanosomes, PMEL undergoes a number of cleavage processing steps by proteases accompanied by sorting to intraluminal vesicles (ILVs) for nucleation of fibrils (Berson et al., 2003; Rochin et al., 2013; Berson et al., 2001; McGlinchey et al., 2009). Unlike canonical ESCRT machinery-dependent ILV sorting, PMEL sorting is mediated via apolipoprotein E (ApoE) and cluster of differentiation 63 (CD63) (van Niel et al., 2015, 2011). Nucleation and extension of PMEL fibrils into PMEL sheets that span across melanosomes results in the ellipsoidal shape of stage II melanosomes. These sheets are clearly visible by EM (**Figure 1.9A**).

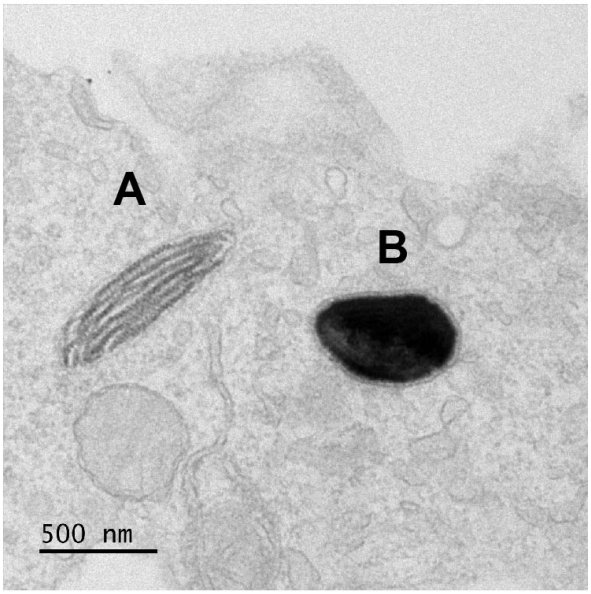

Figure 1.9 Early and late-stage melanosomes
Melan-a cells fixed and processed for EM were imaged using a TEM microscope. **A** early-stage melanosome. **B** late-stage melanosome.

1.3.5. Stage III melanosomes

Stage III melanosomes are characterised by the initiation of the synthesis of melanin which is subsequently deposited onto the established PMEL fibril network. This requires the delivery of melanin synthesising proteins such as tyrosinase, tyrosinase related protein 1 (TYRP1) and TYRP2 (Raper, 1927; Aroca et al., 1991; Del Marmol and Beermann, 1996). These enzymes are delivered specifically to maturing melanosomes following fibril formation (Sitaram and Marks, 2012).

1.3.6. Stage IV melanosomes

Once melanin synthesis is complete and a melanosome is fully pigmented, it is then transferred onto a neighbouring keratinocyte where it performs its role as a nuclear protective cap around the keratinocyte nucleus. An electron micrograph of a stage IV melanosome is shown in **Figure 1.9B**.

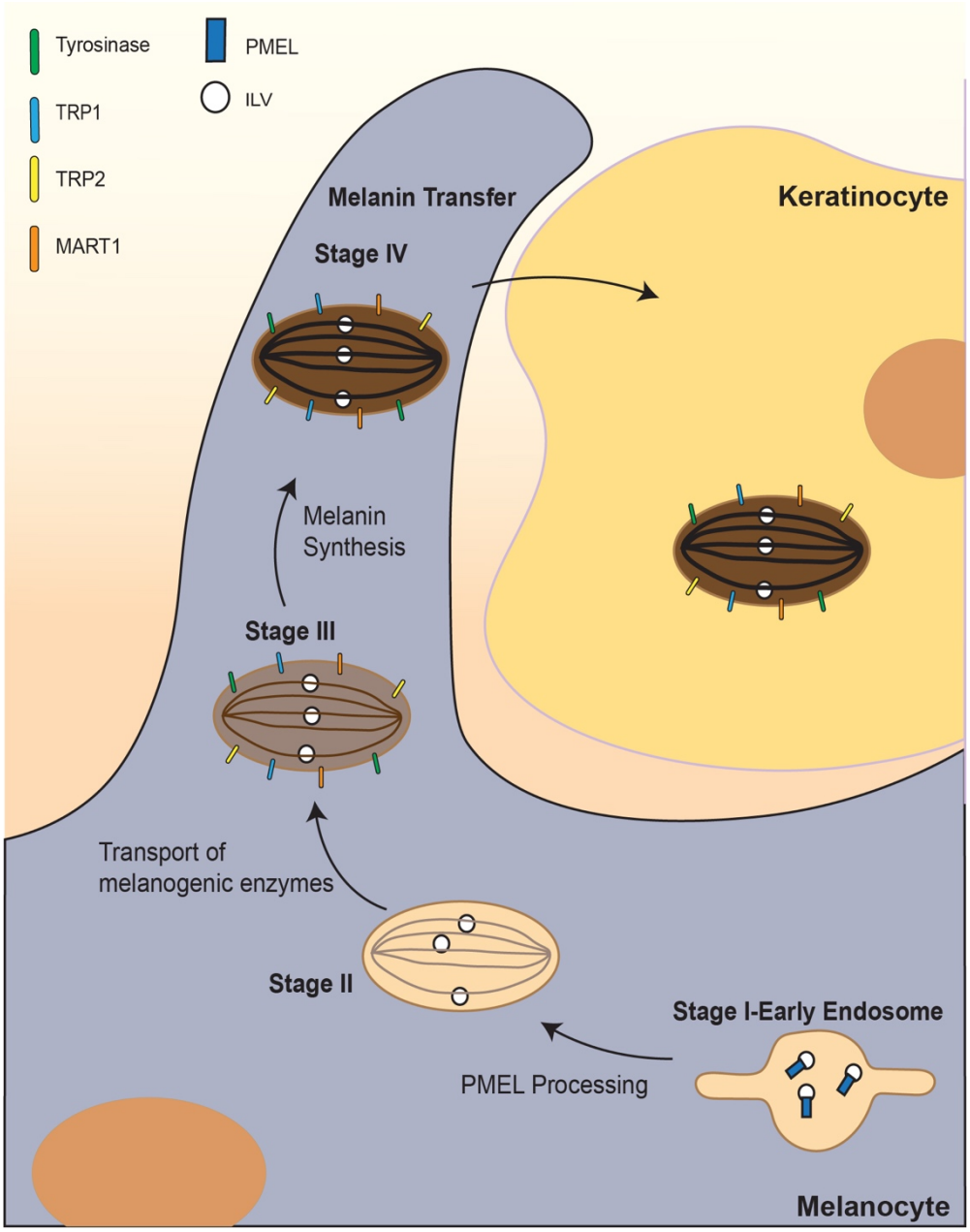

Figure 1.10 Biogenesis of melanosomes
Melanosomes are lysosome related organelles (LRO) which derive from early endosomes. In early-stage pre-melanosomes (stages I and II) PMEL is cleaved to form fibrils. Melanogenic enzymes such as tyrosinase, TYRP1, TYRP2 and MART-1 synthesise the pigment melanin, which is deposited onto the fully formed PMEL fibrils in stage III melanosomes. Stage IV melanosomes are fully pigmented mature melanosomes which are transported along melanocyte dendrites for transport to neighbouring keratinocytes. Adapted from (Raposo and Marks, 2007).

1.3.7. Melanin Synthesis

Melanin, derived from tyrosine, is a cocktail of pigments. In humans, two melanins are produced, eumelanin, which is a brown/black pigment, and pheomelanin, which is a yellow/red pigment. Both pigments share the common precursor dopaquinone, which is derived from the tyrosinase dependent oxidation of L-tyrosine. Dopaquinone is transformed into dopachrome which is oxidoreduced into dihydroxindole (DHI) and DHI carboxylic acid (DHICA) which can polymerise into eumelanin. For pheomelanin, there must be sufficient cysteine present at the conversion of dopaquinone. In this case, cysteinyldopa is generated which can be converted to pheomelanin (Hearing, 2011; Wakamatsu and Ito, 2002). Melanin functions as a protective shield for nuclei in keratinocytes in the skin and protects cells from UV damage via anti-oxidant properties and the scavenging of free radicals (Meredith and Sarna, 2006).

1.3.8. Tyrosinase related proteins

The maturation of melanosomes requires the action of enzymes called tyrosinase related proteins (TYRPs). There are three members: Tyrosinase TYRP1 and TYRP2 (also known as DCT). TYRPs are transmembrane Cu^{++}/Zn^{++} metalloenzymes which also contain 2 characteristic cysteine rich regions. All family members share over 80% homology (Kwon et al., 1987) and contain two copper binding sites essential for enzymatic activity (Wang and Hebert, 2006). The TYRPs are glycoproteins and thus are synthesised and modified via the ER and Golgi apparatus where they undergo glycosylation (Jackson et al., 1992; Liu et al., 2001b; Mikami et al., 2013). Delivery of TYRPs to maturing melanosomes must be timed after the formation of the PMEL fibrils in early melanosomes. The mechanism for this scheduled delivery is known to occur by at least 2 pathways (Raposo and Marks, 2007).

1.3.9. Tyrosinase

Tyrosinase was the first of the TYRPs to be identified. It is responsible for catalysing the rate limiting step of melanin synthesis. In the ER it is bound by chaperones which is essential for the correct folding and the binding of copper to tyrosinase (Branza-Nichita et al., 1999). Tyrosinase can form homo or heterodimers in the ER before being trafficked to the Golgi. From the ER, tyrosinase is trafficked to the Golgi in COPII coated vesicles. At the Golgi the glycosylation modifications on tyrosinase are further modified and some evidence suggests that the Golgi is the site of copper binding (Wang and Hebert, 2006; Setty et al., 2008). Tyrosinase is trafficked from the Golgi to melanosomes in an adaptor protein complex 3 (AP-3)-dependent mechanism. AP-3 can recognise Tyrosinase via a dileucine repeat within its cytoplasmic tail. AP-3 colocalises with tyrosinase at buds at the early endosome thought to be essential to sorting from endosomes to melanosomes (Theos et al., 2005; Höning et al., 1998; Raposo and Marks, 2007). A small pool of tyrosinase can colocalise with AP-1 at early endosomal buds, which are distinct from the AP-3 positive buds. This pool increases with AP-3 depletion indicating that this is a distinct trafficking pathway which may try to compensate for the loss of AP-3 trafficking (Theos et al., 2005). In AP-3 deficient melanocytes tyrosinase is mis-localised to the early endosome and to MVBs. Despite this defect, these cells are still able to produce some melanosomes indicating an AP-3-independent pathway for tyrosinase trafficking. Once at melanosomes tyrosinase catalyses the hydroxylation of tyrosine to dihydroxyphenylalanine (DOPA) and the subsequent oxidation of DOPA to DOPAquinone as well as DHI and DHICA into melanin precursors (Körner and Pawelek, 1982).

1.3.10. TYRP1

TYRP1 (also known as gp 75) is a transmembrane glycoprotein (Ghanem and Fabrice, 2011). Like tyrosinase it is trafficked to the Golgi from the ER before being sorted to melanosomes (Chen et al., 2001; Liu et al., 2001a; Jimbow et al., 1997). Of all the TYRPs, TYRP1's catalytic activity in the melanogenesis pathway is the most poorly understood, with in vitro studies suggesting

catalase and DHIA oxidase activity (Kobayashi 1994, 1994). TYRP1 serves a function in stabilising tyrosinase by forming heterodimers which appear to be crucial to the correct trafficking of these enzymes and therefore crucial to melanogenesis. TYRP1 is bound by AP-1 via its di-leucine sorting sequence and is mis-sorted in AP-1 deficient mice, but not in AP-3 deficient mice, indicating two distinct delivery mechanisms (Raposo and Marks, 2007; Theos et al., 2005). TYRP1 delivery to melanosomes has been found to be via recycling endosome tubular carriers. This process is thought to be dependent on biogenesis of lysosome-related organelle complex 1 (BLOC-1) (Dell'Angelica, 2004). AP-1 can bind kinesin motor KIF13A which helps promote the elongation of the endosomal tubule (Delevoye et al., 2009). AP-1 functions to organise melanosomal proteins into these tubules via their recognition motifs. Following the formation of these tubules, they are then brought into proximity with maturing melanosomes where they are then able to make contact and deliver melanogenic enzymes via fusion with the melanosome membrane (Delevoye et al., 2009).

1.3.11. BLOC Complexes

BLOC-1 is one of 3 BLOC complexes found to have a role in melanogenesis. BLOC-1 is the largest with 8 subunits and thought to operate in the formation of endosome carriers (Dell'Angelica, 2004). BLOC-1 is required for the delivery of copper transporter ATP7A, a cofactor for tyrosinase activity, to melanosomes (Setty et al., 2008, 2007). Loss of BLOC-1 does not affect tyrosinase localisation to melanosomes but results in a loss of tyrosinase activity. This is due to a mislocalisation of ATP7A and leads to a significant pigmentation defect. BLOC-1 colocalises to the tubule carriers for early melanosomes and functions to transport TYRP1 carriers so may function with AP-1 and KIF13A (Setty et al., 2008, 2007).

BLOC-2 is the second largest BLOC complex with 3 subunits and functions downstream of BLOC-1. BLOC-2 defects result in a phenotype where the above-mentioned endosomal tubules are fewer, shorter and establish briefer

contacts with melanosomes, resulting in less efficient delivery of melanogenic enzymes (Dennis et al., 2015). As a result, BLOC-2 deficient mice exhibit a pigmentation defect that is less severe than the defect seen with loss of BLOC-1 (Dell'Angelica, 2004). These results indicate that BLOC-2 promotes tethering of the tubule carriers to melanosomes to promote fusion.

BLOC-3 complex is composed of only 2 subunits and is the least well characterised of the BLOC complexes. In mice BLOC-3 deficiency leads to only a mild coat colour change but leads to an extreme skin hypopigmentation defect (Nguyen and Wei, 2007). BLOC-3 can act as a GEF for Rab32 and Rab38 (discussed below in **section 1.3.12**) and activates their activity (Gerondopoulos et al., 2012). The significance of this activity remains unknown. BLOC-3 has also been implicated in the recycling of components from melanosomes including the SNARE protein VAMP7 (Dennis et al., 2016). VAMP7 is exported from melanosomes via tubular structures which extend from the melanosome body. Rab38 and its effector VARP are also present at these recycling tubules. VAMP7 is the SNARE protein required for the fusion of BLOC-1 mediated endosomal carriers with melanosomes for the delivery of melanogenic enzymes (Dennis et al., 2016). The model proposed in this study suggests that VAMP7 is bound by VARP which locks it in an inactive state and prevents its function while it is recycled (Schäfer et al., 2012). They suggest that VAMP7 is recycled from melanosomes back to the endosome so it can carry out further rounds of fusion and delivery of melanogenic enzymes (Dennis et al., 2016).

1.3.12. Other melanogenesis proteins

Rab proteins Rab32 and Rab38 have specialised roles in cell types which generate lysosome related organelles (LROs) such as melanocytes. These Rab proteins have been found to mediate the selective delivery of tyrosinase and TYRP1 to melanosomes, although the mechanism of this delivery remains unclear (Wasmeier et al., 2006).

Rab6 has been linked to the trafficking of TYRP1 and melanoma antigen recognised by T cells (MART-1) to melanosomes. Vesicular carriers containing these proteins are derived from the TGN via the action of Rab6 which then transports and targets the delivery of these vesicles to melanosomes (Patwardhan et al., 2017). The SNARE protein VAMP-7 is thought to be essential for the fusion of carriers from endosomes with melanosomes for the delivery of TYRP1 (Dennis et al., 2016). In addition, SNARE protein STX13 and Rab protein Rab9 have been linked to the trafficking of melanogenesis enzymes via recycling endosome carriers (Mahanty et al., 2016; Jani et al., 2015). Rab7 has also been linked to melanogenesis. Gomez and colleagues showed that Rab7 could colocalise with TYRP1 positive vesicles and suggested a role for Rab7 in the transport of melanogenic enzymes (Gomez et al., 2001). Neefjes' group published evidence that Rab7 works in concert with Rab27a for melanosome transport (Jordens et al., 2006).

1.3.13. Transport of melanosomes

Following maturation of melanosomes, they then must be transported from their site of development to the cell periphery so they can be transported along the melanocyte projections ready for transport to neighbouring keratinocytes. First, melanosomes are transported the extended distance from the perinuclear area to the cell periphery by kinesins and microtubule networks (Hume and Seabra, 2011). Melanosomes are then docked at the actin cytoskeleton at the plasma membrane. This is mediated by Rab27a. Rab27a is recruited in its active form to mature melanosomes where it binds its effector melanophilin (Wu et al., 2001; Hume et al., 2001). Melanophilin can recruit and activate motor Myosin Va. This heterotrimeric complex can then stimulate the release of melanosomes from the microtubule network and the subsequent transport along the melanocyte projections (Wu et al., 2001, 2005; Hume and Seabra, 2011; Li et al., 2005). In the retinal pigment epithelium (RPE), melanosomes are transported to the apical region and have a similar system where Rab27a, myosin and Rab interacting protein (Myrip) and myosin VIIa

appear to mediate the docking of melanosomes in the apical processes (Lopes et al., 2007b).

1.3.14. Secretion of melanosomes

Once fully matured, melanosomes must be transported to neighbouring keratinocytes. This process is not well understood, and more than one model has been proposed. One proposes that melanosomes are secreted by exocytosis and are subsequently engulfed by keratinocytes. Another suggests that melanosomes are grouped into membrane bound vesicles which either fuse with the plasma membrane of keratinocytes, or are taken up by phagocytosis. Alternatively, it is possible that keratinocytes are able to take up part of the dendritic tip of melanocytes via phagocytosis. Or finally it has been proposed that melanosomes are transferred via a direct fusion of the plasma membrane of both cells creating a direct transfer from one cell to another (Van Den Bossche et al., 2006). More recent studies lean towards a model where melanosomes are in some way first secreted and the taken up by neighbouring keratinocytes. Rab11b has been implicated in this process, with recent work implicating the exocyst complex as an effector for Rab11 in the melanosome secretion process (Tarafder et al., 2014; Moreiras et al., 2020).

1.3.15. Microphthalmia transcription factor

Microphthalmia transcription factor (MITF) is one of four members of the MiT transcription factor family. MITF is a bHLH-leu-ZIP transcription factor which binds to lineage-specific targets in cells such as melanocytes and osteoclasts. It recognises E-Box and M-Box sequences in the promotor regions of genes and is the major transcription factor driving melanogenesis (Napolitano and Ballabio, 2016). Hence, MITF is an integral part of melanocyte development (**Figure 1.6**). As well as driving melanogenesis, MITF is able to drive other processes including cell proliferation, migration and senescence (Hartman and Czyz, 2015). Binding of MITF to the M-Box in the promoter regions of several melanogenesis related genes drives their transcription. This promotes melanosome formation, including the expression of melanin producing

enzymes Tyrosinase, TYRP1 and TYRP2 (Hah et al., 2012; Hemesath et al., 1994a; Sitaram and Marks, 2012). MITF is also responsible for the transcriptional control of Rab27a, the Rab protein responsible for transporting mature melanosomes along the projections of melanocyte cells so that they may be transferred to neighbouring keratinocytes (Chiaverini et al., 2008). MITF binds to DNA either as a homodimer or heterodimer with another member of the MiT transcription family members (Hemesath et al., 1994b). The regulation of MITF is controlled at multiple levels including transcriptional activation, repression, phosphorylation and SUMOylation (Hartman and Czyz, 2015).

1.3.16. MITF and Melanoma

Alterations in MITF expression and transcriptional activity have been linked to melanoma. As well as activating genes required for melanogenesis, it also has a number of pro-tumorigenic targets which have roles in cell death, DNA replication and proliferative pathway. Targets of MITF include CDKN2a (tumour suppressor) and BCL-2 (anti-apoptosis). Studies have shown that MITF is amplified in a subset of melanomas and is commonly upregulated in melanomas harbouring the BRAF (V600E) mutation. Additionally, data suggests that upregulation of MITF promotes cell survival and confers drug resistance to melanomas (Garraway et al., 2005).

Melanoma cells undergo what is known as “phenotypic switching”. This process is reminiscent of the well characterised epithelial-mesenchymal transition (EMT) which is observed in many cancers when gaining metastatic potential (Li et al., 2015). In melanoma there are additional lineage specific gene sets which are altered between the core tumour and invading metastatic cells. MITF is one of the identified markers of melanoma phenotypic switching (Li et al., 2015; Vandamme and Berx, 2014; Hartman and Czyz, 2015). Differential expression of MITF can confer different benefits to different stages of melanoma. Early-stage melanomas have higher MITF activity levels which promotes cell proliferation and cell survival. These characteristics are

advantageous to primary tumour formation and would work collaboratively with other common melanoma mutations in genes such as BRAF and N-RAS (Carreira et al., 2006). Later stages of melanoma have a tendency to down regulate MITF expression, which promotes cell invasiveness beneficial to later stage cancer progression (Carreira et al., 2006). Understanding the expression profiles across this phenotypic switching is of great interest as early-stage disease is very treatable and has a good prognosis. Later stages of disease where metastasis has occurred have a poor prognosis. Therefore prognosis can be better or worse, depending on the expression profile of certain genes, with many genes conferring therapy resistance (Li et al., 2015; Vandamme and Berx, 2014).

1.3.17. Rab7 and melanoma

Rab7 has also been found to have a differential expression pattern in different stages of melanoma. Alonso-Curbelo and colleagues showed that melanoma cells rewire the endolysosomal system to benefit melanoma progression (Alonso-Curbelo et al., 2014). Their study showed that depletion of Rab7 in melanoma cells reduced cell proliferation and colony formation suggesting that enhanced Rab7 expression and activity is beneficial for early-stage melanoma. In contrast they showed that depletion of Rab7 in melanoma cells increased cell invasion, and that cell lines which have high invasive potential in culture had lower basal Rab7 levels. Furthermore, they looked at Rab7 expression across cross sections of melanomas from various stages of disease. They found that melanoma cells had higher levels of expression compared to normal tissue, consistent with a role for Rab7 in melanoma initiation. They also found that Rab7 expression was not consistent across all stages, and that Rab7 expression was decreased at the transition stage where melanoma cells gain invasive potential (Alonso-Curbelo et al., 2014). This data supports Rab7 as a marker for phenotypic switching in melanoma cells, although this study indicated that this effect was independent of the pigmentation status and expression levels of MITF.

1.4. Parkinson's disease (PD)

Parkinson's disease is the second most common neurodegenerative disease after Alzheimer's disease (Tysnes and Storstein, 2017). The substantia nigra pars compacta (SNpc) is the initial site of neuronal loss in PD (**Figure 1.11**). The SNpc forms one of two regions of the substantia nigra in the midbrain- the other being the substantia nigra pars reticular (SNpr). The major function of the SNpc is to operate the motor control of the body; hence defects in motor control in PD patients (Armstrong and Okun, 2020; Fearnley and Lees, 1991; Dickson et al., 2009). Symptoms of PD include (but are not limited to) tremor at rest, bradykinesia (slowness of movement) and muscle stiffness. Post-mortem analysis of brain tissues show pathology arises from a neurodegeneration of the dopaminergic neurons in the SNpc (Fearnley and Lees, 1991; Dickson et al., 2009; Ma et al., 1997; Kordower et al., 2013). These neurons contain the pigment neuromelanin and thus post-mortem tissues show a characteristic loss of this pigmented region of the brain. The remaining neurons routinely contain protein inclusions called "Lewy bodies" (LB). These protein inclusions are protein aggregates which are enriched for the protein α-synuclein (Spillantini et al., 1997, 1998; Lees et al., 2009; Reeve et al., 2014).

Dopaminergic neurons produce the neurotransmitter dopamine (DA) which is released into the striatum to help maintain projections within other parts of the basal ganglia. DA is a catecholamine neurotransmitter which is responsible for motor control, motivation, reinforcement and reward (Barbeau, 1962). As PD results from a loss of the neurons which produce DA, it was hypothesised that by administering DA to PD patients, the progression of the disease could be slowed or stopped. Administering DA is unsuccessful in treating PD as it is unable to cross the blood brain barrier (BBB). DA precursor, levodopa (L-DOPA), is able to cross the BBB, and once entered into the central nervous system, can be converted to DA by the enzyme L-DOPA decarboxylase (Hornykiewicz, 2017; Dorszewska et al., 2014; Hornykiewicz, 2006). Thus, L-DOPA is used to increase the neurological DA levels in PD patients. Although treatment can be successful in reducing symptoms in patients, the efficiency

of this treatment decreases over time and produces substantial adverse side effects (Hornykiewicz, 2017; Dorszewska et al., 2014). Due to the nature of the disease and its progression, there are no conclusive tests to diagnose PD. Instead, a diagnosis is made based on symptom presentation. Additionally, there's currently no cure for PD, only treatments which can lessen the symptoms of patients. Hence there are a large number of clinical trials searching for preventative and more effective treatments (Armstrong and Okun, 2020). Although there is much interest in the field, clinical trials provide a significant challenge as they are both costly and difficult to manage. The lack of a conclusive tests for PD makes it difficult to track the progression of the disease.

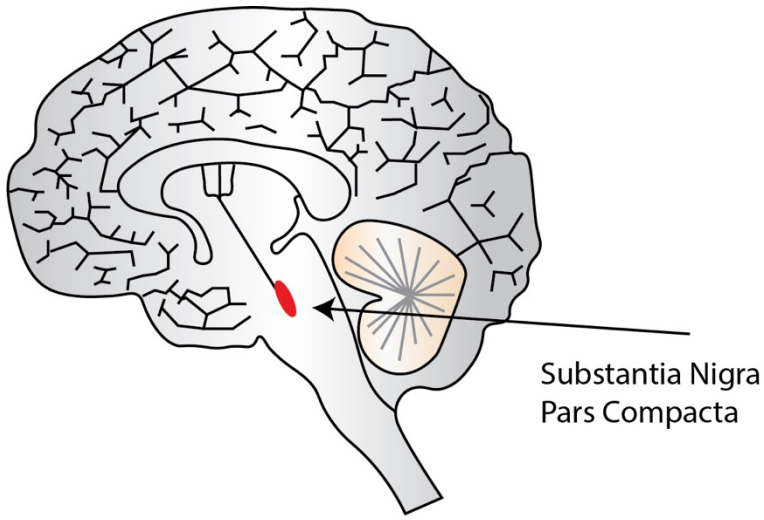

Figure 1.11 Substantia Nigra Pars Compacta (SNpc)
The substantia nigra is a region of the midbrain which is split in to two regions. The substantia nigra pars reticular (SNpr) and the substantia nigra pars compacta (SNpc). The SNpc is the region of the brain associated with the initial loss of neurons in PD.

1.4.1. Aetiology of PD

The majority of PD cases are idiopathic, with only around 10-15% of cases having a familial link (Armstrong and Okun, 2020). There are a number of known genes which have been linked to PD with varied risk factors and

penetrance associated with them (Blauwendraat et al., 2020). These genes appear to broadly fall into two categories- mitophagy dysfunction and endolysosomal trafficking defects- two pathways we know have substantial crosstalk (Armstrong and Okun, 2020). Although only a small percentage of PD cases have a known genetic cause, studying these cases helps to understand the overall disease pathology and may shine some light on the aetiology of "sporadic" cases. One of the greatest challenges in the field of PD research is to connect the associated genes into molecular pathways to further our understanding of disease pathology.

1.4.2. Familial PD genes

Thus far, 18 chromosomal loci have been linked to PD, all termed *PARK* loci. Within each locus are multiple genes, and in some cases, the causative gene within an identified locus has not been determined. There are, however, genes which are unequivocally linked to heritable, monogenic Parkinson's disease (**Table 1.1**). Mutations in SNCA, which encodes alpha synuclein and lies within the PARK1 locus, and mutations in the kinase LRRK2 gene, which lies in the PARK8 locus, result in an autosomal-dominant (AD) form of PD (Zimprich et al., 2004; Paisán-Ruíz et al., 2004; Bardien et al., 2011; Funayama et al., 2005). Mutations in the retromer component VPS35 (PARK17) have also been linked to AD forms of PD (Williams et al., 2017; Vilariño-Güell et al., 2011; Zimprich et al., 2011). There are also mutations in Parkin, PINK1, DJ-1, PLA2G6, FBXO7, SYNJ1 and ATP13A2 which all result in an autosomal recessive (AR) form of PD (Blauwendraat et al., 2020). In addition to these identified chromosomal loci, other genetic risk factors have been identified. For example, alternative splice variants of Rab29 (also known as Rab7L1) in the PARK16 locus have been linked to an increased risk of PD (MacLeod et al., 2013). PD has been linked to the lysosomal storage disease, Gaucher's disease (GD) (Riboldi and Di Fonzo, 2019). People with Gaucher's disease are more likely to develop PD compared to the general population. In both conditions, mutations in the GBA gene have been linked to pathology. GBA encodes the lysosomal enzyme glucocerebrosidase (GCase) (Riboldi and Di

Fonzo, 2019). The links between these two diseases highlight the role of the endolysosomal system in PD pathology.

Table 1.1 Genes associated with PD pathology

Gene	Protein	Inheritance
SNCA (PARK1/PARK4)	α-synuclein	AD
LRRK2 (PARK8)	Leucine rich repeat kinase 2 (LRRK2)	AD
VPS35 (PARK17)	Vacuolar protein sorting-associate protein 35	AD
Parkin (PARK2)	Parkin	AR
PINK1 (PARK6)	PTEN induced kinase-1	AR
DJ-1	DJ-1	AR
SYNJ1	Synaptojanin-1 (SYNJ1)	AR
FBXO7	F-Box only protein 7 (FBXO7)	AR
ATP13A2	Probable cation-transporting ATPase 13A2	AR
PLA2G6	85/88 kDa calcium-independent phospholipase A2	AR
DNAJC6	DnaJ Heat shock protein family (HSP40) member C6	AR

1.4.3. Parkinson's disease and Melanoma

Patients who are diagnosed with PD are less likely to get all types of cancer, except for melanoma, which they are more than twice as likely to get compared to the general population (Huang et al., 2015). Although this data was published in 2015, no subsequent work has shone light on how these diseases are linked, or why melanoma does not follow the same trend as other types of cancer. It is also not known whether there are specific PD related mutations which confer vulnerability to melanoma, or whether these cases fall into the sporadic pool of patients. One obvious factor which links both diseases is the affected cell type. Melanoma is cancer of the pigment producing melanocyte cells (**Section 1.3.1**) and the initial site affected by PD is the pigmented SNpc (Fearnley and Lees, 1991).

1.4.4. Endolysosomal system in Parkinson's disease

Many of the genes outlined in **Table 1.1** have been linked to the endolysosomal system. Additionally, high-throughput sequencing and GWAS studies have identified numerous risk factors for sporadic PD- many of which are functional in the endolysosomal system. Neurons, and in particular dopaminergic neurons, put a high burden on the endolysosomal system. Synaptic vesicles (SVs) are produced in the soma of the cell and transported down axons to the pre-synapse for release. However, newly synthesised SVs are not sufficient to maintain active firing synapses. Therefore, clathrin mediated endocytosis of neurotransmitters from the synaptic junction reforms SVs for re-release into the synapse (Saheki and De Camilli, 2012). Additionally, the rapid firing of synapses in neurons may result in a back log of damaged and exhausted organelles which need to be disposed of. For this, autophagosomal selection and retrograde transport to the lysosomal compartment is required (Yang et al., 2013; Maday et al., 2014). To facilitate this, extended microtubule networks span the axonal distance for transport of vesicles and cargos back and forth from the soma to the pre-synapse (Maday et al., 2014). This higher strain on the endolysosomal system along with their higher dependence on cell/protein homeostasis, makes neurons more susceptible and sensitive to defects in endosomal and lysosomal function. In addition, neurons are post-mitotic and long-lived cells adding another layer of vulnerability.

DNAJC6 also known as auxilin is a PD related gene linked to AR forms of PD. It is a member of the heat shock protein family (Hsp40) (Gorenberg and Chandra, 2017). It acts in the pre-synaptic terminus and is involved in the uncoating of clathrin vesicles following endocytosis. Auxillin recruits the ATPase Hsc70 to the pre-synaptic terminus where it executes its function in catalysing the dissolution of the clathrin coat for recycling of its contents (Gorenberg and Chandra, 2017). In addition, evidence shows that loss of function of auxilin attenuates the effect of a-synuclein overexpression (Song et al., 2017) and auxilin knockout (KO) mice have an increase in the number

of CCVs and empty clathrin cages (Yim et al., 2010). LRRK2 has been found to phosphorylate auxilin, leading to accumulation of oxidised dopamine and α-synuclein. These studies highlight the cross talk between PD related genes (Nguyen and Krainc, 2018).

SYNJ1 is a phosphatase domain containing protein with two phosphatases- a 5-phosphatase and a Sac1 domain (McPherson et al., 1996). The 5-phosphatase works in conjunction with Hsc70 and auxilin in the dissolution of the clathrin coat from endocytosed vesicles from the synaptic junction (Cremona et al., 1999). The Sac1 domain has also been linked to clathrin uncoating, however, this function is less robustly established (Cao et al., 2017). Mutations occur within the Sac1 domain, which are found to cause AR PD (Krebs et al., 2013). Studies have found evidence for Sac1 mutations causing endocytic trafficking defects at the synapse including accumulation of CCVs (Cao et al., 2017; Quadri et al., 2013). There is also evidence that defects in SYNJ1 cause defective autophagy in the synaptic terminal (Vanhauwaert et al., 2017). SYNJ1 can interact with Endophilin A. Endophilin A functions in clathrin independent endocytosis in the synaptic terminal, and promotes membrane bending for vesicle formation (Watanabe et al., 2018; Westphal and Chandra, 2013). Endophilin A recruits SYNJ1 to the pre-synaptic terminus for its function in vesicle recycling. LRRK2 can phosphorylate Endophilin A which impairs its function and results in defects in the endocytic pathway and regulation of autophagy (Soukup et al., 2016; Matta et al., 2012).

α-synuclein is a protein found in the pre-synaptic terminals of neurons as well as many non-neuronal cell types (Kramer and Schulz-Schaeffer, 2007). It is highly expressed in the brain and is found to be enriched in the Lewy body inclusions which are found in the surviving neurons of patient brains post-mortem (Dickson et al., 2009; Fearnley and Lees, 1991). There is a consensus that α-synuclein accumulation is particularly critical to the pathology of PD. As well as pathogenic point mutations in α-synuclein, which are linked to increased aggregation, genomic duplicates and triplicates of the gene have also been linked to disease pathology (Cuervo et al., 2004; Chartier-Harlin et

al., 2004). α-synuclein functions in the transmission of neurotransmitters and the organisation of SVs. Over-expression of α-synuclein has been found to inhibit the release of synaptic vesicles, whereas aggregated α-synuclein impairs synaptic endocytosis (Vargas et al., 2014; Greten-Harrison et al., 2010). Furthermore, there is evidence that α-synuclein aggregates impact SV recycling by impairing the removal of the clathrin coat and impairing Hsc70 activity leading to an accumulation of CCVs (Banks et al., 2020).

1.4.5. Mitochondria Quality control and Mitophagy in PD

Like the endolysosomal system, many of the genes which have been related to PD have been linked to mitophagy. Mitophagy is the selective form of autophagy which deals with the degradation of worn or damaged mitochondria. This is of particular importance in cell homeostasis, as mitochondria produce a variety of molecules (for example, ROS) which could be damaging if released into the cell. Therefore, mitochondria and their contents must be effectively disposed of to prevent toxicity to cells. It is thought that in neurodegenerative diseases, defects in mitophagy result in the inefficient clearance of damaged mitochondria, which leads to accumulation of toxic components in the cell which in turn would lead to neuronal death (Vidyadhara et al., 2019). In particular, there has been much research conducted into the PINK1/Parkin pathway of mitophagy, as these two genes have been robustly linked to AR forms of PD (Bodnar et al., 1998; Vidyadhara et al., 2019). Studies in drosophila found the first mechanistic link between two PD related genes which converged on the mitophagy pathway (Park et al., 2006; Clark et al., 2006). PINK1 acts as a sensor for damaged mitochondria. Under normal conditions, PINK1 enters into the TOMM/TIMM complex on mitochondria and is cleaved by PARL protease (Yamano and Youle, 2013; Jin et al., 2010). PINK1 is extracted and degraded by the proteasome degradation system. In response to mitochondrial depolarisation or damage, PINK1 can no longer enter into the TIMM complex to be cleaved and accumulates on the outer mitochondrial membrane (Narendra et al., 2010; Matsuda et al., 2010). PINK1 then recruits the E3 ubiquitin ligase Parkin to the outer mitochondrial

membrane. PINK1 can phosphorylate Parkin, leading to its activation (Kane et al., 2014; Koyano et al., 2014). Parkin then adds ubiquitin to a number of outer mitochondrial membrane proteins. PINK1 can also phosphorylate ubiquitin on the outer mitochondrial membrane proteins. This generates a feedback loop as Parkin binds phospho-ubiquitin. The ubiquitylated substrates recruit the autophagy machinery to the damaged mitochondria and they are selectively engulfed for degradation. These mitophagosomes are then targeted to the lysosome where they fuse to form autolysosomes, and the damaged mitochondria are degraded. Mutations in PINK1 and Parkin are linked to defects in this pathway leading to ineffective disposal of damaged mitochondria.

1.4.6. Rab7 and mitochondrial dynamics

Rab7 has many well characterised roles in the later stages of the endolysosomal pathway, as well as a role in the melanogenesis pathway (**Section 1.2.8** and **Section 1.3.12**). More recent years have found a growing body of evidence that Rab7 has a key role in mitophagy. Wong at al., showed that Rab7 GTP binding is required for the formation of lysosome-mitochondrial contact sites. They also showed that Rab7 GTP-hydrolysis mediated by TBC1D15, a mitochondrial Rab7 GAP protein, led to the untethering of these contact sites. Finally, this study suggested that these contact sites are important for mitochondrial fission events, and therefore mitochondrial dynamics (Wong et al., 2018). Richard Youle's lab implicated Rab7 in mitophagy, promoting autophagosome formation and morphology via interactions with Fis1 and TBC1D15 (Yamano et al., 2014). They later showed Rab7 to be important for Parkin mediated mitophagy (**Section 1.4.5**). Using immunoelectron microscopy they were able to show that Rab7 can directly interact with the OMM in response to mitophagy induction. Loss of Rab7 by siRNA knockdown resulted in a failure to clear mitochondria and defects in autophagic flux. They also show Rab7 is recruited to damaged mitochondria by the GEF Mon1/CCZ1, downstream of Rab5 and the Rab5 GEF RABGEF1 in a pathway which required Parkin (Yamano et al., 2018). Rab7 is of

increasing interest to the field of PD research as it has been linked to two related familial PD genes, LRRK2 and VPS35 (Jimenez-Orgaz et al., 2018; Gómez-Suaga et al., 2014). This work links Rab7 to yet another familial PD gene.

1.4.7. LRRK2

Leucine-rich repeat kinase 2 (LRRK2) is the most commonly mutated gene in familial PD (Zimprich et al., 2004; Paisán-Ruíz et al., 2004; Bardien et al., 2011; Funayama et al., 2005). At 286 kDa in size, it is a large protein and is unusual in that it contains 2 adjacent catalytic domains- a serine/threonine kinase domain; and a Ras of Complex (ROC)- C-terminal of ROC (COR)-GTPase domain, as well as a number of protein interaction domains. There are a number of pathogenic mutations confirmed within LRRK2, the majority of which lie in the catalytic domains and result in hyperactive kinase activity (Khan et al., 2005; Hur et al., 2019; Cookson, 2010; West et al., 2005). Although the molecular mechanisms of how these mutations manifest into PD remain unclear, the hyperactive kinase activity has made LRRK2 appear an attractive pharmacological target for the treatment and prevention of PD (Yao et al., 2013). In addition, variants in the LRRK2 gene were determined to be risk factors for idiopathic PD (Satake et al., 2009; Rudenko and Cookson, 2014; Simón-Sánchez et al., 2009; Nalls et al., 2014).

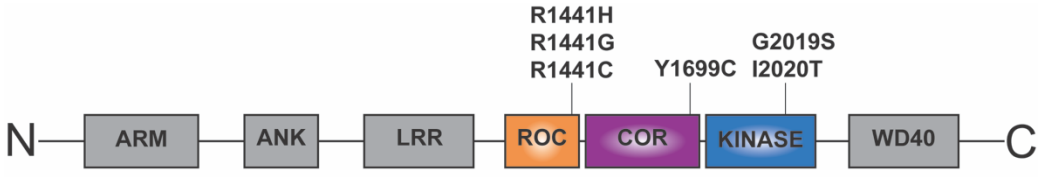

Figure 1.12 LRRK2 protein domains and pathogenic mutations
LRRK2 is a 286 kDa protein containing two catalytic domains: a serine/threonine kinase domain and a ROC-COR GTPase domain. LRRK2 also contains a number of protein interaction domains including an Armadillo repeat domain (ARM), an Ankyrin repeat domain and a WD40 repeat domain. The identified familial PD mutations in LRRK2 largely map to the catalytic domains and result in a hyperactive kinase.

1.4.8. Pathogenic mutations in LRRK2

Multiple heritable pathogenic mutations have been identified within LRRK2 (**Table 1.2**, **Figure 1.12**). The most common is the [G2019S] mutation which lies within the kinase domain and results in a hyperactive kinase 2-fold more active than the wild type (WT) (Jaleel et al., 2007; Khan et al., 2005; West et al., 2005). There are also a number of mutations in the ROC-COR GTPase domain, such as [R1441C/G/H] and [Y1699C], which also result in a hyperactive kinase which is over 3-fold more active than the WT (Khan et al., 2005; Hur et al., 2019; Cookson, 2010; West et al., 2005). This is, however, only the case *in vivo* and is dependent on the increased ability of these mutant proteins to bind GTP and be hyperactivated by an upstream regulator (Steger et al., 2016, 2017; Purlyte et al., 2018; Sheng et al., 2012).

Table 1.2 Pathogenic mutations identified in the LRRK2 gene

Mutation	Domain	Population	Ref
G2019S	Kinase	North American/ European families	(Di Fonzo et al., 2005)
R1441C	ROC-COR	Western Nebraska family D	(Zimprich et al., 2004)
R1441G	ROC-COR	Basque family	(Paisán-Ruíz et al., 2004)
R1441H	ROC-COR	European/ Taiwanese families	(Mata et al., 2005)
Y1669C	ROC-COR	German-Canadian family A	(Zimprich et al., 2004)
I2020T	Kinase	Funayama Japanese family	(Funayama et al., 2005)
N1437H	ROC-COR	Norwegian family F04	(Aasly et al., 2010)

1.4.9. LRRK2 and Rab proteins

Although LRRK2 is thought to be an attractive therapeutic target, the clinically significant substrate(s) of LRRK2 remain unknown. Many potential substrates have been identified via various methodologies, however, there is no consensus in the field which, if any, are the most important in the context of PD. One significant breakthrough came with an unbiased and comprehensive proteomic study which yielded the discovery that LRRK2 can phosphorylate a distinct subset of Rab proteins. Phosphorylation occurs at a conserved serine or threonine residue in their switch II domain (Steger et al., 2016, 2017). This was a great development as LRRK2 had already been linked to a number of

membrane trafficking defects and PD is largely thought of as a disease of membrane traffic (Hasegawa et al., 2017; Bandres-Ciga et al., 2019; Hunn et al., 2015; Clague and Rochin, 2016). Other phosphoproteomic work showed that PINK1 is also able to phosphorylate a separate subset of Rab proteins (Lai et al., 2015a). Additionally, a number of Rab proteins have also been linked to PD, solidifying that membrane traffic, and the role Rab proteins play in its regulation, are somehow key in understanding pathogenesis (Shi et al., 2017; Gao et al., 2018; Gitler et al., 2008; Lai et al., 2015b; Cooper et al., 2006; Mata et al., 2015; Wilson et al., 2014).

16 Rab proteins have been proposed as LRRK2 substrates (Rab1A/B, Rab3A/B/C/D, Rab5A/B/C, Rab8A/B, Rab10, Rab12, Rab29, Rab35 and Rab43) (Steger et al., 2017; Jeong et al., 2018) (**Table 1.3**). In addition to potentially being significant in understanding PD pathology, the phosphorylation of Rab proteins also provides a useful readout for LRRK2 activity. Phos-tag gels produce a mobility shift between the non-phosphorylated and phosphorylated forms of proteins (Ito et al., 2016). This allows for changes in the phosphorylation state of Rabs to be analysed by western blotting. A phospho-specific antibody against the LRRK2 phosphorylation site of Rab10 has been developed as another tool to measure LRRK2 activation and kinase activity (Lis et al., 2018; Mir et al., 2018). Rab29 is unusual in that is has a serine residue at the conserved LRRK2 phosphorylation site with an adjacent threonine residue (Thr71 and Ser72) (Steger et al., 2017). Although it can do both, data suggests that LRRK2 phosphorylates the neighbouring threonine rather than the serine residue, in line with a preference for threonine (Liu et al., 2018). LRRK2 pathogenic mutations which result in hyperactive kinase activity are found to increase the phosphorylation of substrate Rab proteins (Liu et al., 2018; Ito et al., 2016; Steger et al., 2017, 2016; West et al., 2005).

Initial data suggested that LRRK2 phosphorylation of Rab proteins affects their ability to bind effector proteins. In particular, phosphorylation in the switch II domain decreased the ability of Rab proteins to interact with the GDI

chaperone proteins, which remove inactive Rab proteins from their acceptor membrane (**Figure 1.2B**). This was predicted to put a hold on the Rab cycle leaving an increased pool of inactive Rab proteins docked at the membrane (Steger et al., 2016, 2017). The general view in the field now is that the effects of LRRK2 phosphorylation are more complex than this initial model and are likely Rab protein specific.

As well as being substrates of LRRK2, specific Rab proteins have been found to recruit LRRK2 to membranes. The Rab32 subfamily consist of three Rab proteins with high homology. Rab32 and Rab38 are highly similar and act redundantly in many cell types. LRRK2 substrate, Rab29, is also a member of this family. All three family members have been shown to interact with LRRK2, which is proposed to be via LRRK2's ARM domain (Waschbüsch et al., 2014; McGrath et al., 2021). However, some work has proposed that Rab29 interacts with LRRK2's ANK domain (Purlyte et al., 2018). Rab29 has been shown to recruit LRRK2 to the Golgi membrane, whereas Rab32 has been shown to recruit LRRK2 to various endo-lysosomal membranes (Beilina et al., 2020; Purlyte et al., 2018; Liu et al., 2018; Waschbüsch et al., 2014).

Table 1.3 Rab proteins and their LRRK2 phosphorylation site

Rab protein	Phosphorylation site	Localisation	Reference
Rab1A	T75	ER and Golgi	(Jeong et al., 2018)
Rab1B		ER and Golgi	(Jeong et al., 2018)
Rab3A	T86	Secretory vesicles	(Steger et al., 2017)
Rab3B	T86	Secretory vesicles	(Steger et al., 2017)
Rab3C	T94	Secretory vesicles	(Steger et al., 2017; Jeong et al., 2018)
Rab3D	T86	Secretory vesicles	(Steger et al., 2017)
Rab5A	S84	Early Endosome	(Jeong et al., 2018; Steger et al., 2016)
Rab5B	S84	Early Endosome	(Steger et al., 2016)
Rab5C	S85	Early Endosome	(Steger et al., 2016)

Rab8A	T72	Lysosomes, Primary cilia, Golgi	(Steger et al., 2017; Jeong et al., 2018)
Rab8B	T72	Lysosomes, Primary cilia, Golgi	(Steger et al., 2017; Jeong et al., 2018)
Rab10	T73	Lysosomes, mitochondria	(Steger et al., 2017; Jeong et al., 2018)
Rab12	S106	Recycling endosome	(Steger et al., 2017)
Rab29	S72 and T71	Golgi	(Steger et al., 2017)
Rab35	T72	Plasma membrane, recycling endosome	(Steger et al., 2017; Jeong et al., 2018)
Rab43	T82	Golgi apparatus	(Steger et al., 2017)

1.4.10. LRRK2 and the endolysosomal system

LRRK2 activity and its mutations have been found to cause disruption to the endolysosomal system across various models. Fibroblasts from [G2019S] LRRK2 carriers show an enlarged lysosome phenotype with increased clustering to the perinuclear area (Henry et al., 2015; Hockey et al., 2015; Ho et al., 2020; MacLeod et al., 2013). This phenotype is also observed in mouse neurons in aged subjects with the [R1441G] mutation, accompanied by a reduction in lysosomal degradative capacity (Ho et al., 2020). [G2019S] expressing neurons have also been linked to mis-trafficking of the CIMPR (MacLeod et al., 2013). LRRK2 may also impact retrograde traffic through Rab32 and Rab38. As mentioned above, Rab32/38 are LRRK2 interactors. They can also interact with the retromer complex via SNX protein SNX6. Defects in Rab32 have been linked to ineffective retrograde traffic measured by CIMPR distribution (Waschbüsch et al., 2019, 2014). It is not clear if these defects are related to the interaction between LRRK2 and Rab32. Additionally, LRRK2 activity changes have also been linked to lysosome dysfunction via glucocerebrosidase (GCase) activity (Nguyen and Krainc, 2018; Ysselstein et al., 2019). Collectively these studies implicate LRRK2 as a key regulator of the endolysosomal system with a proposed role in trafficking of the lysosomal machinery.

LRRK2 is highly expressed in the kidneys and this region shows the most severe phenotypes. Alterations in lysosomal morphology, size, distribution and activity have been linked to LRRK2 depletion and mutation in mouse kidneys (Hinkle et al., 2012; Tong et al., 2012, 2010a; Baptista et al., 2013; Kuwahara et al., 2016). LRRK2 knockout mice also exhibit defects in autophagy in their kidneys, however, there is some dispute over where in the autophagic pathway the defects lies (Hinkle et al., 2012; Tong et al., 2010a). Some studies suggest that LRRK2 affects autophagic initiation and maturation, whereas others suggest that there is a defect in autophagic flux. It could be that there are issues with autophagic initiation which are exacerbated by defects in lysosomal function. In LRRK2 and LRRK1 double knockout mice brains, there are defects in autophagy accompanied with age dependent dopaminergic neuronal degeneration. In this study, kidney defects were initiated with LRRK2 single knockout. However, knockout of LRRK1 was also required for the neuronal defects (Giaime et al., 2017). This may indicate that the low levels of LRRK2 in the brain can be compensated for by LRRK1 but this is not sufficient for the high endogenous levels in the kidney.

LRRK2 has been shown to phosphorylate Rab5 (Steger et al., 2016). Expression of hyperactive LRRK2 mutants was shown to delay the recruitment of Rab5 to the early endosome and cause subsequent delays in the Rab5 to Rab7 endocytic switch (see **Section 1.1.6**) (Gómez-Suaga et al., 2014). LRRK2 has also been linked to vesicle sorting from lysosomes. Lysosome permeabilization by lysomotrophic reagent L-leucyl-L-leucine methyl ester (LLOME) recruited LRRK2 to lysosomes in a system independent of lysophagy. LRRK2 was localised to tubules emerging from disrupted lysosomes which were also positive for JIP4. The model proposed suggests that LRRK2 phosphorylates Rab35 and Rab10 which are then retained at the lysosomal membrane. This phosphorylation event is required for recruitment of JIP4 which is responsible for the formation of tubular structures which are able to interact with other functional lysosomes (Bonet-Ponce et al., 2020).

1.4.11. LRRK2 and mitophagy

In addition to a role in the endolysosomal system, there has been much evidence supporting a role for LRRK2 in the parallel pathway of mitophagy. LRRK2 kinase activity was able to disrupt the PINK1/Parkin induction of mitophagy by blocking interaction of Parkin with dynamin-like protein 1 (DLP1) (see **Section 1.4.5**). This defect could be rescued by expression of a kinase dead form of LRRK2 or by chemical inhibition of LRRK2 kinase activity (Bonello et al., 2019). LRRK2 substrate Rab10 was shown to accumulate on the mitochondrial membrane and recruit optineurin (OPTN) for the induction of mitophagy. Hyperactivating mutations in LRRK2 were found to result in decreased interaction of Rab10 with OPTN and therefore a reduction in the initiation of mitophagy (Wauters et al., 2020).

As well as the PINK1/Parkin pathway, [G2019S] LRRK2 has been shown to affect basal mitophagy in neuroepithelial cells as marked by a decrease in mitochondrial clearance and an increase in the number of fragmented mitochondria (Walter et al., 2019). The mitochondrial membrane potential and intracellular ATP levels were reduced in LRRK2 [G2019S] derived patient samples (Mortiboys et al., 2010). [G2019S] LRRK2 mutant neurons show an increase in the autophagy markers p62 and LC3 indicating a more general defect in autophagic pathways (Schwab et al., 2017). Finally, LRRK2 has been found to interact with Mitochondrial Rho (Miro), a small mitochondrial GTPase involved in mitochondrial transport and homeostasis. LRRK2 [G2019S] mutation was found to stabilise Miro and impact damaged mitochondrial clearance. This study found that [G2019S] mutation negatively impacted mitophagy initiation which was rescued with depletion of LRRK2 (Wang, 2017; Hsieh et al., 2016).

1.4.12. LRRK2 and the TGN

Rab29 (also sometimes referred to as Rab7L1) is one of 5 genes within the PARK16 locus and has been identified as a genetic risk factor for the development of PD (Tucci et al., 2010; Simón-Sánchez et al., 2009). Rab29 is

reported to primarily localise to the Golgi apparatus as well as tubules emerging from the Golgi (Spanò et al., 2011; MacLeod et al., 2013). Rab29 was originally identified as a phosphorylation target of LRRK2 (Steger et al., 2016, 2017). There is clear evidence that LRRK2 and Rab29 operate in common pathways, although it is currently poorly understood how they are functionally related. Studies have shown that LRRK2 and Rab29 act together to control axonal elongation in *C. elegans* neurons with Rab29 acting upstream of LRRK2 (Kuwahara et al., 2016). LRRK2 hyperactive pathogenic mutations are known to induce reduced neurite process length in rat neurons, which can be rescued by the overexpression of Rab7L1. Knockdown of Rab7L1 was also able to phenocopy LRRK2 hyperactivation (MacLeod et al., 2013). The same study showed that overexpression of retromer component and PD related gene VPS35 was able to rescue the neurite process length phenotype induced by LRRK2 mutation. Genetic studies have found common variants in the LRRK2 and Rab29 loci which function non-additively to affect the risk of Parkinson's disease (Kuwahara et al., 2016; MacLeod et al., 2013).

Additionally it has been shown that Rab29 can recruit LRRK2 to the TGN (Purlyte et al., 2018; Beilina et al., 2020; MacLeod et al., 2013; Liu et al., 2018). Further evidence for Rab29 being upstream of LRRK2 was found when overexpression of Rab29 enhanced the phosphorylation of Rab10 and Rab29 by LRRK2 as well as LRRK2 autophosphorylation (Purlyte et al., 2018; Liu et al., 2018). Data shows that the ROC-COR domain mutants (such as [R1441C/G/H]) are more readily activated by Rab29 compared to WT LRRK2 and [G2019S] mutant LRRK2. Studies speculate this is due to the fact that these LRRK2 mutants more readily bind GTP, and that GTP binding is required for Rab29 activation of LRRK2 (Liu et al., 2018; Purlyte et al., 2018). It has been shown in several studies that hyperactive LRRK2 results in disruption of the TGN, a phenotype which can be rescued by treatment with LRRK2 inhibition. A recent study has shown that Rab29 and LRRK2 can functionally interact with the Golgi Associated Retrograde Protein (GARP) complex (Beilina et al., 2020). LRRK2 and Rab29 can associate via the VPS52 component of the GARP complex at the TGN, and evidence suggests that

Rab29 can recruit the GARP complex when overexpressed. Loss of GARP complex components disrupts Rab29 mediated recruitment of LRRK2 to the TGN. Both LRRK2 and GARP component VPS52 can interact with the SNARE proteins at the TGN (Beilina et al., 2020). This suggests a role for the LRRK2-GARP complex interactions in stabilising the SNARE proteins at the TGN and therefore a role in membrane fusion and trafficking.

1.4.13. VPS35

Vacuolar protein sorting-associated protein 35 (VPS35) makes up one of the three core retromer components alongside VPS26 and VPS29. It is part of the vacuolar protein sorting gene family originally identified in yeast. It binds in a heterotrimeric complex with the other core components, which provides a scaffold for the large multimeric protein retromer complex. VPS35 is therefore essential for the recycling of proteins from the endosomal network to the TGN by retrograde transport. VPS35 is the largest component of the retromer and serves as a platform for VPS26 and VPS29 to bind to (Swarbrick et al., 2011; Seaman, 2004, 2012; Seaman et al., 2009, 1997, 1998).

1.4.14. VPS35 in Parkinson's Disease

Pathogenic mutations have been identified in VPS35 which result in an autosomal dominant inheritance pattern. The most common mutation is the VPS35 [D620N] mutation resulting in a late-onset levodopa-responsive form of PD (Zimprich et al., 2011; Vilariño-Güell et al., 2011; Williams et al., 2017). Other more rare mutations in VPS35 have been linked to PD but the pathogenicity of these mutations is not confirmed (Williams et al., 2017). Because neurons have a long axis between the soma of the cell and the synaptic terminals, there is a greater challenge to both anterograde and retrograde transport through the endolysosomal system (Vidyadhara et al., 2019). VPS35 and the other retromer complex components are therefore essential in maintaining the homeostasis and proteostasis within neurons.

It has been proposed that pathogenic mutations in VPS35 inhibit its ability to associate with the other retromer components therefore impairing retrograde transport (Williams et al., 2017). However, other studies have shown that [D620N] VPS35 is able to form the retromer complex with the same efficiency as wild type (Ishizu et al., 2016). The [D620N] mutation has also been reported to disrupt the interaction of retromer with FAM21, a component of the WASH complex important to retrograde transport (McGough et al., 2014). Mutations in VPS35, as would be expected, led to lysosome dysfunction manifesting in enlarged lysosomes. In addition, studies found that loss of function of VPS35 or depletion led to α-synuclein aggregates, dopaminergic neuron loss and autophagy (Follett et al., 2016; Tang et al., 2015b). Studies showed an increase in the turnover of LAMP2 in VPS35 [D620N] mutant cells which the authors speculated is due to a defect in retrograde transport. Misfolded α-synuclein is turned over by the lysosome, a process where LAMP2 is thought to be important (Tang et al., 2015a). α-synuclein has also been found to disrupt the retromer complex by interacting with the VPS26 and VPS29 core subunits. This results in a reduced binding capacity for VPS35 as well as the SNX-BAR adaptors (Patel and Witt, 2018). Therefore, a vicious cycle ensues where, dysfunction in VPS35 is thought to lead to accumulation of α-synuclein through reduced turnover and accumulated α-synuclein further impairs retromer function via disruption at the core complex.

1.4.15. Retromer and mitochondrial dynamics

The canonical role for the retromer is endosome to TGN retrograde transport through the endolysosomal system. One landmark paper identified a role for the retromer complex in the formation of mitochondrial derived vesicles (MDVs) (Braschi et al., 2010). MDVs are a mitochondrial quality control pathway which is independent of mitophagy (Sugiura et al., 2014).

Steinberg's group showed a role for the retromer in mitophagy. The retromer is a well-established effector of Rab7, with active Rab7 being essential for correct localisation of the retromer to the endosomal network (Rojas et al.,

2008; Seaman et al., 2009). Work from Steinberg's group showed that knockout of VPS35 increased the level of "active", GTP-bound Rab7 in cells. They propose this is via TBC1D5- a Rab7 GAP which can interact with core retromer component VPS29. This study proposes a model where Rab7 recruits the retromer to the endosomal system, and once there, the retromer is able to "switch off" active Rab7 via its interaction with TBC1D5 which allows Rab7 to localise to mitochondria (Jimenez-Orgaz et al., 2018).

Another study has shown that VPS35 mutations cause mitochondrial dysfunction through a relationship with DLP1. DLP1 is a key regulator of mitochondrial fission (Li et al., 2018). The paper showed that overexpression of VPS35 induced mitochondrial fragmentation and dysfunction which was further enhanced by VPS35 pathogenic mutation. They show that VPS35 interacts with DLP1 and is responsible for DLP1 turnover via its role in MDV formation (Sugiura et al., 2014).

1.4.16. LRRK2 as part of a Parkinson's network

Both LRRK2 and VPS35 have been linked to both major pathways implicated in PD and there is significant evidence that they operate in common and overlapping pathways (**Figure 1.13**). The pathogenic mutations in LRRK2 and VPS35, as discussed in **Sections 1.4.10, 1.4.11** and **1.4.14**, have been shown to cause a variety of different phenotypes, depicted in **Figure 1.14**. There is some disagreement in the literature regarding the effect of the [D620N] mutation on VPS35 activity. Loss of binding interactions of VPS35 would suggest a loss of function mutation. VPS35 [D620N] mutation has been found to hyperactivate LRRK2 kinase activity, suggesting VPS35 is upstream of LRRK2 (Mir et al., 2018). Heterozygous mutation of VPS35 resulted in an increase in Rab10 phosphorylation by LRRK2 which would suggest this is a gain of function.

LRRK2 and VPS35 have both been shown to regulate Rab7 activity. It is predicted that a VPS35 [D620N] gain of function mutation would result in

inactivation of Rab7. LRRK2 has been reported to negatively regulate Rab7, with hyperactive LRRK2 [G2019S] decreasing GTP-Rab7 in patient derived fibroblasts relative to WT (Gómez-Suaga et al., 2014). Interestingly, Rab7 is not a direct substrate of LRRK2, but is in fact a substrate of its homologue, LRRK1 (Malik et al., 2020). It has not been determined whether the effect of VPS35 on Rab7 is mediated by its activation of LRRK2 kinase activity, or whether these two PD related proteins negatively regulate Rab7 by two distinct mechanisms. It has been suggested that LRRK2, VPS35 and Rab29 are three PD related genes which operate in the same pathway, with VPS35 and Rab29 being upstream regulators of LRRK2 activity (**Figure 1.14**) (MacLeod et al., 2013; Liu et al., 2018; Purlyte et al., 2018). However, it still remains unclear if the action of VPS35 and Rab29 on LRRK2 is the PD causing mechanism.

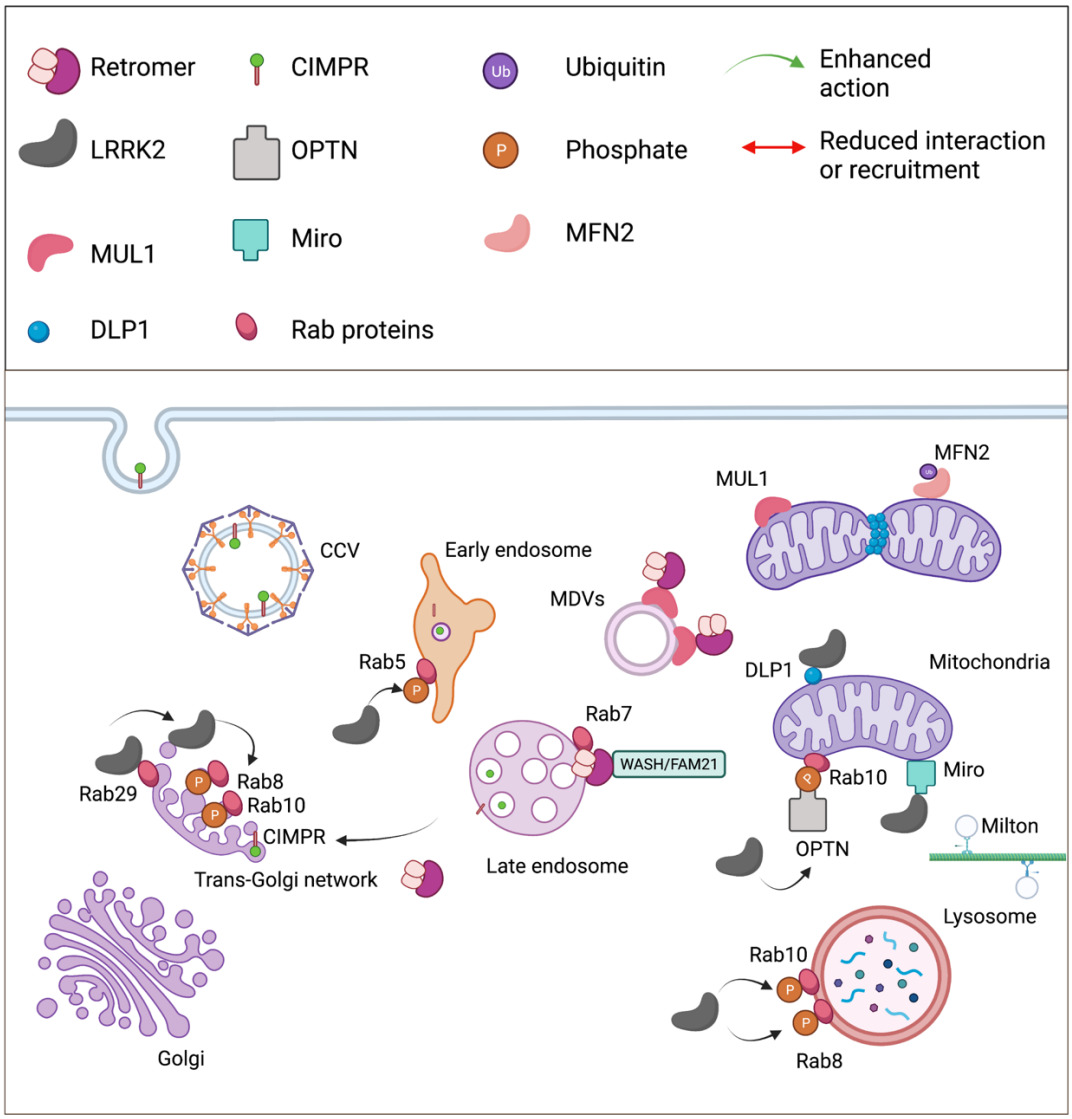

Figure 1.13 LRRK2, VPS35 and Rab29 work in an interconnected PD network

Parkinson's disease related proteins LRRK2, VPS35 and Rab29 have been shown to operate in a variety of cell biology pathways. LRRK2 can phosphorylate a subset of Rab proteins including Rab5, Rab10 and Rab8. These phosphorylation events have been linked to deficient endolysosomal trafficking and protein homeostasis. Additionally, LRRK2 can be recruited to the TGN by Rab29. LRRK2 is able to interact with DLP1 and Miro at mitochondria. Phosphorylation of Rab10 was shown to increase OPTN recruitment to mitochondria for mitophagy. The retromer has been shown to function in the MDV quality control pathway, as well as in its canonical role in retrograde trafficking. It acts as a Rab7 effector at MVBs and is able to recruit the WASH complex. Created with biorender.com. Adapted from figure by Charlotte Menzies.

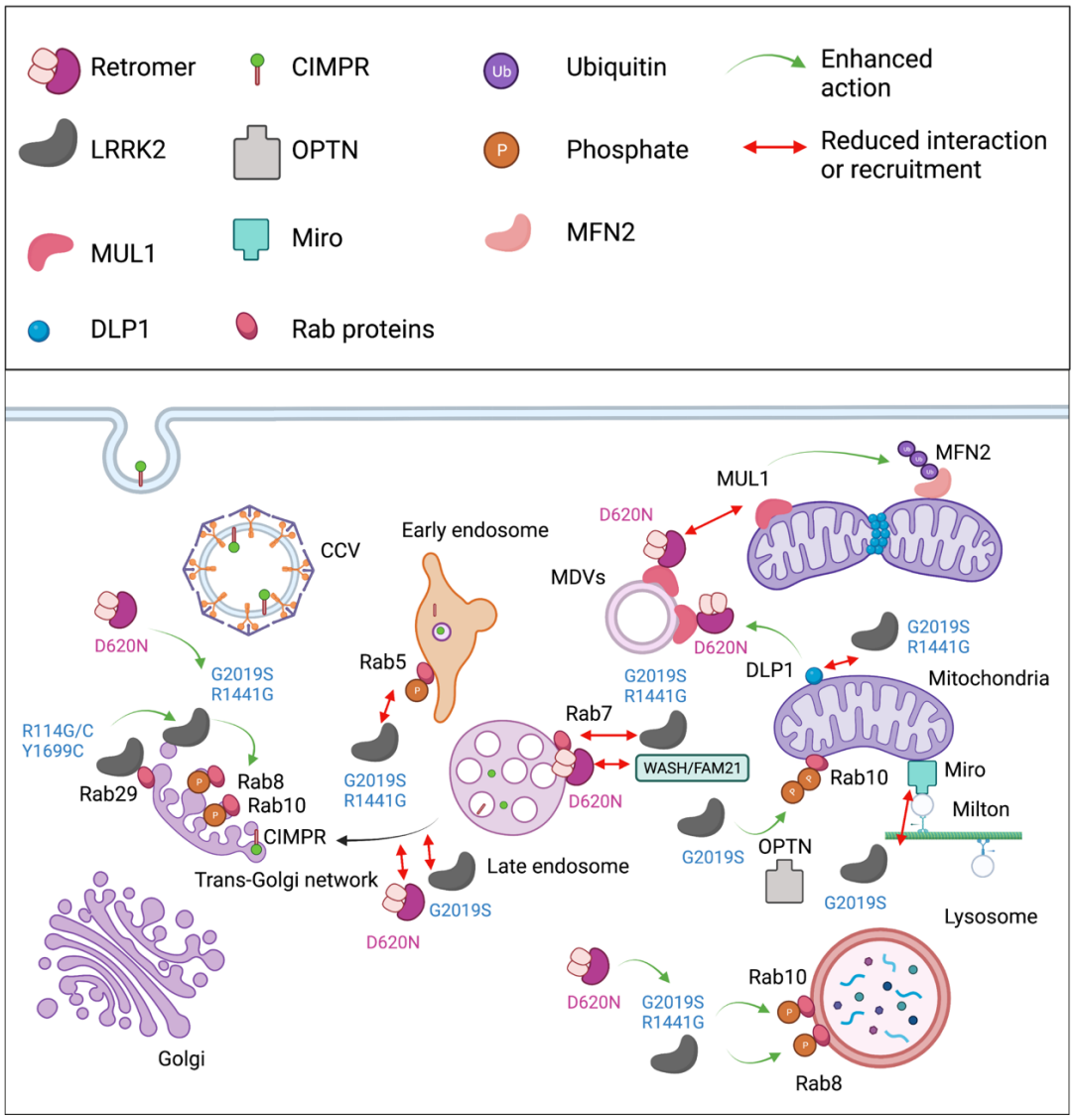

Figure 1.14 Mutations in LRRK2 and VPS35 cause a wide array of trafficking and homeostasis defects

ROC-COR LRRK2 mutations are hyperactivated by Rab29 overexpression and are more efficiently recruited to the TGN. Most LRRK2 mutations cause a hyperactive kinase leading to excessive phosphorylation of target Rab proteins. They also lead to defects in efficient endolysosomal trafficking of proteins, lysosome function and general protein homeostasis. LRRK2 mutations are also associated with reduced quality control of mitochondria and mitophagy clearance. The PD associated [D620N] mutation in VPS35 has been shown to hyperactivate LRRK2 kinase activity suggesting it lies upstream of LRRK2 in a common pathway. [D620N] has also been shown to alter retrograde traffic in the endolysosomal system, recruitment of the WASH complex as well as altering mitochondrial dynamics and homeostasis. Created with biorender.com. Adapted from figure by Charlotte Menzies.

1.5. Aims of study

LRRK2 functions in a wide variety of pathways and these functions overlap with other PD related proteins. Understanding the physiological function of LRRK2 in these processes is as important as understanding its pathophysiology, especially as LRRK2 represents an attractive therapeutic target. I thus aimed to gain a better understanding of the physiological role of LRRK2 in cells, and how this would relate to other PD linked proteins. I also aimed to investigate if LRRK2 plays a role in the relationship between PD and melanoma, as data from the cancer cell line encyclopaedia shows that LRRK2 is highly expressed across melanoma cell lines. In addition to this, early work showed LRRK2 is inversely related to the expression of pigmentation markers in melanoma cells.

In Chapter 3, I generate tools which provide a platform to study the physiology of both LRRK2 and VPS35 in the context of their pathogenic mutations. In particular, I have generated the tools required to study the effect of both LRRK2 and VPS35 on the activity of Rab7.

In Chapter 4, I will show the effect of LRRK2 depletion and inhibition on a number of organelle markers in the context of melanoma cells and melanocytes. Prior to this thesis there were multiple studies indicating a role for LRRK2 in membrane traffic in the endolysosomal system, however, the mechanisms underpinning these pathways remain poorly understood.

Finally, in Chapter 5, I will report on a role for LRRK2 in melanogenesis and melanoma progression phenotypes. PD has been linked to an increase in the incidence of melanoma compared to the general populations, but the reason for this is not known. Although LRRK2 mutations only account for a small proportion of PD patients, LRRK2 is highly expressed across melanoma cell lines and has also been linked to sporadic cases of PD.

2. Chapter 2: Materials and Methods

2.1. Cell Culture

2.1.1. Materials and Reagents

RPMI 1640 W/GLUTAMAX-I (#61870-036), Dulbecco's Modified Eagle's Medium, high glucose, GlutaMAX™ Supplement, pyruvate (DMEM, #31966-021), DMEM F12 GlutaMAX™ (#10565018), AIM V™ Medium (#31035025), Trypsin 0.5% EDTA, 10X (#15400054), Penicillin-Streptomycin (#15140122), MEM Non-Essential Amino Acids Solution (MEM NEAA, #11140-035), Sodium Pyruvate (#11360070), Fetal bovine serum (#10270106) were all purchased from Invitrogen (UK). GeneJuice (#70967), Phorbol 12-myristate 13-acetate (TPA, #P8139), N-Phenylthiourea (PTU, #P7629) Doxycycline (Dox, D9891), and G418 (#4727878001) were purchased from Sigma. Flp-In kit (#K601002), Blasticidin (#R21001) and Zeocin (#R25005) were purchased from Thermo Fisher scientific. LRRK2 lentivirus was purchased from Ku Leuven (Error! Reference source not found.). Polybrene (#TR-1003) was purchased from Merk-Millipore. All plasticware was purchased from Corning Inc. (NY, USA).
For work in Sheffield Minimum Essential Medium (MEM), with Earle's Salts, with L-Glutamine(#E15-825) and Foetal Bovine Serum (FBS) Gold (#A15-151) were purchased from PAA. Penicillin / Streptomycin Solution (100X concentrate) (#17-602E), MEM Vitamins Solution (100X) (#11120-037), MEM Non-Essential Amino Acids (100X) (#11140-035) and Na Pyruvate (#13-115E) were all purchased from Lonza (USA). Uridine (#U-3003) was purchased from Sigma.

2.1.2. Cell lines

Melan-a melanocyte cell line was obtained from E. Sviderskaya (London, UK). Parental human telomerase reverse transcriptase immortalised retinal-pigment epithelial Flp-In (hTERT-RPE1 Flp-In (RPE1 Flp-In)) cells were provided by Dr Jon Pine (ICR, London). The WM266.4 cell line was obtained from R. Marais (Manchester, UK). HEK293 Flp-In cells were purchased from

Invitrogen. MNT1 cells were obtained from Graca Raposo (Institut Curie, Paris).

Fibroblast lines derived from patient skin punches were cultured at the Sheffield Institute of Translational Neuroscience (SiTraN) under the supervision of Dr Heather Mortiboys. iNPCs were derived from reprogramming patient fibroblasts carried out by Dr Heather Mortiboys. Dopaminergic neurons were derived from these iNPCs as per protocol in **Section 2.1.10** under the supervision of Dr Heather Mortiboys.

2.1.3. Cell line culture

Melan-a cells were maintained in RPMI 1640 W/GLUTAMAX-I gassed at 10% CO_2, supplemented with 10% non-heat-inactivated fetal bovine serum, 200 nM TPA. TPA was added to cells fresh with each passage. Media was also supplemented with 200 µM PTU for the first 3 days of culture. Cells were split 1:3 every 2-3 days up to a maximum passage number of 30 and were maintained in a humidified 10% CO_2 atmosphere at 37°C. WM266.4 cells and HEK293 Flp-In cells were maintained in DMEM + GlutaMAX™ supplemented with 10% heat-inactivated fetal bovine serum, 1% MEM NEAA in a humidified 5% CO_2 atmosphere at 37°C. Cells were split 1:6 every 2-3 days. RPE1 Flp-In cells were maintained in DMEM F12 (1:1) supplemented with 10% heat-inactivated fetal bovine serum, 1% MEM NEAA in a humidified 5% CO_2 atmosphere at 37°C. MNT1 cells were maintained in DMEM + GlutaMAX™ supplemented with 20% FBS, 10% AIM-V, 1% NEAA and 1% sodium pyruvate in a humidified 5% CO_2 atmosphere at 37°C.

2.1.4. Flp-In™ T-REx™ System

The Flp-In T-Rex system is a system marketed by Themo Fisher Scientific for the rapid generation of cell lines using a Flp recombination target (FRT) site. This system utilises cells that have two plasmids (pCDNA6/TR and pFRT/lacZeo, **Figure 2.1**) stably integrated into their genome. The pFRT/lacZeo plasmid has the FRT site required for the integration of a gene

of interest into the genome of the cell at a transcriptionally active locus. The pCDNA6/TR plasmid contains the TetR gene which results in the expression of the Tet repressor protein. In this system, the gene of interest (GOI) integrated into the cell's genome is only expressed with the addition of doxycycline or tetracycline. They can displace the Tet repressor protein from the promotor region of the gene and allows for transcription and expression (**Figure 2.2**). The pCDNA6/TR and pFRT/lacZeo plasmids each have their own antibiotic selection marker- Blasticidin and Zeocin respectively (**Figure 2.1**). These antibiotics are used to maintain the cells prior to transfection to ensure cells have retained the plasmids stably integrated into their genome. It is also important cells only have one FRT site within their genome- as this ensures that each GOI is only integrated into one site and that cell lines are comparable.

The GOI is cloned into a pCDNA5/FRT/TO plasmid with a resistance gene for selection of clones. The plasmid is co-transfected with a pOG44 plasmid which encodes the recombinase enzyme required for the integration (**Figure 2.3**). In the original system, the pCDNA5/FRT/TO plasmid has hygromycin as the selection marker for stably transfected cells. One benefit of this system is the generation of isogenic models for different mutations of the same protein. Integration at the FRT site means that WT and mutant forms of a protein should be expressed at the same levels- something which cannot be guaranteed in overexpression models.

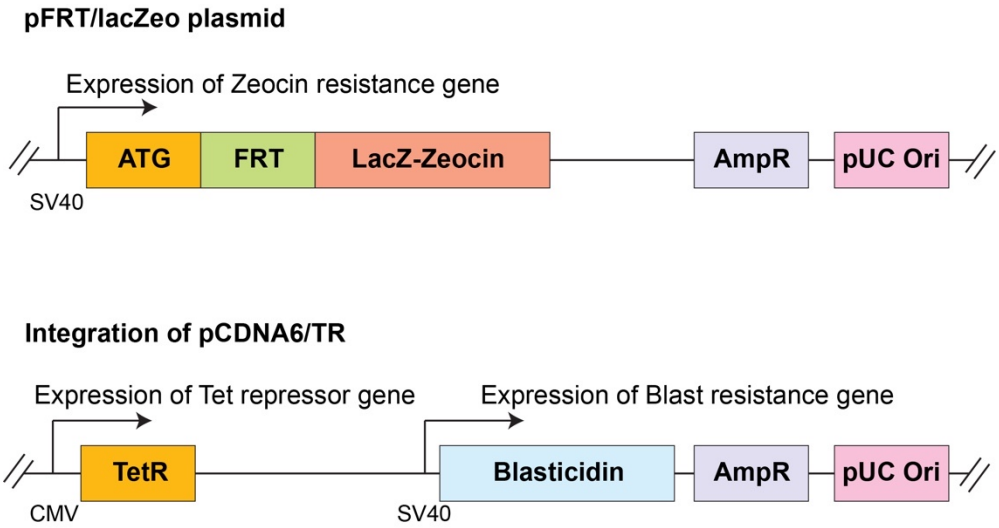

Figure 2.1 Plasmids stably integrated into the genome of Flp-In cells
pFRT/lacZeo and pCDNA6/TR plasmids are stably integrated into Flp-In cells. This ensures that the integrated gene of interest is added at a transcriptionally active locus. It also ensures that the expression of the gene of interest is controlled by the Tet repressor and therefore can be induced with doxycycline.

In the case of my project, we wanted to generate hTERT-RPE1 (RPE1) Flp-In cells with GOI VPS35 WT or VPS35 [D620N]. In this case the GOI was cloned into a pCDNA5 FRT/TO Neo plasmid, as RPE1 cells are already resistant to hygromycin (Bodnar et al., 1998). RPE1 cells were co-transfected with one of two VPS35 plasmids (VPS35 WT or [D620N]) alongside pOG44 plasmid and positive clones were selected with G418 selection media. Clones were screened for VPS35 expression +/- doxycycline followed by western blotting. Workflow for generation of cell lines shown in **Figure 2.4**.

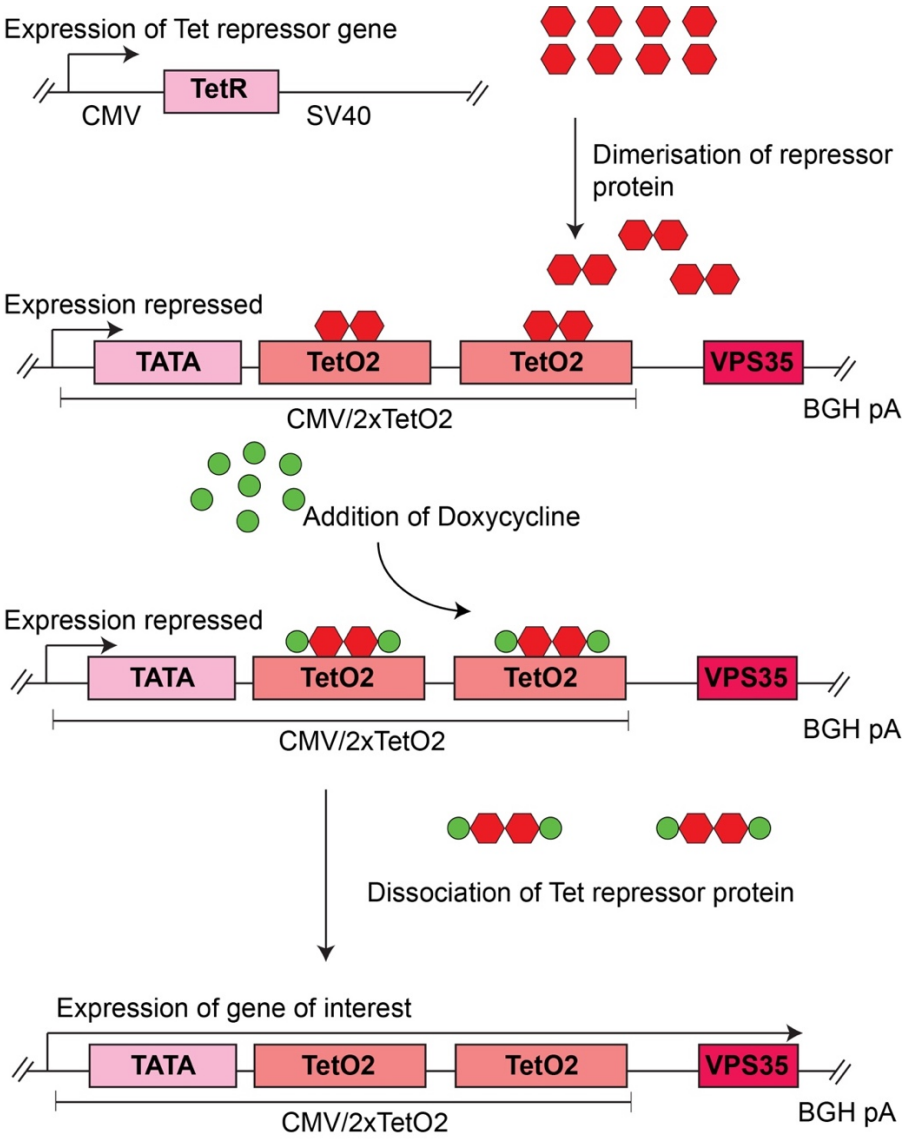

Figure 2.2 Repression of gene of interest expression in Flp-In cells

RPE1 Flp-In cells contain a Tet repressor (TetR) gene. The gene of interest is cloned into a locus under the control of the Tet repressor protein. Addition of doxycycline displaces the Tet repressor protein and activates expression of the gene of interest. This allows for an inducible system.

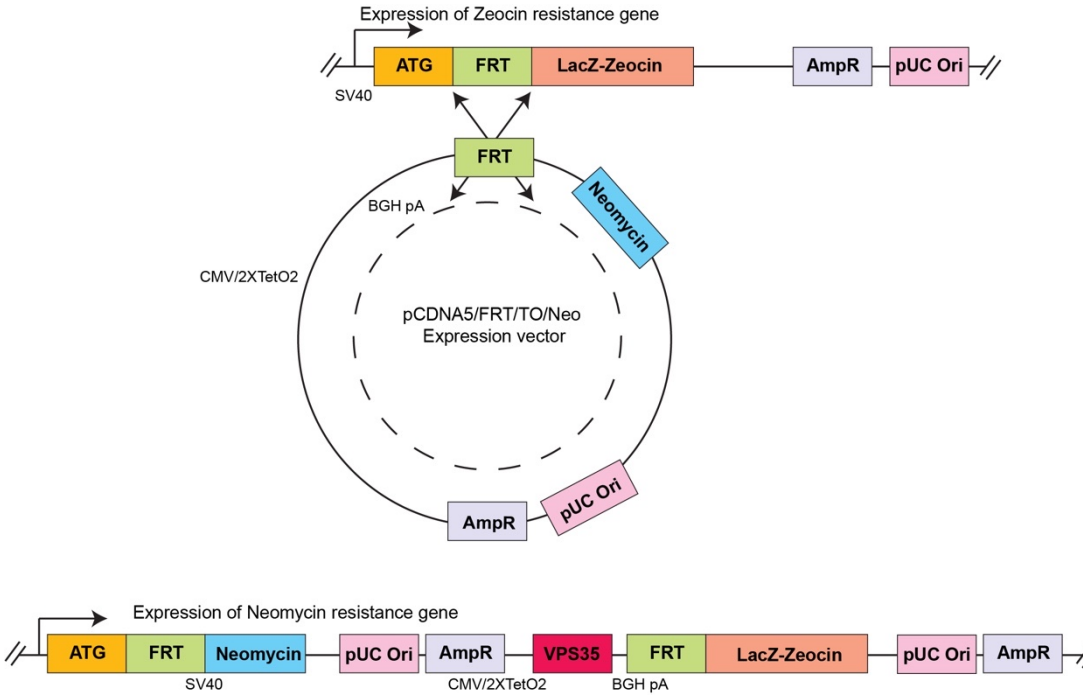

Figure 2.3 Integration of GOI into FRT site by a recombinase enzyme

Transfection of a pCDNA5 FRT/TO plasmid encoding the gene of interest alongside a plasmid encoding the recombinase results in the integration of the gene of interest at the FRT site. This ensures the integration occurs at a transcriptionally active locus and that cell lines are comparable as they should have even levels of expression.

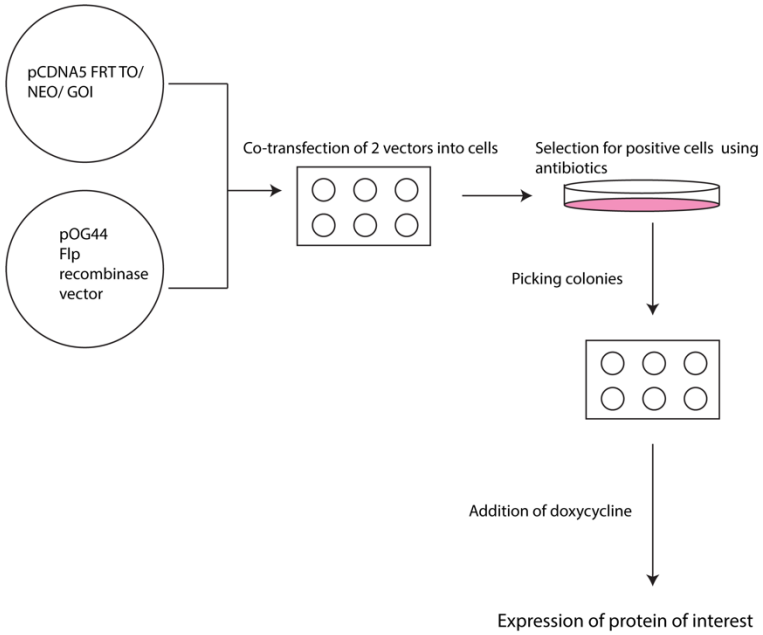

Figure 2.4 Workflow of generation of RPE1-VPS35 Flp-In cell lines
pCDNA5 FRT TO vector containing the gene of interest (GOI) was co-transfected with pOG44 Flp vector containing the recombinase enzyme. Cells were split from a 6 well plate into a 10 cm dish and put under antibiotic selection. Colonies were picked from the 10 cm dish into multi-well plates and screened by adding doxycycline to induce expression. Clones were screened by western blotting and immunofluorescence.

2.1.5. Generating VPS35 Flp-In Cell lines

On day 1, RPE1 Flp-In parental cells were co-transfected with pCDNA5 FRT/TO Neo plasmids generated with HA-VPS35 (WT or [D620N] mutant) (100 ng) and pOG44-Flp plasmid (900 ng) using Genejuice transfection reagent (see below). An additional well was transfected with GFP plasmid to check transfection efficiency. Transfection efficiency was approximately 30%. On day 2, cells were split 1:4 from a 6-well plate into a 10 cm dish in selection media (DMEM F12 + Blasticidin + G418) in order to get single colonies. Once single colonies were visible, they were picked into 24-well plates and from there expanded for screening. This work was carried out in collaboration with Katy McCarron.

2.1.6. Screening VPS35 Flp-In clones

Selected colonies were seeded into 6-well plates and treated +/- doxycycline (1 µg/ml) for 24 hours. Cells were lysed and screened by western blot, probing for HA and VPS35 (see below for methods). Cells were also screened by IF staining for HA expression to check if cells were single clones. This work was carried out in collaboration with Katy McCarron.

2.1.7. Single cell dilution of mixed clones

Mixed clones were trypsinised and counted using a haemocytometer. Cells were diluted 1:100. 150 cells were then split across 3 x 96 well plates to obtain single clones. Clones were expanded from 96 well plates and then screened as above. This work was carried out in collaboration with Katy McCarron.

2.1.8. Generating LRRK2 Lentivirus cell lines

Single RPE1 Flp-In clones, VPS35 WT 3B4 and VPS35 [D620N] 1F3, generated **in section 2.1.7** were transduced with LRRK2 lentivirus purchased from Ku Leuven (see **Table 2.1**). From the viral titre, a multiplicity of infection (MOI) of 0.8 was calculated for each virus. Cells were transduced with virus in full media with polybrene. Media was exchanged after 48 hours. Cells were expanded to 15 cm dishes. Cells were then trypsinised, washed in PBS then resuspended in FACS buffer (PBS + 1% FBS). GFP-positive cells were sorted using FACS (carried out by Ailbhe Brazel). Polybrene only control was used to set the gating. Positive cells were expanded and screened by live cell imaging and western blotting for GFP and LRRK2.

Table 2.1 LRRK2 lentiviruses

Production number	Virus	Functional titre
PD-12-197.2	LV-CMV-eGFP-LRRK2 wild-type	5.52E+06
PD-12-289	LV-CMV-eGFP-LRRK2 G2019S	1.18E+07
PD-12-279	LV-CMV-eGFP-LRRK2 G2019s/D1994A	1.22E+07
PD-12-233	LV-CMV-eGFP (control)	2.13E+13

2.1.9. Fibroblast cell culture

Patient derived fibroblasts were maintained in MEM supplemented with 10% Foetal bovine serum gold, 1% MEM vitamins solution, 1% MEM Non-Essential Amino Acids, 1% Penicillin/Streptomycin, 1% sodium pyruvate and Uridine (200 µM). Cells were maintained in a humidified 5% CO_2 atmosphere at 37°C. Cells were split 1:3 once a week and fed every other day with a full media change.

2.1.10. Dopaminergic neuron differentiation

iNPCs were plated into a 6-well plate in DMEM/F-12 medium with Glutamax supplemented with 1% NEAA, 2% B27 supplement. Cells were cultured for 2 days with full media plus DAPT (2.5 µM). After 2 days, DAPT media was removed, and replaced with full media supplemented with SAG and FGF8 (1 µM) factors. Cells were maintained in these factors for 10 days, changing the media every day. On day 12, neurons were re-plated into plates for assaying. Following this, factors were replaced with BDNF (30 ng/ml), GDNF (30 ng/ml), TGF-β3 (2 mM) and dCAMP (2 mM) for 15 days. On the final day cells were assayed or fixed for staining.

2.2. Cell Biology

2.2.1. Materials and reagents

Lipofectamine RNAiMAX (#13778075), Lipofectamine LTX with PLUS (#15338100), Opti-MEM™ Reduced Serum Medium, GlutaMAX™ Supplement (#51985034), and RPMI 1640 no phenol red (11835030), LysoTracker™ Red DND-99 (#L7528), were all purchased from Invitrogen (UK). MLi-2 (#5756) and Torin1 (#4247) were purchased from TOCRIS (Abingdon, UK). GSK2578215A (#S7664), GNE-0877 (#S7367), Rapamycin (#S1039) were purchased from Selleckchem (TX, USA). HG-10-102-01 (#438195) and GeneJuice Transfection Reagent (#70967) were purchased from Merck Millipore (Dorset, UK). Cycloheximide (CHX) (#C7698), were obtained from Sigma- Aldrich (Merck). Magic Red Cathepsin B Kit (#ICT937) was purchased from Bio-Rad (Deeside, UK). Cathepsin D activity assay kit (#ab65302) was purchased from abcam (Cambridge, UK). siRNA oligonucleotides were purchased from Dharmacon (Cambridge, UK). IBIDI products purchased from Thistle Scientific (Glasgow, UK). Hoechst 33342 (#62249) was purchased from Thermo Fisher Scientific.

2.2.2. siRNA knockdown

Melan-a cells were seeded into 6 well plates at a density of $2x10^5$ per well on day 1. WM266.4 and RPE1 Flp-In cells were seeded into 6 well plates at a density of $1.5x10^5$ on day 1. On day 2 cells were transfected with siRNA (40 nM) using Lipofectamine RNAiMAX in Opti-MEM medium at a 1:1 ratio according to manufacturer's protocol. The reaction was added to cells for 6 hours before it was exchanged for normal media. Reactions were left for 72 hours. Cells were lysed or fixed on day 5.

Table 2.2 siRNA oligonucleotide sequences
All siRNAs were purchased from Dharmacon (CO, USA)

Target	Cat. No.	Species	ON-TARGET Plus	Sequence
NT1	D-001810-01	-	-	
LRRK2	L-006323-00-0005	Human	SMARTpool	5'-GAAAUUAUCAUCCGACUAU-3' 5'-GGAGGGAUCUUCUUUAAUU-3' 5'-UUACCGAGAUGCCGUAUUA-3' 5'-CAAGUUAUUUCAAGGCAAA-3'
LRRK2	J-006323-05-0002	Human	Individual	5'-UUACCGAGAUGCCGUAUUA-3'
Lrrk2	L-049666-00-0005	Mouse	SMARTpool	5'-CAAGAUUGAUUAACCGAUU-3' 5'-GGUAGGCUCUGAAGUCUUA-3' 5'-CCAGAUAAGUCAUCCAAUU-3' 5'-GAACGAAGUGCAUGUCUUU-3'

Lrrk2	J-049666-05-0002	Mouse	Individual	5’-CAAGAUUGAUUAACCGAUU-3’
MITF	L-008674-00-0005	Human	SMARTpool	5’-UGGCUAUGCUUACGCUUAA-3’ 5’-AGAACUAGGUACUUUGAUU-3’ 5’-AGACGGAGCACACUUGUUA-3’ 5’-GAACACACAUUCACGAGCG-3’
Mitf	L-047441-00-0005	Mouse	SMARTpool	5’-CGAAGAAGAAGAUUUAACA-3’ 5’-GGAGCUAGGUACUCUGAUC-3’ 5’-GAAGAAAUUUUGGGCUUGA-3’ 5’-AGGCAGACCUGACAUGUAC-3’
TFEB	L-009798-00-0005	Human	SMARTpool	5’-GCAGAUGCCCAACACGCUA-3’, 5’-UGAAAGGAGACGAAGGUUC-3’, 5’-

				GCAGCCACCUGAAUGUGUA-3’, 5’-CAACAGUGCUCCCAAUAGC-3’
Tfeb	L-050607-02-0005	Mouse	SMARTpool	5’-GGAUCAAGGAGCUGGGAAU-3’ 5’-CAUCAGAAGGUUCGGGAGU-3’ 5’-GGUGUGAAGUAGCCGCCUA-3’ 5’-CUAAUUGAGAGAAGACGCA-3’
Rab27a	L-060970-01-0005	Mouse	SMARTpool	5’-CGGAUGGAGAUUACGAUUA-3’ 5’-CAGGAGAGGUUUCGUAGCU-3’ 5’-GUACAGAGCAAUGGGCCA-3’ 5’-GGGCAUUGAUUUCAGGGAA-3’
TBC1D5	L-020775-01-0005	Human	SMARTpool	5’-AGAUAAAGAACUUCGAUCA-3’ 5’-GAAUUAAGAGCAUGGUAUA-3’

				5’-CCGAAUCACAAUUUAGAAU-3’ 5’-AUCCAAGACCAGUGACUUA-3’

2.2.3. Transfections

For HEK293 Flp-In and RPE1 Flp-In cells, Genejuice transfection reagent was used as per the manufacturers protocol. In short, cells were seeded on Day 1 to be at 70% confluency on day 2 for transfection. On day 2, Genejuice transfection reagent was diluted in Opti-MEM serum free medium and incubated at room temperature for 5 min. DNA was added to the mixture and incubated at room temperature for 15 min. Genejuice was used at a ratio of 3 µL per 1 µg of DNA. Media was exchanged on cells for fresh full media and the reagent/DNA mixture was added dropwise over cells. Cells were imaged or harvested after either 24 or 48 hours.

2.2.4. Drug treatments

Melan-a cells were treated with PTU (200 µM) for the first 3 days of culture to inhibit melanogenesis. Melan-a cells were incubated for 72 hours with 1 µM Rapamycin to increase pigmentation. To inhibit LRRK2 activity, cells were treated with 200 nM MLi-2 for 1-72 hours or 500 nM GNE-0877, HG-10-102-01 or GSK2578215A for 1-72 hours. For RPE1 Flp-In cells VPS35 expression was induced with doxycycline at 0.1 µg/ml for the time point indicated in figures. All drug treatments were carried out in full regular culture media. The duration of each treatment is indicated on the respective figures.

2.2.5. LysoTracker Assay

Cells were seeded at the desired density into IBIDI glass bottomed plates and treated with the relevant siRNA or inhibitor. Following the desired incubation LysoTracker Deep Red fluorescent dye was added to the cells in full media

along with 1 µg/ml Hoechst nuclear dye and incubated for 1 hour at 37°C. LysoTracker media was removed, and cells washed 2 x 1 min in RT PBS. Media without phenol red was then added and cells immediately imaged live.

2.2.6. Magic Red-Cathepsin B Lysosome activity assay

To measure the activity of lysosomal Cathepsin B, Magic Red-Cathepsin B (Magic Red) reagent was used. Magic Red is a fluorescent probe which consists of a cresyl violet fluorophore with two target sequences for Cathepsin B attached. With both target sequences attached, the fluorophore is held in a non-fluorescent state. Entry of the Magic Red reagent into active lysosomes results in the cleavage of one or both of the target sequences by active Cathepsin B resulting in the cresyl violet emitting fluorescence. A schematic of how Magic Red-Cathepsin B reagent works is depicted in **Figure 2.5**.
Cells were seeded at the desired density into IBIDI glass bottomed plates for live imaging and the appropriate treatments carried out. Magic Red reagent was incubated with cells in full media at 20 µL per 500 µL of cells at 10^6 cells/ml along with 1 µg/ml Hoechst nuclear dye. Reagents were incubated with cells for 1 hour at 37°C. Media was removed and cells washed 3 x 1 minutes in room temperature PBS. Media without phenol red was then added and cells immediately imaged live.

2.2.7. Cathepsin D activity assay

To measure the proteolytic activity of Cathepsin D, a commercially available activity assay from Abcam (ab65302) was used according to the manufacturers protocol. Briefly, Melan-a cells were lysed in the kit lysis buffer for 10 mins on a wheel in the cold room. Lysates were clarified by spinning for 20 mins at 23,000 g at 4°C. The supernatant was collected. Reactions were set up in triplicate in a 96 well plate with kit reaction buffer and Cathepsin D substrate. Plates were incubated at 37°C for 2 hours before measuring the fluorescent output per well using a microplate reader.

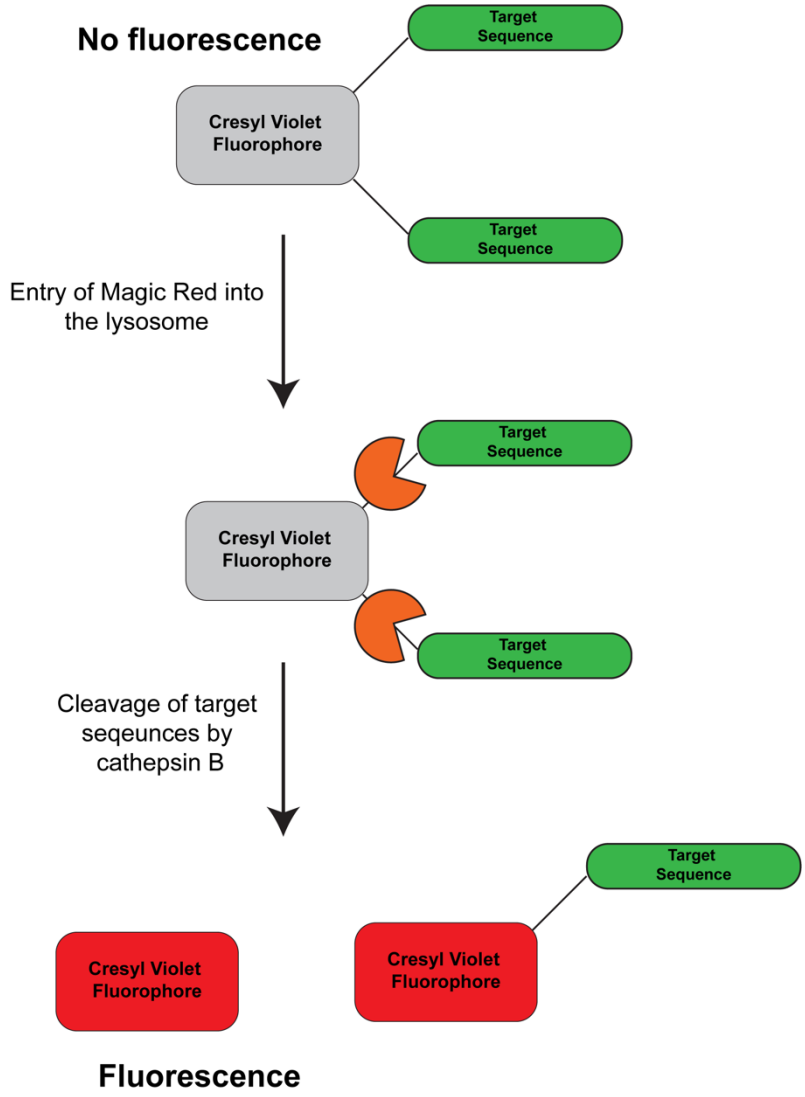

Figure 2.5 Schematic to show principle of Magic Red-Cathepsin B assay
Magic Red fluorescent probe is a readout for cathepsin B activity. The cresyl violet fluorophore is attached to two target sequences for Cathepsin B cleavage. Prior to cleavage of either target sequence there is no fluorescence. Cleavage of one or both of the target sequences by Cathepsin B results in fluorescence.

2.2.8. Incucyte cell proliferation assays

WM266.4 cells were seeded for siRNA knockdown on day 1, and the reaction was carried out as stated in section 2.2.2. After 48 hours cells were replated into the final assay vessel (usually a 24 well plate) at a low density. After a further 24 hours (72 hours post KD) the plate was placed in an Incucyte live imaging system. Multiple fields of view were imaged per well at regular

intervals for 3 days. After the final acquisition, image analysis was carried out using the Incucyte software. Images were segmented to identify cells and calculate the percentage confluence in each frame. This was then plotted over time to measure the speed of cell proliferation.

2.2.9. Cell tracking experiments

For experiments requiring siRNA knockdown, WM266.4 cells were treated as detailed in **Section 2.2.2**. 48 hours post knockdown, cells were replated into a fresh 6 well plate with 40,000 cells per well. 24 hours later (72-hour post knockdown), time-lapse imaging was set up. For experiments with inhibitor treatments, 20,000 WM266.4 cells were seeded per well into a 6 well plate. Cells were treated with MLi-2 for 24 hours on day 2. Time-lapse imaging experiments were set up on day 3. Time-lapse imaging experiments were acquired with a NIKON Ti-Eclipse Microscope with a CFI Plan Fluor DLL x10 objective. Brightfield images were acquired every 15 minutes for 24 hours. Cells were maintained at 37°C and 5% CO_2 for the duration of the experiment.

2.3. Molecular Biology and Protein Preparation

2.3.1. Materials and Reagents

The RNeasy Mini kit (#74106), QIAshredder (#79656), QIAprep MiniPrep Kit (#27106), PCR clean up kit (#28104) and HiSpeed Maxiprep kit (#12633) were purchased from Qiagen. All primers for qPCR were ordered from Eurofins Scientific. All restriction digest enzymes, T4 DNA ligase reagents, 1Kb DNA ladder (#N3232) and 100bp DNA ladder (#N3231) as well as BL21 competent cells (#C2530H) were purchased from New England Biolabs. TAE buffer was purchased from National Diagnostics. S.O.C. medium (#1554-034), DH5α subcloning efficiency cells (#18265-017), SYBR Safe DNA gel stain (#S33102) and electrophoresis grade agarose were obtained from Invitrogen. PCR nucleotide mix (#C1441) and RNasin plus RNAse inhibitor (#N2611) as well as standard PCR reagents were purchased from Promega. Reverse Transcriptase (#10121360) and Reverse transcriptase buffer (#10512703) were purchased from Fisher Scientific (Loughborough, UK). iTaq Universal

SYBR Green Supermix was purchased from Bio-Rad. Nuclease free water (#W4502), Bacterial protease inhibitors (#P8465) and all other chemicals were obtained from Sigma-Aldrich.

Table 2.3 Table of plasmids

Plasmid name	GOI	Obtained from
pCDNA5 FRT TO VPS35 WT	VPS35	MRC PPU
pCDNA5 FRT TO VPS35 [D620N]	VPS35 [D620N]	MRC PPU
pGEX-4T-3-mR7BD	RILP domain	Addgene
pCDNA5 FRT TO Neo	Backbone	
pGEX-6P-1	Backbone	Addgene

2.3.2. DNA PCR for cloning and subcloning process

For this project I was required to make constructs for the generation of VPS35 Flp-In cell lines. We obtained pCDNA5/FRT/TO HA-VPS35 (WT and [D620N]) constructs from Dundee which encode a hygromycin resistance gene. These constructs were not suitable for use in the RPE1 Flp-In cells which are already hygromycin resistant. I therefore needed to subclone the HA-VPS35 WT and HA-VPS35 [D620N] into a pCDNA5/FRT/TO Neo backbone which has a neomycin resistance gene instead. A schematic of the workflow used is shown in **Figure 2.6**. The VPS35 inserts were amplified by PCR for insertion into the neomycin resistance vector. I designed primers to retain the N-terminal HA tag on VPS35 and introduce an N-terminal KpnI restriction site for cloning into the destination vector (**Table 2.5**). The reverse primer retained the NotI restriction site at the C-terminus for cloning into the destination vector. The reaction mixture used for the amplification is shown in **Table 2.4**. The amplification product was run on a 1% agarose gel by electrophoresis and a band of the expected size was extracted. The linear product was digested with KpnI and NotI restriction enzymes. The digested PCR product was then purified with a PCR clean up kit. The destination vector was also double digested and run on

a gel to extract the digested backbone. The two digested products were ligated together using a T4 DNA ligase reaction mixture Table 2.6). All plasmids were then sent for sequencing. This work was carried out in collaboration with Katy McCarron.

Table 2.4 PCR reaction mixture for DNA amplification

per reaction µl	
H_2O	adjusted
10x Pfu-buffer	5
dNTPs (25mM)	0.5
Primer Forward (10µM)	1
Primer Reverse (10µM)	1
DNA template (100ng)	adjusted
HS Ultra-II Pfu fusion	1
Total	45µl

Table 2.5 DNA PCR Primers

Gene	Primer No	Used for	Sequence
VPS35	2545	PCR-up	5' GACGGTACCGCCACCATGTACCCATACG
	2546	PCR-up	5'AAGCGGCCGCTTAAAGGATGAGACCTT CAT

Table 2.6 T4 DNA ligase reaction mixture

Reagent	**Per Reaction 20 µl**
T4 DNA ligase buffer (10X)	2 µl
Vector (5 kb)	50 ng
Insert (2.5 kb)	150 ng
Nuclease free water	Varied
T4 DNA ligase	1 µl

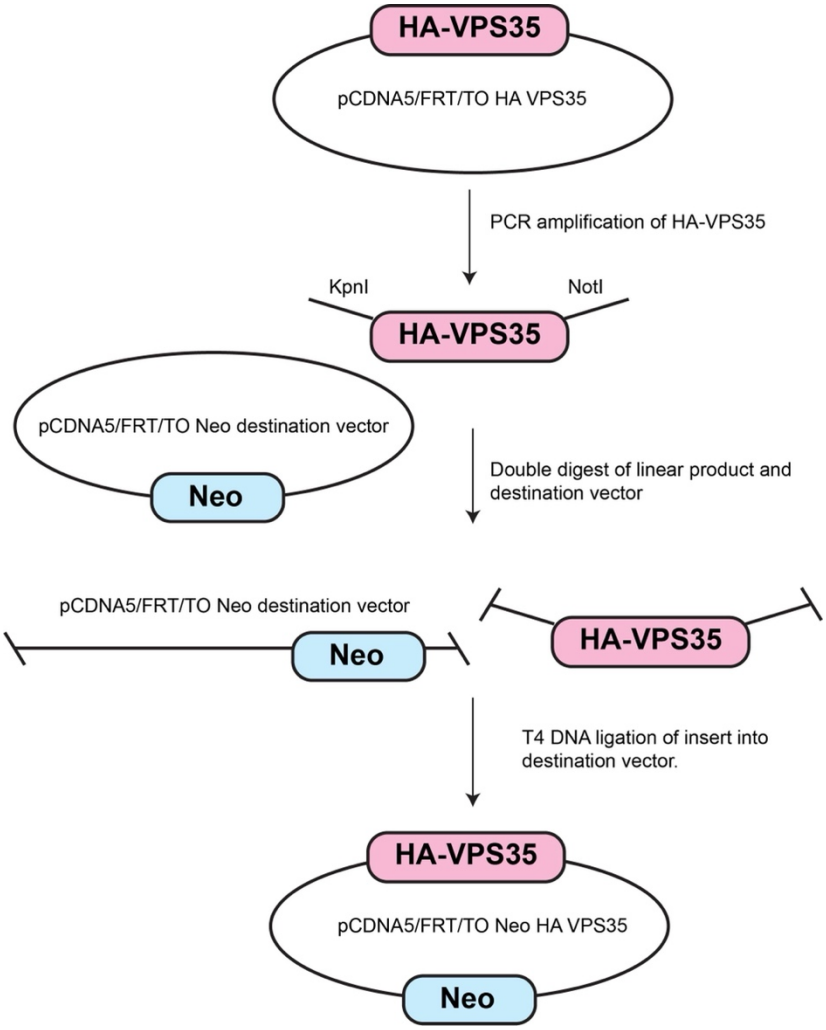

Figure 2.6 Schematic for the cloning process for VPS35 Neo plasmids
The HA-VPS35 WT and [D620N] cDNA was amplified by PCR from the pCDN5/FRT/TO plasmids purchased from Dundee MRC PPU. Primers were designed to include the appropriate restriction sites. PCR products and destination vectors were digested with the relevant restriction enzymes. The digest products were ligated together to give the pCDNA5/FRT/TO Neo HA-VPS35 (WT/[D620N]) plasmids required to generate RPE1 Flp-In cells.

2.3.3. mRNA extraction and cDNA synthesis

mRNA was extracted from cells using QIAshredder columns to homogenise cells, followed by an RNeasy mini kit according to the manufacturers protocol. Concentration of extracted RNA was measured using a NanoDrop Spectrophotometer ND100 at 260 nm. The quality of extracted mRNA was determined using the A260/280 and A260/A230 ratios. For use in qPCR 1 µg

of mRNA was reverse transcribed to cDNA. An 11 µl solution was prepared which contained a total of 1 µg of mRNA and 1 µl of Oligo DT primer in sigma water. The solution was incubated at 70 °C for 5 minutes. During incubation reverse transcription buffer was prepared as per Table 2.6 below. 8 µl of reverse transcription buffer was added to each reaction and this mixture incubated at 37°C for 5 minutes followed by the addition of 1 µl of MuLV reverse transcriptase. The final mixture was incubated for 1 hour at 42°C before a final incubation at 70°C for 10 minutes. The cDNA synthesis products were diluted 1:4 in sigma water ready for qPCR analysis.

Table 2.7 Reverse transcription reaction buffer

Per reaction	
5x Reverse transcription buffer	4 µl
PCR nucleotide mix	2 µl
RNasin	0.5 µl
Nuclease free ddH_2O	1.5 µl

2.3.4. Quantitative real-time polymerase chain reaction (qRT-PCR)

Primers used for qRT-PCR are listed in Table 2.8. Prior to qRT-PCR analysis of samples, primers were tested in an end-point PCR reaction to ensure that they only produce one amplicon of the correct number of base pairs. For each primer pair a reaction master mix was assembled as listed in Table 2.9 and 6 µl of this reaction added to all relevant wells of a qPCR plate. 4 µl of cDNA was spiked into the relevant wells before qRT-PCR was performed using the CFX Connect Real-Time PCR Detection system (Bio-Rad). The incubation cycle used is as follows: 95°C for 3 minutes for denaturation of the cDNA, 40 cycles of a two-step amplification protocol: 95°C for 10 seconds and 60°C for 30 seconds before a final incubation at 72°C for 10 minutes. The Ct values were taken for the analysis and were normalised to the readings for

housekeeping gene Actin (ΔCt). These values were expressed as $2^{-\Delta Ct}$ and the relative values to the control sample are shown as ΔΔCt.

Table 2.8: qRT-PCR Primers

Gene	Species	Primer No.	Sequence
Actin	Human and Mouse	1610	F-CACCTTCTACAATGAGCTGCGTGTG
		1611	R-ATAGCACAGCCTGGATAGCAACGTAC
LRRK2	Human	2092	F- CCCTGCCATACGAGATTACC
		2093	R- GCACATTTTTACGCTCCG
TFEB	Human	2407	F- CAGTGCTCCCAATAGCCCCA
		2406	R- CTGCTGGACAGGGGTAGCGT
Lrrk2	Mouse	2414	F- GGAAATACGGGGAGCGG
		2415	R- GGGTCATGAAGTGGGGGT
Tfeb	Mouse	2412	F- CCTTCAGAGCGAGGGAG
		2413	R- TCAGACAGATACTCCCGAACC
Tyrosinase	Mouse	2766	F- CAGGCTCCCATCTTCAGCAGAT
		2766	R- ATCCCTGTGAGTGGACTGGCAA
TYRP1	Mouse	2768	F- AGCCACAGGATGTCACTCAGTG
		2769	R- GCAGGGTCATATTTTCCCGTGG

Table 2.9 qRT-PCR Reaction mixture

Per reaction AND per primer pair	
H_2O	0.7 µl
SyBrGreen Biorad Supermix	5 µl
Forward Primer (20 µM)	0.15 µl
Reverse Primer (20 µM)	0.15 µl

2.3.5. Bacterial Transformation

DH5α and BL21 Escherichia coli cells were used for plasmid DNA preparation and protein preparation respectively. 50 µl of competent cells were thawed on ice before adding 100 ng of plasmid DNA. Cells were incubated on ice for 20 minutes then heat shocked for 60 seconds in a 42°C water bath. Cells were then placed on ice for 2 minutes. 350 µl SOC media was added to cells followed by shaking at 245 rpm for 1 hour at 37°C. Reactions were plated on LB agar plates with an antibiotic selection marker and incubated at 37°C overnight.

For screening DH5α colonies, multiple clones were picked into 5 ml of LB broth + antibiotic and grown shaking at 245 rpm at 37°C overnight. Plasmid DNA was isolated using a Qiagen MiniPrep kit. Preps were first tested by double restriction digest and colonies that gave the appropriate dropout bands were sent for sequencing at the DNA sequencing service (MRC-PPU, Dundee).
For verified constructs, a glycerol stock was made by inoculating the original culture into 250 ml antibiotic supplemented LB broth for overnight culture. 5 ml of the overnight culture was pelleted at 4000 rpm. The pellet was resuspended into 40% glycerol/LB broth and stocks kept at -80°C.

2.3.6. Restriction Digests

Restriction digests were used routinely to initially screen isolated plasmid DNA. For digest reactions 1 µg of plasmid DNA was used per reaction and incubation conditions and buffers were adjusted depending on the restriction enzymes to be used. For each digest, single digest and uncut plasmid controls were run to check the activity of both enzymes.

2.3.7. Agarose gel electrophoresis

DNA was resolved in 1% agarose gels using electrophoresis. Electrophoresis grade agarose was mixed with TAE buffer and heated using a microwave to dissolve the agarose. The mixture was allowed to cool before the addition of

SYBR Safe DNA gel stain (1x). Gels were cast into a running cassette and allowed to set. Samples were diluted in 6X loading buffer without SDS before loading. Gels were run in a horizontal midi electrophoresis tank (Fisher Scientific) in TAE buffer at 120V for 45 minutes. DNA was visualized using an ultraviolet (UV) light.

2.4. Biochemistry

2.4.1. Materials and Reagents

2-mercaptoethanol (#M6250), Bovine IgG (immunoglobulin G), Ponceau stain (#P7170), Goat Serum Donor Herd (#G6767) and mammalian protease inhibitor (#P8340) were obtained from Sigma-Aldrich (Poole, UK). Marvel skimmed milk powder was ordered from Premier Brands, UK. BCA protein assay kit (#23225) was ordered from Pierce Biotechnology (Rockford, IL, USA). Nu-PAGE Bis-Tris 4-12% gels (#NP0321BOX, #NP0303BOX) as well as NuPAGE MOPS and MES running buffers, SimplyBlue SafeStain (#LC6060), DAPI (4'6-Diamidino-2-Phenylindole Dihydrochloride) (#D1306) were purchased from Invitrogen (Paisley, UK). Amersham Protran 0.45 µm nitrocellulose membrane (#10600002), Glutathione Sepharose 4B (#17075601) and GSTrap 1ml columns (#17528101) were purchased from GE healthcare. Reduced glutathione (#G4251), PD-10 Columns (GE17-0851-01), Lysozyme (#1052810001), IPTG (#I6758), DNase (#DN25), Protease inhibitor cocktail powder (#P8465), cOmplete, Mini, EDTA-free protease inhibitor cocktail (#11836170001) and Mowiol (#475904) were purchased from Merck Millipore (Darmstadt, Germany). Pre-stained broad range molecular weight marker (#P7708S) as well as unstained broad range marker (#P7704) were ordered from New England Biolabs (NEB) (Hitchin,UK). Bovine serum albumin (BSA, #40-00-410) was purchased from First Link (UK).

2.4.2. Cell lysis

Plates for lysis were placed on ice and washed twice in ice cold PBS before the addition of RIPA buffer (10mM Tris-HCL pH 7.5, 150mM NaCl, 1% Triton-x100, 0.1% SDS, 1% sodium deoxycholate). RIPA buffer was always

supplemented with mammalian protease inhibitor cocktail (1:250). For Melan-a cells, cells were scraped into lysis buffer and transferred into eppendorfs on ice for 15 minutes. Cells were then sonicated 3 x 10 seconds with a sonicator probe on a low setting. For all other cell lines, RIPA buffer was added, and the plate rocked on ice for 15 minutes. Lysates were then centrifuged at 21,000 g for 30 minutes at 4°C.

For hot lysis, cells were washed 2x in warm PBS before addition of pre heated hot lysis buffer (2% SDS, 1 mM EDTA, 50 mM NaF). Cells were scraped into hot lysis buffer and boiled at 110°C for 10 mins, vortexing at 2-minute intervals. Lysates were then clarified at 21,000g for 20 mins at RT.

2.4.3. Membrane fractionation

Plates for fractionation were placed on ice and washed twice in ice cold PBS. Cells were scraped into PBS and pelleted at 200 g for 4 mins. Pellets were washed in HIM buffer (200 mM Mannitol, 70 mM sucrose, 1 mM EGTA, 10 mM HEPES, pH 7.5) and pelleted again at 200 g for 4 mins. Pellets were resuspended in HIM buffer supplemented with mammalian protease inhibitor cocktail (1:250). For Melan-a cells, cells were passed through a 23G needle 7 times before passing through a cell cracker with an 8.01 mm ball approximately 10 times until cells had been homogenised. The nuclear fraction was removed by spinning homogenate at 600 g for 10 mins. Post nuclear supernatant (PNS) was collected, and nuclear fraction discarded. A sample of PNS was retained for western blotting. The remainder was spun in an ultracentrifuge at 100,000 g for 30 mins. The supernatant was removed and labelled cytoplasmic fraction. The membrane pellet was resuspended in 20% of the total homogenisation volume, in HIM buffer supplemented with MPIs.

2.4.4. Melanosome fractionation

Melan-a cells (2x 15cm dish per condition) were placed on ice and washed twice in ice cold PBS. Cells were scraped into PBS and pelleted at 200 g for 4 mins. Pellets were washed in HIM buffer (200 mM Mannitol, 70 mM sucrose,

1 mM EGTA, 10 mM HEPES, pH 7.5) and pelleted again at 200 g for 4 mins. Pellets were resuspended in HIM buffer supplemented with mammalian protease inhibitor cocktail (1:250). Cells were passed through a 23G needle 7x before passing through a cell cracker with an 8.01 mm ball approximately 10x until cells had been homogenised. The nuclear fraction was removed by spinning homogenate at 600 g for 10 mins. Post nuclear supernatant (PNS) was collected, and nuclear fraction discarded. A sample of PNS was retained for western blotting. The PNS was loaded onto a sucrose cushion (2 M) and spun for 30 mins at 11,000 g. The melanosome rich fraction was collected and spun for a further 60 mins at 100,000 g. The resulting pellet was resuspended in 50 µl of HIM buffer. Once resuspended 50 µl of 2x RIPA buffer was added. Samples were analysed by BCA and made up in sample buffer to run by WB.

2.4.5. Protein assay and sample preparation

A BCA protein assay kit was used to determine the protein concentration of collected lysates. Bovine IgG in duplicate was used to create a standard curve. 3 repeats of 3 µl of sample was used for each assay. BCA assay kit reagents were made up in a ratio of 50:1 Reagent A: Reagent B respectively. After addition of the kit reagents, plates were incubated at 37°C for 30 minutes before reading at OD_{562} using a Thermo Labsystems Multiskan Spectrum plate reader. For pierce 660 protein assay, provided protein standards were set up in duplicate to generate a standard curve. 3 repeats of 3 µl of sample was used for each assay. 150 µl of pierce reagent was added per well and incubated at RT for 5 mins before scanning using a Thermo Labsystems Multiskan Spectrum plate reader. Once protein concentrations were determined, samples were diluted to the same concentrations in lysis buffer. Samples were diluted in 5x sample buffer ((312.5mM Tris-HCl, pH6.8, 15% w/v SDS, 50% w/v glycerol, 16% w/w 2-Mercaptoethanol, 0.05% w/v Bromophenol Blue) (to 1x final) before boiling at 95°C for 5 minutes .

2.4.6. Sodium Dodecyl Sulphate Polyacrylamide gel electrophoresis (SDS-PAGE) and Western Blotting

Equal amounts of protein per condition were resolved on a 4-12% Bis-Tris precast NuPAGE gel in MOPS or MES running buffer. In general, gels were run at 150V for 90 minutes. For western blots, resolved proteins were transferred onto a nitrocellulose membrane is transfer buffer (3.03g Tris, 14.4g Glycine, 200ml methanol, topped up to 1L with distilled H20) at a constant current 1A, 25V for 2 hours on ice or 1 hour at RT. Transfer and loading efficiency was preliminarily checked using Poncaeu. Poncaeu staining was removed by incubation in blocking buffer for 5 minutes. Membranes were then transferred into fresh blocking buffer for 1 hour. Unless otherwise stated, membranes were blocked in 5% Marvel milk powder/ TBS-T (0.1% w/v Tween 20). For some antibodies blocking and antibody incubation was in 5% bovine serum albumin (BSA)/ TBS-T. Primary antibodies were then incubated with membranes as per conditions stated in **Table 2.10**. Membranes were then washed 3 x 5 minutes in TBS-T before incubation with the appropriate secondary antibodies, incubation conditions stated in **Table 2.11**. Membranes were washed a further 3x 5 minutes in TBS-T with a final 5-minute wash in TBS. Membranes were scanned using a LI-COR Odyssey imaging system.

2.4.7. Western blot quantification

All quantification for western blots was carried out in Image Studio Lite software. The analysis tab was used to draw around the relevant bands and subtract the background. The final signal values were exported to excel.

Table 2.10 Primary Antibodies used for western blot

Target	Species	Source/Catalogue No.	Incubation Conditions
LRRK2	Mouse	Neuromab N241A/34	1:50, o/n, 4°C
TYRP1	Mouse	Abcam, ab178676	1:1000, 1 hr, RT
PMEL (Pep13)	Rabbit	Dawn Harper and M. Marks Philadelphia	1:200, o/n, 4°C

LAMP1	Mouse	DSHB Iowa, 1D4B	1:100, o/n, 4°C
Rab32	Rabbit	Sigma, SAB4200086	1:1000, 1 hr, RT
Cathepsin D	Rabbit	Cal Biochem, 219361	1:2000, 1 hr, RT
MITF	Mouse	Santa Cruz, SC-56725	1:1000, o/n, 4°C
Actin	Mouse	Proteintech, 66009-1-Ig	1:10000, 1 hr, RT
Actin	Rabbit	Proteintech, 20536-1-AP	1:10000, 1 hr, RT
E Cadherin	Mouse	Cell signalling, 3195	1:1000, o/n, 4°C
MART-1	Mouse	Abcam ab3168	1:200 o/n, 4°C
β-catenin	Mouse	BD Biosciences, 610154	1:1000, 1 hr, RT
N-Cadherin	Mouse	BD Biosciences, 610921	1:1000, 1 hr, RT
Rac1	Mouse	Upstate 05-389	1:1000, 1 hr, RT
TFEB	Goat	Novus Biologicals NB100-1030)	1:400, 1 hr, RT
RAB27A	Sheep	R&D systems AF7245	1:400 o/n, 4°C
RAB10	Rabbit	Cell signalling Technologies 8127	1:1000, 1 hr, RT
pThr73-RAB10	Rabbit	Abcam ab230267	1:1000, 1 hr, RT, BSA
RAB7a	Rabbit	Abcam ab137029	1:1000, 1 hr, RT
pS935-LRRK2	Rabbit	MRX PPU Dundee, Dundee UK	1:1000, 1 hr, RT
VPS35	Goat	Abcam ab10099	1:1000, 1 hr, RT
VPS26	Rabbit	Abcam ab23892	1:400, o/n 4°C
TBC1D5	Mouse	Santa Cruz sc-376296	1:1000, 1hr, RT
HA	Mouse	Covance, MMS-101P	1:1000, 1 hr, RT

Table 2.11: Secondary antibodies used for western blot.

Secondary Antibody	Source/Catalogue No.	Incubation conditions
Donkey anti-mouse IR Dye 800CW	LI-COR (926-32212)	1:10,000, 1 hr, RT
Donkey anti-mouse IR Dye 680CW	LI-COR (926-32222)	1:10,000, 1 hr, RT
Donkey anti-rabbit IR Dye 800CW	LI-COR (926-32213)	1:10,000, 1 hr, RT
Donkey anti-rabbit IR Dye 680CW	LI-COR (926-32223)	1:10,000, 1 hr, RT
Donkey anti-goat IR Dye 800CW	LI-COR (925-32214)	1:10,000, 1 hr, RT
Donkey anti-sheep IR Dye 680CW	LI-COR (92632224)	1:10,000, 1 hr, RT
Goat anti-rat IR Dye 800CW	LI-COR (926-32219)	1:10,000, 1 hr, RT

2.4.8. GST and GST-R7BD Production

For the production of GST fused to the Rab7 binding domain of RILP (GST-RILP) The cDNA for this domain was subcloned into the pGEX-6P-1 backbone vector. The cDNA for the domain was double digested out from pGEX-4T-3-mR7BD plasmid from Addgene alongside a double digest of pGEX-6P-1 destination vector. Digests were run on a 1% agarose gel, and the drop out band and digested backbone were extracted. Vector and insert were ligated together using a T4 DNA ligation reaction, see **Table** 2.6**,** to produce pGEX-6P-1-RILP plasmid.

For production of GST control protein and GST-RILP (GST-mR7BD), plasmids pGEX-6P-1 and pGEX-6P-1-RILP were transformed into BL21 bacteria as in **section 2.3.5**. Colonies were selected on ampicillin LB-Agar plates and picked into a 5-10 ml starter culture grown for 16 hours. The starter culture was inoculated into a 1 or 2-litre maxi culture the following day. The culture was

grown to an OD_{600} of 0.6-0.8. A 1 ml pre-induction sample was taken. Protein production was induced with IPTG (0.5 mM). For GST, bacteria were shaken for 4 hours at 37°C. For GST-RILP, the culture was shaken at 20°C for 20 hours for an overnight induction. A 1 ml post-induction sample was taken. Bacteria were pelleted at 4500 rpm for 15 minutes at 4°C. Pellets were washed with PBS and then re-pelleted as before. Bacteria were flash frozen in liquid nitrogen and stored at -80°C until lysis. Pellets were lysed in PBS + 0.5 mg/ml lysozyme + DNase (10 µg/ml) + Bacterial protease inhibitors (1:500) on ice for 30 minutes. Lysates were sonicated on ice with a sonicator probe set to high for 10 x 20 seconds. Lysates were pelleted in an ultracentrifuge at 100,000 g at 4°C for 25 minutes. The supernatant was filtered before it was run through an ÄKTA purification system.

2.4.9. Running pre- and post-induction pellets

1 ml pre- and post-induction samples were pelleted in a table-top centrifuge and the supernatant was removed. The pellet was resuspended in hot lysis buffer and boiled at 110°C for 10 mins, vortexing every 2 mins. 10x sample buffer was added to samples which were boiled for a further 5 mins at 95°C. Samples were spun at max speed for 5 mins to pellet any debris. 10 µl of samples were loaded onto a gel and run as normal. Resolved proteins were stained with SimplyBlue SafeStain.

2.4.10. Purification of GST using Sepharose beads

1 ml of glutathione-sepharose beads were washed 3x 5 mins in PBS. Washed beads were incubated with the supernatant containing the GST control protein for 4 hours on a wheel at 4°C. The beads were pelleted, and the supernatant was removed. Beads were washed 3x in PBS as before. Bound proteins were eluted using 50 mM Tris-HCL, 10 mM reduced glutathione. Eluted protein was dialysed in 2.5 litres of dialysis buffer (HEPES-KOH (pH 7.6) (20 mM), KCl (100 mM), DTT (0.2 mM) for 2 hours and a fresh 2.5 litres overnight. The concentration of the dialysed protein was measured using a pierce protein 660

assay. Aliquots of recombinant protein were flash frozen in liquid nitrogen and stored at -80°C until ready to carry out the assay.

2.4.11. Purification of GST-RILP using a GSTrap column

The supernatant from lysed GST-RILP pellets was loaded onto an ÄKTA purification system and GST-RILP protein was captured on a 1 ml GSTrap column. The column was washed with 3 ml PBS (3 column volumes) to remove sticky proteins. Bound proteins were eluted from the column with 50 mM Tris-HCL, 10 mM reduced glutathione. 500 µl fractions were collected and a UV trace was used to determine which fractions contained GST-RILP. Relevant fractions were pooled for buffer exchange. PD10 columns were equilibrated with GST storage buffer (10% glycerol, 50 mM Tris (pH 7.4), 150 mM NaCl, 5 mM $MgCl_2$, and 1 mM DTT). The pooled fractions were spun through the column to remove reduced glutathione and exchange GST-RILP into storage buffer. Aliquots of the purified protein were flash frozen in liquid nitrogen and stored at -80°C until ready to use for assay. Collected fractions were also run by SDS-PAGE and the gel stained with Simply blue Safe stain to determine purity of collected fractions. This work was carried out in collaboration with Katy McCarron.

2.4.12. GST-RILP-Rab7 pulldown assay

The night before the assay, 20 µl of sepharose beads per condition were washed 3x in PBS. GST or GST-RILP recombinant protein (250 µg/ml) was added to the washed beads and incubated on a wheel in the cold room overnight. The morning of the assay, beads were washed 3x in assay wash buffer (Tris-HCl (pH7.8, 20 mM), NaCl (50 mM), $MgCl_2$ (3 mM)). On the day of the assay cells were lysed in a high magnesium buffer (Tris-HCl (pH 7.8, 20 mM), NaCl (50 mM), 0.5% Triton x-100, 1 mM $MgCl_2$, Roche protease inhibitor without EDTA) for 15 mins on a wheel in the cold room. Lysates were clarified at 21,000 g for 20 mins. Protein concentrations were determined using a BCA assay kit. Samples were made up to the same concentration and a 50 µg input was taken per sample. 250-800 µg of sample was incubated with GST or GST-

RILP beads for 2 hours at 4°C on a wheel. Beads were pelleted and the unbound fraction discarded. Beads were washed 3 times in assay wash buffer (Tris-HCl (pH7.8, 20 mM), NaCl (50 mM), $MgCl_2$ (3 mM)). Washed beads were dried, and bound proteins were eluted in 2x sample buffer. Beads were boiled at 95°C for 5 mins and eluted proteins were resolved by SDS-PAGE.

2.4.13. Immunofluorescence

The type of fixation used was selected based on the primary antibody datasheet guidelines and in some cases both methods were tried in the optimisation. The fixation method used in each experiment is stated in the figure legends. Details of antibody dilutions and incubation is listed in **Table 2.12**. Cells were seeded onto glass coverslips on day 1 of the experiment. siRNA and drug treatments were carried out as indicated for each experiment. For methanol fixed coverslips, cells were washed with room temperature PBS before fixing with 1 ml ice cold methanol for 5 minutes at -20°C. For PFA fixed coverslips, cells were washed twice with room temperature PBS before fixing with 1 ml 4% PFA in PBS for 15 minutes. The reaction was quenched with 50 mM NH_4Cl for 10 minutes. Coverslips were then permeabilised with 0.2% Triton x-100 for 4 minutes. For staining, unless otherwise stated, coverslips were blocked in 10% Goat serum in PBS for 30 minutes. Coverslips were then incubated with the primary antibody diluted in 5% goat serum unless otherwise indicated in **Table 2.12**. Coverslips were washed 3x 4 minutes in PBS followed by incubation with the relevant secondary antibody for 30 mins (
Table 2.13). Coverslips were washed 3x 4 minutes before being dipped in Millipore H_2O and mounted onto glass slides using Mowiol with or without 1:5000 DAPI. Coverslips were dried overnight then stored at 4°C.

Table 2.12 Primary antibodies used for immunofluorescence

Target	Species	Source/Catalogue Number	Fixation/Dilution
TYRP1 (TA99)	Mouse	Abcam, ab3312	PFA 1:200 BSA + saponine, 1 hr
PMEL (Pep13)	Rabbit	Dawn Harper and M.Marks, Philadelphia, USA	PFA 1:200, 1 hr
PMEL (HMB45)	Mouse	Abcam, ab787	PFA 1:200 BSA + saponine, 1 hr
LAMP1	Mouse	DSHB Iowa, ID4B	PFA 1:100, 1 hr
EEA1	Mouse	BD Transduction Laboratories, 610456	PFA 1:2000, 1 hr
TOMM20	Rabbit	Sigma, HPA011562	PFA, 1:1000, 1hr
CIMPR	Rabbit	Gifted by Paul Luzio	PFA, 1:500, 1 hr
Rab7	Rabbit	Abcam, ab137029	PFA, 1:500, 1 hr
F-Actin	488 Conjugated	Invitrogen, A12379, Phalloidin -488	PFA, 1:40, 1 hr
HA	Mouse	Covance MMS-101P	PFA, 1:1000, 1 hr
HA	Rat	Roche 11867423001	PFA, 1:500, 1 hr
p230	Mouse	BD 611281	PFA, 1:500, 1 hr
HRS	Goat	Everest Biotech. EB07211	MeOH, 1:200, 1hr
LAMP2	Mouse	DSHB Iowa, H4B4	PFA, 1:50, 1 hr
FAM21	Rabbit	Abcam ab137029	PFA/MeOH, 1:1000, 1 hr
WASH	Rabbit	Atlas HPA002689	PFA, 1:100, 1 hr

Table 2.13 Secondary antibodies used for immunofluorescence

Secondary Antibody	Source/ Catalogue Number	Incubation
Donkey anti-mouse AF488	Invitrogen, A21202	1:500
Donkey anti-mouse AF594	Invitrogen, A21203	1:500
Donkey anti-rabbit AF488	Invitrogen, A21206	1:500
Donkey anti-rabbit AF594	Invitrogen, A21207	1:500
Donkey anti-sheep AF594	Invitrogen, A11016	1:500
Donkey anti-rat AF647	Invitrogen A21247	1:500

2.5. Live and fixed cell imaging and quantification

2.5.1. Live Imaging

Confocal live imaging experiments were carried out using a Marianas spinning disk confocal microscope (3i, Intelligent Imaging Innovations, Germany) with a Plan-Apo 63x/ 1.4NA Oil objective M27. All live cell imaging was carried out at 37°C, 5% CO_2 in a humidified chamber for live cell imaging.

2.5.2. Fixed Cell imaging

Widefield brightfield and fluorescence images were acquired with a NIKON Ti-Eclipse Microscope with a CFI Plan Fluor DLL 10X objective, a CFI Plan Apo 40x objective or a CFI Plan Apochromat VC 60X objective lens. Confocal images were acquired with a Marianas spinning disk confocal microscope (3i, Intelligent Imaging Innovations, Germany) with a Plan-Apo 40x/1.3NA oil objective M27 or a Plan-Apo 63x/ 1.4NA Oil objective M27. Confocal images

were also acquired using a Zeiss LSM800 or Zeiss LSM900 with Airyscan confocal laser scanning microscope (CLSM) using a 63x 1.4 NA Zeiss Plan Apochromat objective or a 40x LD C-Apochromat objective.

2.5.3. Electron microscopy

Samples for EM were plated on day 1 and treated with MLi-2 as indicated for each experiment. Cells were fixed and processed for EM by Alison Beckett at the Biomedical Electron Microscopy unit at the University of Liverpool. Samples were mounted onto grids and images were acquired using a FEI 120kV Tecnai G2 Spirit BioTWIN TEM microscope.

2.5.4. ER-Mitochondria contact site quantification

Images were acquired at 4200x, imaging the whole cell. The total perimeter of mitochondria per image was measured first using the ROI tool in FIJI. Mitochondria were categorised based on the number of contact sites per mitochondria. The length of each contact site was measured using the free hand line tool. Contact sites were defined as the ER and mitochondrial outer membrane being within 30 nm of each other.

2.5.5. LysoTracker quantification

For LysoTracker images, the background labelling was too high to be able to resolve individual punctae. Therefore, the total intensity per cell was measured to quantify acidic organelles. Images were thresholded and the total intensity of each cell was measured using the ROI selection tool.

2.5.6. LAMP1 quantification

For the analysis of LAMP1 positive vesicles, the analyse particles tool in FIJI was used. Cells were selected using the ROI tool. LAMP1 positive vesicles were identified, and the number of spots was measured from thresholded images.

2.5.7. TGN morphology quantification

To analyse the morphology of the TGN, images from cells stained with p230 were used. For the mixed RPE1 Flp-In clones, cells were co-stained with HA to ensure that only positive cells were quantified. The ROI selection tool in FIJI was used to draw around the space occupied by the TGN and the area of each ROI was taken.

2.5.8. Phalloidin cell morphology quantification

To identify cell morphology changes with LRRK2 inhibition, cells were drawn around using the ROI selection tool in FIJI. The shape descriptors tool was selected in the “set measurements” window in FIJI. The roundness and aspect ratio measurements were then taken for each cell.

2.5.9. Cell tracking analysis

Time lapse images of WM266.4 cells (**section 2.2.9**) were uploaded into MATLAB CellTracker graphic user interface (GUI). The manual tracking feature was used to generate tracks for individual cells. These manual tracks were used to generate coordinates which were then input into Chemotaxis software (ibidi). Chemotaxis software was used to generate data for individual cells including the accumulated distance.

2.5.10. OPERA imaging

For fluorescent images taken in Sheffield, an OPERA Phoenix High Content Screening Imaging System was used. The objective used is indicated in individual figure legends. For imaging with the OPERA, cells were seeded into glass bottom, black-walled 96 well plates.

2.5.11. Opera imaging quantification

Quantification measurements from OPERA images were taken using Harmony High Content Imaging and Analysis Software from PerkinElmer. The

total cell area across images to be analysed was selected using a minimum signal parameter. The number of nuclei per image was also counted for per cell calculations. LAMP1, Rab7, and Magic Red positive puncta were counted using the find spots tool. Parameters were kept the same across each condition to ensure there wasn't any bias in the analysis. A schematic of the work-flow is depicted in **Figure 2.7**.

2.5.12. IN Cell Analyser 2200 imaging

For brightfield images of neurons taken over their differentiation, an IN Cell Analyser 2200 imaging system (GE healthcare) was used. Images were taken in the last 15 days of the differentiation protocol. Images were acquired with a 10X objective in brightfield only. Random fields of view from wells were acquired to prevent bias.

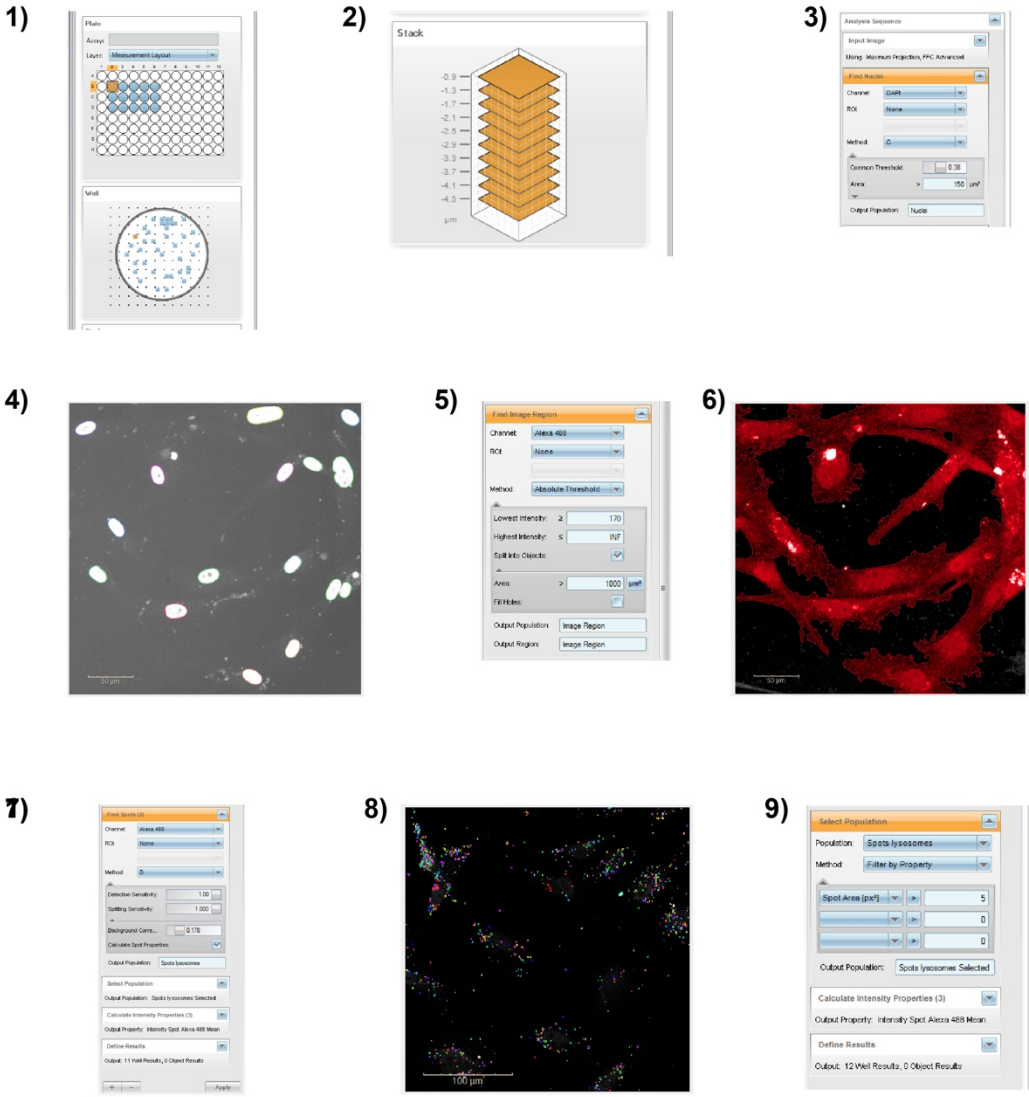

1) Select well(s) and position(s) to be analysed
2) Select Z planes to be analysed
3) Set paramaters to find nuclei
4) Find nuclei example
5) Set parameters to find image region
6) Find image region example
7) Set parameters to find spots
8) Find spots example
9) Select population to be counted based on spot size
10) Select population example

Figure 2.7 Schematic of OPERA Image quantification workflow

3. Chapter 3: Generation and Optimisation of Project tools

3.1. Introduction

It is now well accepted that Parkinson's disease (PD) and melanoma are linked; in contrast to the relationship between PD and all other types of cancer, there is a higher incidence of melanoma in PD patients relative to the general population (Huang et al., 2015). However, there has been no progress in determining the molecular mechanisms which link these two seemingly unrelated diseases. One of the issues faced when addressing such a question is that 85-90 % of PD patients are idiopathic, meaning there is no specific target to pursue. It has not been determined whether one of the identified familial genes in PD is relevant to the link between dopaminergic neuron loss and melanoma. It is, however, interesting that the substantia nigra, the primary region of the brain affected by PD, is pigmented, which provides a loose link between the cell types affected by the two diseases.

For my project, my aim was to look at specific aspects of LRRK2 function within melanosomes and melanoma. One reason for pursuing this avenue is that LRRK2 is the most commonly mutated gene in familial PD, and so has the widest reach of familial pathogenic targets. Another compelling reason for selecting LRRK2 as the primary focus is the high level of LRRK2 expression across melanoma cell lines, as can be observed by referring to the Cancer Cell line Encyclopaedia (**Figure 3.1**) (Broad institute, MIT and Harvard) https://portals.broadinstitute.org/ccle (Barretina et al., 2012) .

The work carried out in this chapter generating Flp-In cells and establishing the GST-RILP pulldown assay was carried out in collaboration with Katy McCarron.

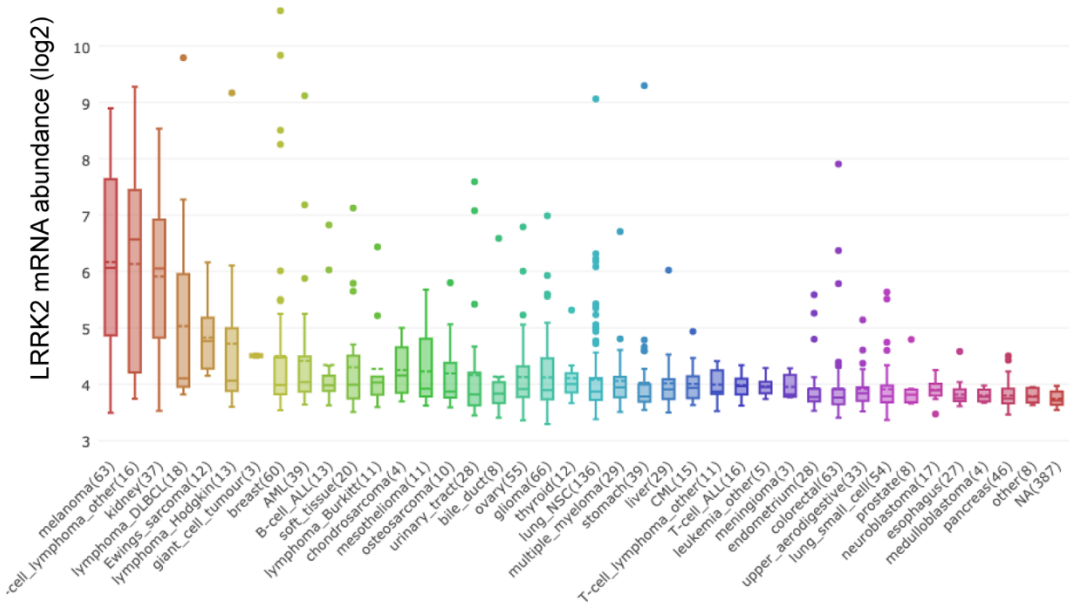

Figure 3.1 LRRK2 mRNA abundance across cell lines
Plot showing mRNA expression of LRRK2 across cancer cell lines taken from the Cancer Cell Line Encyclopaedia. Data are gene expression profiles of 917 human cancer cell lines. The number of lines used for each cancer type is shown in brackets. mRNA abundance for each line obtained using Affymetrix U133 plus 2.0 arrays. RMA normalisation was used. Data is shown as log2 gene expression signal. (Barretina et al., 2012) https://portals.broadinstitute.org/ccle

3.2. Characterisation of cell lines expressing endogenous LRRK2

3.2.1. LRRK2 is highly expressed across melanoma cells

I determined the endogenous levels of LRRK2 expression across both melanoma and non-melanoma cell lines by probing lysates available in the laboratory by western blotting. The melanoma cell lines tested were A375P, 501-mel, WM266.4 and MNT1 cell lines, a mixture of pigmented and non-pigmented lines. The non-melanoma cell lines included RPE1, SK-N-BE-2, SH-SY5Y and HeLa lines (**Figure 3.2A**). I also looked at pigmentation markers across these cell lines such as melanogenic transcription factor MITF, and late melanosome markers TYRP1 and MART-1 (**Figure 1.10**). Western blotting showed the levels of LRRK2 protein were higher in the melanoma cell lines

relative to the non-melanoma cell lines. LRRK2 signal was quantified using Image studio software (LI-COR) to measure the total intensity of the LRRK2 band (**Figure 3.2B**). This is consistent with the data from the Cancer Cell Line Encyclopaedia (CCLE) which indicates that there is an enrichment of LRRK2 across melanoma cell lines.

This pattern observed in **Figure 3.2** also suggests an inverse relationship between LRRK2 and pigmentation markers; in cell lines where levels of LRRK2 are high, the levels of pigmentation proteins are low. For example, the highest levels of LRRK2 were seen in the WM266.4 cell line. This is a highly metastatic, non-pigmented and advanced melanoma cell line, which has largely lost expression of MITF, TYRP1 and MART-1 in accordance with the loss of pigmentation in this cell line. Comparatively, the levels of LRRK2 are approximately 6-fold lower (**Figure 3.2B**) in the MNT1 cell line- a melanoma cell line which has retained its pigmentation along with high levels of expression of pigmentation-related proteins. It is also noteworthy that the non-melanoma cell line which showed the highest levels of expression of LRRK2 was the hTERT-immortalised retinal pigmented epithelial (RPE1) cell line which has a low level of pigmentation.

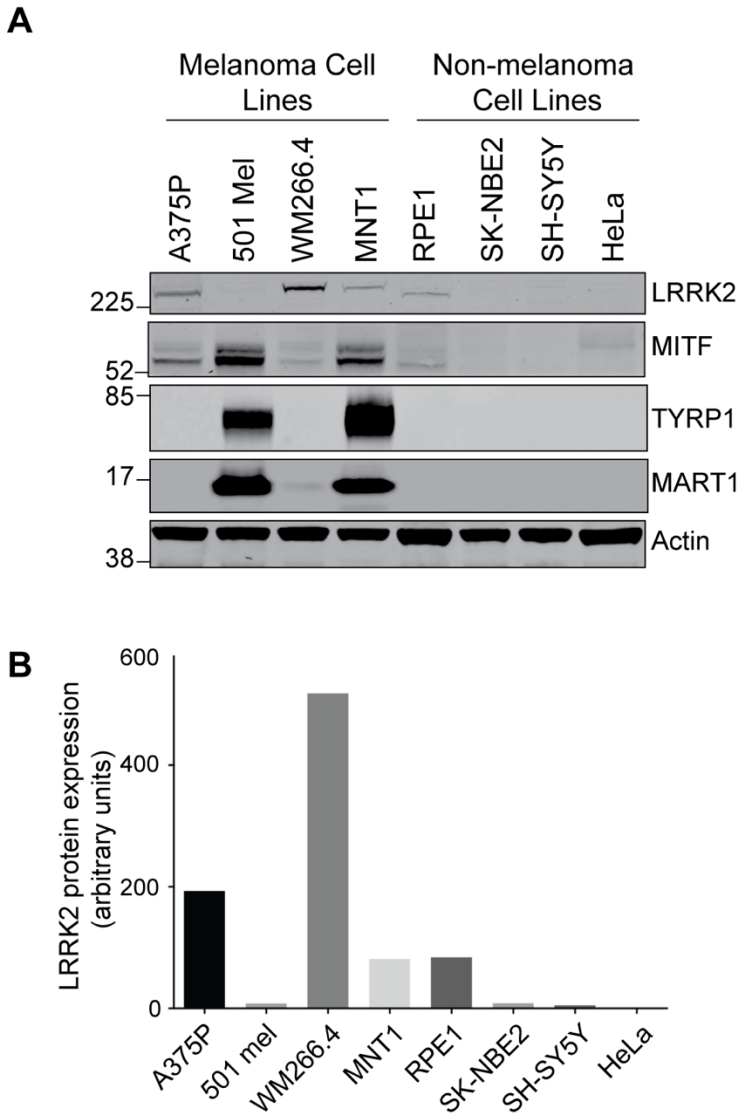

Figure 3.2 Protein expression of LRRK2 and melanosome markers across a panel of melanoma and non-melanoma cell lines.
A 20 µg of protein per cell line was resolved by SDS-PAGE and analysed by western blotting. Lysates were probed for LRRK2, as well as melanogenesis markers MITF, TYRP1 and MART-1. **B** LRRK2 protein signal across cell lines was quantified using LI-COR image studio software with no normalisation. n=1.

3.2.2. Western blotting as a readout for LRRK2 activity

The majority of pathogenic mutations identified in LRRK2 result in hyperactive kinase activity (West et al., 2005). This makes LRRK2 inhibitors attractive as potential therapeutic agents. As a result, there are a number of commercially available LRRK2 inhibitors suitable for use in the laboratory. These include GNE-0877 (GNE), GSK2578215A (GSK), HG-10-102-01 (HG-10) and MLi-2 (Estrada et al., 2014; Choi et al., 2012; Fell et al., 2015; Reith et al., 2012). Furthermore, the discovery that LRRK2 phosphorylates a subset of Rab proteins, including Rab10, has led to the development of a phospho-specific Rab10 antibody. This recognises Rab10 phosphorylated at the LRRK2 target site-threonine 73 (Thr73) (Lis et al., 2018). Lysates from WM266.4 cells treated with one of these distinct LRRK2 inhibitors were run via western blot and the level of LRRK2 inhibition was measured by the reduction in phosphorylation of Rab10 at Thr73 (**Figure 3.3A**). For all inhibitors, reduction in Rab10 phosphorylation shows effective inhibition of LRRK2 kinase activity, with MLi-2 being the most effective inhibitor. LRRK2 contains an autophosphorylation site at serine 1292. However, the efficiency of the antibody for this site varies greatly between cell lines and has not been used in this project. LRRK2 possesses a number of upstream kinase sites, including serine 935, which become rapidly dephosphorylated upon LRRK2 inhibition. There has been much speculation about which kinases phosphorylate LRRK2 at these sites, and many candidates have been proposed including casein kinase 1α (CK1α), the IκB family and protein kinase A (PKA) (Berwick et al., 2019). Lysates from WM266.4 cells treated with 40 nM siRNA targeting LRRK2, or MLi-2 LRRK2 inhibitor, were run by western blot (**Figure 3.3B**). The reduction in total and pSer935-LRRK2 as well as pThr73-Rab10 in the siRNA treated cells demonstrates effective depletion of LRRK2. Reduction of both pSer935-LRRK2 and pThr73-Rab10 (but not total LRRK2) in MLi-2 treated cells shows effective inhibition of LRRK2 activity. These results show that both the antibody against pSer935-LRRK2 and pThr73-Rab10 are viable readouts for LRRK2 activity in WM266.4 cells, and that both siRNA depletion and chemical inhibition are effective ways of depleting LRRK2 activity.

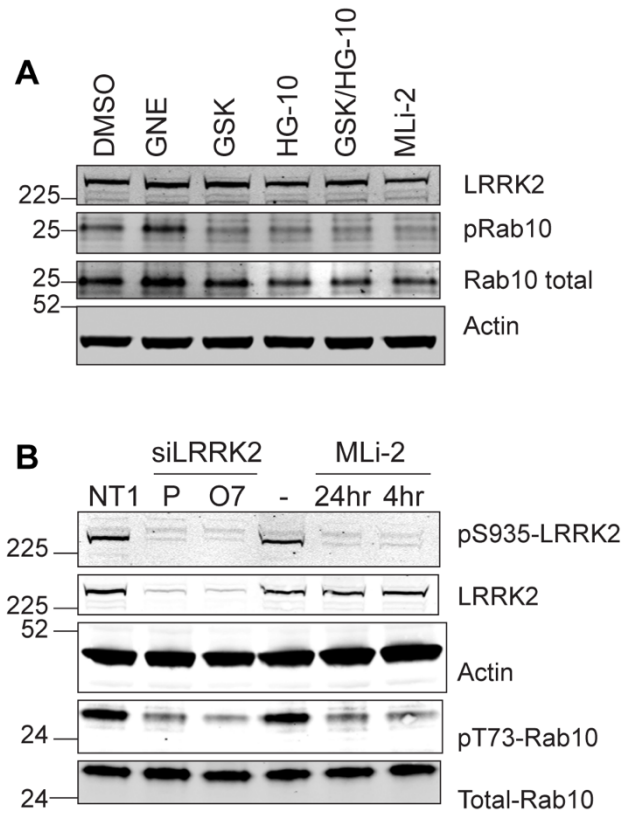

Figure 3.3 LRRK2 kinase activity can be depleted by chemical inhibition and siRNA depletion
A Lysates from WM266.4 cells treated with LRRK2 inhibitors for 24 hours (500 nM except for MLi-2 which was 200 nM) were analysed by western blotting probing for the indicated antibodies. n=1. **B** Lysates from WM266.4 cells treated with either 40 nM siRNA (Smartpool (SP) or single oligonucleotide (O7)) for 72 hours, or MLi-2 inhibitor (200 nM) for the indicated time points were analysed by western blotting probing for the indicated antibodies. n=1.

3.2.3. Optimisation of Reagents in WM266.4 cells

HG-10-102-01 (HG-10) and MLi-2 were selected as the most effective LRRK2 inhibitors guided by the western blot data presented in **Figure 3.3A**. Depletion of LRRK2 with 40 nM siRNA for 72 hours was tested using both a pool of 4 oligonucleotides and an individual oligonucleotide. Lysates from siRNA knockdowns were analysed by western blot. Probing with LRRK2 antibody revealed effective depletion of LRRK2 by both the pool and single oligonucleotides (**Figure 3.4A**). To inhibit LRRK2 kinase activity, cells were treated with two concentrations of HG-10 for 48 hours. The level of inhibition was measured with the pS935-LRRK2 antibody. Results showed HG-10 treatment for 48 hours at 500 nM strongly inhibited LRRK2 activity. Replenishing media after 24 hours was deemed unnecessary.

WM266.4 cells were treated with MLi-2 across two concentrations and multiple time points. Lysates were analysed by western blot and the efficiency of inhibition was determined using the pS935-LRRK2 antibody (**Figure 3.4B**). 200 nM was deemed the optimal concentration for LRRK2 inhibition. A time course of MLi-2 inhibitor was carried out in WM266.4 cells and lysates probed with pThr73-Rab10 antibody. (**Figure 3.4C**). The level of pThr73- Rab10 was depleted 1-hour post-treatment and did not decrease further with the longer time points. Therefore, acute inhibition of LRRK2 is sufficient to reduce the phosphorylation status of Rab10.

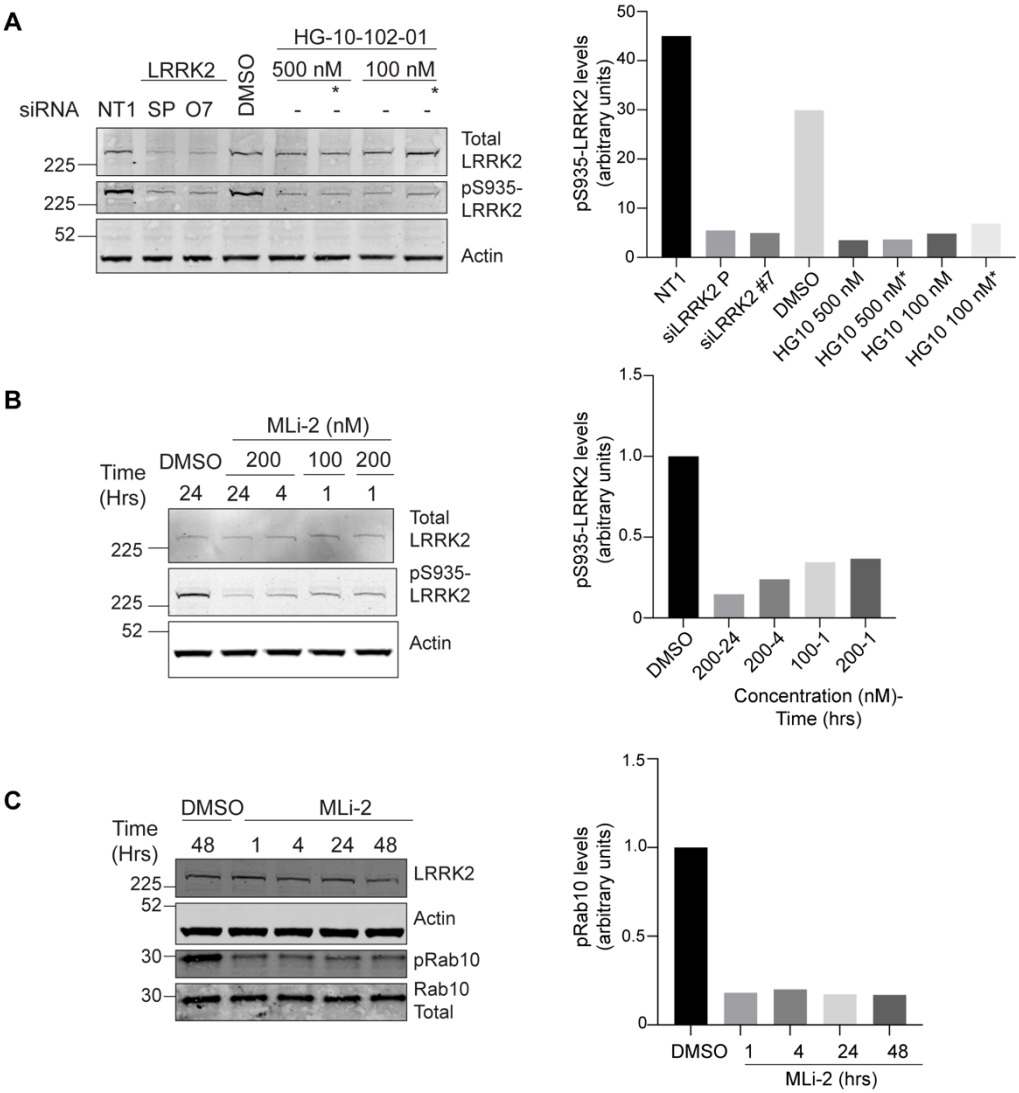

Figure 3.4 Optimisation of LRRK2 reagents in WM266.4 cells **A** Lysates from WM266.4 cells treated with HG-10-102-01 (HG-10) for 48 hours, or 40 nM siRNA for 72 hours, were analysed by western blotting probing for the indicated antibodies. Lanes marked with a * had their media exchanged with fresh inhibitor after 24 hours. n=1. **B** Lysates from WM266.4 cells treated with MLi-2 at the indicated concentrations and time points were analysed by western blotting probing for the indicated antibodies. n=1. **C** WM266.4 cells treated with a time course of MLi-2 (200 nM) were lysed and analysed by western blotting probing for the indicted antibodies. n=1. All quantification was carried out in image studio lite software.

3.2.4. Melan-a cells as a pigmented model for studying LRRK2

WM266.4 cells were selected as a non-pigmented melanoma model due to their high level of expression of LRRK2. For a pigmented model, MNT1 cells were initially considered due to their relatively high level of expression of LRRK2 relative to other pigmented melanoma cell lines (**Figure 3.2**). However, due to their high pigmentation, the length of time you can culture MNT1 cells before they reach maximal pigmentation is very limited. As we were interested in studying pigmentation, the Melan-a cell line was selected as the main pigmented model for this study. Melan-a cells are a non-tumorigenic, immortalised, mouse melanocyte cell line which are pigmented at a much lower level relative to the MNT1 cell line (Bennett et al., 1987). As with the WM266.4 cell line, the efficiency of depleting LRRK2 levels and activity by siRNA and inhibition was tested. We also tested the ability of the pThr73-Rab10 antibody to detect changes in LRRK2 activity in a mouse cell line. 72-hour depletion with both a pool of siRNA oligonucleotides as well as single oligonucleotides targeting LRRK2 resulted in depletion of LRRK2 protein levels (**Figure 3.5A**). A time course of the MLi-2 inhibitor was carried out in Melan-a cells and protein lysates were analysed by western blot (**Figure 3.5B**). As seen by a reduction in pThr73-Rab10, inhibition of LRRK2 was seen as early as 1-hour post-treatment, consistent with data from WM266.4 cells.

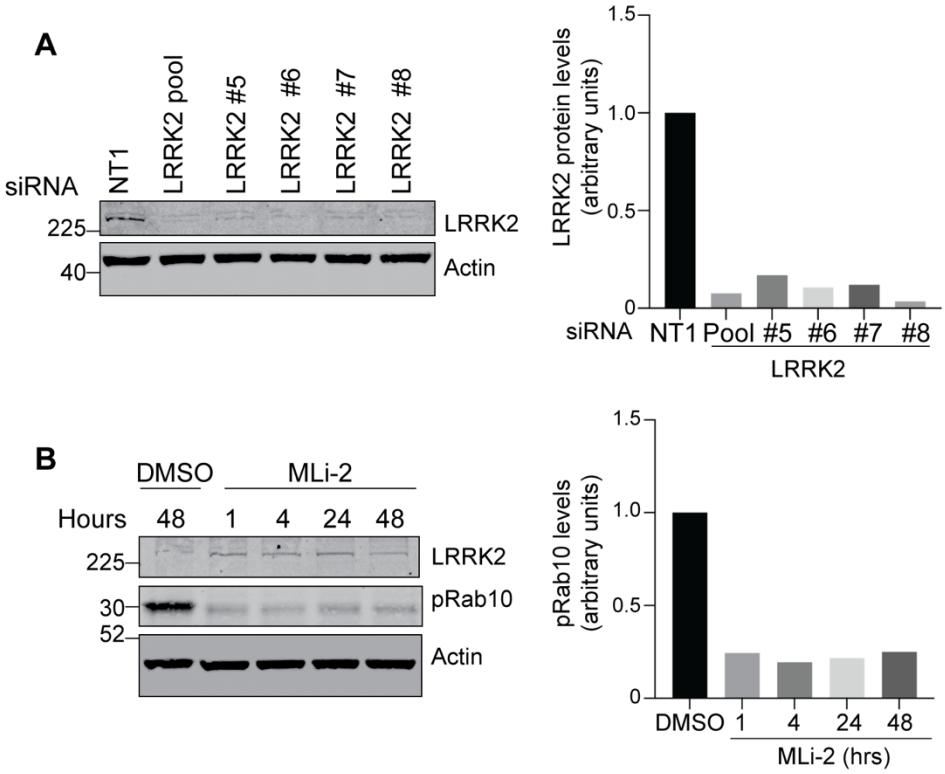

Figure 3.5 Optimisation of reagents in Melan-a cells
A Lysates from Melan-a cells treated with 40 nM siRNA targeting LRRK2 for 72 hours were analysed by western blotting, probing for the indicated antibodies. n=1. **B** Lysates from Melan-a cells treated with a time course of MLi-2 (200 nM) were analysed by western blotting, probing for the indicated antibodies. n=1. For **A** and **B,** bands were quantified using image studio lite software. Samples were normalised to actin and the control sample.

3.3. Generating Project tools

3.3.1. GST-RILP Protein production

One of the aims of this project was to determine if there is a link between the effect of hyperactive LRRK2 on Rab7 activity and the effect of VPS35 knockout on Rab7 activity (Jimenez-Orgaz et al., 2018; Gómez-Suaga et al., 2014) (see Section 1.4.16). The PD-related mutation [D620N] in VPS35 has been found to hyperactivate LRRK2 kinase activity, resulting in hyperphosphorylated Rab proteins. This is in contrast to loss of VPS35 which was shown to suppress LRRK2 kinase activity (Mir et al., 2018). We therefore

wanted to determine if VPS35's action on Rab7 activity is via LRRK2 or an independent pathway.

To answer this question, it was important to have a reliable assay to measure the activity levels of Rab7. To do this, we set up an already characterised assay within the laboratory. The assay exploits the Rab7 binding domain of RILP (mR7BD), which is only able to bind to "active" or GTP-bound Rab7 (Sun et al., 2009) (**Section 2.4.12**). This domain was produced by protein preparation with a GST tag attached. The GST tag was used to bind the recombinant protein to glutathione beads which were used to pull down active Rab7 from cell lysates. cDNA for mR7BD was digested out from the pGEX-4T3-mR7BD construct from Addgene. The excised insert was then ligated into pGEX-6P-1 vector backbone to generate GST-mR7BD. This was preferable as the pGEX-4T3 backbone has a thrombin cleavage site between the GST tag and the gene of interest (GOI), whereas pGEX-6P-1 has a precision cleavage site between GST and the GOI. The precision cleavage site is a longer linker and is more stable than the thrombin site, meaning less of the produced protein is cleaved from the tag (**Figure 3.6A**). The pGEX-6P-1-mR7BD construct was transformed into BL21 competent E. coli and positive colonies were picked into a starter culture overnight. The following day the starter culture was used to inoculate a 2-litre culture. GST-RILP expression was induced with IPTG, followed by shaking for 20 hours at 20°C. Pre- and post-induction sample pellets were run on a gel to check efficiency of induction (**Figure 3.6B**). Gels showed successful induction of GST-RILP production indicated by the band appearing in post induction samples indicated with a *.

Bacterial pellets were lysed with sonication on ice and lysates were clarified by ultracentrifugation at 100,000 g for 20 minutes. The supernatant was filtered and GST-RILP protein was immobilised by running samples through a GSTrap column using an AKTA chromatography system. Once bound to the column, GST-RILP was eluted using reduced glutathione. The UV trace over the course of the elution was used to determine which fractions to collect (**Figure 3.7A**). Fractions were also run on a gel to determine the purity of

fractions collected (Figure 3.7B). Fractions A3-A9 were selected to be pooled. The gel showed that the purification was clean, however, the presence of a lower band indicated the purification of some GST alone.

3.3.2. Validation of GST-RILP Rab7 Binding assay

To check that the GST-RILP produced was suitable for pulling down GTP-bound Rab7, HEK293 Flp-in cells were transfected with constructs expressing either: GFP, GFP-Rab7 WT or a GFP-dominant negative form of Rab7 (GFP-Rab7 DN). Transfections were also carried out for LRRK2 constructs; however, the transfection efficiency was very low for these samples, and they should be disregarded. 24 hours after transfection cells were lysed in Rab7 assay lysis buffer and an input sample was taken. Lysates were incubated with GST-RILP beads and bound proteins were eluted. Samples were analysed by immunoblot for Rab7 (Figure 3.8). The levels of total Rab7 in WT and DN transfected inputs are comparable. Transfection with GFP-Rab7 gave a strong band in the GST-RILP pulldown lane, much stronger than the endogenous active Rab7. This band was not present in the GFP-Rab7 DN transfected lane. GST control protein was also produced and no Rab7 was pulled down with beads conjugated to GST alone (Appendix 1). This data shows that the GST-RILP Rab7 binding assay is specific and an accurate readout for Rab7 activity. We also validated the assay by knocking down TBC1D5. TBC1D5 is a Rab7 GAP. Therefore, depletion of TBC1D5 should increase the levels of GTP-bound Rab7. RPE1 Flp-In parental cells were treated with siRNA targeting TBC1D5 and the assay carried out as above. Input and pulldown samples were run by western blot (Figure 3.9). Depletion of TBC1D5 resulted in a clear increase in GTP-bound Rab7, with no increase in the total Rab7 in the input samples. This result is what we would expect and shows that the GST-RILP Rab7 binding assay is specifically pulling down active Rab7.

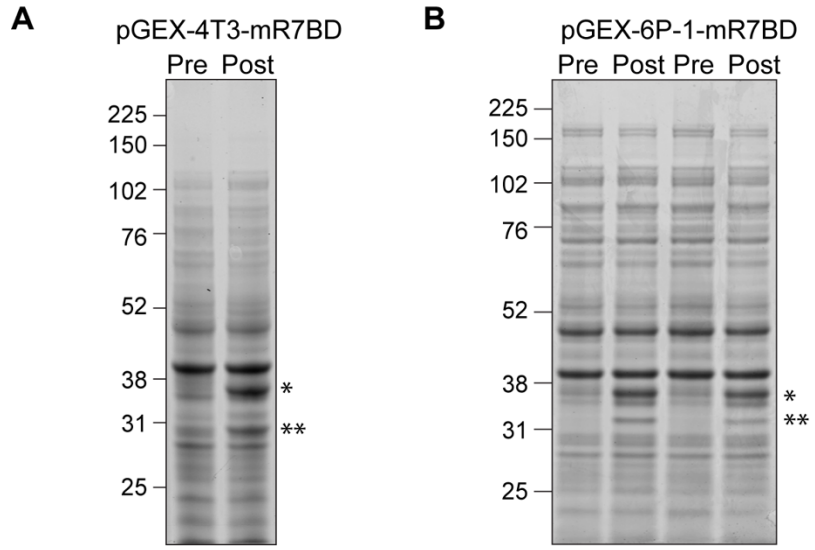

Figure 3.6 Induction of GST-RILP Protein expression in BL21 bacteria

A BL21 bacteria were transformed with pGEX-4T3-mR7BD plasmid and selected on Amp plates. Positive colonies were picked into a starter culture which was used to inoculate a 1 litre maxi culture. **B** BL21 bacteria were transformed with pGEX-6P-1-mR7BD plasmid and selected on Amp plates. Positive colonies were picked into a starter culture which was later used to inoculate two 1 litre maxi cultures. For both **A** and **B** cultures were grown to an OD_{600} of 0.6 and a pre-induction sample was taken. Protein expression was induced with IPTG (0.5 µM). Bacteria were shaken for 20 hours at 20 °C and a post- induction sample was taken. Pre- and post-induction samples were resolved by SDS-PAGE and gels stained for total protein. The band indicating induced GST-RILP expression is indicated with a * and GST alone is indicated with **.

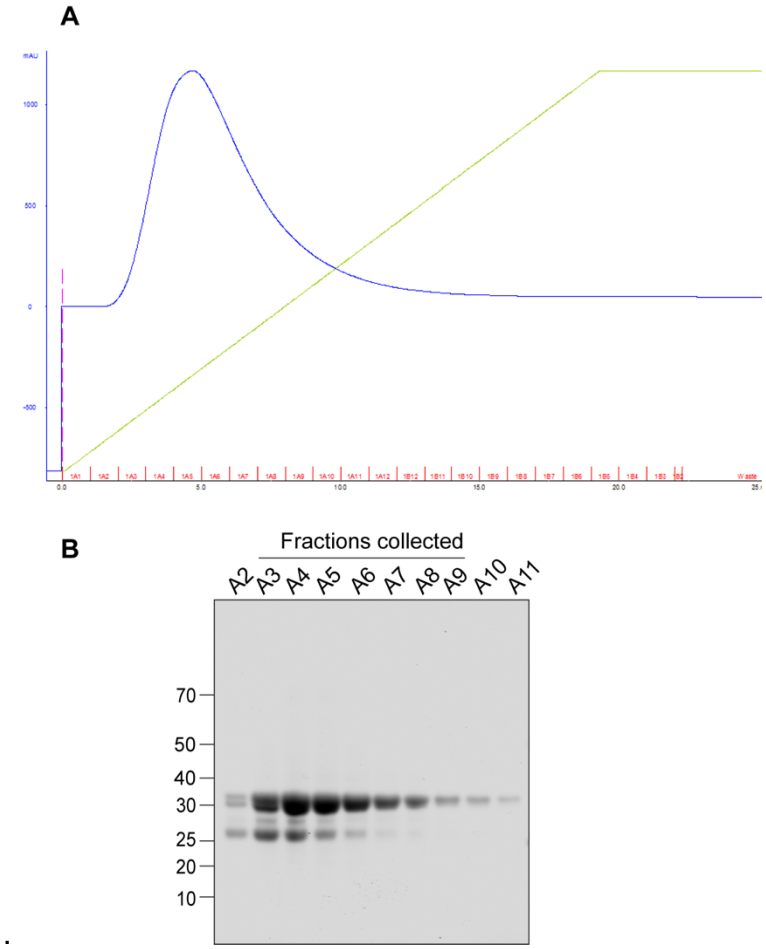

Figure 3.7 Purification of GST-RILP Protein
Lysates from induced BL21 bacterial pellets were passed through an AKTA purification system and GST-tagged proteins were collected using a GSTrap column. Bound proteins were eluted with reduced glutathione (10 mM) in 500 µl fractions. **A** A UV trace was used to determine which fractions contained GST-RILP. The blue line shows the UV trace. The fractions are indicated by red intervals. The increasing concentration of the reduced glutathione gradient is indicated by the green line. The pink dashed line shows the sample injection at the beginning of the run. **B** Collected fractions were resolved by SDS-PAGE and stained for total protein to determine their purity.

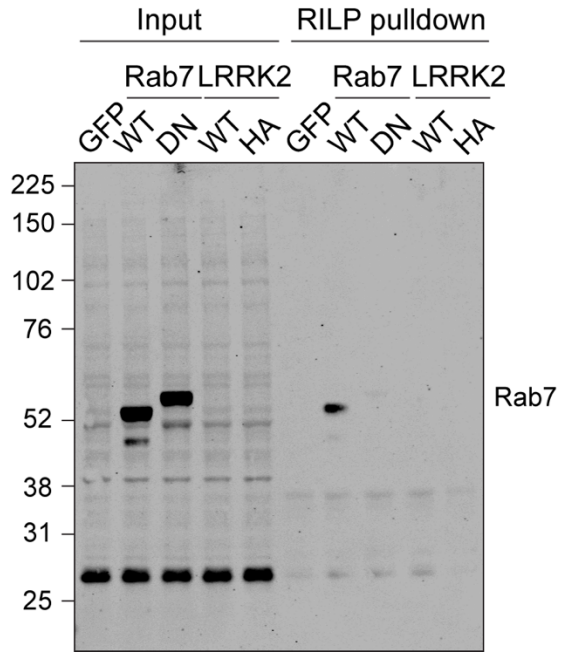

Figure 3.8 Validation of GST-RILP Rab7 binding assay
HEK293 Flp-In cells were transfected with the indicated constructs containing either GFP or a GFP-tagged Rab7 protein or a GFP-tagged LRRK2 protein (WT-Wild type, DN-dominant negative, HA-Hyperactive). 24 hours after transfection, cells were lysed, and samples were incubated with GST-RILP beads for 2 hours. Captured proteins were eluted and analysed by western blot probing for Rab7. n=1.

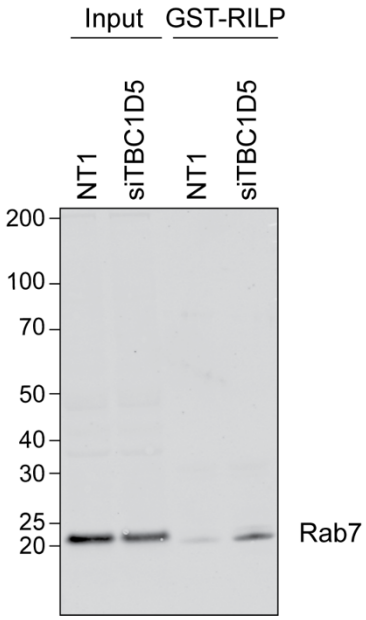

Figure 3.9 Validation of GST-RILP Rab7 binding assay with TBC1D5 depletion
RPE1 Flp-In parental cells were treated with 40 nM siRNA targeting TBC1D5 for 72 hours. Cells were lysed and samples were incubated with GST-RILP beads for 2 hours. Captured proteins were eluted and analysed by western blot probing for Rab7. n=1.

3.3.3. Generating VPS35 Flp-In plasmids

Another useful tool we wanted to establish for the project were RPE1 Flp-In T-REx cell lines with control WT VPS35 and PD related mutant [D620N] VPS35. This cell line was selected for multiple reasons. It is a diploid cell line which is commonly used in my laboratory. We have an already established work-flow for generating knockouts in these cells which may be useful for further studies. These cells express a reasonable level of LRRK2 (**Figure 3.2**). RPE1 cells are also lightly pigmented which gave the possibility of cross talk between this branch of my project and the melanocyte work. We also wanted to use the Flp-In system as this would allow us to have inducible control over the expression of exogenous VPS35 (**Section 2.1.4**).

pCDNA5 FRT/TO HA VPS35 (WT and [D620N]) plasmids were obtained from Dundee. These plasmids use hygromycin as the selection marker. RPE1 Flp-

In cells are already resistant to hygromycin (Bodnar et al., 1998). Therefore, we generated plasmids which use neomycin (G418) as the antibiotic selection. The HA-VPS35 WT and HA-VPS35 [D620N] inserts were amplified by PCR with appropriate restriction sites for subcloning into the new backbone. The destination vector used was a pCDNA5/ FRT/TO Neo plasmid containing the G418 resistance gene. Double digests of the PCR products and the destination vector were then ligated together using a T4-DNA ligase reaction. All methodologies for subcloning are outlined in more detail in **Section 2.3**.

3.3.4. Generating and screening RPE1 Flp-In VPS35 cell lines

RPE1 Flp-In parental cells were transfected with a pCDNA5/FRT/TO Neo VPS35 plasmid (WT or [D620N] mutant) alongside a pOG44-Flp recombinase expression plasmid. Transfected cells were split 1:4 from a 6-well plate into a 10 cm dish to select for single colonies. Cells were from this point maintained in selection media containing blasticidin and G418. Cells were grown for approximately 2 weeks before colonies were picked into 24 well plates. Colonies were expanded before cells were treated +/- doxycycline for 24 hours before lysing for screening by western blot (**Figure 3.10**). Lysates were probed with an antibody against HA to identify exogenous VPS35 expression. A number of positive clones were identified for both WT and [D620N] VPS35 cell lines. Full methods are shown in **section 2.1.5** and **section 2.1.6**.

3.3.5. Initial Characterisation of Flp-In Cells

Induction of HA-VPS35 expression with doxycycline was optimised using a time course experiment. Two concentrations of doxycycline, across a number of time points were tested in two clones per line and resulting VPS35 levels were analysed by western blotting (**Figure 3.11**). It was determined that all clones produced similar levels of VPS35 across both WT and mutant clones. There appeared to be no difference in the levels of VPS35 induction between the 0.1 µg/ml and 1 µg/ml doxycycline treated cells. Therefore, 0.1 µg/ml was selected as the working concentration for future experiments. At 4 hours post-induction only a small amount of VPS35 expression was induced, as can be

seen in both the HA and VPS35 blots. Treatment with doxycycline for 20 and 24 hours gave a much more pronounced induction of VPS35 expression (Figure 3.12). 24-hour treatment was selected as the preferred time point for future experiments.

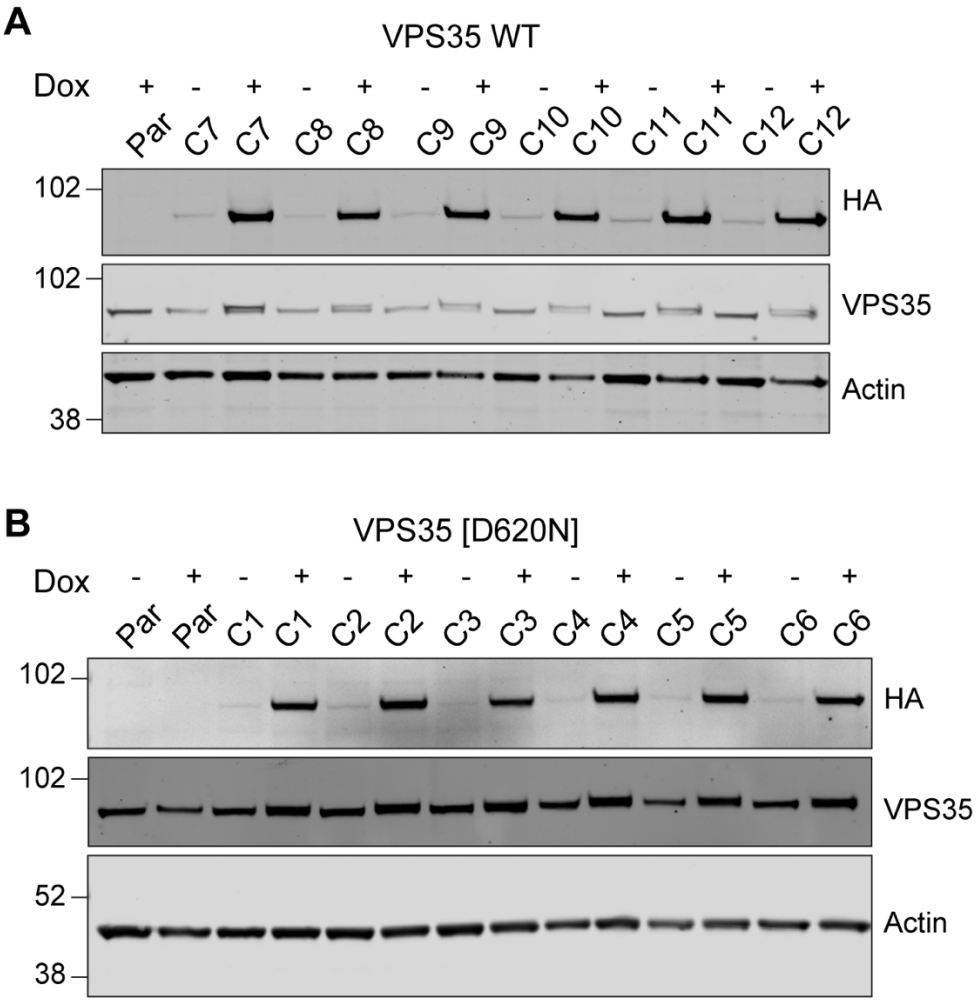

Figure 3.10 Screening RPE1 Flp-In VPS35 cell lines
Parental non-transfected cells (Par), **A**, WT or **B** [D620N] mutant HA-VPS35 RPE1 Flp-In colonies picked from transfected cells were treated +/- Doxycycline (1µg/ml) for 24 hours. Cells were lysed and protein resolved by SDS-PAGE before processing for western blot and immunoblotting for the indicated antibodies. n=1.

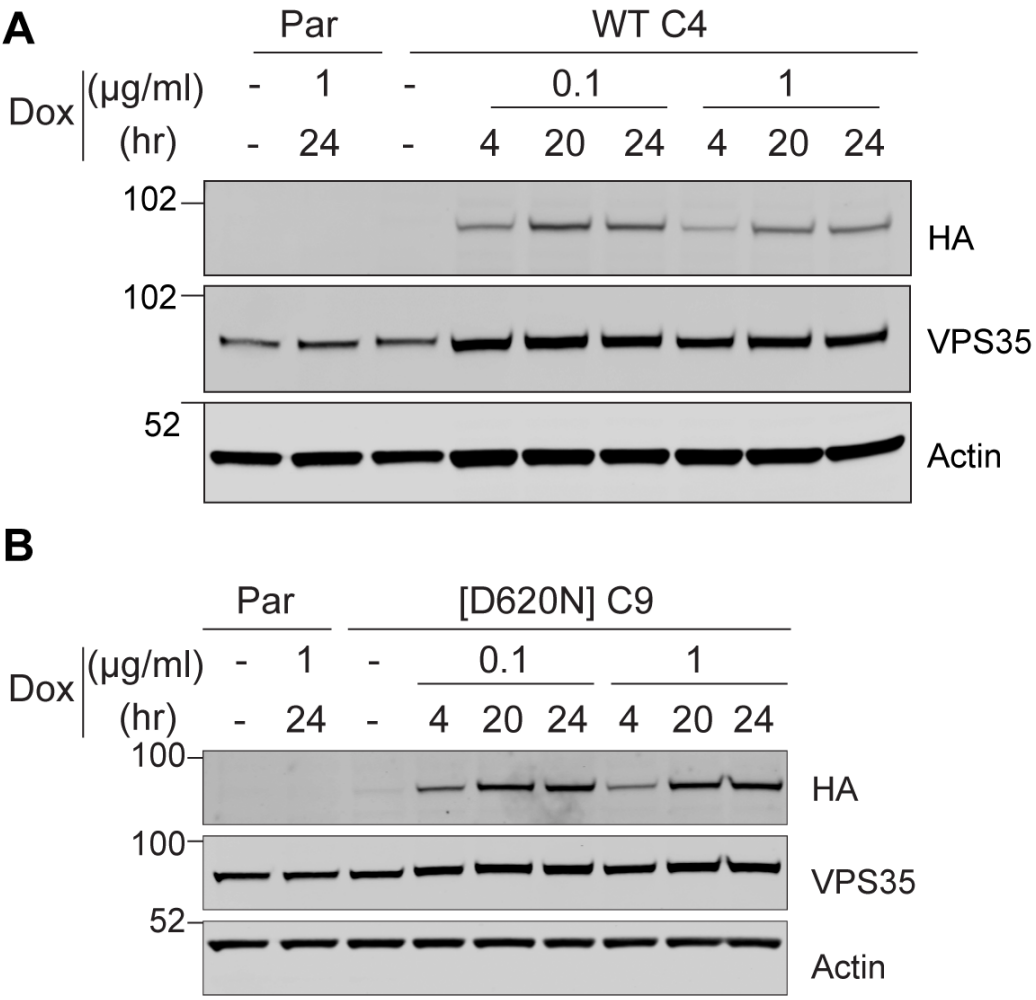

Figure 3.11 Optimisation of HA-VPS35 expression in RPE1 Flp-In cell lines

A WT or **B** [D620N] mutant HA-VPS35 RPE1 Flp-In cells were treated with the indicated concentrations of doxycycline for the indicated time points. Cells were lysed and proteins resolved by SDS-PAGE before processing for western blot and immunoblotting for the indicated antibodies. n=1.

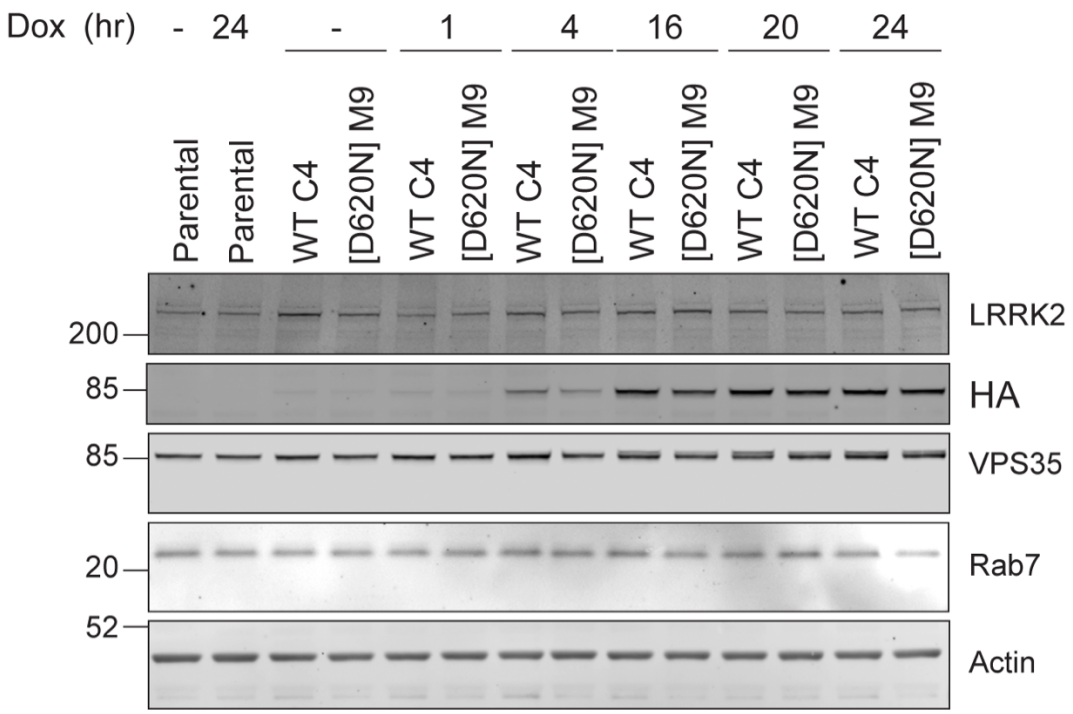

Figure 3.12 Doxycycline induction time course in RPE1 Flp-In VPS35 clones
WT or [D620N] VPS35 RPE1 Flp-In cells were induced with doxycycline (0.1 µg/ml) for the indicated time points. Cells were lysed and proteins resolved by SDS-PAGE before processing for western blot and immunoblotting for the indicated antibodies. n=1.

3.3.6. Characterisation of RPE1 Flp-In VPS35 lines by IF

We next characterised the VPS35 RPE1 Flp-In cells using various markers and immunofluorescence (IF). First, cells were induced with doxycycline for 24 hours and then fixed and stained for HA and early endosome marker EEA1 (Figure 3.13). As expected, HA-VPS35 WT was found to localise to vesicle structures which partially overlapped with EEA1 staining. The staining for EEA1 in the [D620N]-positive cells showed no change in distribution or colocalisation compared with HA-VPS35 (Figure 3.13). This suggests that there is no change in the ability of VPS35 to localise to early endosomes with the pathogenic mutation. This experiment also revealed that many cells in this culture were not positive for HA staining, meaning that cells were not from a single positive clone. Following this discovery, these cells were used for IF experiments to be able to compare HA-VPS35-positive and -negative cells

side by side. It was however, decided that for biochemistry experiments such as the GST-RILP pulldown assay, a 100% pure population from a single clone would be more optimal.

Next, cells were fixed and stained for various cellular markers alongside the HA-tagged VPS35. Cells were stained for mitochondrial marker TOMM20, TGN marker p230 (**Figure 3.14**) or late endosome/lysosomal markers Rab7, LAMP1 or LAMP2 (**Figure 3.15**). Co-staining HA with the lysosomal proteins LAMP1 and LAMP2 revealed no change in these proteins' distribution or colocalisation with HA-VPS35 (**Figure 3.15**). Staining for late endosomal marker Rab7 revealed that there was what appeared to be an increase in colocalisation between Rab7 and HA-VPS35. Other groups have shown that the [D620N] mutation in VPS35 results in mitochondrial dysfunction and fragmentation (Wang et al., 2016; Hanss et al., 2021). It has also been shown that VPS35 is able to regulate the activity of Rab7 (Jimenez-Orgaz et al., 2018), which has been shown to regulate mitochondrial dynamics (**Section 1.4.6**). In our cells the staining of TOMM20 showed there was no change in mitochondrial networks in the pathogenic mutant cells (**Figure 3.14**). This could, however, be due to the use of a different cell type.

We wanted to look at the morphology of the TGN as hyperactivation of LRRK2 has been shown to induce a disrupted network, and [D620N] VPS35 is reported to hyperactivate LRRK2 (Mir et al., 2018; Purlyte et al., 2018) (**Section 1.4.16**). Co-staining for Golgi marker p230 and the HA tag revealed the TGN appeared to be disrupted and more dispersed in the [D620N] positive cells compared with the WT positive cells (**Figure 3.14**). To confirm this, we quantified the area of the TGN in HA positive cells. This confirmed that there was an increase in p230 area and therefore an increase in TGN dispersal with the [D620N] mutation when compared with the WT (**Figure 3.16**).

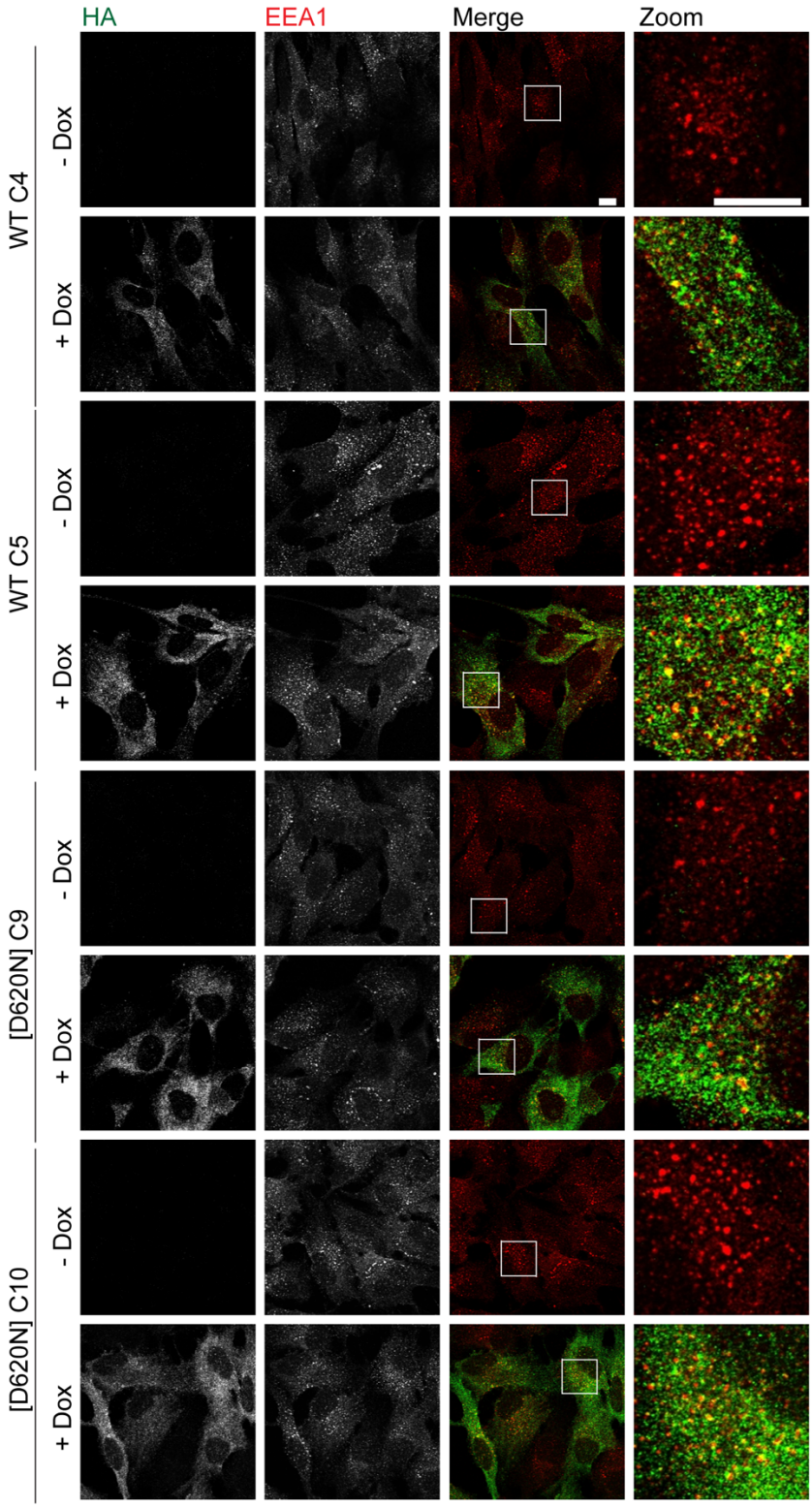

Figure 3.13 Distribution of VPS35 and EEA1 in HA-VPS35 RPE1 Flp-In cells

WT and [D620N] HA-VPS35 RPE1 Flp-In cells were induced with 0.1 µg/ml doxycycline for 24 hours. Cells were fixed in 4% PFA before processing for IF. Images were acquired with a Zeiss LSM800 scanning confocal x63 objective. Scale bar is 10 µm. 350 nm slice. n=1.

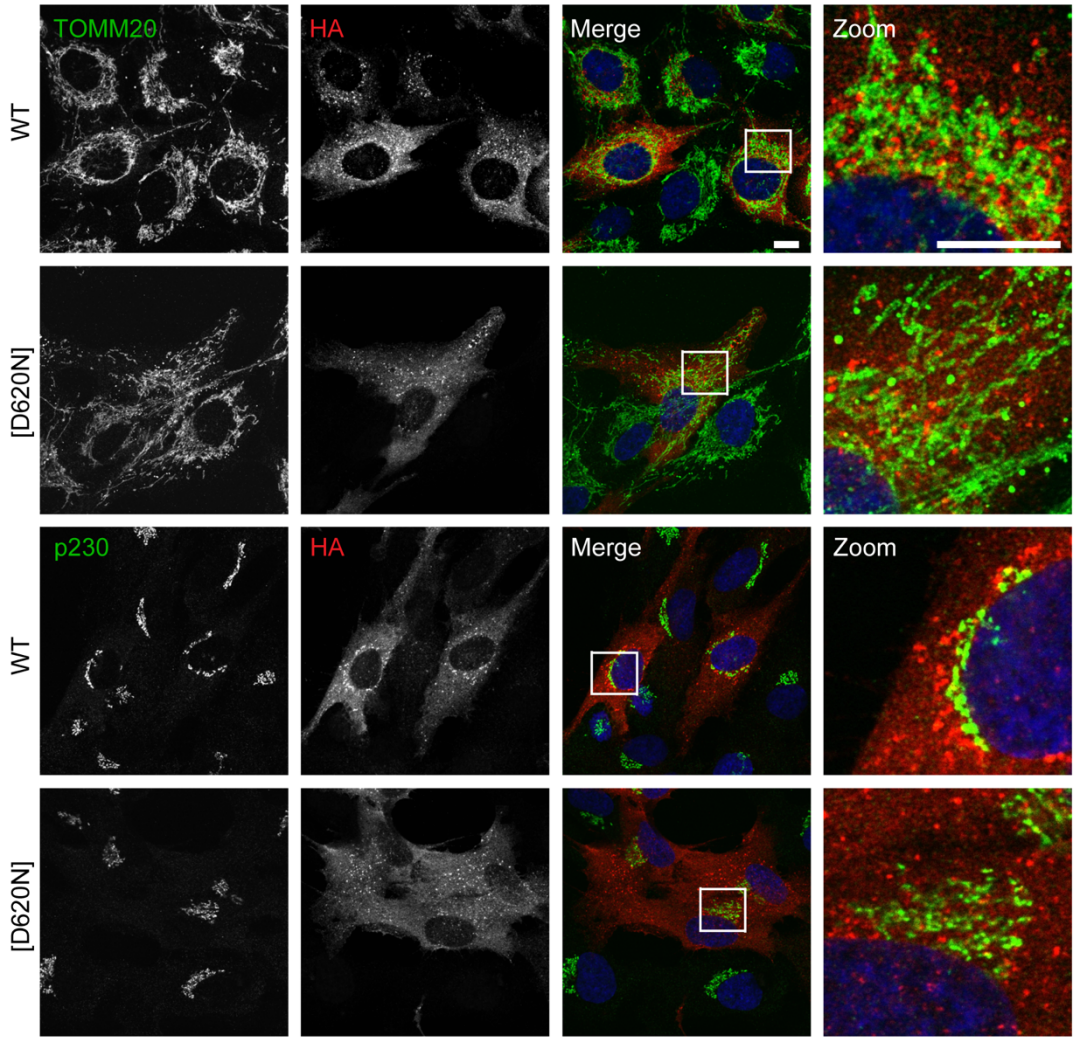

Figure 3.14 Mitochondrial and Trans-Golgi markers in HA-VPS35 RPE1 Flp-In cells

WT and [D620N] HA-VPS35 RPE1 Flp-In cells were induced with 0.1 µg/ml doxycycline for 24 hours. Cells were fixed in 4% PFA before processing for IF. Cells were stained for the TGN marker p230 or the mitochondrial marker TOMM20 alongside HA. Coverslips were mounted on Moviol supplemented with 4',6-diamidino-2-phenylindole (DAPI). Images were acquired with a Zeiss LSM800 scanning confocal x63 objective. Scale bar 10 µm. 350 nm slice. n=1.

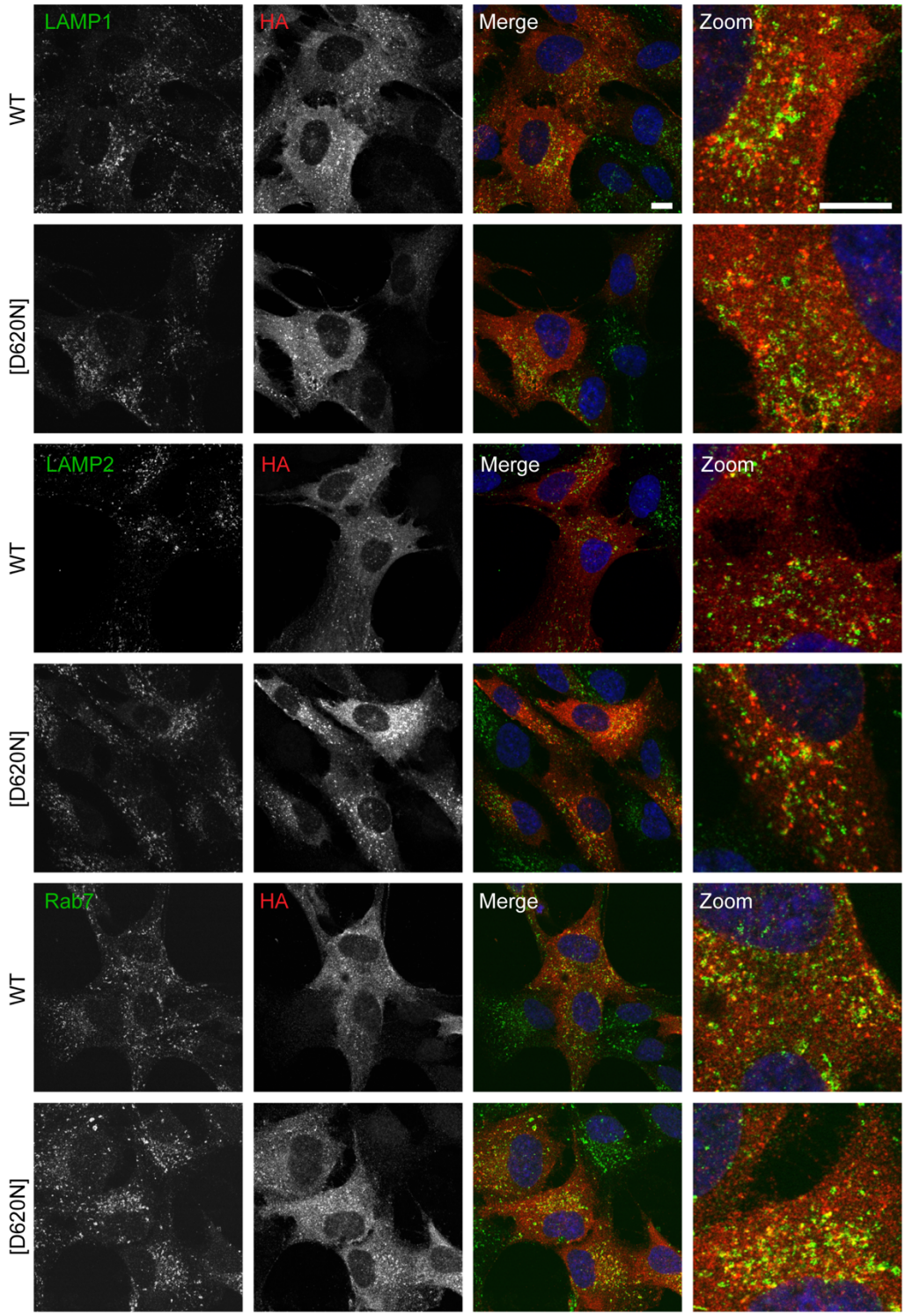

Figure 3.15 Late endosome and lysosomal marker distribution in HA-VPS35 RPE1 Flp-In cell lines
WT and [D620N] HA-VPS35 RPE1 Flp-In cells were induced with 0.1 µg/ml doxycycline for 24 hours. Cells were fixed in 4% PFA before processing for IF. Coverslips were mounted on Moviol supplemented with 4',6-diamidino-2-phenylindole (DAPI). Images were acquired with a Zeiss LSM800 scanning confocal x63 objective. Scale bar 10 µm. 350 nm slice. n=1.

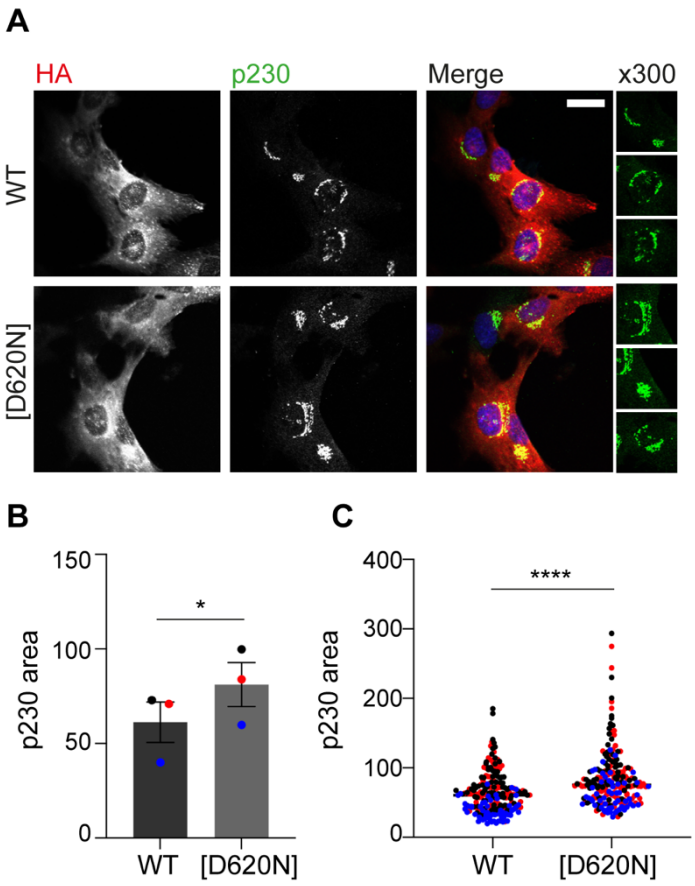

Figure 3.16 VPS35 [D620N] mutation induces disruption of the TGN

A RPE1 Flp-In VPS35 WT or [D620N] cells were induced with 0.1 µg/ml doxycycline for 24 hours. Cells were fixed in 4% PFA before processing for IF. Images were acquired using a Zeiss LSM900 confocal microscope. Scale bar 20 µm. 350 nm slice. **B** Average p230 area per cell. TGN area was quantified using p230 signal in HA-positive cells using FIJI. Analysis: Paired t test (* $p<0.05$) n=3 biological replicates. Error bars: SEM. Minimum 40 cells quantified per condition per repeat. **C** p230 area values for individual cells. Analysis: Unpaired t test (**** $p<0.0001$).

Steinberg's group showed data suggesting that a pool of Rab7 localised with the mitochondria which is disrupted by VPS35 knockout (Jimenez-Orgaz et al., 2018). We were interested to see if the [D620N] mutation would affect the localisation of Rab7 to mitochondria. Both WT and [D620N] mutant cells were induced with doxycycline and stained for HA, TOMM20 and Rab7 (Figure 3.17). Unlike the previous study we were unable to identify a pool of Rab7 colocalised with mitochondria. TOMM20 showed clear mitochondrial network staining whereas Rab7 staining was clearly on vesicles. There was no change

in the staining with in the [D620N] expressing cells. This could be due to the use of a different cell type or the use of different fixation protocols.

The same study also showed that knockout of VPS35 resulted in a change in the colocalisation of Rab7 and LAMP2, with a redistribution of Rab7 across the endolysosomal network. We tested to see if the [D620N] mutation altered Rab7 and LAMP2 colocalisation. HA-VPS35 WT and [D620N] RPE1 Flp-In cells were induced with doxycycline and stained for HA, Rab7 and LAMP2 (**Figure 3.18A**). Initial studies indicated that there is an increase in colocalisation of Rab7 and LAMP2 in the VPS35 mutant cells compared to the WT cells. The Mander's overlap coeffecient was slightly increased with the [D620N] mutation (**Figure 3.18B**). Further repeats would be needed to determine if there is a redistribution of Rab7 across the endolysosomal network with the [D620N] mutation, as observed by others with VPS35 knockout (Jimenez-Orgaz et al., 2018).

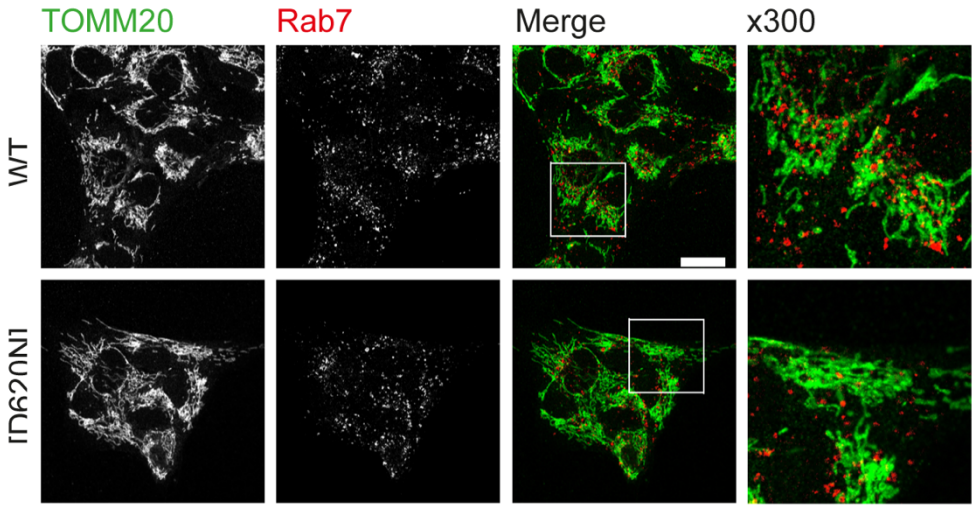

Figure 3.17 Rab7 and TOMM20 do not colocalise at mitochondria in HA-VPS35 RPE1-Flp-In cells
WT and [D620N] HA-VPS35 RPE1 Flp-In cells were induced with 0.1 µg/ml doxycycline for 24 hours. Cells were fixed in 4% PFA before processing for IF. Images were acquired using a Zeiss LSM900 confocal microscope. Scale bar 20 µm. 350 nm slice. n=1.

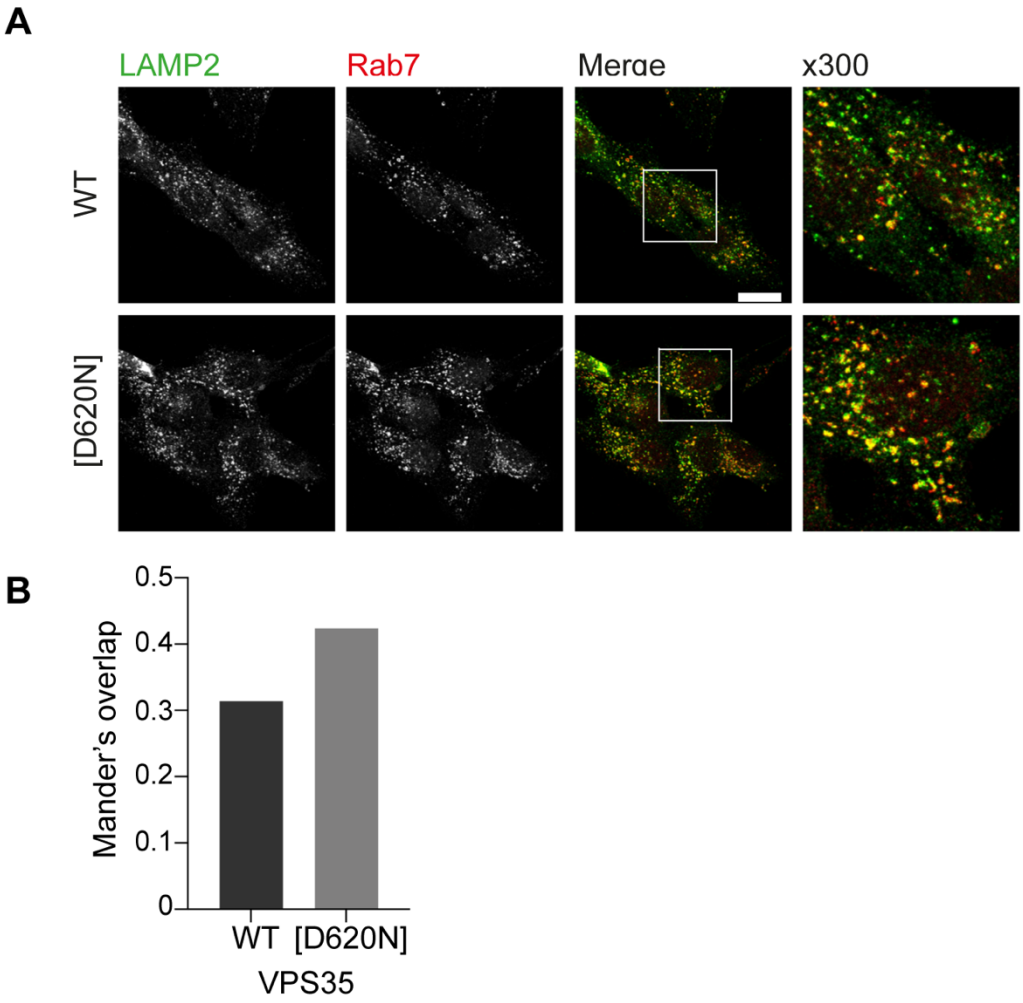

Figure 3.18 Colocalisation of Rab7 and LAMP2 may be altered with VPS35 [D620N] mutation

A WT and [D620N] HA-VPS35 RPE1 Flp-In cells were induced with 0.1 µg/ml doxycycline for 24 hours. Cells were fixed in 4% PFA before processing for IF. Images were acquired using a Zeiss LSM900 confocal microscope x63 objective. Scale bar 20 µm. 350 nm slice. **B** Mander's overlap coefficient was calculated using FIJI Coloc2 plugin and corresponds to the fraction of Rab7 overlapping with the LAMP2 signal. n=1.

3.3.7. Single cell diluting HA-VPS35 RPE1 Flp-In clones

Following the discovery that WT C4 and [D620N] M9 were not from a single clone, cells were single cell diluted into 96 well plates to obtain true positive single clones. Once plated, cells were put into selection media for 10 days. Colonies that grew were expanded until they could be screened by western blot. Clones were also seeded onto coverslips and screened by fixing and staining for the HA tag (**Figure 3.19** and **Figure 3.20**).

From the images acquired it was determined that the clones which were from a single cell and had the most comparable expression of HA-VPS35 were WT 3B4 and [D620N] 1F3. Cells were also screened by WB following 24-hour induction with doxycycline (**Figure 3.21**). Western blotting confirmed that clones such as [D620N] 1D1 were still not pure, reflected by their lower levels of HA and VPS35 following induction with doxycycline. In addition to blotting for VPS35 and HA, lysates were also probed for other key proteins-of-interest such as retromer component VPS26, LRRK2 and Rab7. There did not appear to be an effect on the levels of any of these related proteins with doxycycline induction in the clones analysed.

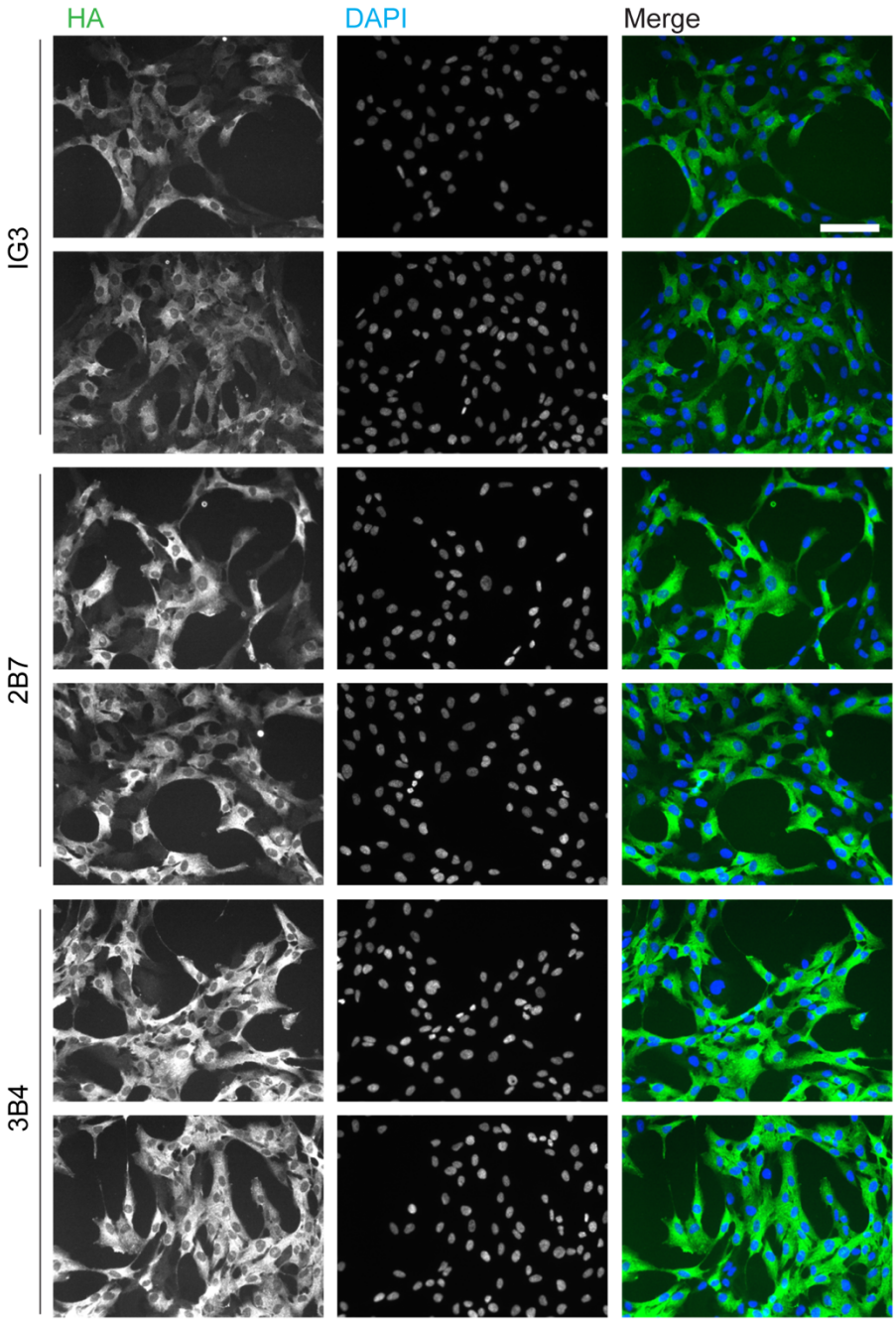

Figure 3.19 Screening RPE1 Flp-In VPS35 WT single cell diluted clones by IF

HA-VPS35 WT RPE1 Flp-In clones from single cell dilution of WT C4 were induced with doxycycline (0.1 µg/ml) for 24 hours. Cells were fixed in 4% PFA before processing for IF. Cells were stained with an antibody against the HA tag. Images were acquired using a NIKON Ti-Eclipse widefield microscope x20 objective. Scale bar 100 µm.

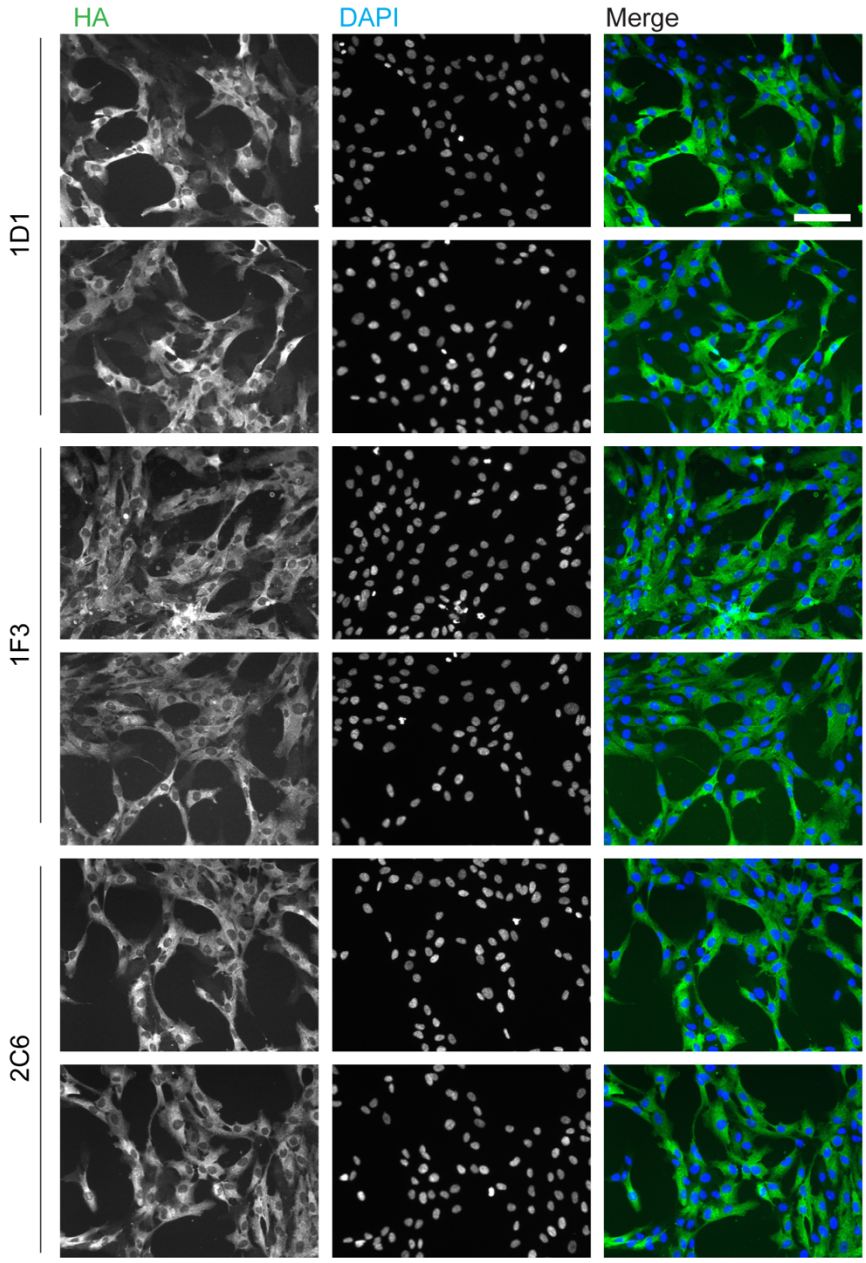

Figure 3.20 Screening RPE1 Flp-In VPS35 [D620N] single cell diluted clones by IF

HA-VPS35 [D620N] RPE1 Flp-In clones from single cell dilution of [D620N] M9 were induced with doxycycline (0.1 µg/ml) for 24 hours. Cells were fixed in 4% PFA before processing for IF. Cells were stained with an antibody against the HA tag. Images were acquired using a NIKON Ti-Eclipse widefield microscope x20 objective. Scale bar 100 µm.

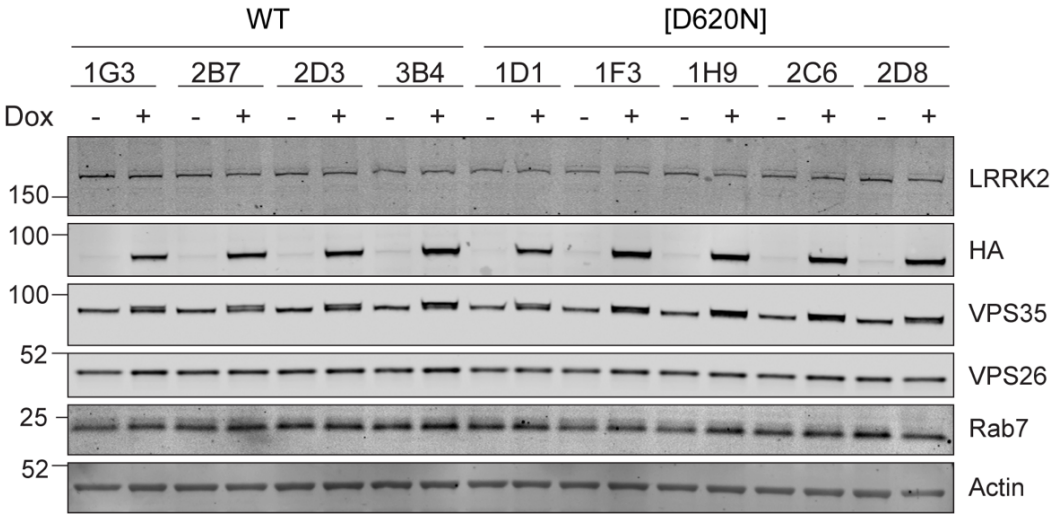

Figure 3.21 Screening single cell diluted clones by western blot

WT or [D620N] HA-VPS35 RPE1 Flp-In cells were induced with doxycycline (0.1 µg/ml) for 24 hours. Cells were lysed and proteins resolved by SDS-PAGE before processing for western blot and immunoblotting for the indicated antibodies. n=1.

3.4. Generating LRRK2 WT and Mutant HA-VPS35 RPE1 Flp-In Cells

3.4.1. Lentiviral Transduction

WT and [D620N] HA-VPS35 RPE1 Flp-In cells (clones 3B4 and IF3 respectively) generated in **section 3.3.7** were transduced with GFP-LRRK2 lentiviruses detailed in **Table 1.1**. Each virus was used at a MOI of 0.8 to ensure only one integration per cell. After expansion cells were sorted by FACS to collect the GFP-positive population. FACS work was carried out by Dr Ailbhe Brazel. The positive pool was expanded, and aliquots frozen for use in experiments. Confirmation of GFP and GFP-LRRK2 expression was obtained by fluorescence microscopy (**Figure 3.22**).

3.4.2. Characterisation of LRRK2 lentivirus lines

Next, we confirmed the activity of LRRK2 in these pools by western blot (**Figure 3.23A**). The level of phosphorylated Rab10 was confirmed using the phospho-Thr73 antibody and the signal was quantified. The level of phospho-Rab10 was then normalised to the level of total LRRK2 expression (**Figure 3.23B**). The LRRK2 [G2019S/D1994A] construct was expressed at a lower level than both the WT and [G2019S] mutant constructs. Cells transduced with LRRK2 [G2019S] hyperactive mutant showed higher levels of Rab10 phosphorylation relative to WT LRRK2 transduced cells when normalised to the level of LRRK2 expression. LRRK2 [G2019S/D1994A] harbouring the kinase-dead mutation did not increase the levels of Rab10 phosphorylation confirming that this increase is dependent on LRRK2 kinase activity. As part of ongoing work in the laboratory, these cells are being single cell diluted to have lines with comparable expression of WT, [G2019S] and [G2019S/D1994A] LRRK2.

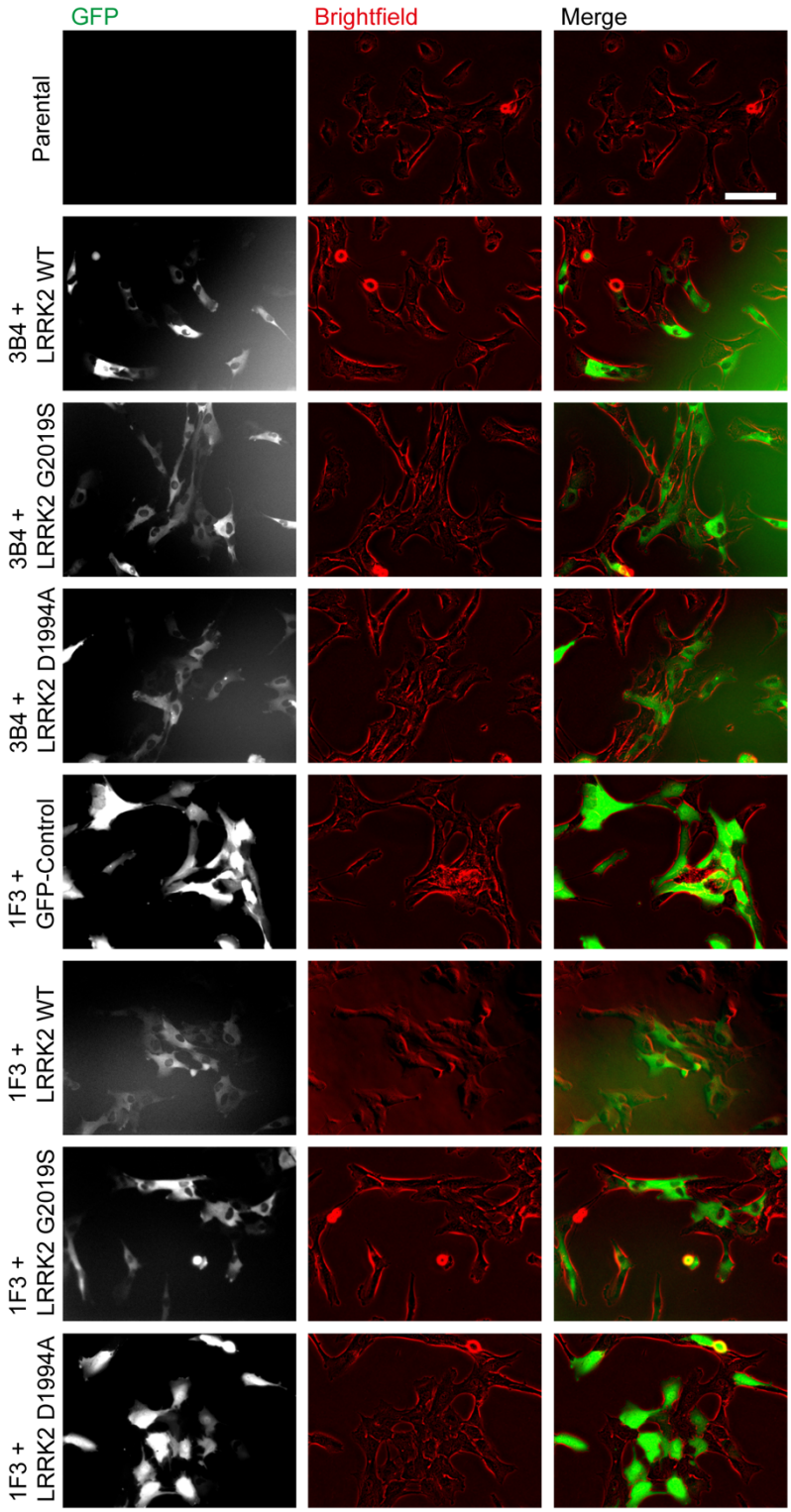

Figure 3.22 Generation of RPE1 Flp-In VPS35 + LRRK2 Lentivirus lines

RPE1 Flp-In cells generated in section 3.3.7 were transduced with LRRK2 lentiviruses detailed in Table 1.1. Positive cells were sorted by FACS and the positive pool expanded. FACS work carried out by Dr Ailbhe Brazel. Images were acquired using a Nikon Ti-Eclipse widefield microscope. Scale bar is 100 µm.

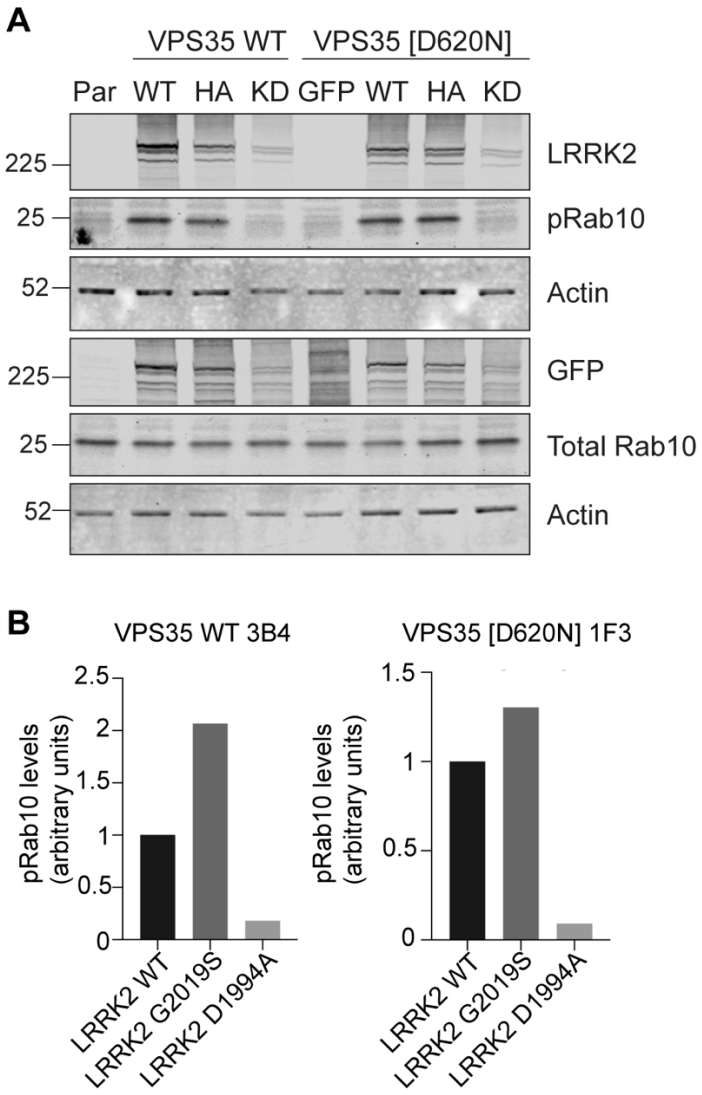

Figure 3.23 Phosphorylation of Rab10 in RPE1 Flp-In VPS35 + LRRK2 lentivirus lines

A Lysates from RPE1 Flp-In VPS35 + LRRK2 lentivirus lines generated in section 3.4.1 were run by western blot and probed for total LRRK2 and phosphorylated Rab10 (WT-Wild type LRRK2, HA-Hyperactive [G2019S] LRRK2, KD-Kinase dead [D1994A] LRRK2) **B** Phospho-Rab10 signal was quantified using image studio lite software and normalised to the level of LRRK2 expression. n=1.

3.5. Discussion

In this chapter I outline several optimisation steps carried out for this project as well as tools which were generated for use in this project and overlapping projects. As LRRK2 is a hot topic in PD research there are a number of well-established commercially available reagents which were found to be suitable for use in both the human and mouse cell lines selected for the project. Although there are no published papers on LRRK2 in melanoma, the finding that LRRK2 is highly expressed in melanoma cell lines could suggest a potential role for LRRK2 in linking PD and the increase incidence of melanoma. Melanoma progression is often characterised by the so-called "Phenotypic switch" (Li et al., 2015). In this phenomenon the core tumour producing cells express a distinct set of genes which drive proliferation and other cellular functions that are required for tumour formation and maintenance. A different pattern of genes is often expressed in the invasive metastatic cells from the same original cancer. For example, both MITF and Rab7 are examples of early drivers of tumour formation and growth by driving proliferation and cell survival. However, they become down-regulated to promote metastasis in later stages of cancer progression (Goodall et al., 2008; Hoek and Goding, 2010; Alonso-Curbelo et al., 2014) (**Sections 1.3.16** and **1.3.17**). The pattern of LRRK2 expression across melanoma cells is inverse to that seen with Rab7 and MITF and could represent a novel marker of phenotypic switching in melanoma cells. It may be the case that melanoma cells upregulate LRRK2 expression as a beneficial gene to promote late-stage melanoma progression. In PD the pathogenic LRRK2 mutations identified are gain-of-function. If a higher level of LRRK2 expression (and therefore presumably higher levels of LRRK2 activity) is a driver for melanoma, then PD related mutations in LRRK2 could also be a positive driver for melanoma progression. The effect of LRRK2 on key characteristics associated with melanoma will be explored in more detail in Chapter 5.

In this chapter we also set up the GST-RILP Rab7 binding assay for measuring the levels of active, GTP-bound Rab7, which we validated using various Rab7 constructs and depletion of TBC1D5. Although LRRK2 is known to

phosphorylate a subset of Rab proteins, Rab7 is not a direct substrate (**Table 1.3**). More recent studies have reported that Leucine Rich Repeat Kinase 1 (LRRK1) is able to directly phosphorylate Rab7 (Malik et al., 2020). Despite not being a direct substrate, data has shown that LRRK2 is able to mediate the activity levels of Rab7, with hyperactivating mutations in LRRK2 causing a reduction in Rab7 activity (Gómez-Suaga et al., 2014). This could be significant as Rab7 is one of the best characterised late endosomal/lysosomal Rab proteins and alterations in its activity could be relevant to the trafficking defects observed in LRRK2 mutant cells and in PD related models in general.

We also made RPE1 Flp-In cell lines with inducible VPS35 WT or VPS35 [D620N] mutant. We made both mixed clones to be used for IF and single "pure" clones to be used for biochemical assays. The [D620N] mutation in VPS35 causes familial PD, but the exact mechanisms that underpin this are poorly understood. We found that the localisation of [D620N] VPS35 alongside many markers was unchanged compared to the WT, consistent with previous studies (Ishizu et al., 2016). VPS35 has been found to function in a common pathway with LRRK2 and Rab29, both PD related genes (MacLeod et al., 2013; Mir et al., 2018) (**Section 1.4.16**). [D620N] VPS35 results in hyperactivation of LRRK2, suggesting that VPS35 lies upstream of LRRK2. VPS35 has also been linked to Rab7 with KO of VPS35 inducing increased active Rab7. It is not currently known the effect of the [D620N] mutation on the levels of active Rab7. We were particularly interested in identifying if the effects of LRRK2 and VPS35 on Rab7 activity are part of the same pathway or distinct pathways. The cell lines and assay established provide us with the tools to answer this question. This is part of ongoing work being carried out within the laboratory. I will revisit the relationship between LRRK2 and Rab7 later (**Section 4.3.7**). Additionally, we also made pools of LRRK2 lentivirus transfected cells in both the VPS35 WT and [D620N] Flp-In cells. This will allow us to look at the effects of the hyperactive and kinase dead LRRK2 mutants and help to overcome the potential issue of using a cell line with low endogenous levels of LRRK2 expression.

When characterising the localisation of various compartmental markers in the RPE1 Flp-In cells, the WT and [D620N] mutation mostly appeared unchanged. Previous work has suggested that KO of VPS35 results in a re-localisation of Rab7 to the late endosomal/lysosomal compartment as marked by colocalisation with LAMP2 (Jimenez-Orgaz et al., 2018). We looked with triple staining of the RPE1 Flp-In VPS35 lines to see if a similar phenotype was observed with the [D620N] mutations. Initial studies showed a slight increase in the colocalisation of Rab7 and LAMP2 with VPS35 pathogenic mutation, however, more repeats are needed to confirm this finding. Confirmation would indicate a change in the trafficking of Rab7 in the late endosomal/lysosomal system consistent with what is seen with VPS35 knockout.

We also noticed that the TGN marker p230 appeared to be more dispersed in the cells expressing the VPS35 [D620N] mutation compared with the WT expressing cells. LRRK2 overexpression and hyperactivation has been found to induce disruption of the TGN, a phenotype which can be rescued following treatment with LRRK2 inhibitor (Purlyte, 2018). This will be discussed in further detail in Chapter 4 (**Section 4.4.5**). Recruitment of LRRK2 to the Golgi network and the downstream effects are suggested to be mediated by Rab29. The finding that the pathogenic mutations in both LRRK2 and VPS35 have the same effect on TGN integrity provides further evidence that these proteins operate in a common pathway and solidifies the link between these two PD-related proteins.

4. Chapter 4: LRRK2 and LROs

4.1. Introduction

The proteins and pathways known to be associated with PD (as well as many other neurodegenerative diseases) can largely be assigned to one of two categories- mitophagy dysfunction or endolysosomal dysfunction (Liu et al., 2019; Malik et al., 2019; Dauer and Przedborski, 2003; Perrett et al., 2015) (**Sections 1.4.4 and 1.4.5**). We know that there is significant crosstalk between these two quality control pathways which are predicted to be significant to PD pathogenesis (Plotegher and Duchen, 2017). It is important to understand the physiological functions of LRRK2, as well as understanding the pathophysiology relating to PD. In this chapter I present data which shows that LRRK2 plays a significant role in membrane dynamics within a specialised cell type- specifically in the context of lysosomes and lysosome related organelles.

Within research into neurodegenerative diseases, a wide variety of models are used to study the pathogenic mutations that have been identified in the field. These range from cell lines to in vivo models, such as drosophila and mouse models, all of which have their own benefits and draw backs. For example, many cell lines used are not physiologically relevant to PD. In drosophila, LRRK1 and LRRK2 homologues are represented by one protein Lrrk. Some data has also been gathered from human post-mortem brain samples, however, the information drawn from these samples is limited by the fact that most dopaminergic neurons have already been lost, making it impossible to study the pathogenesis of disease.

Many laboratories have used reprogramming techniques to provide cellular models from patients which harbour known pathogenic mutations. A common model is induced pluripotent stem cells (iPSCs) derived from patient skin fibroblasts. These dedifferentiated cells can be pushed to differentiate into various cell types (Unternaehrer and Daley, 2011). One major draw-back of using this kind of model to study neurodegenerative disease is that the

reprogramming for iPSCs removes the aged, epigenetic phenotype of these cells which is likely to be significant when studying an ageing disease (Meyer et al., 2014; Ebrahimi et al., 2019). Induced neural progenitor cells (iNPCs) are an alternative model to differentiate dopaminergic neurons. In this model fibroblasts derived from patients and controls are reprogrammed so that they retain their aged phenotype (Meyer et al., 2014; Kim et al., 2011a). From these cells, treatment with several factors can then be used for differentiation into astrocytes or dopaminergic neurons.

4.2. LRRK2 and MiT transcription factors

4.2.1. LRRK2 is inversely related to MITF and TFEB in Melan-a cells

Following the finding that LRRK2 expression is inversely related to the levels of pigmentation markers (**Figure 3.2**), I performed an siRNA knockdown of LRRK2 or pigmentation related transcription factor MITF in Melan-a. cells. A fellow member of the MiT transcription factor family, TFEB, was knocked down as a control. The levels of proteins were measured by western blot (**Figure 4.1A**). All proteins were efficiently depleted by siRNA. Loss of LRRK2 resulted in an increase in the level of MITF protein levels. As expected, depletion of MITF resulted in a decrease in the levels of both MITF and Rab27A- one of its transcriptional targets (Chiaverini et al., 2008) (**Appendix 2**). Interestingly, loss of MITF also resulted in an increase in the levels of LRRK2. Furthermore, depletion of LRRK2 induced an increase in the levels of TFEB and loss of TFEB resulted in an increase in the levels of LRRK2 protein- larger than that seen with loss of MITF. These results were quantified using Image Studio software (**Figure 4.1B**). This demonstrates an inverse relationship between LRRK2 and both MITF and TFEB in Melan-a cells.

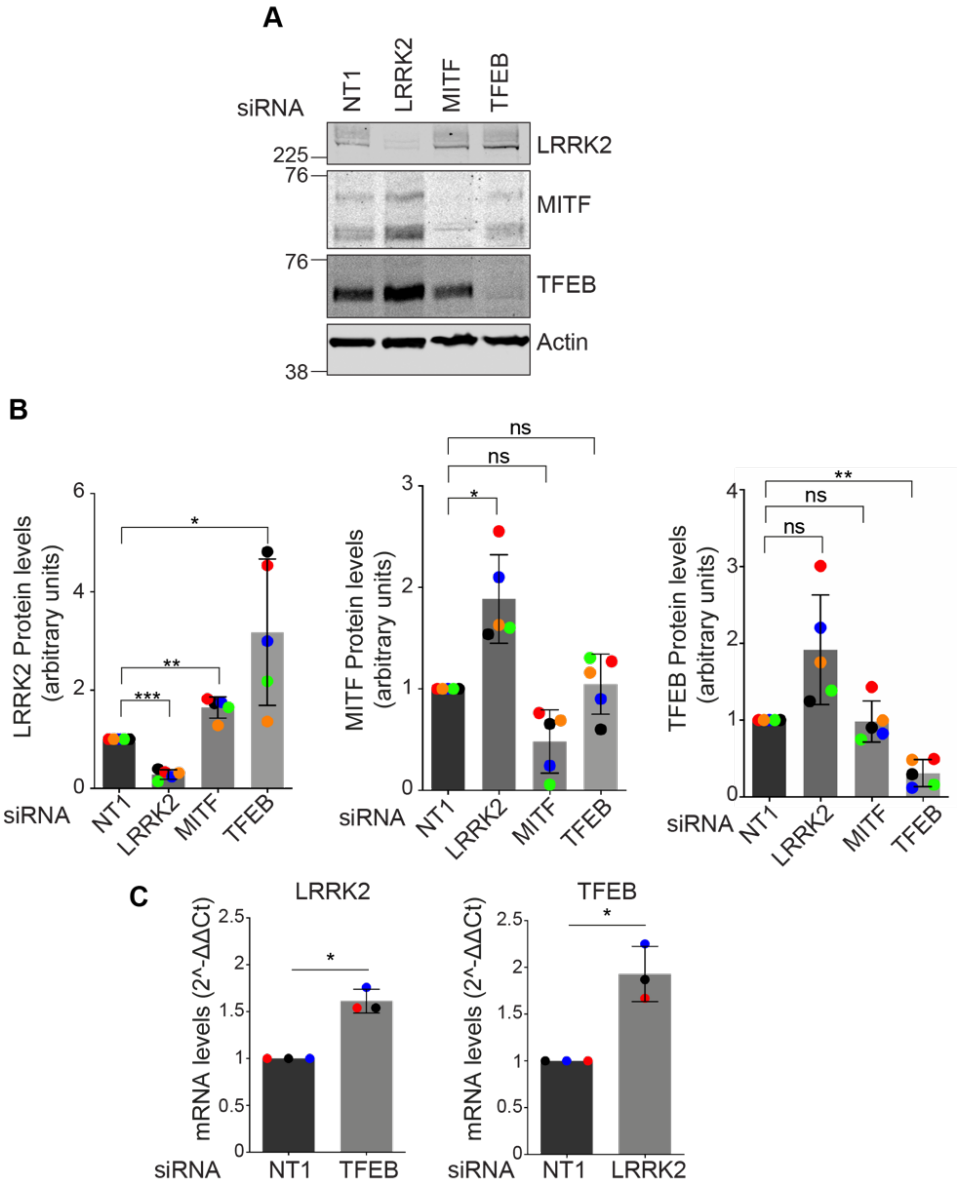

Figure 4.1 Identification of an inverse relationship between LRRK2 and two related MiT transcription factors

A Lysates from Melan-a cell treated with 40 nM siRNA for 72 hours were analysed by western blot and probed with the indicated antibodies. Blot is representative of 5 biological repeats. **B** Bands from western blots were quantified using image studio lite software and normalised to NT1. n=5 biological replicates. Error Bars: SD. Analysis: one-way ANOVA with Turkey's multiple comparison test. (* $p<0.05$, ** $p<0.01$, *** $p<0.001$. **C** Melan-a cells were treated with 40 nM siRNA targeting LRRK2 or TFEB for 72 hours. mRNA was extracted and reverse transcribed. Resulting cDNA was analysed by RT-qPCR using primers against LRRK2 or TFEB. 2^-ΔΔCt values normalised to NT1. n=3 biological replicates. Error bars: SD. Individual repeats displayed in different colours. Analysis: Unpaired t test (* $p<0.05$).

4.2.2. mRNA levels of LRRK2 and TFEB with knockdowns

To determine if the changes in protein level seen by western blot were occurring at a transcriptional level, RT-qPCR was used to determine the mRNA levels of LRRK2 and TFEB following siRNA knockdown (**Figure 4.1C**). When quantified, depletion of TFEB resulted in a 2-fold increase in the levels of LRRK2 mRNA transcripts. Similarly, a loss of LRRK2 resulted in a 1.5-fold increase in the levels of TFEB mRNA. These results support the reciprocal relationship between LRRK2 and TFEB seen by western blot and suggest that the increase in protein level is at least in part a result of an increase in mRNA expression.

4.3. LRRK2 and Lysosome related organelle number and function in Melan-a cells

4.3.1. Depletion of LRRK2 increases LRO number in Melan-a cells

I next investigated the effect of depletion of LRRK2 protein on lysosomes and lysosome related organelles (LROs). LRRK2 was depleted with siRNA for 72 hours. Cells were labelled with LysoTracker Deep Red fluorescent dye and imaged live using confocal microscopy. LysoTracker compounds are cell permeable fluorophores which are highly specific for acidic organelles. Organelles expected to be labelled with LysoTracker red include some late endosomes, lysosomes, early melanosomes, and peroxisomes (**Section 1.2.7**). Depletion of LRRK2 protein increased the number of LysoTracker positive vesicles by eye (**Figure 4.2A**). This was quantified by taking the total intensity per cell and averaging over the number of cells analysed. Quantification confirmed there was an increase in LysoTracker intensity with LRRK2 knockdown (**Figure 4.2B**).

Next, I looked to confirm this result by imaging the number of lysosome-associated membrane protein 1 (LAMP1) positive vesicles in fixed cells using immunofluorescence. Confocal imaging of fixed cells stained with LAMP1

confirmed that depletion of LRRK2 increased the number of LROs in Melan-a cells relative to NT1 treated cells (Figure 4.3A). Depletion of LRRK2 also increased the number of Rab7 positive vesicles in Melan-a cells further supporting an effect on the late endosomal/ lysosomal pathway (Figure 4.4).

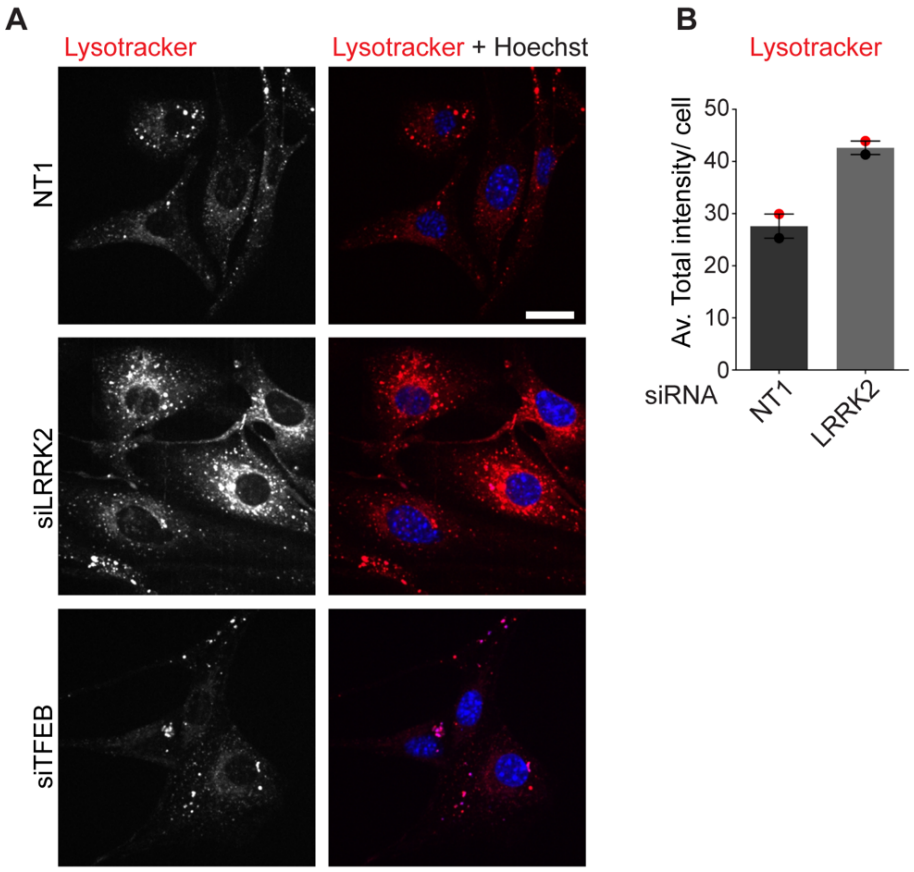

Figure 4.2 Depletion of LRRK2 in Melan-a cells increases LysoTracker labelling in Melan-a cells
A Melan-a cells treated with 40 nM siRNA oligos against LRRK2 and TFEB for 72 hours were incubated with LysoTracker Deep Red fluorescent dye (0.5 μM) for 1 hour. The nuclei were labelled with Hoechst. Live images were acquired using a 3i spinning disk confocal microscope x63 objective. Scale bar: 20 μm. 350 nm slice. **B** Total intensity of LysoTracker signal was quantified per cell. Minimum of 25 cells analysed per condition. n=2 biological replicates. Error bars: Range.

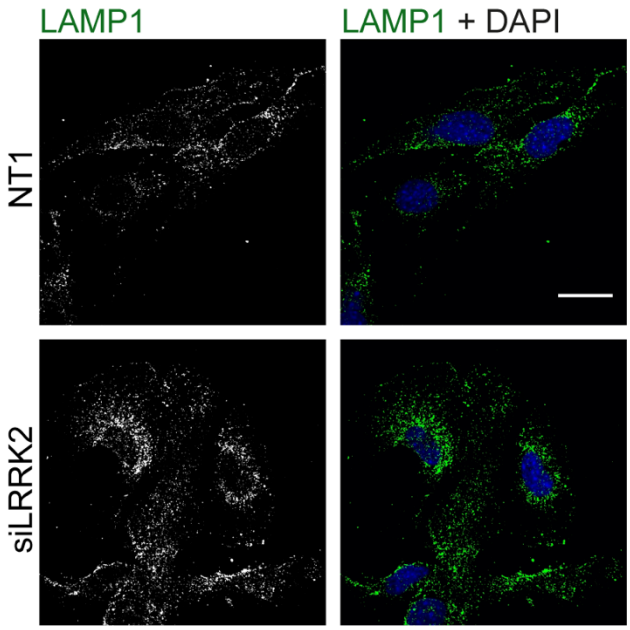

Figure 4.3 Depletion of LRRK2 increases the staining of LAMP1 in Melan-a cells.
Melan-a cells treated with 40 nM siRNA oligos for 72 hours were fixed with 4% PFA before processing for IF. Coverslips were mounted on Moviol supplemented with 4',6-diamidino-2-phenylindole (DAPI). Images were acquired with a 3i spinning disk confocal microscope x63 objective. Scale bar: 20 µm. 350 nm slice n=3 biological replicates.

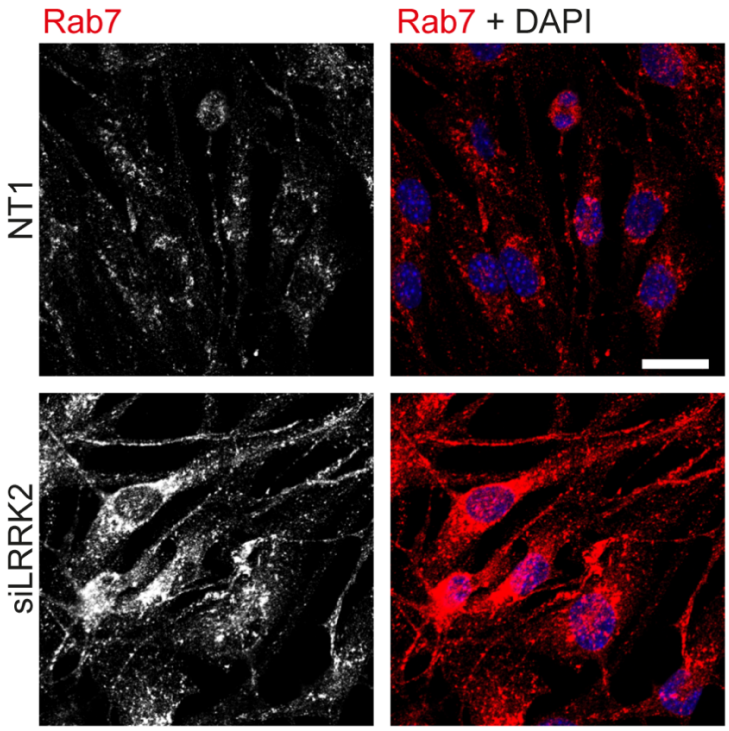

Figure 4.4 Depletion of LRRK2 increases the number of Rab7 positive vesicles in Melan-a cells.
Melan-a cells treated with 40 nM siRNA oligos for 72 hours were fixed with 4% PFA before processing for IF. Coverslips were mounted on Moviol supplemented with 4',6-diamidino-2-phenylindole (DAPI). Images were acquired using a Zeiss LSM800 confocal microscope x63 objective. Scale bar: 20 µm. 350 nm slice. n=3 biological replicates.

4.3.2. Inhibition of LRRK2 increases LRO number in Melan-a cells

To further support the results seen with LRRK2 knockdown, I then looked at the number of acidic organelles in Melan-a cells with LRRK2 inhibition. Melan-a cells were treated with inhibitors HG-10-102-01 (HG-10) and MLi-2 for 48 hours then labelled with LysoTracker. Cells were imaged by live confocal microscopy. Inhibition of LRRK2 increased the number of acidic organelles relative to DMSO treated cells (**Figure 4.5A**). LysoTracker images were quantified by taking the total intensity of LysoTracker signal per cell and averaging this value for the total number of cells quantified (**Figure 4.5B**). Quantification confirmed an increase in LysoTracker signal with LRRK2 inhibition.

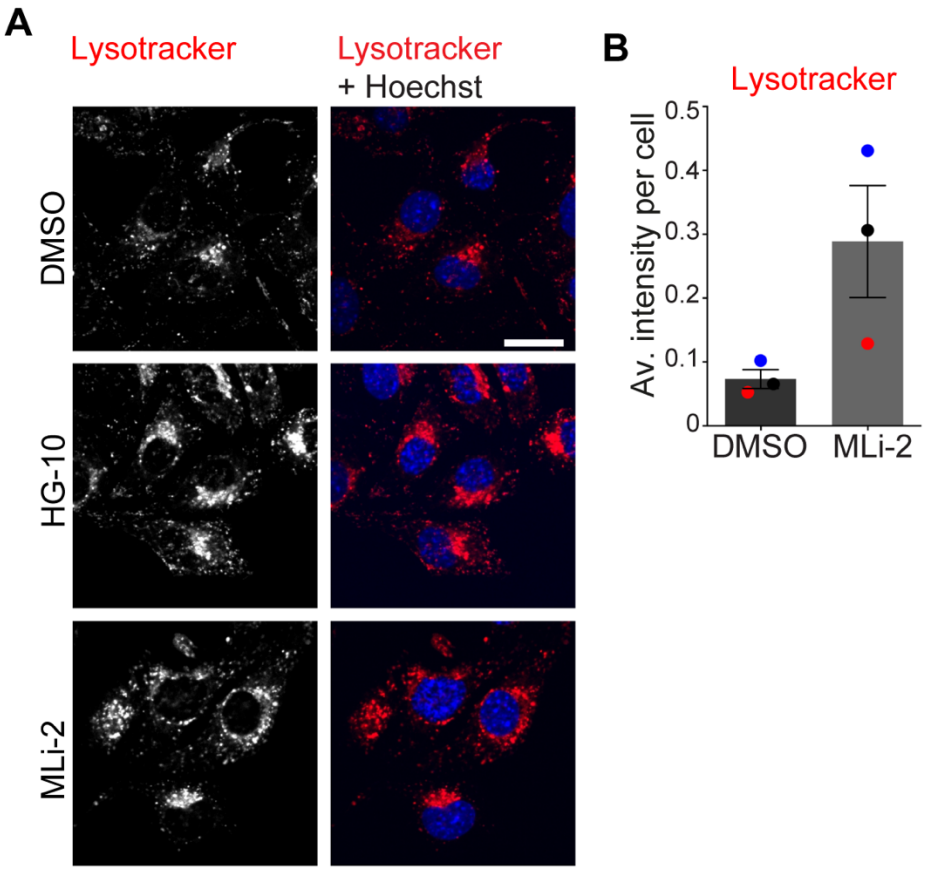

Figure 4.5 Inhibition of LRRK2 increases LysoTracker labelling in Melan-a cells
A Melan-a cell treated with HG-10-102-01 (HG-10, 500 nM) or MLi-2 (200 nM) for 48 hours were incubated with LysoTracker Deep red (0.5 µM) for 1 hour. Cells were imaged live using a 3i spinning disk confocal microscope Scale bar: 20 µm. 350 nm slice. **B** Total intensity of LysoTracker signal was quantified per cell. Minimum of 25 cells quantified per condition per repeat. n=3 biological replicates. Error bar: SEM.

Next, I looked to confirm this result by imaging the number of LAMP1 positive vesicles in fixed cells. Melan-a cells treated with HG-10 and MLi-2 inhibitors for 48 hours were fixed and stained for LAMP1 and coverslips imaged by confocal microscopy (Figure 4.6A). Inhibition of LRRK2 was shown to increase the number of LAMP1 vesicles relative to the control treated cells. The number of vesicles per cell was quantified using the analyse particles plugin in FIJI, and the average taken across three independent experiments (Figure 4.6B). Quantification showed an increase in the number of LAMP1 positive vesicles per cell with LRRK2 inhibition, which is consistent with what was seen with the LysoTracker fluorescent dye experiments.

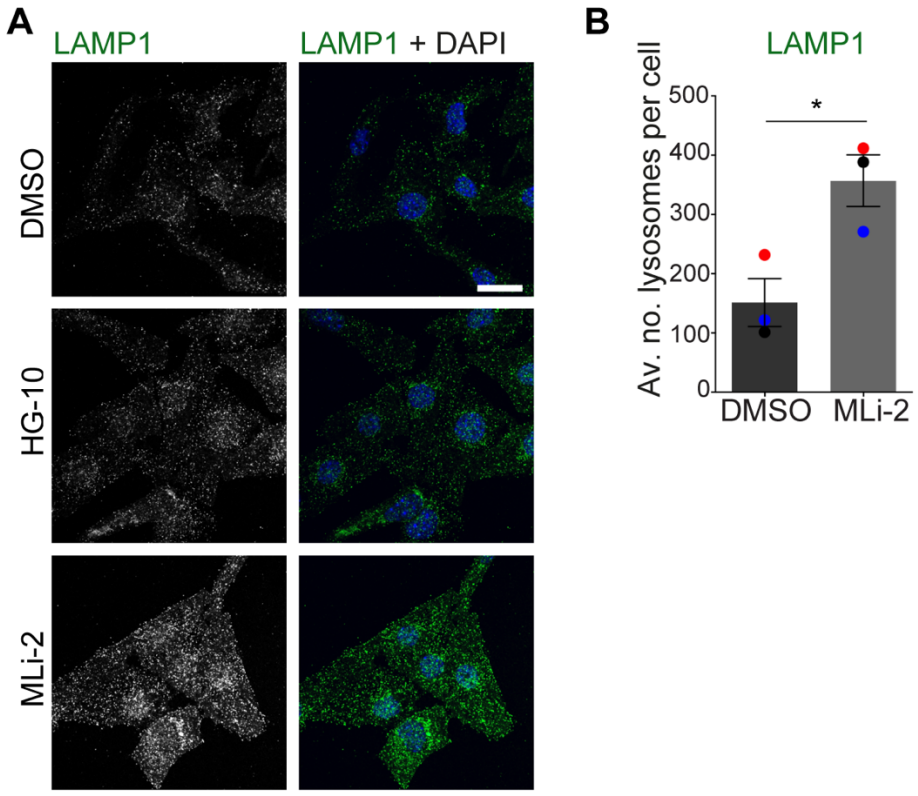

Figure 4.6 Inhibition of LRRK2 increases the number of LAMP1 positive vesicles
A Melan-a cells treated with LRRK2 inhibitors HG-10 (500 nM), or MLi-2 (200 nM) for 48 hours were fixed with 4% PFA before processing for IF. Coverslips were mounted on Moviol supplemented with 4',6-diamidino-2-phenylindole (DAPI). Images were acquired with a 3i spinning disk confocal microscope x63 objective. Scale bar: 20 µm. 350 nm slice. **B** The number of LAMP1 vesicles per cell was quantified using the analyse particles function in FIJI. Graph shows average number of vesicles per cell across 3 biological repeats. Minimum 25 cells analysed per condition per repeat. Error bars: SEM. Analysis: Unpaired t test (* $p<0.05$).

4.3.3. Inhibition of LRRK2 does not increase lysosome function

To determine if the lysosomal activity of these cells had also increased, I utilised the Magic Red-Cathepsin B fluorescent probe (see schematic Figure 2.5). This probe only becomes fluorescent within an active lysosomal compartment. The probe consists of a fluorophore conjugated to two cleavage peptides for Cathepsin B hydrolase. Prior to cleavage the probe is not fluorescent. Cleavage of one or both of the target peptides by cathepsin B in

the lysosome results in release of the fluorophore and a fluorescent signal (Van Noorden et al., 1997). Melan-a cells treated with LRRK2 inhibitors for 24 hours were labelled with Magic Red-Cathepsin B and imaged live by confocal microscopy (**Figure 4.7A**). Melan-a cells treated with LRRK2 inhibitors did not show an increase in fluorescent signal. This indicated there was not a significant change in the activity of Cathepsin B. It must be noted that Cathepsin B has a broad pH optimum which does limit the conclusions we can draw from this assay, as the activity of more pH sensitive proteins may be affected by the changes seen in acidic organelles.

I also used a plate reader assay to measure the activity of another lysosomal cathepsin protein- Cathepsin D. This works in a similar format to the Magic red probe in that cleavage of a target sequence by Cathepsin D results in a fluorescent signal read by a plate reader. Lysates from Melan-a cells treated with MLi-2 were incubated with Cathepsin D substrate and then the fluorescence per well quantified. Fluorescence was normalised to the amount of protein loaded onto the assay (**Figure 4.7B**). As with the Magic Red assay, there was no increase in the activity of Cathepsin D with LRRK2 inhibition. This data, together with that from the LysoTracker experiments, would indicate that with LRRK2 inhibition the number of LROs is increasing, but that there isn't a concomitant increase in the degradative capacity of lysosomes.

I also checked to see if inhibition of LRRK2 changed the Cathepsin D protein levels. Melan-a cells were treated with LRRK2 inhibitor and lysates probed with an antibody against cathepsin D. Cathepsin D exists as an immature "pro" form prior to delivery to the lysosome (**Section 1.2.5**). Neither the pro-, nor cleaved-cathepsin D bands showed any change with LRRK2 inhibition (**Figure 4.7C**). Therefore, neither the pro-form levels, nor the active form of lysosomal hydrolases are increased with LRRK2 inhibition, consistent with no change in the lysosomal activity assays.

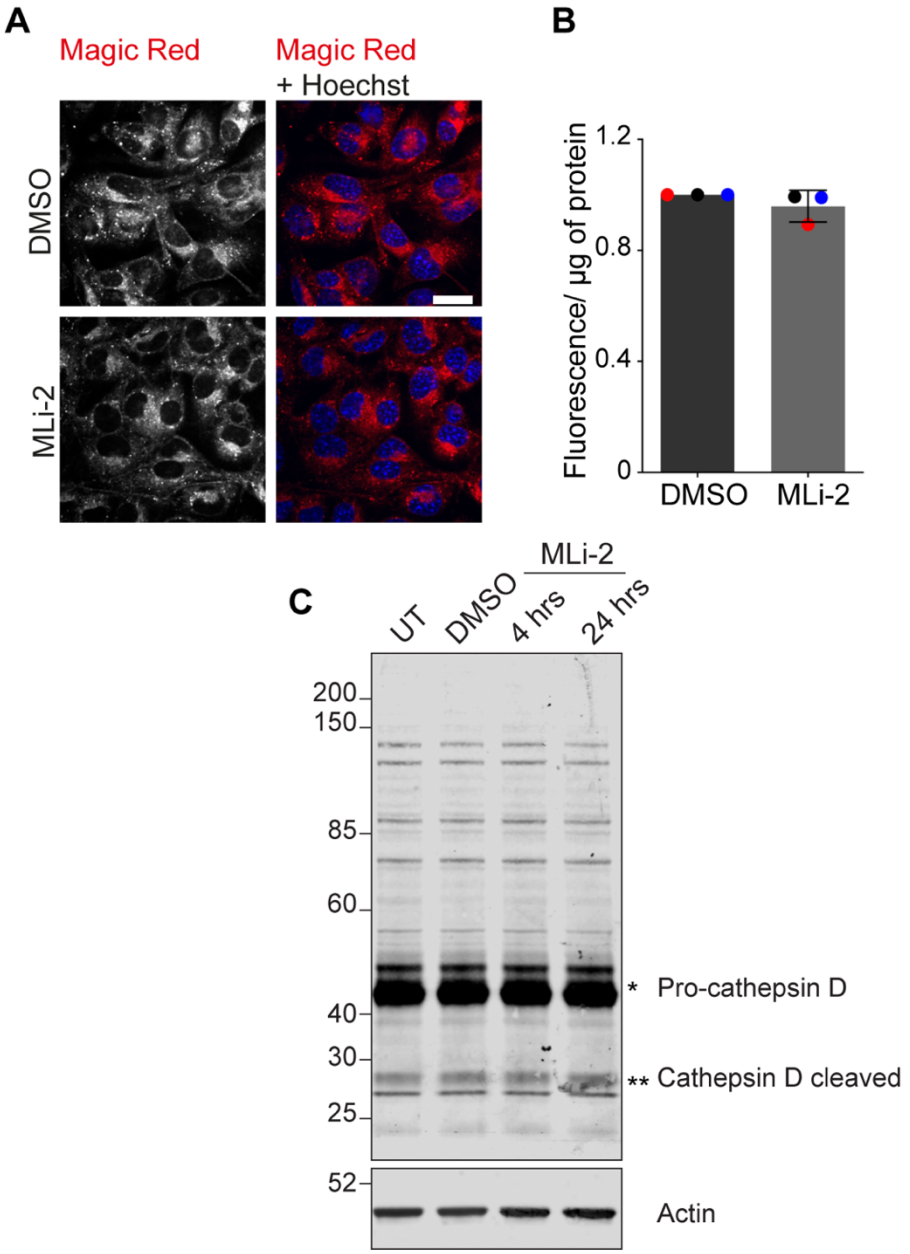

Figure 4.7 Inhibition of LRRK2 in Melan-a cells does not increase Cathepsin B or D proteolytic activity

A Melan-a cells treated with LRRK2 inhibitor MLi-2 (200 nM) for 24 hours were incubated with Magic Red-Cathepsin B fluorescent probe for 1 hour before live imaging with a 3i spinning disk confocal microscope x63 objective. Scale bar 20 µm. 350 nm slice. n=3 biological replicates. **B** Lysates from Melan-a- cells treated with LRRK2 inhibitor MLi-2 (200 nM) for 24 hours were analysed with Cathepsin D activity assay kit. Signal was normalised to DMSO. n=3 biological replicates. Individual repeats displayed in different colours. Error bars: SD. **C** Lysates from Melan-a cells treated with MLi-2 (200 nM) for the indicated time points were probed with the indicated antibodies. Both pro (*) and cleaved (**) forms of Cathepsin D indicated.

4.3.4. LRRK2 inhibition results in a striking rapid change in late endosome and LRO markers in Melan-a cells

I was next interested to determine the kinetics of this change in LRO number. Melan-a cells were treated with LRRK2 inhibitor for a range of time points and labelled with LysoTracker for 1 hour. For the 1-hour treatment, MLi-2 and LysoTracker were added simultaneously. Cells were imaged live using widefield microscopy. Imaging revealed that there was a large increase in the level of LysoTracker labelling after just 1 hour of treatment that recedes over time, indicating that LRRK2 is having a major acute effect on acidic organelles. (**Figure 4.8A**). To confirm this result, I repeated the experiment with just the 1-hour time point but looked with confocal microscopy which confirmed there is an increase in acidic organelles after just 1 hour (**Figure 4.8B**).

I next looked at fixed cells stained with a late endosome/lysosome marker to see if I could again observe an increase after 1 hour. Imaging of fixed cells treated with MLi-2 for various time points showed that there is an increase in staining of Rab7 in Melan-a cells after just 1 hour (**Figure 4.9**). Importantly, early endosomal markers EEA1 and HRS staining did not change with LRRK2 inhibition (**Figure 4.10**) indicating a change in a later stage of the endolysosomal pathway.

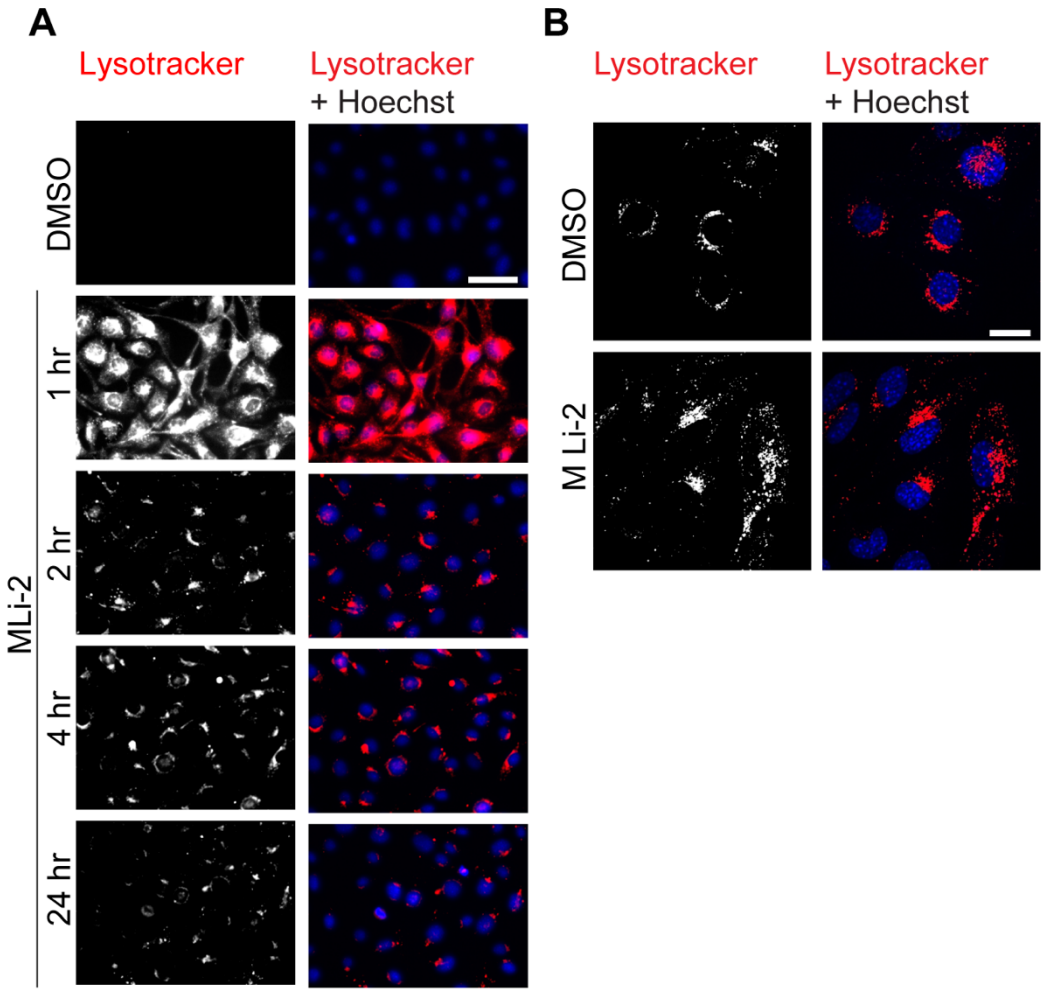

Figure 4.8 LRRK2 inhibition results in a rapid increase and subsequent dissipation in LysoTracker labelling
A Melan-a cells treated with MLi-2 (200 nM) for the indicated time points were labelled with LysoTracker Deep Red fluorescent dye (0.5 μM) for 1 hour before images were acquired live using a Nikon Ti-Eclipse microscope x40 objective. Scale Bar: 50 μm. **B** Melan-a cells treated with MLi-2 (200 nM) for 1 hour were labelled with LysoTracker Deep Red fluorescent dye. Images were acquired live using a 3i spinning disk confocal. Scale Bar: 20 μm. 350 nm slice. n=3 biological replates.

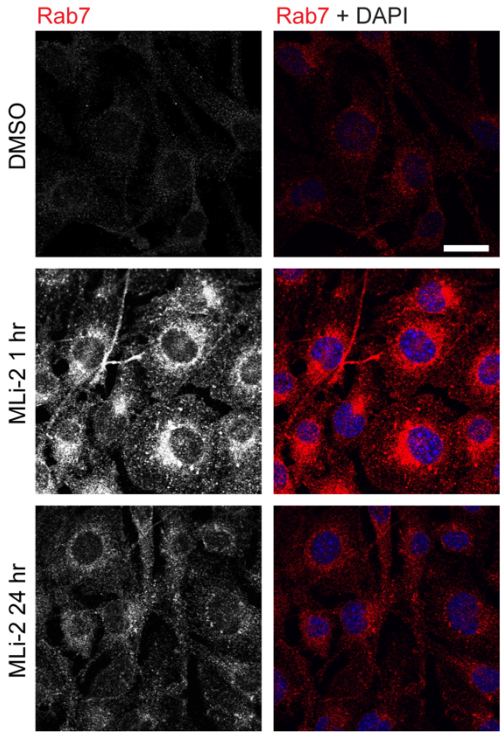

Figure 4.9 Acute inhibition of LRRK2 increases Rab7 staining in Melan-a cells

Melan-a cells were treated with MLi-2 LRRK2 inhibitor (200 nM) for the indicated time points before being fixed in 4% PFA and processed for IF. Coverslips were mounted with Moviol supplemented with 4',6-diamidino-2-phenylindole (DAPI). Images were acquired using a Zeiss LSM800 confocal microscope x63 objective. Scale bar 20 μm. 350 nm slice. n=3 biological replicates.

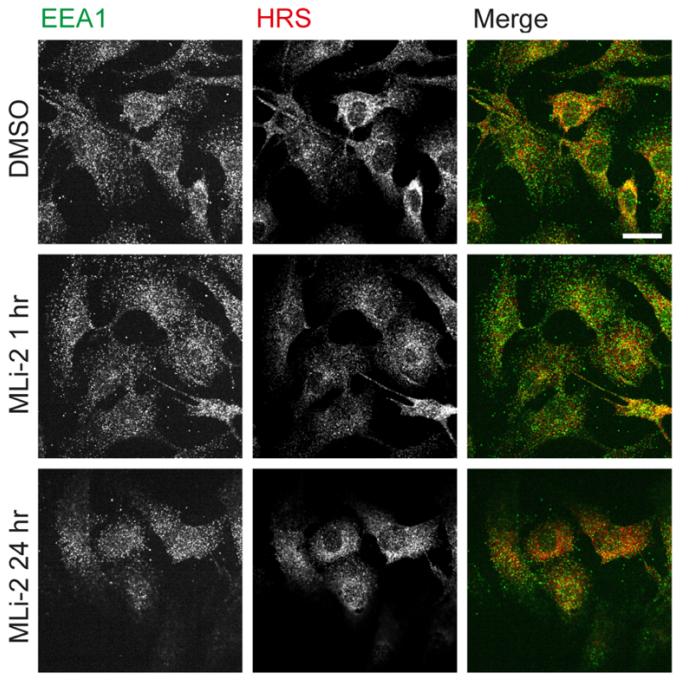

Figure 4.10 LRRK2 inhibition doesn't change EEA1 and HRS staining in Melan-a cells
Melan-a cells were treated with MLi-2 LRRK2 inhibitor (200 nM) for the indicated time points before being fixed in 4% PFA and processed for IF. Cells were stained for the indicated antibodies. Coverslips were mounted with Moviol supplemented with 4',6-diamidino-2-phenylindole (DAPI). Images were acquired using a Zeiss LSM800 confocal microscope x63 objective. Scale bar 20 µm. 350 nm slice. n=1.

In addition to the confocal images taken of fixed cells, quantification was carried out for Melan-a cells stained with LAMP1 antibody by IF using an OPERA high content screening system. Cells were treated with MLi-2 for multiple time points before fixing and staining for LAMP1 and nuclear stain Hoechst. Random fields of view were then imaged for each well. Quantification was carried out using Harmony software to select cell area, cell nuclei and "spots" (LAMP1 positive vesicles). Calculations were then run in the harmony software to determine values such as average number of lysosomes per cell, average number of lysosomes per cell area, average intensity of lysosomes and average size of lysosomes (Figure 2.7). Quantification showed that there was a striking increase in the number of lysosomes per cell area at the 1-hour time point, which then dropped down by 2 hours but remained above baseline,

consistent with what had been seen by IF (Figure 4.11A). There was not an increase in the intensity or area of LAMP1 positive vesicles (Figure 4.11B-C).

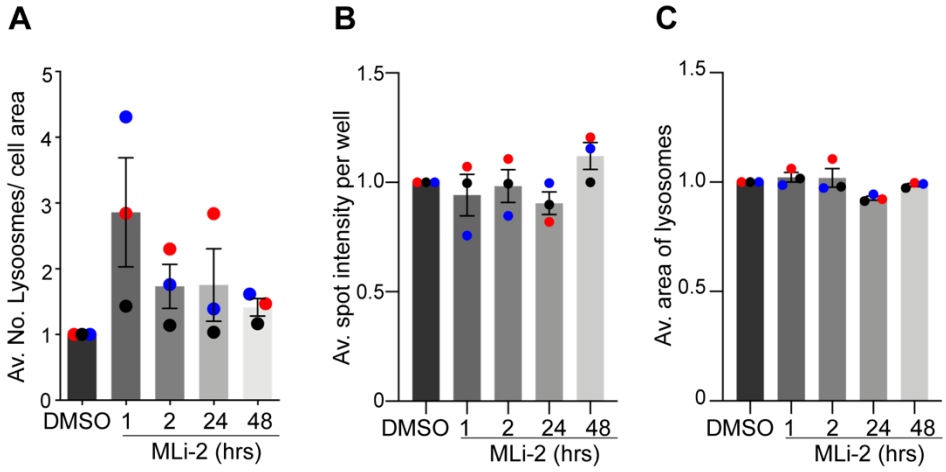

Figure 4.11 Acute inhibition of LRRK2 increases the number of LAMP1 positive vesicles in Melan-a cells
Melan-a cells were treated with LRRK2 inhibitor MLi-2 (200 nM) for the indicated time points. Cells were fixed in 4% PFA before processing for IF. Cells were stained with a LAMP1 antibody and nuclei labelled with Hoechst. An OPERA phoenix high content screening system was used to image cells at random throughout conditions. **A** Harmony software was used to quantify the average number of lysosomes per cell. **B** Harmony software was used to calculate the average intensity of spots measured. **C** Harmony software was used to measure the average area of LAMP1 positive spots. Samples were normalised to the DMSO sample. n=3 biological replicates. Minimum 500 cells quantified per condition per repeat. Error bars: SEM.

4.3.5. The effect of LRRK2 on lysosomes is independent of TFEB

My initial interest in LRRK2 and lysosomes came from the early finding that LRRK2 knockdown results in an increase in the levels of TFEB at both a protein and mRNA transcript level. However, the later finding that there is an effect on LROs as early as 1 hour after treatment suggests that this process is too quick for translation to be involved. Therefore, I sought to determine if the changes seen in LysoTracker and LRO marker labelling were independent of TFEB. To do this I first knocked down TFEB in Melan-a cells and then

treated them with LRRK2 inhibitor MLi-2. I then fixed and stained them with an antibody against Rab7. Cells were imaged by confocal microscopy (**Figure 4.12**). Treatment with LRRK2 inhibitor in TFEB depleted cells resulted in an increase in Rab7 staining.

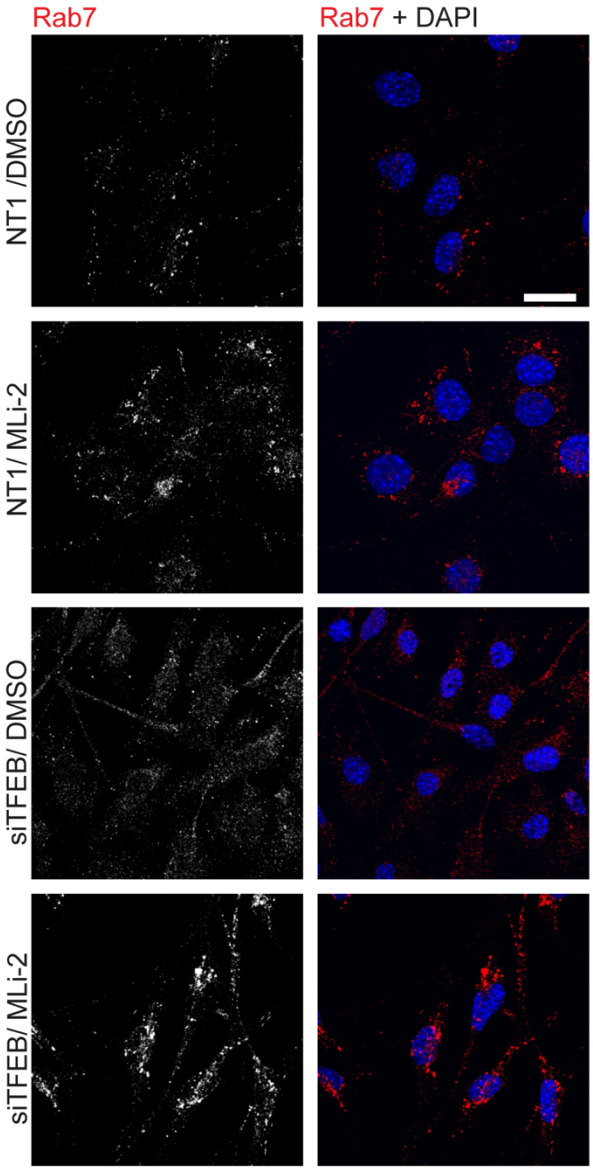

Figure 4.12 The effect of LRRK2 on lysosomes in Melan-a cells is independent of TFEB
Melan-a cells were treated with 40 nM siRNA against TFEB for 48 hours before the addition of MLi-2 (200 nM) for an additional 24 hours. Cells were fixed in 4% PFA before processing for IF. Images were acquired with a 3i spinning disk confocal microscope x63 objective. Scale bar 20 µm. 350 nm slice. n=1.

4.3.6. Total levels of lysosomal proteins do not change with LRRK2 inhibition or depletion

To determine if the changes seen by IF were due to an increase in protein levels of these markers, or a change in dynamics, Melan-a cells were treated with LRRK2 inhibitors HG-10 or MLi-2 or siRNA targeting LRRK2. Lysates were probed for total levels of late endosome/lysosome associated proteins LAMP1 and Rab7 (Figure 4.13). There were no changes in the total levels of either LAMP1 or Rab7 with LRRK2 inhibition or with 72-hour knockdown.

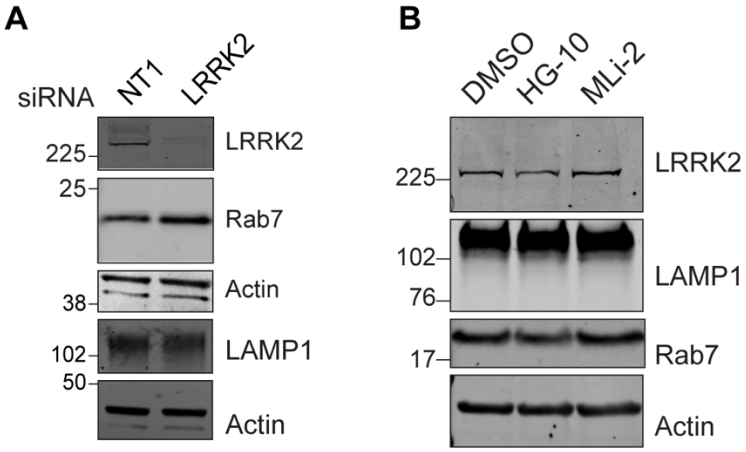

Figure 4.13 Total levels of lysosomal proteins do not change with LRRK2 inhibition or siRNA depletion
A Melan-a cells were treated with 40 nM siRNA targeting LRRK2 for 72 hours **B** Melan-a cells were treated with HG-10 (500 nM) and MLi-2 (200 nM) LRRK2 inhibitors for 24 hours. Lysates were analysed by western blot. Membranes were probed with the indicated antibodies. n=3 biological replicates. Representative blots shown.

4.3.7. Inhibition of LRRK2 increases GTP-bound active Rab7

To determine if the Rab7 phenotype observed in Melan-a cells could be due to a change in the nucleotide binding status of Rab7 I used the GST-RILP binding assay described in Chapter 3 (Section 3.3.2). Melan-a cells were treated with MLi-2 inhibitor for 1 hour or 24 hours. Cells were lysed, and lysates were incubated with GST-RILP beads to pulldown active Rab7. Eluates from

beads were analysed by western blot (Figure 4.14A). Active Rab7 signal was quantified and normalised to the total Rab7 in the input sample (Figure 4.14B). Both at the 1-hour and 24-hour time points an increase was seen in the amount of GTP-bound active Rab7.

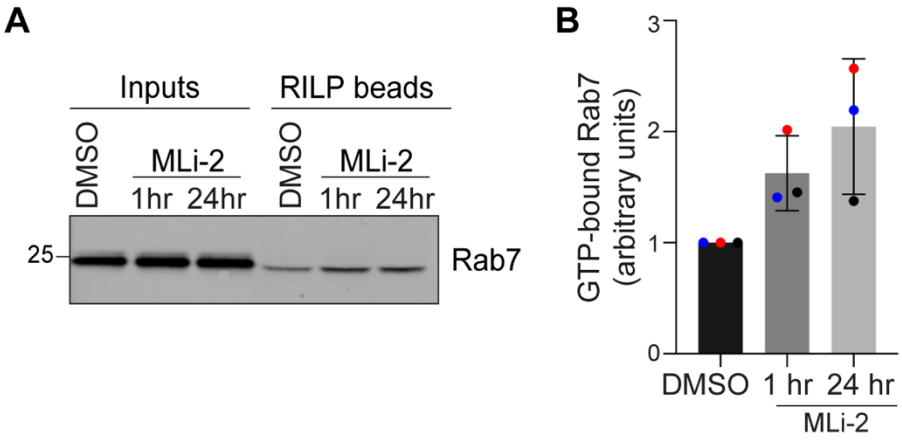

Figure 4.14 LRRK2 inhibition increases GTP-bound Rab7
A Melan-a cells were treated with MLi-2 (200 nM) for the indicated time points. Cells were lysed in Rab7 assay lysis buffer and lysates loaded onto GST-RILP beads. Bound proteins were eluted and analysed by western blot. 10 µg input loaded. **B** Levels of GTP-bound active Rab7 were quantified using image studio software. Levels were normalised to total Rab7 levels from input. Values were then normalised to DMSO. n=3 biological replicates. Error bars: SD.

4.4. LRRK2 in iNPC derived dopaminergic neurons

4.4.1. Differentiation of iNPCs into dopaminergic neurons

In order to look at LRRK2 in a more physiologically relevant setting, under the supervision of Heather Mortiboys at The Sheffield Institute for Translational Neuroscience (SITraN), I carried out work in dopaminergic neurons derived from iNPCs. Skin samples were taken from 2 healthy age-matched controls and 2 individuals carrying the [G2019S] LRRK2 mutation. One of the individuals with the [G2019S] LRRK2 mutation is symptomatic for PD, and derived samples will be referred to as manifesting mutant (MM). The other donor carries the mutation but has not been diagnosed with PD, and derived

samples will hereafter be referred to as the non-manifesting mutant (NMM). Skin samples were used to extract fibroblasts for cell culture. Cells were reprogrammed from fibroblasts to iNPCs by Heather Mortiboys. From iNPCs, dopaminergic neurons were differentiated over a 27-day protocol. The full methods for dopaminergic neuron differentiation are given in **section 2.1.10**. Representative images of Control 1 cells undergoing the final stretch of differentiation are shown in **Figure 4.15**.

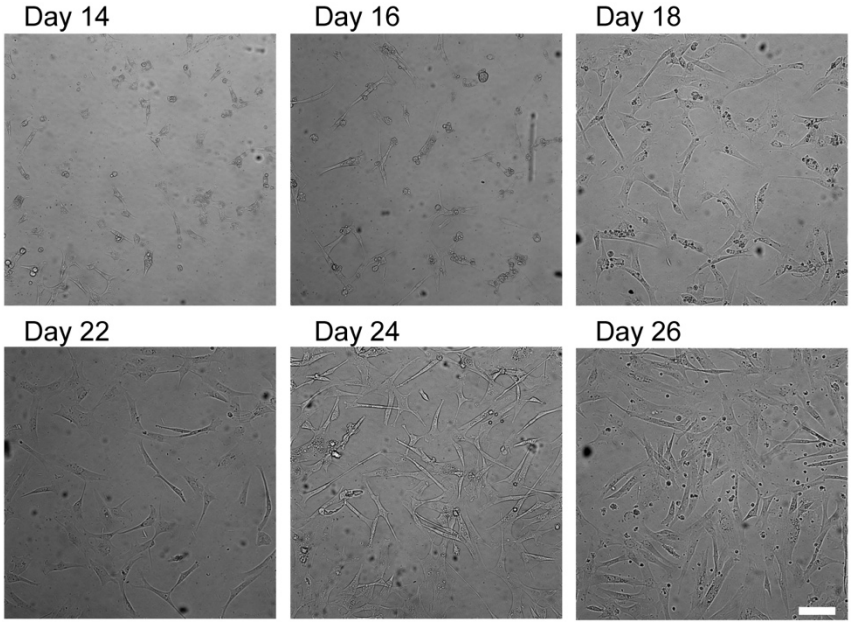

Figure 4.15 Differentiation of dopaminergic neurons from control 1 iNPCs
iNPCs were differentiated into dopaminergic neurons across a 27-day protocol outlined in section 2.1.10. On day 12 cells were re-plated into the final assay vessel and grown in BDNF (30 ng/ml), GDNF (30 ng/ml), TGF-β3 (2 mM) and dCAMP (2 mM) for 15 days. Images were acquired on the indicated days of the protocol to show morphology changes and monitor differentiation progress. Cells were imaged with an IN Cell Analyser 2200 imaging system x10 objective. Scale bar 100 µm

4.4.2. LRRK [G2019S] mutation increases LAMP1 staining in dopaminergic neurons

Dopaminergic neurons differentiated from iNPCs from control and mutant donors were fixed and stained for lysosomal marker LAMP1. Staining was

then visualised using an OPERA Phoenix high content screening imaging system. Random fields of view from each well were captured to remove bias. Representative images of each neuron line are shown in **Figure 4.16A**. Both the non-manifesting and manifesting [G2019S] mutant lines showed an increase in LAMP1 staining compared to control lines. Harmony high content imaging and analysis software was used to quantify the number of cells (number of nuclei), cell area analysed and the number of spots (number of LAMP1 positive vesicles). From this the number of LAMP1 positive spots per cell/cell area was quantified. Quantification analysis confirmed what was evident by eye, that there was an increase in the number of LAMP1 positive vesicles in the mutant lines relative to the control lines. This quantification workflow is shown in more detail in **Figure 2.7**. Quantification also showed that there was an increase in the area of lysosomes, but only in the case of the manifesting mutant (**Figure 4.16B**).

4.4.3. LRRK2 [G2019S] does not increase lysosomal activity

Following the increase in LAMP1 staining, I was next interested in the lysosomal activity in the mutant neurons compared to the control neurons.
In order to look at this I utilised the same Magic Red-Cathepsin B assay used in the melanocytes (see **Section 4.3.3**). Neurons were differentiated from iNPCs, and on the final day of the differentiation protocol were labelled with Magic Red-Cathepsin B probe. Neurons were imaged live using an OPERA Phoenix high content screening imaging system. Random fields of view were captured for each neuron line to prevent bias. Representative images are shown in **Figure 4.17A**. The number of active lysosomes was quantified using Harmony high content imaging and analysis software as above. Cells were counted by nuclei staining and cell area and active lysosomes (number of spots) quantified. In contrast to the LAMP1 staining, there was not an increase in the number of active lysosomes in LRRK2 mutant neurons relative to the control neurons (**Figure 4.17B**). In fact, there was a decrease in lysosomal activity in the non-manifesting mutant line. This was also the case for

measurements taken for active lysosome (signal) intensity and active lysosome area.

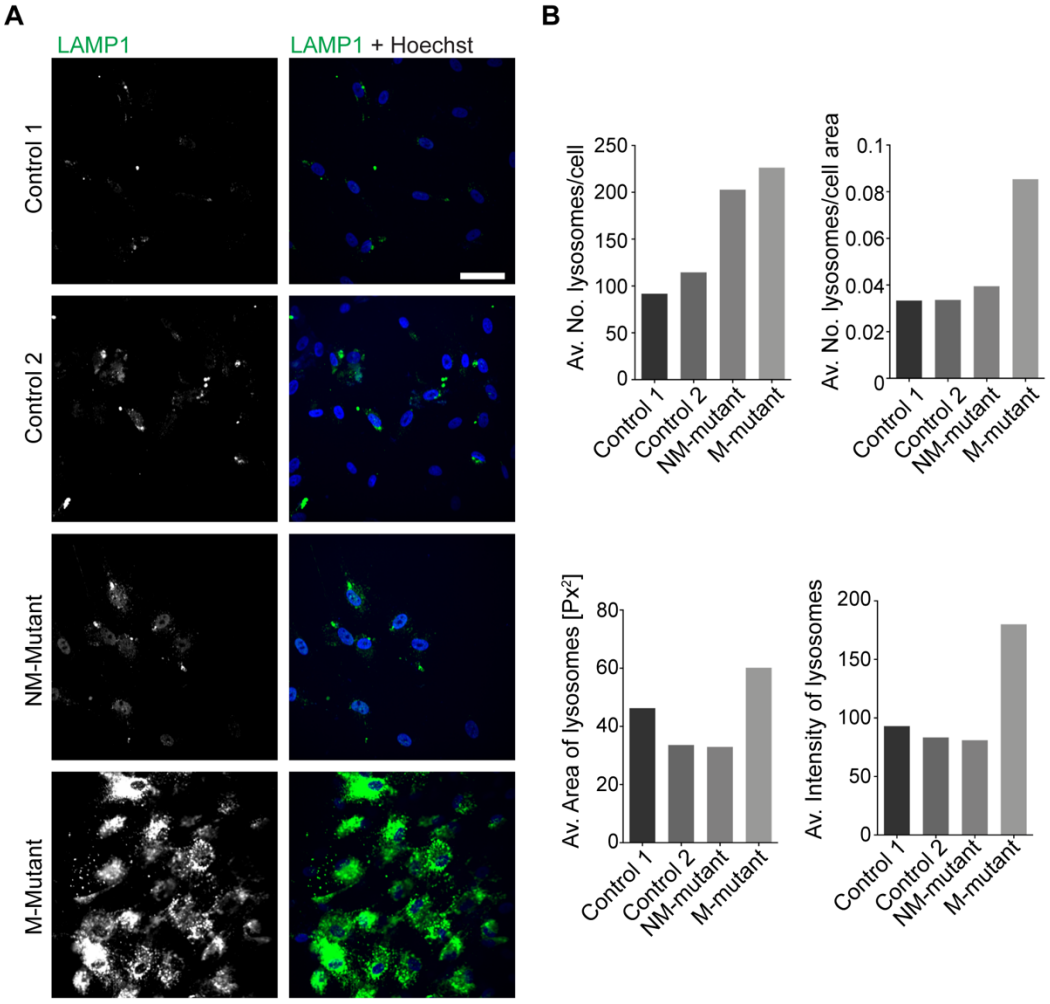

Figure 4.16 LRRK2 [G2019S] mutation increases LAMP1 staining in iNPC derived dopaminergic neurons
A Dopaminergic neurons were differentiated from iNPCs and fixed in 4% PFA before processing for IF. Cells were stained with a primary antibody against LAMP1 and imaged using an OPERA high content screening imaging system. x40 objective used. Maximum projection shown. **B** The number, intensity and area of LAMP1 positive vesicles was quantified using Harmony high content imaging and analysis software. Minimum of 526 cells quantified per line. Scale bar 40 µm.

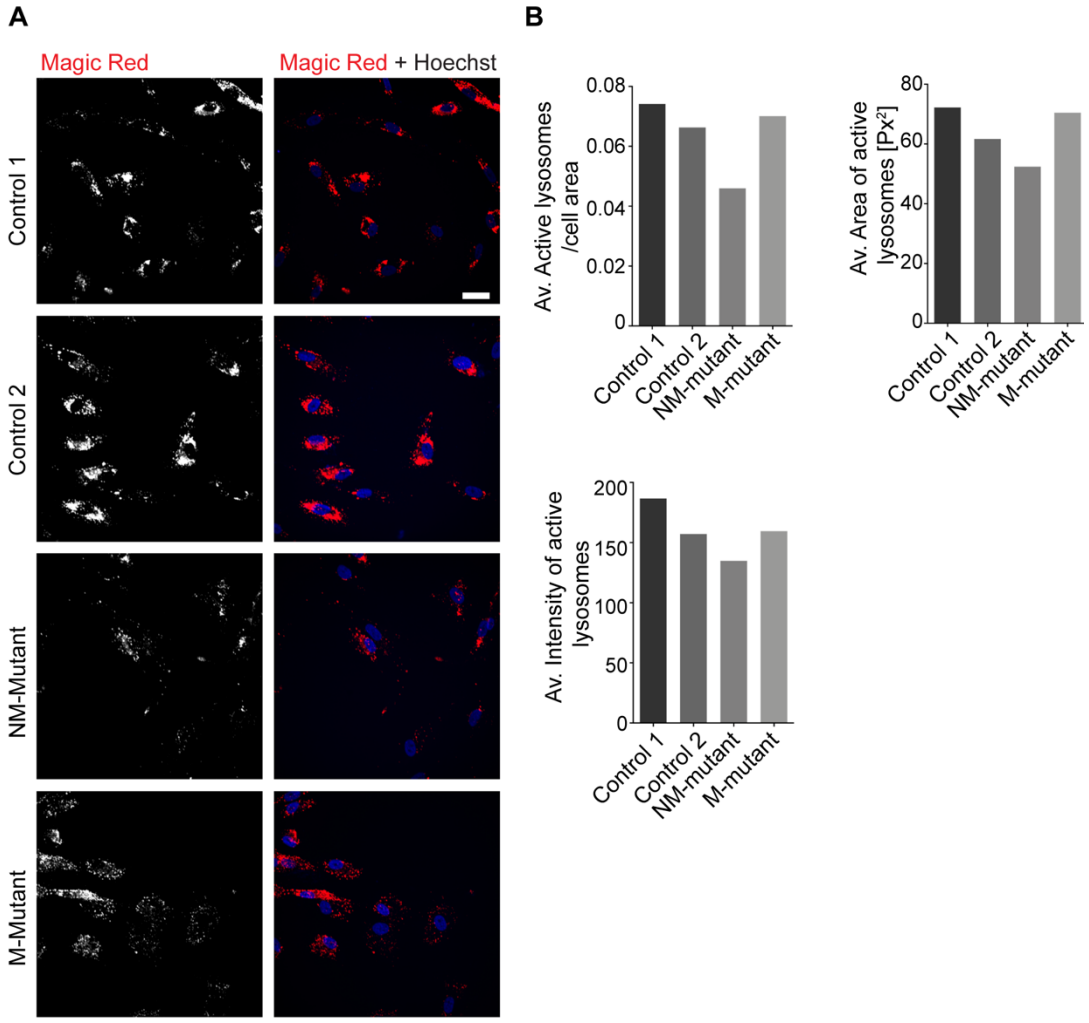

Figure 4.17 LRRK2 [G2019S] mutation doesn't increase lysosome activity

A Dopaminergic neurons were differentiated from control and [G2019S] mutant iNPCs lines. Cells were labelled with Magic-Red Cathepsin B reagent at the end of the differentiation protocol and imaged live with an OPERA high content screening imaging system x40 objective. Scale bar 20 µm. Maximum projection shown. **B** The number, intensity and area of active lysosomes was quantified using Harmony high content imaging and analysis software. Minimum of 251 cells quantified per line.

4.4.4. LRRK2 [G2019S] manifesting mutant dopaminergic neurons have reduced Rab7 staining

I next wanted to see if the increase in LAMP1 staining was due to a general issue within the endolysosomal system. Dopaminergic neurons differentiated from iNPCs were fixed on the final day of differentiation and stained with an antibody for Rab7. Images were acquired with an OPERA Phoenix high content screening imaging system. Random fields of view from each well were captured to remove bias. Representative images of each neuron line are shown in **Figure 4.18A**. For manifesting mutant cells there was a dramatic reduction in the Rab7 signal when compared to the control neuron lines. Quantification was carried out as above to determine the number of Rab7 positive vesicles per cell (**Figure 4.18B**). This confirmed there is a significant decrease in the number of Rab7 positive vesicles in the manifesting mutant [G2019S] neuron line compared with the control lines. The non-manifesting mutant showed no difference in staining compared with the control lines.

4.4.5. LRRK2 [G2019S] mutants have a disrupted TGN

It has previously been shown that hyperactive mutation of LRRK2 affects the morphology of the TGN in a number of cell models (Purlyte et al., 2018; Liu et al., 2018) (**Section 1.4.12**). To further investigate the finding that there is not an increase in the activity of lysosomes despite there being an increase in the number of total lysosomes, I next looked at the distribution of the mannose-6-phosphate receptor (CIMPR). Neurons were differentiated from iNPCs and fixed and stained with an antibody for CIMPR on the final day of differentiation. Images were acquired with an OPERA Phoenix high content screening system. Representative images are shown in **Figure 4.19**. The CIMPR would be expected to reside in the Golgi apparatus and TGN at steady state, with only a small portion trafficking back from the endosomal network (Cooper and Stevens, 1996). This was the case in both control and mutant lines. However, as previously reported, the morphology of the Golgi and the TGN was affected by the [G2019S] mutation in both the non-manifesting and manifesting mutant cells. In control cells, the Golgi and TGN was compact in the perinuclear area.

In both [G2019S] LRRK2 mutant lines, the Golgi and TGN was more dispersed and stretched out further from the nucleus compared to control lines.

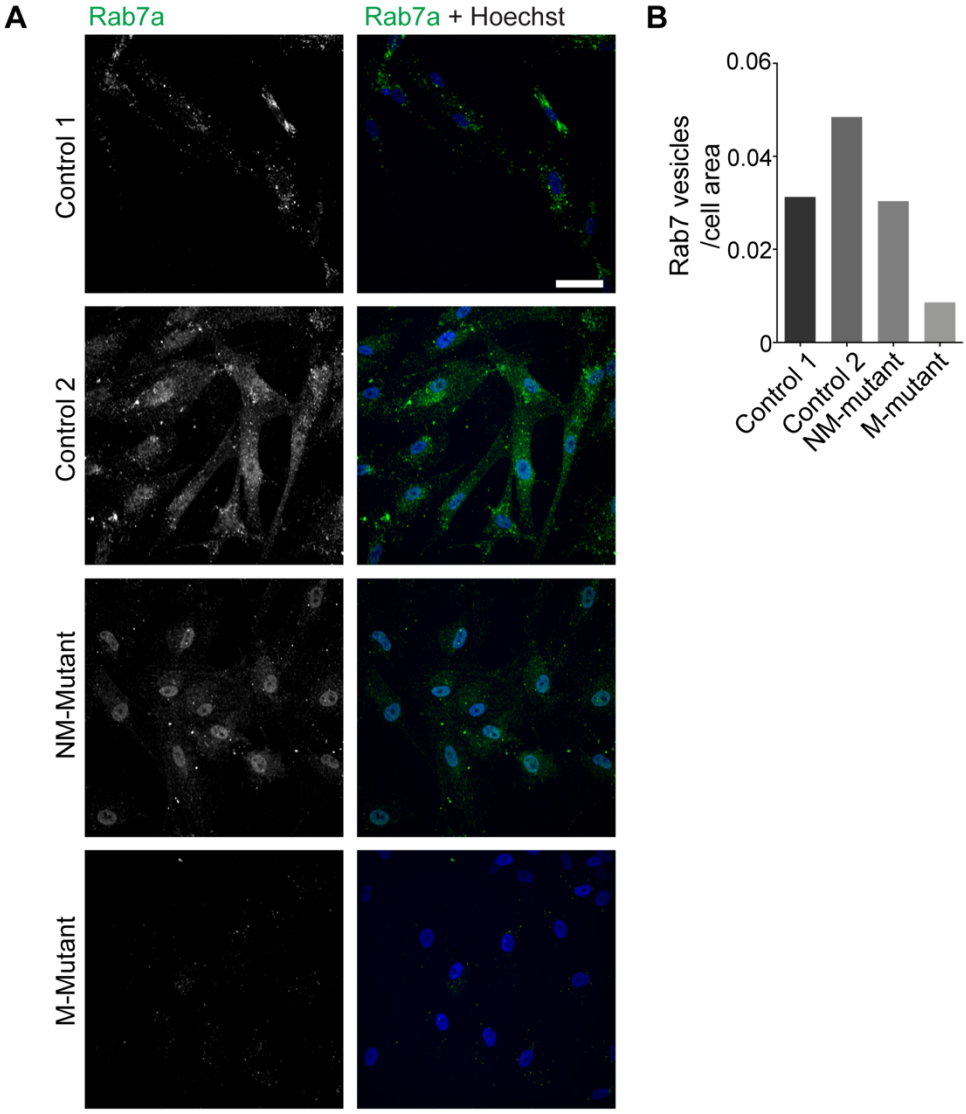

Figure 4.18 Manifesting [G2019S] LRRK2 mutant neurons have reduced Rab7 staining
A Control and [G2019S] mutant neurons differentiated from iNPCs were fixed on the final day of differentiation in 4% PFA before processing for IF. Cells were stained with an antibody against Rab7. Cells were imaged with an OPERA high content screening imaging system x40 objective. Scale bar 50 µm. Maximum projection shown. **B** The number of Rab7 positive vesicles per cell was quantified using Harmony high content imaging and analysis software. Minimum of 541 cells quantified per line.

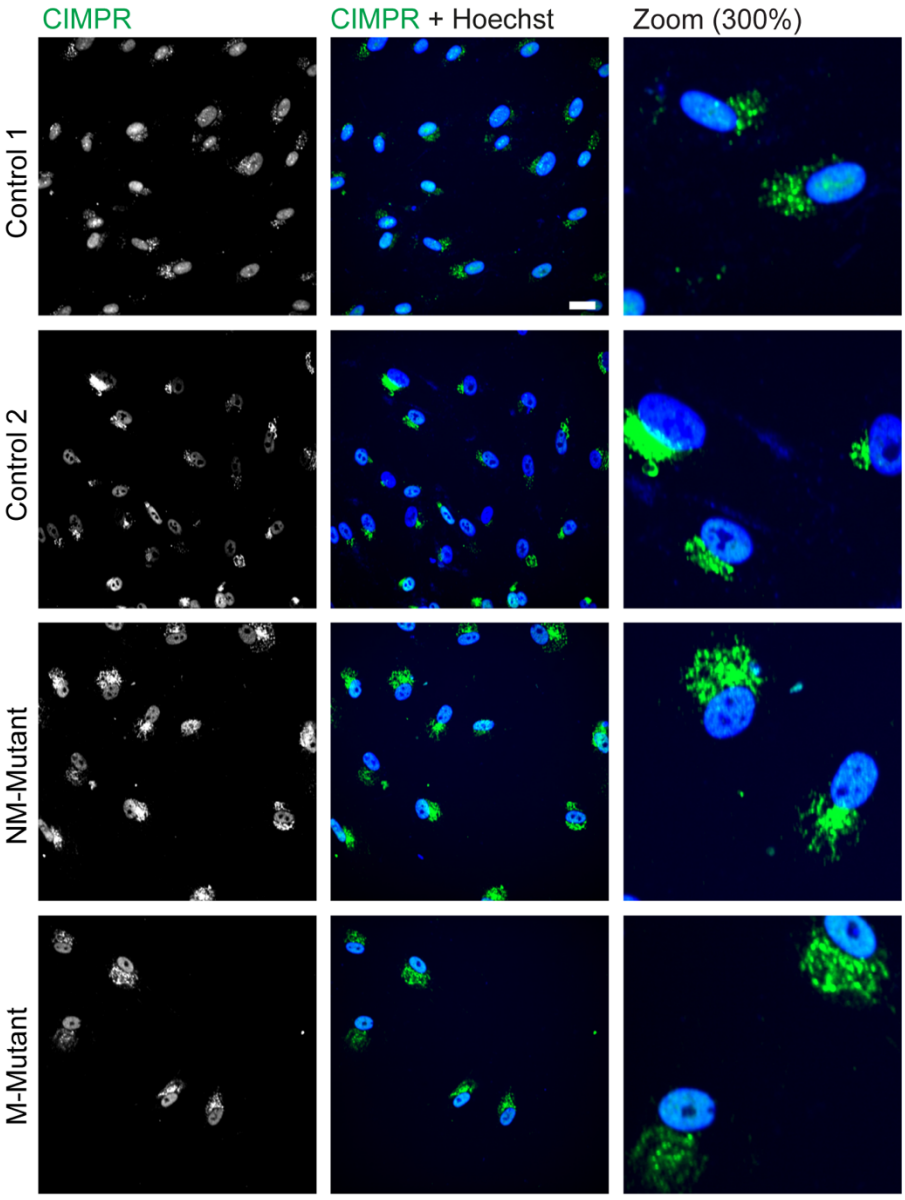

Figure 4.19 LRRK2 [G2019S] mutation disrupts the TGN
Control and [G2019S] mutant neurons differentiated from iNPCs were fixed on the final day of differentiation in 4% PFA before processing for IF. Cells were stained with an antibody against CIMPR. Cells were imaged with an OPERA high content screening imaging system x40 objective. Scale bar 20 µm. Maximum projection shown. n=1.

4.5. Discussion

In this chapter I identified a relationship between LRRK2 and two related transcription factors which drive related organelle biogenesis pathways, MITF and TFEB (**Figure 1.6**). The inverse relationship between MITF and LRRK2 is consistent with the pattern of LRRK2 expression seen in Melanoma cells shown in **Figure 3.2**, where high levels of LRRK2 correlate with low levels of pigmentation markers and vice versa. Although LRRK2 has been linked to many trafficking defects, in particular within the endolysosomal system, LRRK2 has not previously been linked to the lysosome biogenesis transcription factor TFEB. Western blotting showed a striking increase in LRRK2 levels with TFEB KD and an increase in TFEB protein with LRRK2 depletion. However, the qPCR data showed a much smaller fold change in mRNA levels compared to total protein levels. This suggests that the inverse relationship between LRRK2 and TFEB is only in part due to changes in transcription, and instead post translational changes are relevant. The data in this chapter indicates LRRK2 inhibition leads to dysfunction in the late stages of the endolysosomal pathway. No changes were observed in early endosomal markers. The inverse relationship with TFEB made us question whether this was due to an increase in lysosome biogenesis. Changes seen in staining for acidic organelles as well as LAMP1 and Rab7 occur as early as 1 hour post inhibition of LRRK2 suggesting this is not the case. It does not seem conceivable that changes observed could be due to the generation of new organelles in such a short time frame. This is also supported by the finding that total amounts of late endosome/lysosome proteins are unchanged with LRRK2 inhibition or depletion.

It has recently been shown that LRRK2, and Rab29 interact with Vps52 (Beilina et al., 2020). Vps52 is a component of the GARP complex- a tethering factor responsible for the retrograde transport from the endosomal system to the TGN (Bonifacino and Hierro, 2011). Knockdown of LRRK2 was shown to reduce the normal trafficking of CIMPR and CtxB to the TGN and was proposed to do this through its interaction with GARP. This would suggest that LRRK2 serves an integral role in the maintenance of lysosomal enzyme traffic

and therefore lysosome function and homeostasis (Beilina et al., 2020). In our model, LRRK2 inhibition did not alter lysosomal enzyme activity. The lack of an increase in lysosomal hydrolase activity would suggest that the degradative capacity of cells is unchanged. This supports the assumption that we do not generate more lysosomes, as you would expect a concomitant increase in lysosomal protein and activity. Therefore, this phenotype is more likely to be due to changes in fission/fusion events, or recruitment of markers to membranes. The occurrence of such events could be based on an initial response at shorter time points, that is independent of TFEB, or one in which TFEB plays a role in the sustained effect on the endolysosomal system following longer inhibition or knockdown periods.

Rab7 staining by immunofluorescence was dramatically increased after 1-hour inhibition of LRRK2 and was sustained at longer time points, as well as with LRRK2 depletion. Although LRRK2 can phosphorylate a subset of Rab proteins (Steger et al., 2016), Rab7 is not a direct substrate of LRRK2 (**Table 1.3**). LRRK1, a paralogue of LRRK2, is able to phosphorylate Rab7 (Malik et al., 2020). Despite not being a substrate, Rab7 activity has been linked to LRRK2 kinase activity. Hyperactivating mutations in LRRK2 negatively regulate Rab7, resulting in an increase in Rab7-GDP (Gómez-Suaga et al., 2014). The mechanism through which LRRK2 exerts its regulatory function on Rab7 is not currently known. You would expect the hyperactivating mutations in LRRK2, and inhibition of LRRK2 activity to have opposing phenotypes. In this case you would expect that inhibition of LRRK2 would induce a higher proportion of Rab7-GTP, or “active Rab7”. In Melan-a cells LRRK2 inhibition increased GTP-bound active Rab7 with both acute and longer inhibition time points. Rab proteins are inserted into membranes via their lipid-based geranylgeranyl PTM, after which they can exchange GDP for GTP, with the help of their GEF (Zerial and McBride, 2001; Zerial and Stenmark, 1993). You would expect that GTP bound Rab7 would be localised to membranes as opposed to the cytoplasm. Under baseline conditions, only a small percentage of total Rab protein is in the active GTP bound form. One explanation for the results seen could be that acute inhibition of LRRK2 blocks Rab7 hydrolysis

of GTP and prevents the progression of the Rab cycle. This would prevent the extraction of Rab7 from the membrane and give the appearance of an increase in Rab7 positive punctae. The change in staining pattern could also be related to Rab7's function in late endosome- lysosome fusion events and lysosomal positioning. Rab7 interacts with the HOPS complex which tethers late endosomes and lysosomes together prior to fusion (Khatter et al., 2015; Lin et al., 2014). Therefore, there could be an increase in tethering of Rab7 positive vesicles in response to LRRK2 inhibition. In imaging experiments changes were observed in Rab7, LAMP1 and LysoTracker, with varying responses. Since there is a large body of data already linking LRRK2 to the endolysosomal system, and PD being a disease of membrane traffic, it would be reasonable to assume that these vesicles are lysosomes. Due to the initial data linking LRRK2 and TFEB this was also my initial assumption.

One caveat that should be noted is that many late endosomal markers are also present at melanosomes. LAMP1 has been identified as residing at melanosomes (Zhou et al., 1993). Rab7 has also been reported to be a melanosome associated protein (Jordens et al., 2006; Gomez et al., 2001). As melanosomes are lysosome related organelles, which originate from the same system, it is logical that they would share many markers. The rapid change in LysoTracker signal with acute LRRK2 inhibition indicates a rapid acidification process. Lysosomes are well characterised as having a low pH essential to their function. Early-stage melanosomes are also acidic. Via the action of a v-ATPase isoform, they are acidified during the early stages of melanogenesis, then neutralised at the later stages prior to melanosome transfer (Ohbayashi and Fukuda, 2020)(**Section 1.2.7**). It therefore must be considered that the changes seen could all be the result of an effect on melanosomes as well as lysosomes. This would be consistent with the relationship observed between LRRK2 and MITF, and the inverse relationship seen between LRRK2 and pigmentation markers. No previous role for LRRK2 in melanogenesis has been identified. It would be beneficial to identify a marker which is a "true lysosomal marker". However, it was difficult to find a lysosomal protein which has not also been reported to localise to melanosomes. This makes it difficult

to differentiate fully between the two compartments in this cell type. I will revisit this issue later in chapter 5, as well as looking at Rab7 and the acidification phenotypes in other cell lines. It is also possible that the changes observed are due to alterations in both pathways and that they share some regulatory machinery where LRRK2 plays a role.

The work carried out in Sheffield utilising the differentiated dopaminergic neurons allowed me to look at LRRK2 biology in a more physiologically relevant setting, and to look at cells which are expressing a LRRK2 pathogenic mutation, rather than looking at LRRK2 depletion or inhibition. The finding that LAMP1 positive vesicles are increased in the non-manifesting and manifesting [G2019S] mutant is consistent with previous studies showing that LRRK2 mutation results in trafficking defects in the lysosomal pathway (Ho et al., 2020; Henry et al., 2015; Hockey et al., 2015; MacLeod et al., 2013). Labelling of these cells with Magic Red-Cathepsin B did not indicate that there is an increase in the lysosomal activity within these cells. This is consistent with the phenotypes observed in the melanocytes with LRRK2 inhibition, despite the change in LRRK2 activity being in the opposite direction. This data contrasts with what was previously reported showing that the interaction between LRRK2 and GARP affects the trafficking of lysosomal hydrolases (Beilina et al., 2020). In our data, LRRK2 [G2019S] mutation in the dopaminergic neurons resulted in a more dispersed staining of CIMPR. The staining was clearly consistent with TGN morphology, indicating that the CIMPR is localising normally, but that the morphology of the TGN itself is changed. This is consistent with previous studies which also show that hyperactive mutations in LRRK2 result in a more dispersed Golgi staining, which can be rescued by treating cells with MLi-2 (Liu et al., 2018; Purlyte et al., 2018). In these studies, they suggest that Rab29 and its ability to recruit LRRK2 to the TGN is significant to this disruption. This phenotype is also consistent with the data shown in chapter 3 where VPS35 [D620N] induced disruption of the TGN. This is consistent with the reports that VPS35 is upstream of LRRK2 and that the [D620N] mutation hyperactivates LRRK2 kinase activity (Mir et al., 2018).

The staining for Rab7 in the dopaminergic neurons indicated that the manifesting mutant neurons had a lower number of Rab7 positive vesicles relative to the control cells and the non-manifesting mutant. This, unlike the LAMP1 and Magic Red data, is the opposite phenotype observed in the melanocytes with LRRK2 inhibition. The paper mentioned above suggests that hyperactive mutations in Rab7 increase the Rab7-GDP bound form (Gómez-Suaga et al., 2014). Inactive Rab7 is more likely to be cytosolic and could account for the lack of Rab7 positive dots. However, it is unclear why the manifesting and non-manifesting [G2019S] mutants show different phenotypes for this marker. Unlike the melanocytes, the dopaminergic neurons do not have melanosomes which removes the ambiguity regarding whether we are looking at lysosomes or another related organelle. The data suggest that hyperactivating mutations in LRRK2 in this cell type result in wide scale defects in the endolysosomal system.

The work in this chapter highlights that hyperactivating mutations in LRRK2 and inhibition or depletion of LRRK2 do not always have opposite effects. It is possible that because LRRK2 is related to Rab proteins, changes in kinase activity in either direction cause dysfunction in a Rab cycle which can result in the same overall effect.

5. Chapter 5: LRRK2 and pigmentation

5.1. Introduction

Data in Chapter 4 showed clear trafficking defects in Melan-a cells following depletion of LRRK2 and inhibition of kinase activity. I next wanted to confirm exactly which compartment was affected in this cell type, i.e., is the effect specific to melanosomes or lysosomes or are both related compartments changed with LRRK2 disruption. The issue experienced previously was that many markers used to look at lysosomes would also be markers for melanosomes. In order to overcome this, I focused on looking at the pigmentation of cells by brightfield and EM as well as looking at specific melanosome markers. I also looked at two other cell lines, a pigmented and a non-pigmented melanoma cell line, to try and distinguish between effects on melanosomes and lysosomes. I also wanted to try and determine the mechanisms which underpin the rapid acidification phenotype observed with acute LRRK2 inhibition. Whilst working with the melanoma cells, I also looked at other key processes affected in melanoma including cell morphology, cell growth and cell migration, and the effect of loss of LRRK2.

5.2. LRRK2 and pigmentation in Melan-a cells

5.2.1. LRRK2 KD increases pigmentation in Melan-a cells

Following the finding that depletion of LRRK2 increased the protein levels of MITF (**Figure 4.1**), I next looked at Melan-a cells by both brightfield and immunofluorescence microscopy to investigate the effect of LRRK2 depletion or inhibition on pigmentation. For immunofluorescence, antibodies against PMEL and TYRP1 were used as early and late melanosome markers respectively (Raposo and Marks, 2007).

Rab27A is the Rab protein responsible for transporting mature melanosomes along the melanocyte projections for keratinocyte transfer (Jordens et al., 2006; Chiaverini et al., 2008; Wu et al., 2001; Lopes et al., 2007a; Futter et al., 2004). Loss of Rab27A resulted in a redistribution of melanosomes around the

perinuclear area (Figure 5.1). Loss of MITF halted melanosome production resulting in a decrease in pigmentation. With MITF depletion, any pre-existing melanosomes were redistributed to the peri-nuclear space, reflecting loss of Rab27A which is itself under the transcriptional control of MITF (Appendix 2) (Chiaverini et al., 2008). Melan-a cells also appeared highly stressed with MITF depletion with frequent cell death observed (Figure 5.1 x10 images). In the case of both Rab27A and MITF depletion, the signal for TYRP1 appeared more intense around the perinuclear area due to the concentration of melanosomes to the perinuclear space. Depletion of LRRK2 using siRNA resulted in a moderate increase in the pigmentation of Melan-a cells (Figure 5.2) visible from both the brightfield and TYRP1 stained images. This data would suggest that depletion of LRRK2 activity results in an increase in pigmentation in Melan-a cells.

5.2.2. Inhibition of LRRK2 increases pigmentation

I wanted to see if these results could be reproduced with LRRK2 inhibition. Rapamycin was used as a positive control. It has previously been shown that inhibition of the mTOR pathway using Rapamycin induces melanogenesis in melanocytes (Hah et al., 2012). Phenylthiourea (PTU) is an inhibitor of the enzyme tyrosinase, preventing the synthesis of melanin. Previously, treatment of melanocytes with PTU has been shown to result in an increase in early stage melanosomes (Chang, 2009) (Figure 5.3).

Inhibition of LRRK2 kinase activity with MLi-2 for 72 hours resulted in an increase in pigmentation in Melan-a cells (Figure 5.4). These results suggest that LRRK2 acts as a negative regulator of pigmentation in this cell type. Although we did see increases in both the TYRP1 staining, as well as changes in the brightfield images with LRRK2 inhibition, these cells are very heterogenous when it comes to their pigmentation. This means that there was great variation between cells imaged side by side. Staining with PMEL by IF comes with the issue that once cells begin to pigment and melanin is deposited on to the PMEL fibrils, antibodies cannot always reliably recognise PMEL.

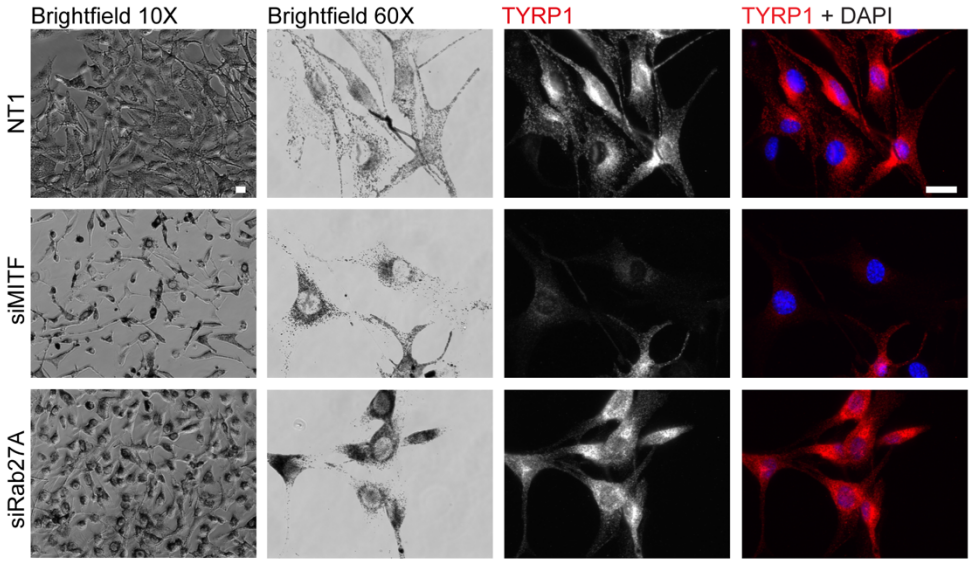

Figure 5.1 Loss of MITF and Rab27A causes melanosome defects

Melan-a cells treated with 40 nM siRNA for 72 hours were fixed in 4% PFA before processing for IF. Cells were stained for the late melanosome marker TYRP1. Coverslips were mounted on Moviol supplemented with 4',6-diamidino-2-phenylindole (DAPI). Images were acquired with a Nikon Ti-Eclipse widefield microscope x10 or x60 objective. Scale bar: 20 μm. n=3 biological replicates.

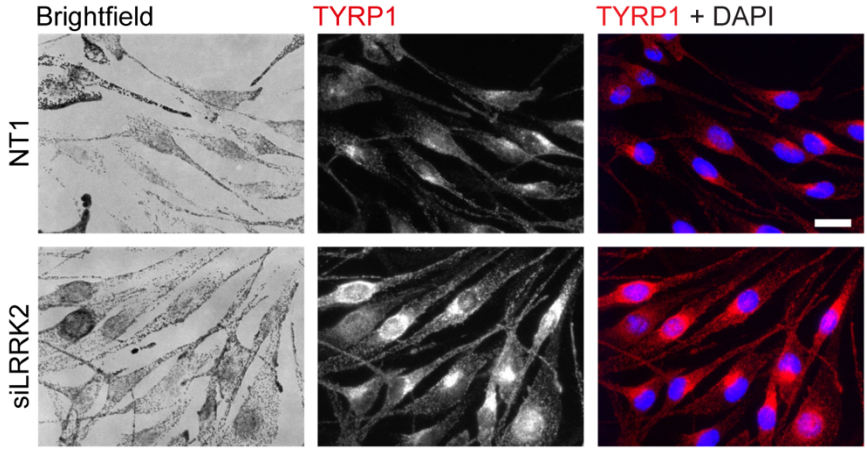

Figure 5.2 Depletion of LRRK2 increases pigmentation in Melan-a cells

Melan-a cells treated with 40 nM siRNA for 72 hours were fixed in 4% PFA before processing for IF. Cells were stained for the late melanosome marker TYRP1. Coverslips were mounted on Moviol supplemented with 4',6-diamidino-2-phenylindole (DAPI). Images were acquired with a Nikon Ti-Eclipse widefield microscope x10 or x60 objective. Scale bar: 20 μm. n=3 biological replicates.

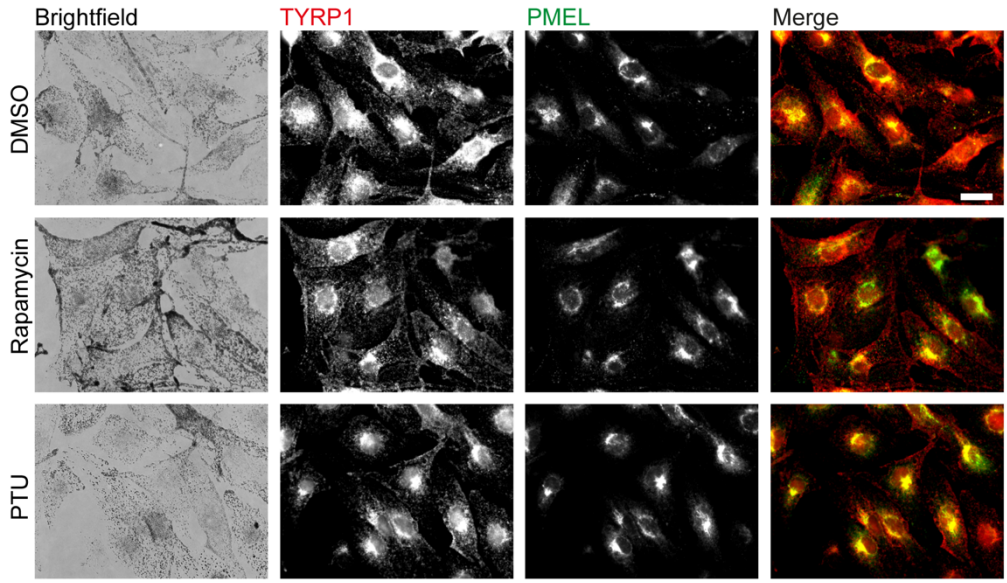

Figure 5.3 Rapamycin and PTU and pigmentation markers in Melan-a cells
Melan-a cells treated with Rapamycin (1 μM) or PTU (200 μM), for 72 hours were fixed in 4% PFA before processing for IF. Cells were stained for early melanosome marker PMEL and late melanosome marker TYRP1. Coverslips were mounted on Moviol supplemented with 4',6-diamidino-2-phenylindole (DAPI). Images were acquired with a Nikon Ti-Eclipse widefield microscope x60 objective. Scale bar: 25 μm. n=3 biological replicates

Additionally, I found that the TYRP1 antibody staining did not always reflect pigmentation as seen by brightfield imaging. For example, in the cell projections in **Figure 5.4**. I therefore determined brightfield imaging to be the most reliable way of looking at pigmentation. I next took lower magnification images of cells treated with MLi-2 to get a more global look at pigmentation (**Figure 5.5**). Inhibition of LRRK2 resulted in an increase in pigmentation after 24 hours, but not 1 hour treatment.

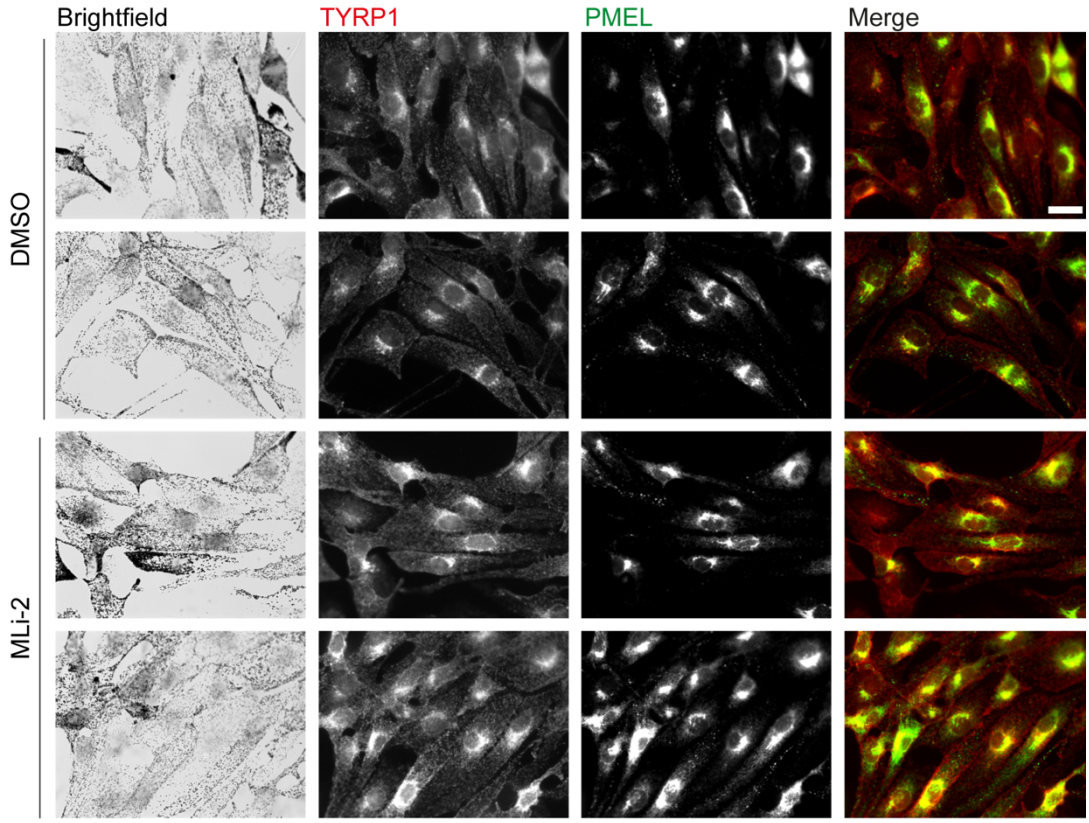

Figure 5.4 Inhibition of LRRK2 increases pigmentation in Melan-a cells

Melan-a cells treated with MLi-2 (200 μM) for 72 hours were fixed in 4% PFA before processing for IF. Cells were stained for early melanosome marker PMEL and late melanosome marker TYRP1. Coverslips were mounted on Moviol. Images were acquired with a Nikon Ti-Eclipse widefield microscope x60 objective. Scale bar: 25 μm. n=3 biological replicates.

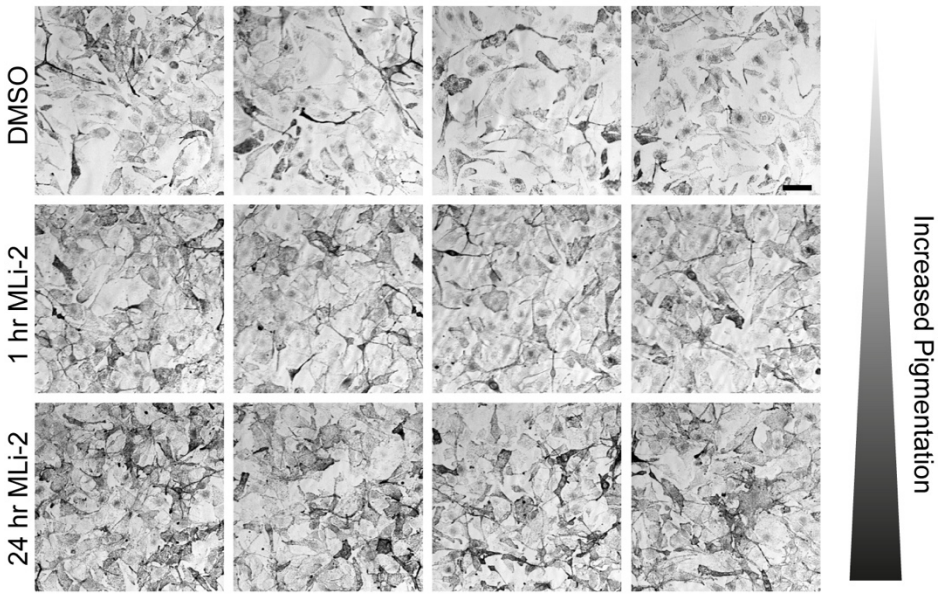

Figure 5.5 LRRK2 inhibition increases pigmentation in Melan-a cells
Melan-a cells were treated with LRRK2 inhibitor MLi-2 (200 nM) for the indicated time points. Cells were fixed in 4% PFA and coverslips were mounted on Moviol. Images were acquired using an LSM800 confocal microscope x20 objective. Scale bar: 50 µm. 350 nm slice. n=3 biological replicates

5.3. LRRK2 and LRO in Melanoma cells

5.3.1. Inhibition of LRRK2 increases acidification in MNT1 cells

One of the most striking phenotypes observed in Melan-a cells reported in chapter 4 was the rapid and sustained acidification following LRRK2 inhibition or depletion. I next wanted to see if the effect of LRRK2 inhibition on acidification was specific to Melan-a cells or could be replicated in another cell line. To do this, I used the MNT1 melanoma cell line. As discussed in chapter 3, MNT1 cells are highly pigmented, human melanoma cells which have a good level of LRRK2 expression (**Figure 3.2**). MNT1 cells treated with LRRK2 inhibitors HG-10-102-01 and MLi-2 for 48 hours were labelled with the LysoTracker Deep Red fluorescent dye and imaged live using confocal microscopy (**Figure 5.6**). LysoTracker images showed an increase in the number of acidic organelles with LRRK2 inhibition in MNT1 cells relative to control cells.

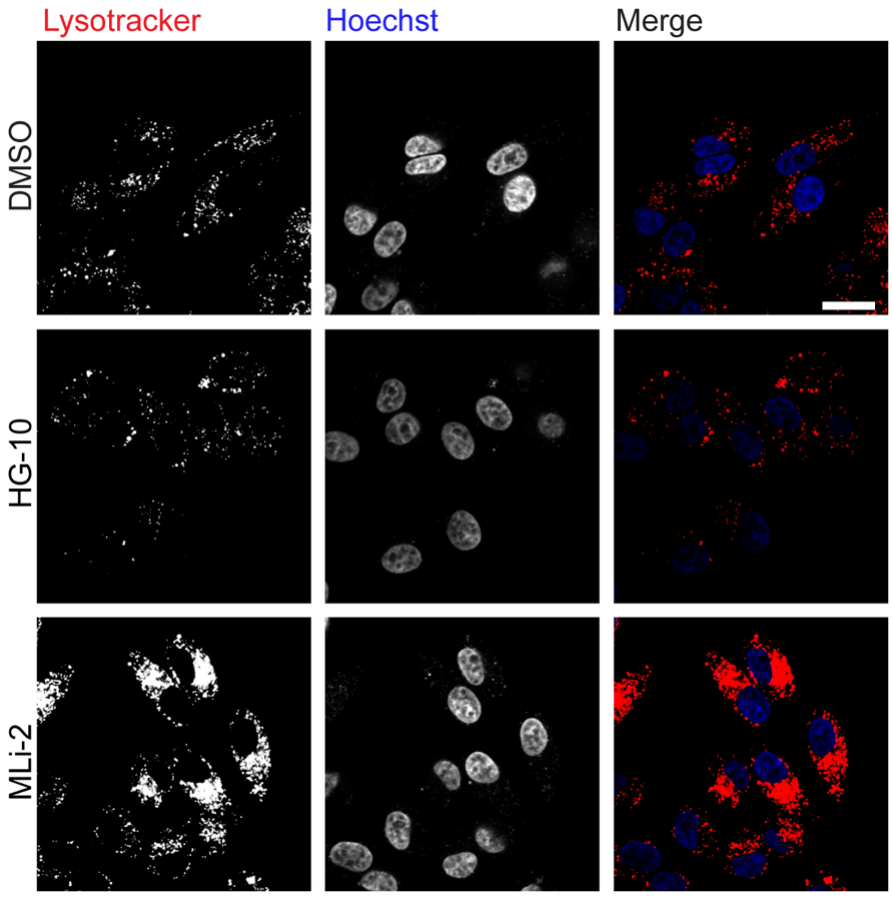

Figure 5.6 Inhibition of LRRK2 in MNT1 cells increases the number of acidic organelles
MNT1 cells treated with LRRK2 inhibitors HG-10-102-01 (500 nM) and MLi-2 (200 nM) for 48 hours were incubated with 0.5 μM LysoTracker Deep Red and nuclear dye Hoechst for 1 hour before live imaging with a 3i spinning disk confocal microscope x63 objective. Scale bar: 20 μm. 350 nm slice. n=3 biological replicates.

In Melan-a cells, we saw an accumulation of acidic organelles 1 hour after treatment. I wanted to see if this rapid phenotype could be recapitulated in the MNT1 line. MNT1 cells were treated with MLi-2 for 1 hour and labelled with LysoTracker Deep Red (**Figure 5.7**). Cells were imaged live to visualise acidic organelles. There was a big increase in LysoTracker labelling after 1 hour of LRRK2 inhibition in MNT1 cells, consistent with what I had previously observed in Melan-a cells.

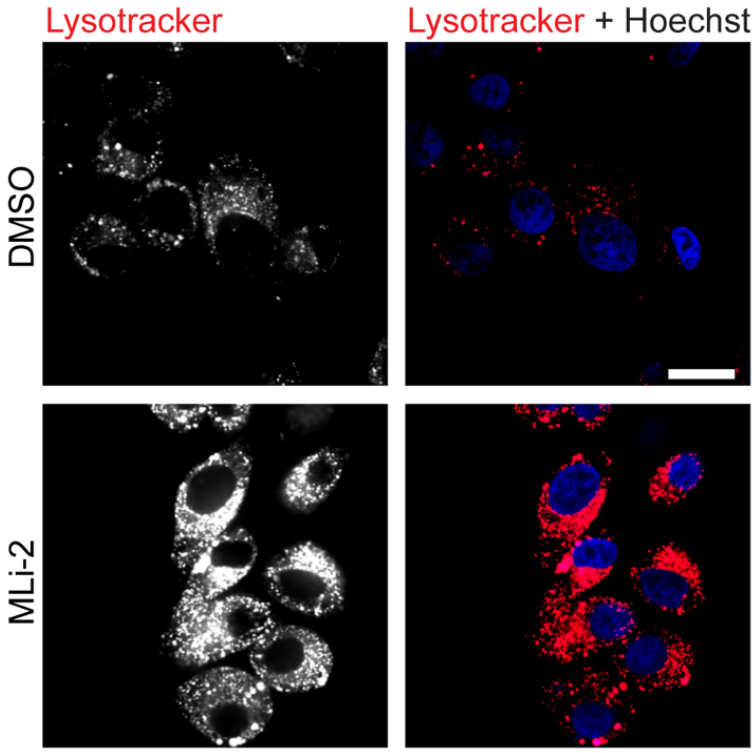

Figure 5.7 Acute inhibition in MNT1 cells increases acidic organelles
MNT1 cells were treated with MLi-2 inhibitor (200 nM) for 1 hour and labelled with LysoTracker Deep Red and nuclear dye Hoechst for 1 hour before live imaging with a 3i spinning disk confocal microscope x63 objective. Scale bar: 20 µm. 350 nm slice. n=1.

Unlike Melan-a cells, MNT1 cells are very homogenous in terms of their pigmentation. We therefore looked at the effect of LRRK2 inhibition on staining of TYRP1 in these cells. LRRK2 inhibition resulted in an increase in TYRP1 staining much more consistent than that seen in the Melan-a cells (**Figure 5.8**). The data from MNT1 cells gives support to the idea that the data seen in chapter 4 relates to changes in melanosomes.

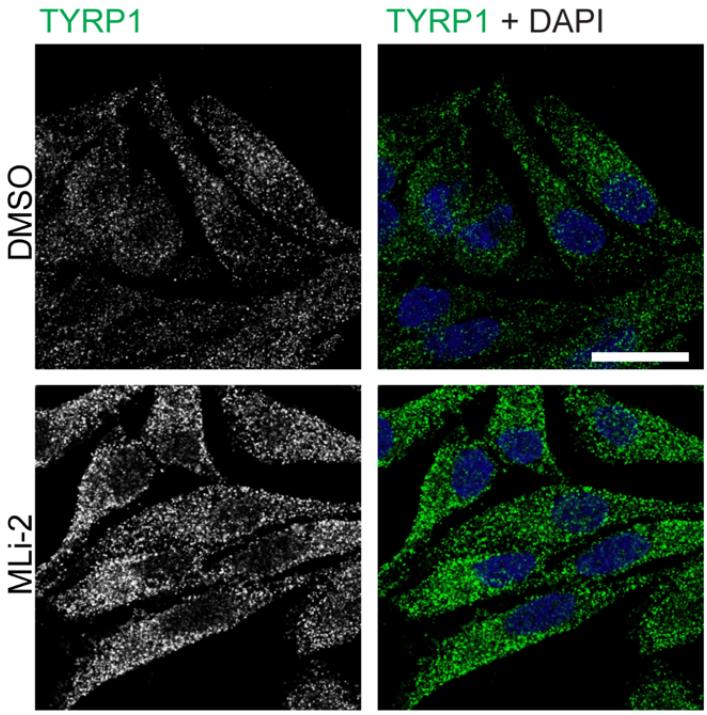

Figure 5.8 LRRK2 inhibition increases TYRP1 staining in MNT1 cells
MNT1 cells were treated with MLi-2 (200 nM) for 24 hours. Cells were fixed in 4% PFA before processing for IF. Coverslips were mounted on Moviol supplemented with 4',6-diamidino-2-phenylindole (DAPI). Cells were stained for late melanosome marker TYRP1. Images were acquired with an LSM900 confocal microscope. Scale bar 20 µm. 350 nm slice. n=1.

5.3.2.2 Inhibition of LRRK2 has no effect on LRO number in WM266.4 cells

Next, I investigated if the same increase in LRO number could be observed in the non-pigmented human melanoma WM266.4 cells. WM266.4 cells were treated with MLi-2 for 48 hours before they were labelled with LysoTracker Deep Red fluorescent dye. Cells were imaged live using confocal microscopy (Figure 5.9). LRRK2 inhibitor treated cells did not show an increase in LysoTracker signal relative to control treated cells.

WM266.4 cells treated with the same LRRK2 inhibitor were fixed after 48 hours treatment and stained with an antibody against LAMP1 (Figure 5.10). Coverslips were imaged using confocal microscopy. Inhibition of LRRK2 did

not result in an increase in the number of LAMP1 positive vesicles in WM266.4 cells. Collectively the LysoTracker and LAMP1 data indicate that the phenotypes observed in the Melan-a and MNT1 cell lines are not conserved in the WM266.4 melanoma cell line. This could indicate that the changes observed in chapter 4 are specific to melanosomes rather than lysosomes, as these phenotypes cannot be recapitulated in a cell line which has lost its pigmentation.

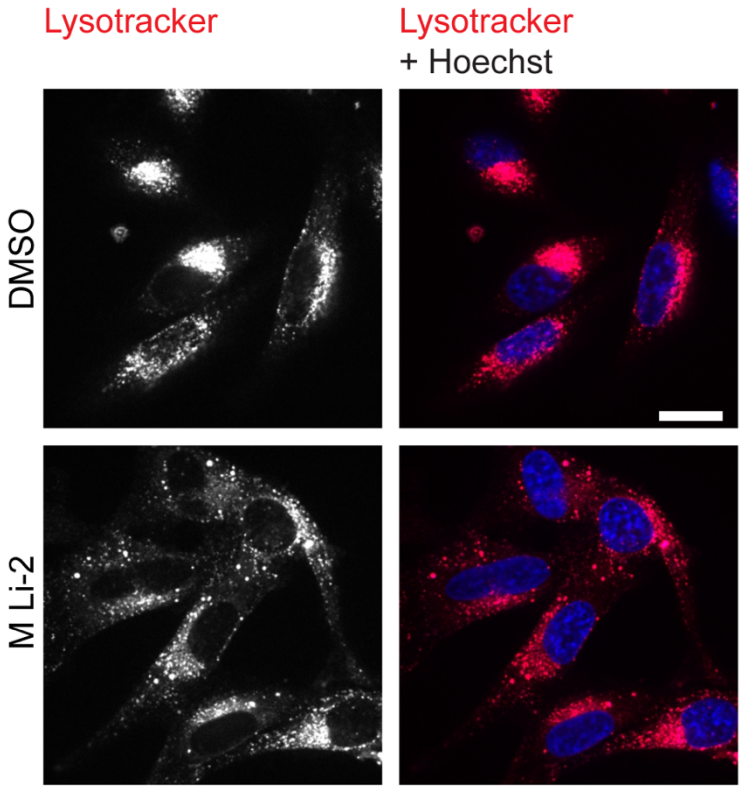

Figure 5.9 Inhibition of LRRK2 in WM266.4 cells does not affect the number of acidic organelles
WM266.4 cells treated with LRRK2 inhibitor MLi-2 (200 nM) for 48 hours were incubated with 0.5 μM LysoTracker and nuclear dye Hoechst for 1 hour before live imaging with a 3i spinning disk confocal microscope x63 objective. Scale bar: 20 μm. 350 nm slice. n=3 biological replicates.

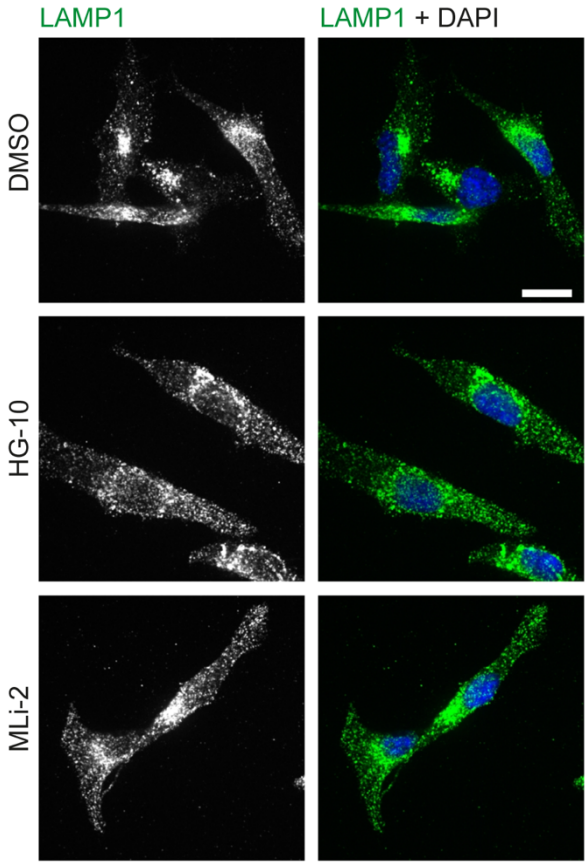

Figure 5.10 Inhibition of LRRK2 in WM266.4 cells has no effect on lysosome number.
WM266.4 cells treated with LRRK2 inhibitors HG-10-102-01 (500 nM) or MLi-2 (200 nM) were fixed in 4% PFA and processed for IF. Coverslips were mounted with Moviol supplemented with 4',6-diamidino-2-phenylindole (DAPI). Images were acquired with a 3i spinning disk confocal microscope x63 objective. Scale bar: 20 µm. 350 nm slice. n=1.

5.4. LRRK2 and cell invasion in Melanoma

5.4.1. LRRK2 expression correlates with invasion markers in melanoma cells

In melanoma, the loss of pigmentation is often simultaneous with an increase in invasive potential of cells. I was interested in the relationship between LRRK2 and invasion markers. The EMT switch is associated with solid tumours gaining malignancy (Kozar et al., 2019). A classical marker of EMT is the loss of E-cadherin and an increase in N-cadherin. Lysates from the melanoma and non-melanoma cell lines used in the chapter 3 blot for

pigmentation markers were also blotted for their expression of invasion markers Figure 5.11. In the melanoma cell lines tested, the levels of LRRK2 were highest in cells which have high levels of N-Cadherin. For example, LRRK2 is highly expressed in the WM266.4 and A375-P cell lines which are highly metastatic cells, as well as having lost their pigmentation markers. We also blotted for the receptor tyrosine kinase, Axl, which is another protein differentially expressed at different stages of melanoma (Flem-Karlsen et al., 2020; Simmons et al., 2020). High levels of Axl expression have been linked to slow cycling, highly invasive, drug resistant melanomas (Kozar et al., 2019).

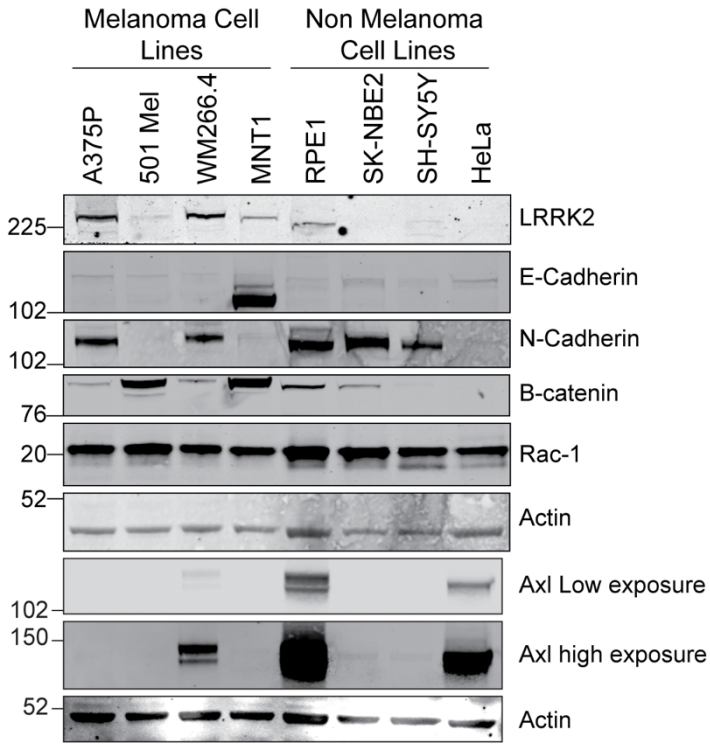

Figure 5.11 Expression of LRRK2 and cell invasion markers across cell lines
20 µg of protein lysate per cell line was analysed by western blot probing for the indicated antibodies. n=1.

5.4.2. Inhibition of LRRK2 induces cell morphology changes

When looking at the effect of LRRK2 inhibition in both melanoma cells and the melanocytes, I noticed that loss of LRRK2 activity induced a change in morphology, resulting in more elongated cells. To confirm this, cells were

treated with MLi-2 inhibitor and stained with F-actin probe phalloidin (Figure 5.12A). This was used to draw around cells, and changes in morphology were determined using the shape descriptors tools in FIJI (Figure 5.12B). For the WM266.4 cells I decided that the Aspect Ratio measurement was the most appropriate due to the irregular morphology of these cell under baseline conditions. The aspect ratio gives the major axis/minor axis. Inhibition of LRRK2 resulted in an increase in the aspect ratio of cells. This data shows that cells become more elongated with LRRK2 inhibition.

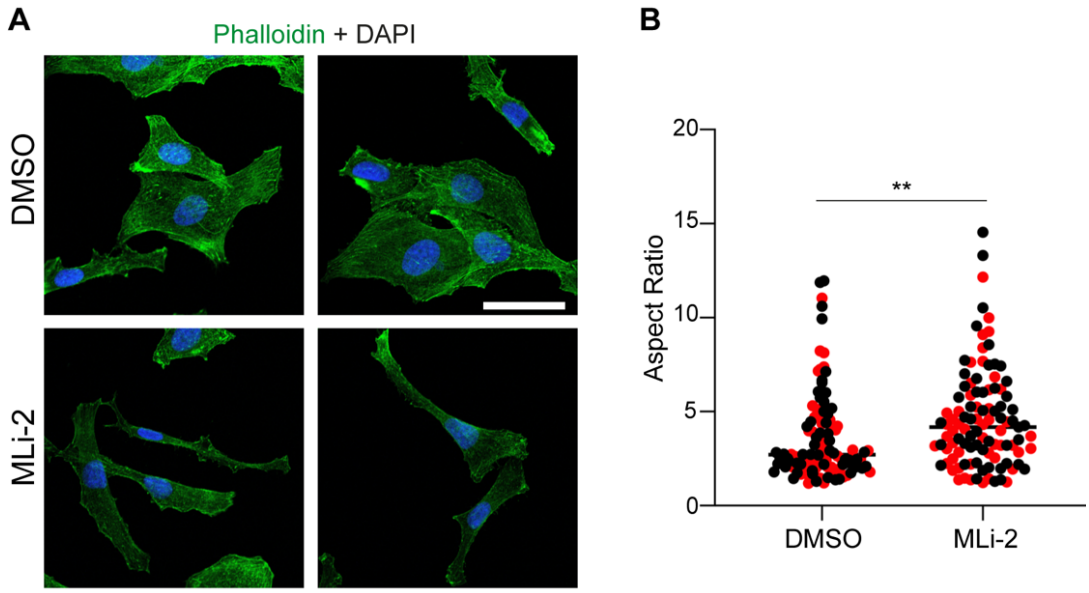

Figure 5.12 LRRK2 inhibition in WM266.4 cells alters cell morphology

A WM266.4 cells were treated with MLi-2 (200 nM) for 24 hours. Cells were fixed in 4% PFA before processing for IF. Cells were stained with Phalloidin-488 dye and coverslips mounted on Moviol supplemented with 4',6-diamidino-2-phenylindole (DAPI). Images were acquired with an LSM900 confocal microscope x40 objective. Scale bar: 50 µm. 350 nm slice. **B** Phalloidin stain was used to draw round cells and the shape descriptors tool in FIJI was used to analyse cell morphology. Aspect ratio measurements were used for WM266.4 cells. Each dot represents an individual cell. Different colours represent different experiments. n=2 biological replicates. Analysis: Unpaired t test (** $p<0.01$). Minimum 52 cells quantified per condition per repeat.

5.4.3. LRRK2 inhibition changes cell morphology in Melan-a cells

I next wanted to see if the same morphology change occurred with LRRK2 inhibition in Melan-a cells. Melan-a cells were treated with MLi-2, fixed, then stained with Phalloidin (**Figure 5.13A**). Changes in morphology were analysed as above. Quantification showed that that there was an increase in the aspect ratio of cells with LRRK2 inhibition (**Figure 5.13B-C**). This is consistent with the data from the WM266.4 cells and indicates that indeed LRRK2 inhibition results in a more elongated cell morphology.

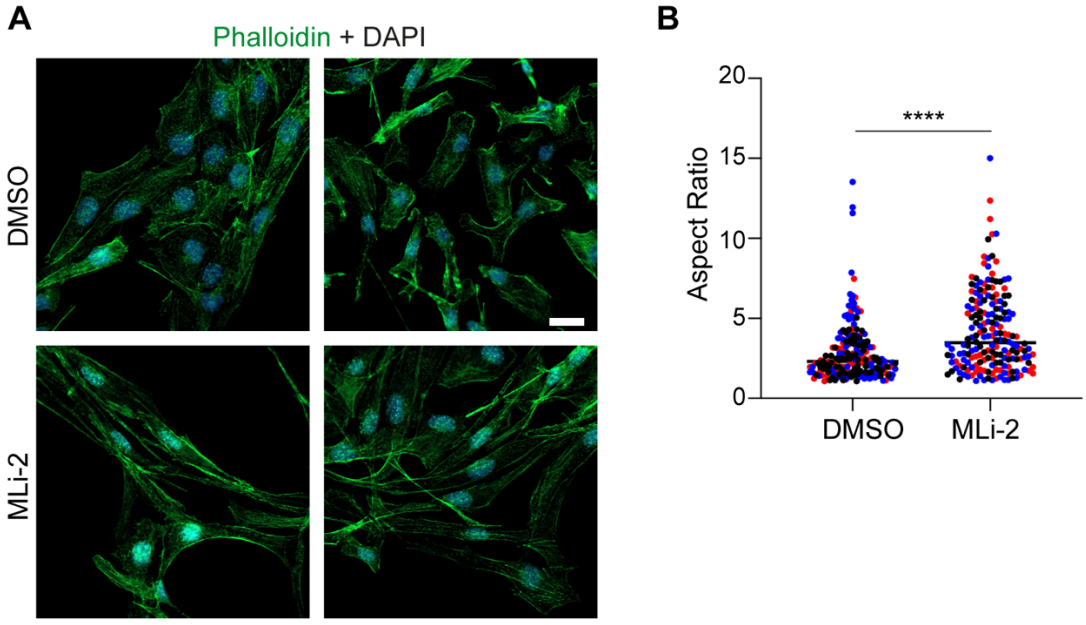

Figure 5.13 Inhibition of LRRK2 alters cell morphology of Melan-a cells
A Melan-a cells were treated with MLi-2 (200 nM) for 24 hours. Cells were fixed in 4% PFA before processing for IF. Cells were stained with Phalloidin-488 dye and coverslips mounted on Moviol supplemented with 4',6-diamidino-2-phenylindole (DAPI). Images were acquired with a LSM900 confocal microscope x40 objective. Scale bar: 50 µm. 350 nm slice. **B** Phalloidin stain was used to draw round cells and the shape descriptors tool in FIJI was used to analyse cell morphology. Aspect ratio measurements were used for Melan-a cells. Each dot represents an individual cell. Different colours represent different experiments. Analysis: Unpaired t test (**** $p<0.0001$). n=3 biological replicates. Minimum 52 cells quantified per condition per repeat.

5.4.4. LRRK2 depletion does not affect cell proliferation in WM266.4 cells

I was interested to see if LRRK2 depletion would change the rate of proliferation in melanoma cells. WM266.4 cells were treated with siRNA targeting LRRK2 for 72 hours. After 48 hours, cells were re-plated at two densities. The plate was then placed in an Incucyte imaging system and cells were imaged at regular intervals over 3 days to monitor cell growth. Images were then segmented, and cell density was plotted over time. Loss of LRRK2 did not have any effect on the rate of cell growth at either density seeded (Figure 5.14). Depletion of Rab7 has previously been shown to be essential for the high proliferative potential of melanoma cells (Alonso-Curbelo et al., 2014). Knockdown of Rab7 resulted in a decrease in cell proliferation or cell survival, relative to the control, as previously reported.

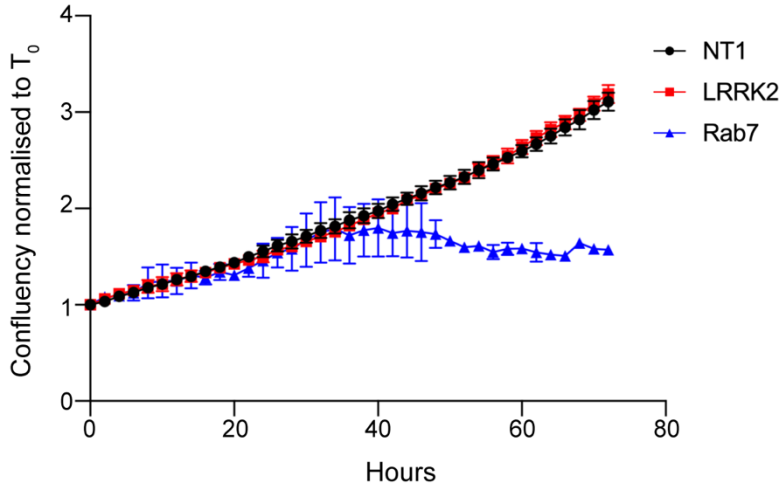

Figure 5.14 LRRK2 depletion has no effect on cell growth in WM266.4 cells
WM266.4 cells were treated with 40 nM siRNA for 72 hours. After 48 hours cells were replated into a new plate. After 72 hours cells were placed into an Incucyte live imaging system and imaged for 72 hours. Incucyte software was used to segment cells and the confluency per well was calculated over time. Plot shows confluency normalised to confluency at T_0. The average of 3 technical replicates is shown. Error bars: SD.

5.4.5. Loss of LRRK2 activity decreases cell motility

I wanted to determine if the loss of LRRK2 kinase activity would affect cell motility as LRRK2 expression correlated with cell invasion markers (Figure 5.11). To do this, WM266.4 cells were seeded at a low density and treated with either DMSO or MLi-2 for 24 hours. Cells were then imaged live at regular intervals for 24 hours. Cells were then manually tracked using the CellTracker GUI in MATLAB. Tracks were input into Chemotaxis software which then generated values for each individual cell including the accumulated distance (Figure 5.15). Inhibition of LRRK2 resulted in a decrease in the accumulated distance of cells over time. This would indicate that LRRK2 activity promotes cell motility and may account for the higher expression of LRRK2 in highly invasive melanoma cell lines like the WM266.4 cells.

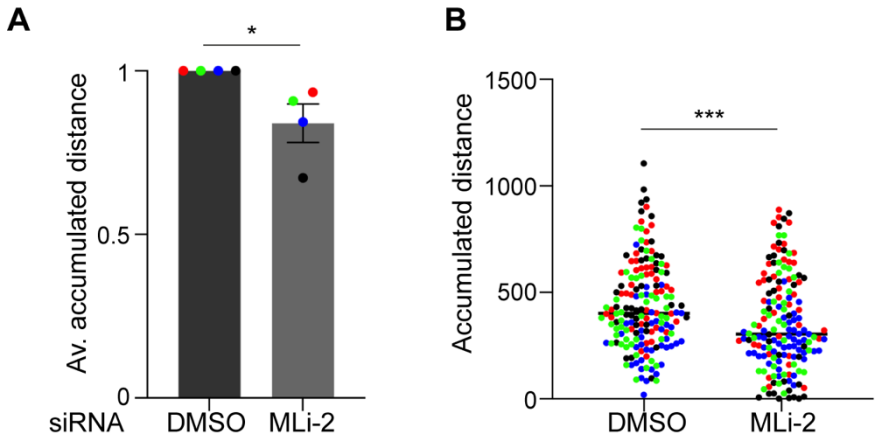

Figure 5.15 Inhibition of LRRK2 decreases cell motility in WM266.4 cells
WM266.4 cells were treated with LRRK2 inhibitor MLi-2 (200 nM) for 24 hours and then imaged live for the following 24 hours. Images were acquired with a Nikon Ti-Eclipse widefield microscope x10 objective. Cells were maintained at 5% CO_2, 37 °C throughout imaging. Manual tracks were generated using MATLAB CellTracker GUI and the resulting tracks were analysed using chemotaxis software. **A** Average accumulated distance per cell. Normalised to DMSO. n=4 biological replicates. Error bars: SEM. Analysis: Unpaired t test (* $p<0.05$) **B** Accumulated distance values for individual cells. n=4 biological replicates. Analysis: Unpaired t test (*** $p<0.001$). Different colours represent different biological replicates. Minimum 35 cells tracked per condition per repeat.

To confirm the inhibitor data, I repeated the same experiment with LRRK2 siRNA knockdown in WM266.4 cells. Cells were treated with siRNA targeting LRRK2 and after 48 hours were replated at a low density. After a total of 72 hours, cells were imaged live for a further 24 hours at regular intervals and manual tracking data generated as above. The accumulated distance for each cell was calculated and plotted (Figure 5.16). Depletion of LRRK2 confirmed that loss of LRRK2 kinase activity results in a decrease in the accumulated distance of cells. The changes seen with knockdown were more significant than those seen with the inhibitor treatment. I used a 72-hour knockdown, whereas MLi-2 treatment was for 24 hours which may indicate that this phenotype takes longer to manifest, or the defect can accumulate over time.

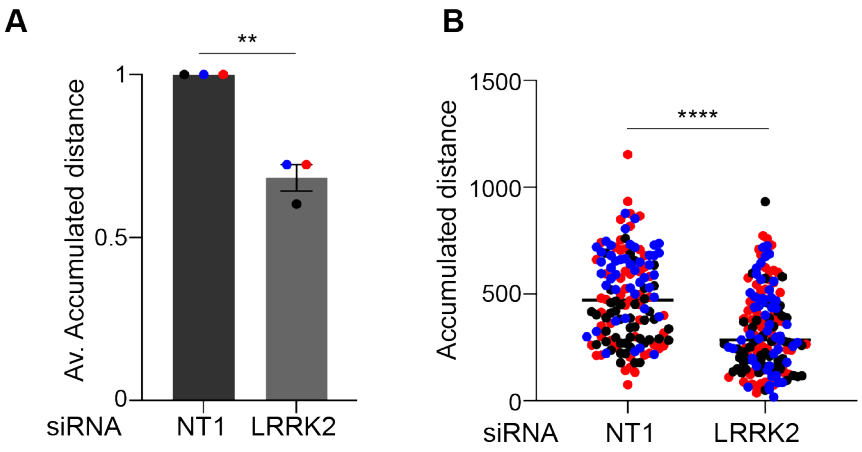

Figure 5.16 LRRK2 depletion decreases cell motility in WM266.4 cells
WM266.4 cells were treated with 40 nM siRNA targeting LRRK2 for 72 hours and then imaged live for the following 24 hours. Images were acquired with a Nikon Ti-Eclipse widefield microscope x10 objective. Manual tracks were generated using MATLAB CellTracker GUI and the resulting tracks were analysed using chemotaxis software. **A** Average accumulated distance per cell normalised to NT1. n=3 biological replicates. Error bars: SEM. Analysis: Unpaired t test (** $p<0.01$) **B** Accumulated distance values for individual cells. n=3 biological replicates. Analysis: Unpaired t test (**** $p<0.0001$). Different colours represent different biological replicates. Minimum 35 cells tracked per condition per repeat.

5.5. LRRK2 and pigmentation by EM

5.5.1. LRRK2 inhibition increases the number of melanosomes by EM

The lack of acidification and LAMP1 phenotypes observed in the WM266.4 cells could suggest that the phenotypes observed in Melan-a cells and MNT1 cells are the result of changes in the melanogenesis pathway. This would explain why no changes are seen in acidic organelles or LAMP1 staining in WM266.4 cells, as this cell line has lost its pigmentation.

To confirm if inhibition of LRRK2 increases the number of melanosomes in the Melan-a cell line, we treated cells with LRRK2 inhibitor MLi-2 for 1 or 24 hours before cells were fixed, and samples processed for EM. Whole cells were imaged and the total number of melanosomes per cell was quantified (**Figure 5.17**). Cells treated with MLi-2 for 24 hours had a clear increase in the number of melanosomes per cell. As well as an increase in the number of melanosomes, the area of melanosomes was increased at the 24-hour timepoint but not after 1-hour treatment.

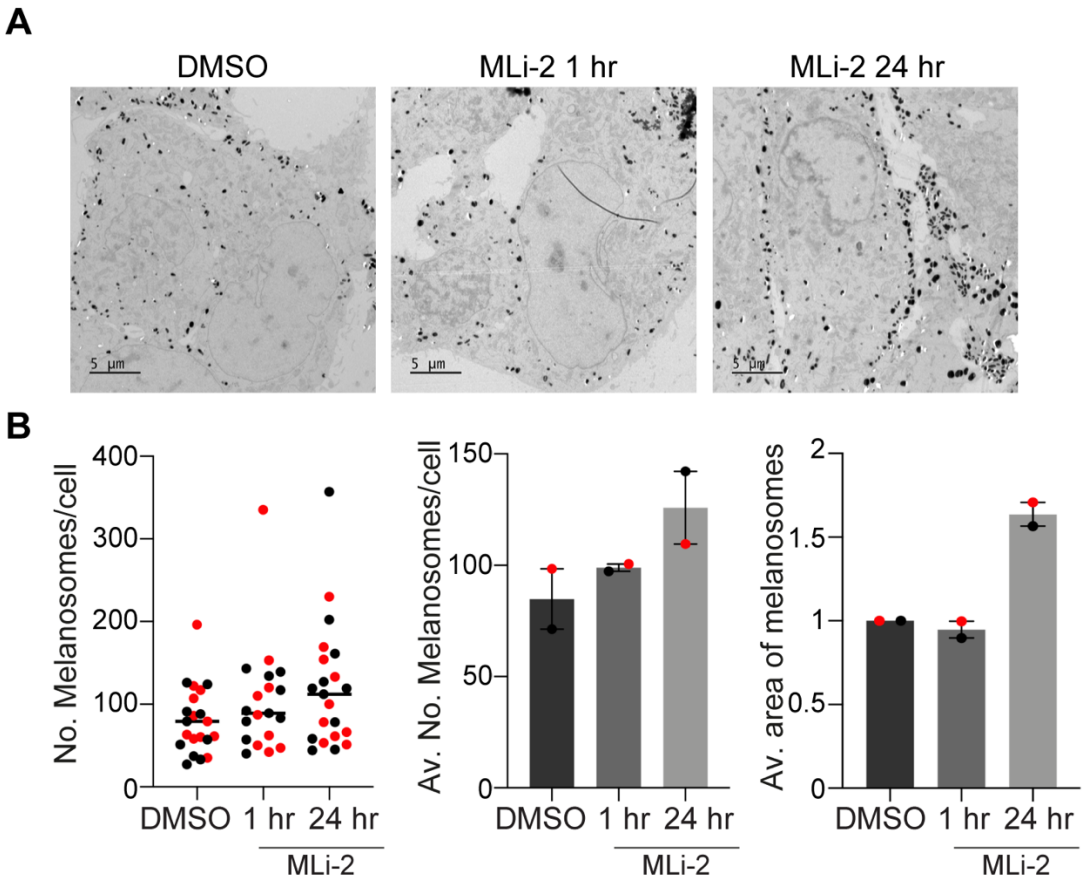

Figure 5.17 LRRK2 inhibition increases melanosomes per cell and the area of individual melanosomes
A Melan-a cells were treated with MLi-2 inhibitor (200 nM) for the indicated time points. Cells were fixed and processed for EM and overview images were acquired. **B** The number and area of individual melanosomes was quantified. Error bars: Range. n=2 biological replicates. Minimum 10 cells quantified per condition per repeat. Different colours represent different experiments.

5.5.2. LRRK2 inhibition does not increase total levels of melanogenic markers

I next checked if these changes in melanosomes were reflected in changes to total melanosome marker proteins by western blot. LRRK2 kinase activity was inhibited with MLi-2 and lysates analysed by western blot. Total protein levels of TYRP1 and PMEL were not changed (Figure 5.18). Melan-a cells were treated with siRNA against LRRK2 for 72 hours and lysates analysed by western blot. Following LRRK2 depletion the levels of melanosomal proteins TYRP1 and PMEL did not show a significant change (Figure 5.19).

To confirm, cDNA made from RNA extracted from Melan-a cells treated with siRNA targeting LRRK2 was analysed by RT-qPCR using primers against TYRP1 and tyrosinase. Neither melanosome marker showed a reproducible significant change following LRRK2 depletion confirming the results seen by western blot (Figure 5.20).

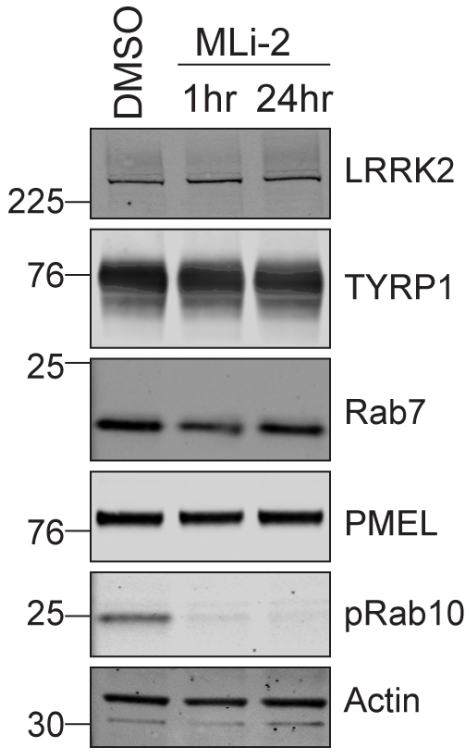

Figure 5.18 LRRK2 inhibition does not increase the levels of melanosome markers
Representative western blot from Melan-a cells treated with MLi-2 inhibitor (200 nM) for the indicated time points probed with the indicated antibodies. n=3 biological replicates.

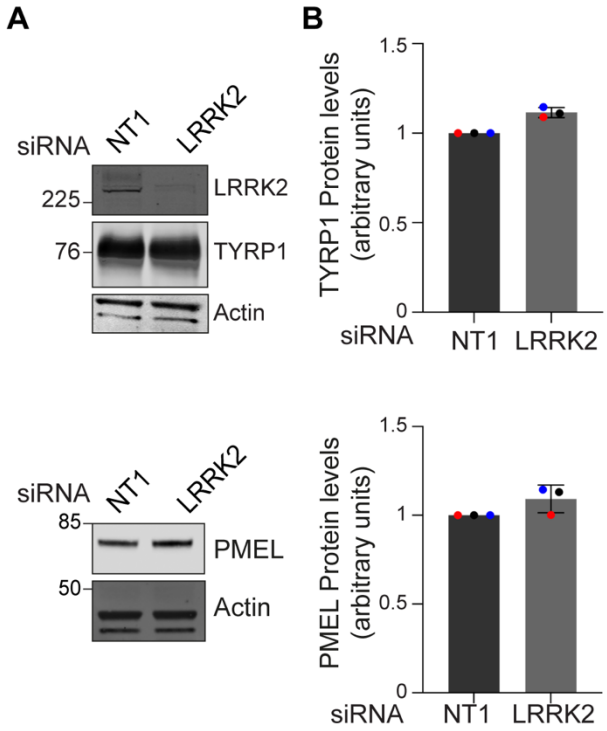

Figure 5.19 LRRK2 depletion does not increase melanosome protein expression

A Representative western blots of Melan-a cells treated with siRNA targeting LRRK2 for 72 hours probed for the indicated antibodies. **B** Quantification of **A**. Error bars: SD. n=3 biological replicates represented in different colours.

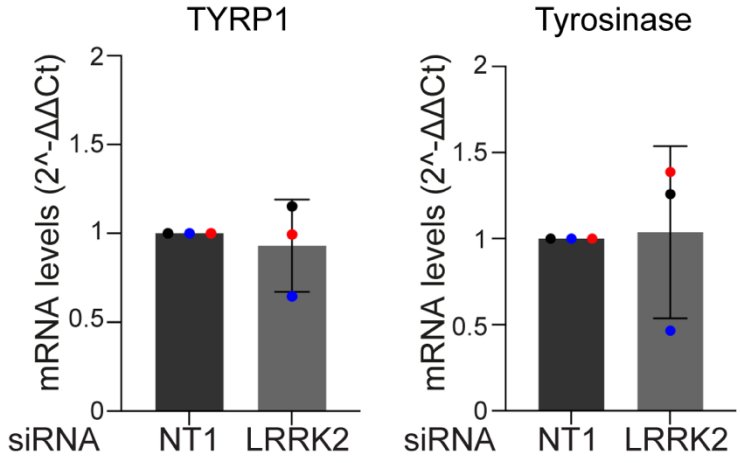

Figure 5.20 LRRK2 depletion does not affect melanosome marker transcript levels

Quantitative RT-qPCR reactions for TYRP1 and tyrosinase were performed with cDNA from Melan-a cells transfected with siRNA targeting LRRK2 for 72 hours. 2^-ΔΔCt values normalised to NT1. n=3 biological replicates. Error bars: SD. Individual repeats represented by different colours.

5.5.3. Acute LRRK2 inhibition changes melanosome morphology

It could be possible that the acute change in acidic organelles with LRRK2 inhibition are related to the recycling of the v-ATPase from melanosomes. Early melanosomes are acidic via the action of an isoform of the v-ATPase and are then neutralised in later stages of melanogenesis (Maxson and Grinstein, 2014; Tabata et al., 2008). Therefore, the v-ATPase must be removed from later stage melanosomes, and ion transporters act to neutralise melanosomes prior to transfer. Studies have shown that tubules can extend from melanosomes which are thought to recycle melanogenesis machinery and cargo (Ripoll et al., 2018). I next looked at EM samples, using a higher magnification, at the morphology of melanosomes with LRRK2 inhibition. Melanosomes were grouped into four categories: round, elongated, fibrils (early) or "halo" (**Figure 5.21A-B**). The first three categories are typical of the four stages of melanogenesis characterised previously (Raposo and Marks, 2007) (**Figure 1.10**). I also identified a fourth category I have called the halo phenotype. These melanosomes presented with a loose outer membrane separating from the main body of the melanosome. There was an increase in the number of melanosomes that had the so called "halo" phenotype after 1 hour of LRRK2 inhibition. It is important to note that these melanosomes were also present in the DMSO condition, but at a much lower abundance than in the 1 hour treated condition. The number of each phenotype was quantified and plotted as a percentage of the total number of melanosomes (**Figure 5.21C**). There was an increase in the percentage of melanosomes with the halo phenotype after 1 hour of treatment which then dropped back down at the 24-hr time point.

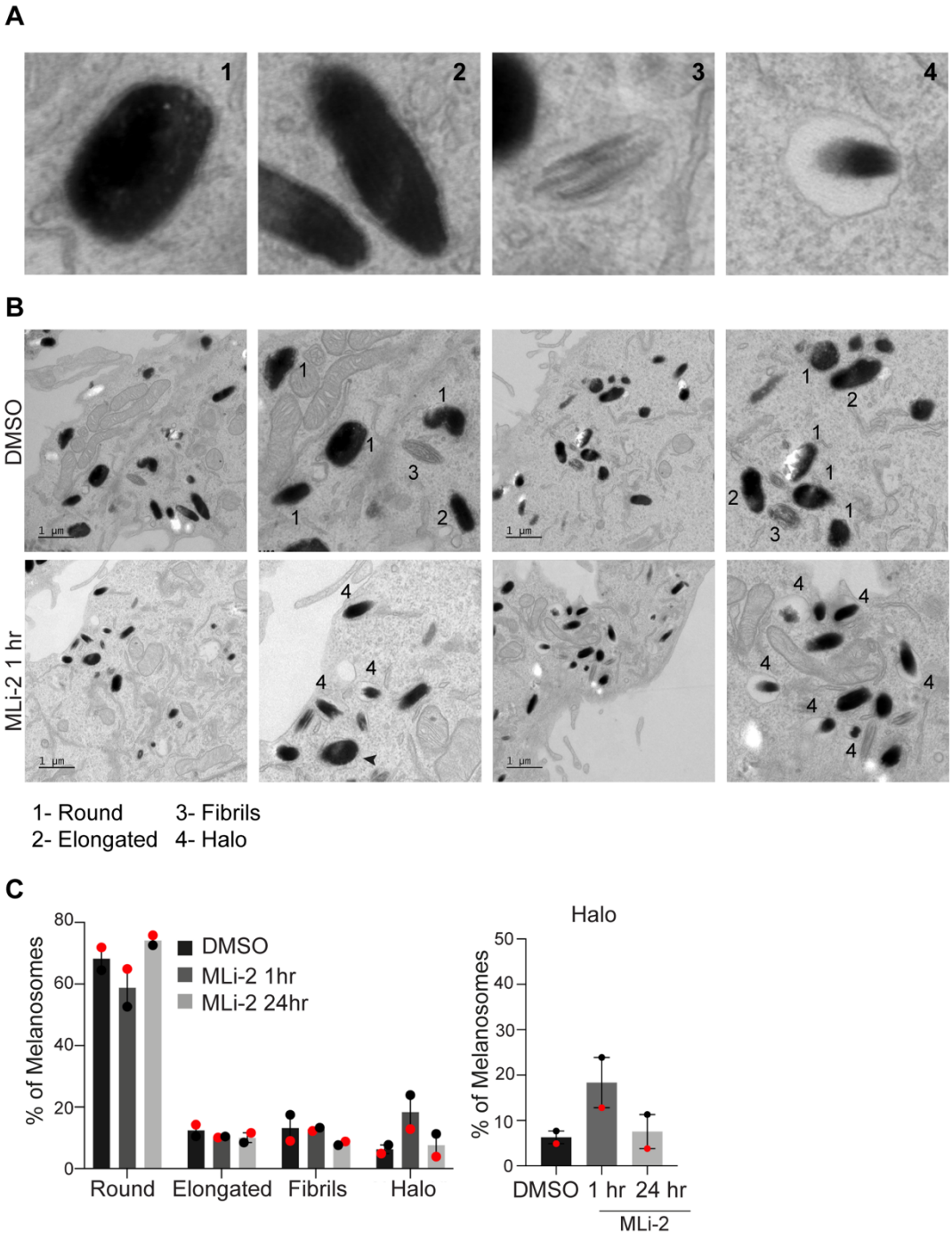

Figure 5.21 Acute LRRK2 inhibition alters melanosome morphology

A x720 zoom images from **B** showing characteristic melanosomes from categories 1-4 **B** Melanosomes from images of Melan-a cells treated with MLi-2 (200 nM) for 1-hour were split into 4 categories. Minimum 10 cells quantified per condition per repeat. **C** Categories outlined in **A** and **B** were plotted as a percentage of the total number of melanosomes. Different colours represent individual experiments. Error bars: Range. n=2 biological replicates.

5.5.4. Generating melanosome enriched fraction from MLi-2 treated cells

In order to get a better idea of what is mechanistically happening at melanosomes with LRRK2 inhibition, melanosome enriched fractions were prepared from Melan-a cells treated with LRRK2 inhibitor for 1 hour or 24 hours. Fractions were analysed by western blot, loading PNS and melanosome fractions in a 5:1 ratio (**Figure 5.22**). LRRK2 appeared enriched in the melanosome enriched fraction following 24-hour treatment with inhibitor. Rab7 also appeared enriched in this fraction at both 1 hour and 24-hour treatment with LRRK2 inhibitor. The levels of TYRP1 in the melanosome enriched fraction was slightly increased by eye with LRRK2 inhibition. The level of Rab32 at this fraction after 24 hours of treatment was increased relative to controls but not after 1-hour of inhibition. Quantification of these experiments indicated that although these results followed the same trends in each repeat, this did not reach statistical significance. There was a high amount of variability between repeats of this experiment. This may reflect the difference in pigmentation of cells at the time of the experiment, variability in the signal given by the antibodies in the western blot and the tricky nature of preparing melanosome enriched fractions. However, by eye it was clear that LRRK2, Rab7 and Rab32 followed the same trends in all 3 repeats. All western blots for the three repeats are shown in **Appendix 3**.

I also did total membrane fractionations of Melan-a cell treated with MLi-2 for 1 hour or 24 hours (**Figure 5.23**). The level of LRRK2 and Rab7 in the total membrane fractions did not increase with LRRK2 inhibition. This together with the melanosome enriched fractions supports a model where LRRK2 is recruited to melanosomes.

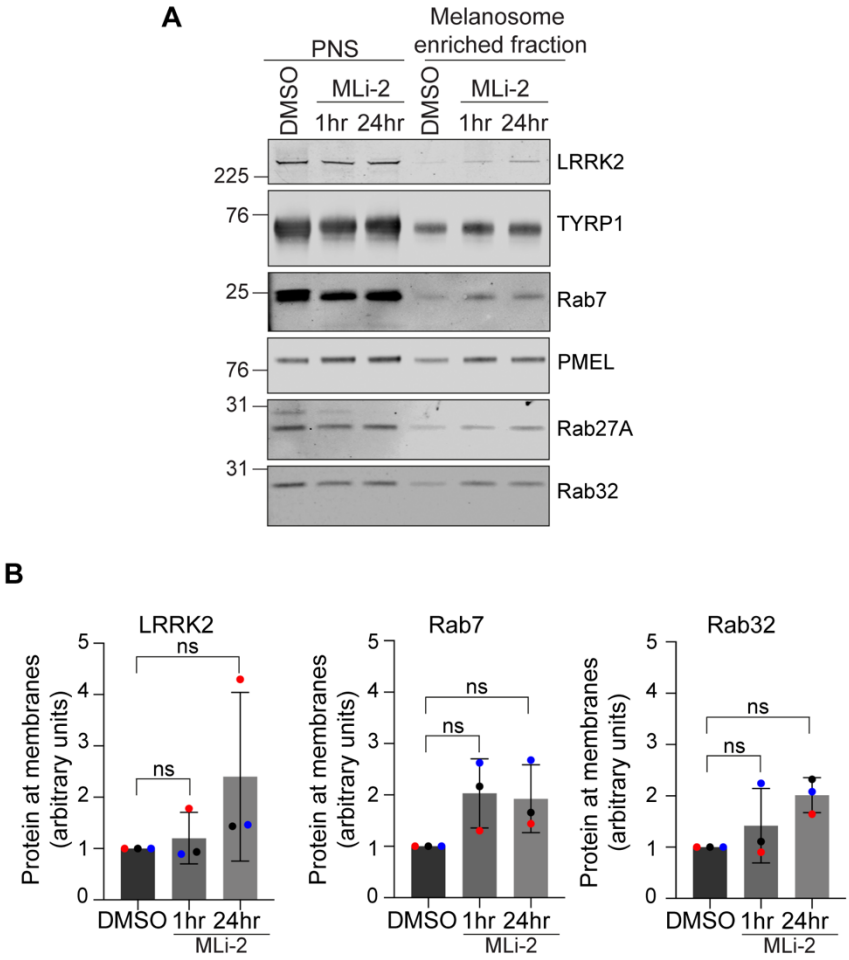

Figure 5.22 Generation of melanosome enriched fractions from Melan-a cells treated with LRRK2 inhibitor

A Melan-a cells were treated with MLi-2 (200 nM) for the indicated time points. Cells were homogenised, and then subjected to a series of spins to collect a melanosome enriched fraction. Fractions were analysed by WB probing for the indicated antibodies. The PNS and melanosome enriched fractions were loaded in a 5:1 ratio. Representative blot shown. **B** Quantification for **A** Samples were normalised to DMSO. n=3 biological replicates. Error bars: SD. Individual repeats represented in different colours.

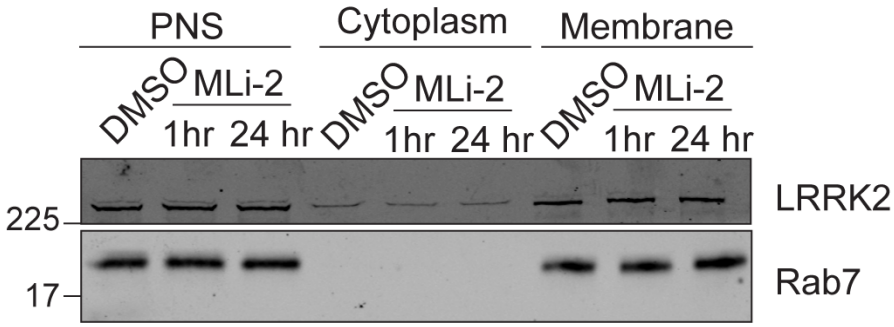

Figure 5.23 Total membrane fractionation with LRRK2 inhibition
Melan-a cells were treated with MLi-2 (200 nM) for the indicated time points. Cells were homogenised, and total membrane fractions were collected from the PNS with a 100,000 g spin. Fractions were analysed by WB probing for the indicated antibodies. Representative blot shown. n=2 biological replicates.

5.6. Inhibition of LRRK2 increases ER-mitochondrial contact sites

Whilst looking at EM images of Melan-a cells treated with LRRK2 inhibitor, it appeared that there was a change in the number of ER- mitochondrial contact sites (**Figure 5.24A**). I therefore quantified the number of ER mitochondrial contact sites per mitochondria as well as the percentage of the total mitochondrial perimeter in a contact site (**Figure 5.24B**). Contact sites were defined as the mitochondrial membrane and ER being within 30 nm of each other. Treatment with LRRK2 inhibitor for 1 hour increased the number of ER- mitochondrial contact sites, a phenotype which was further increased at the 24-hour time point. No change was seen in contact site length (**Figure 5.24F**).

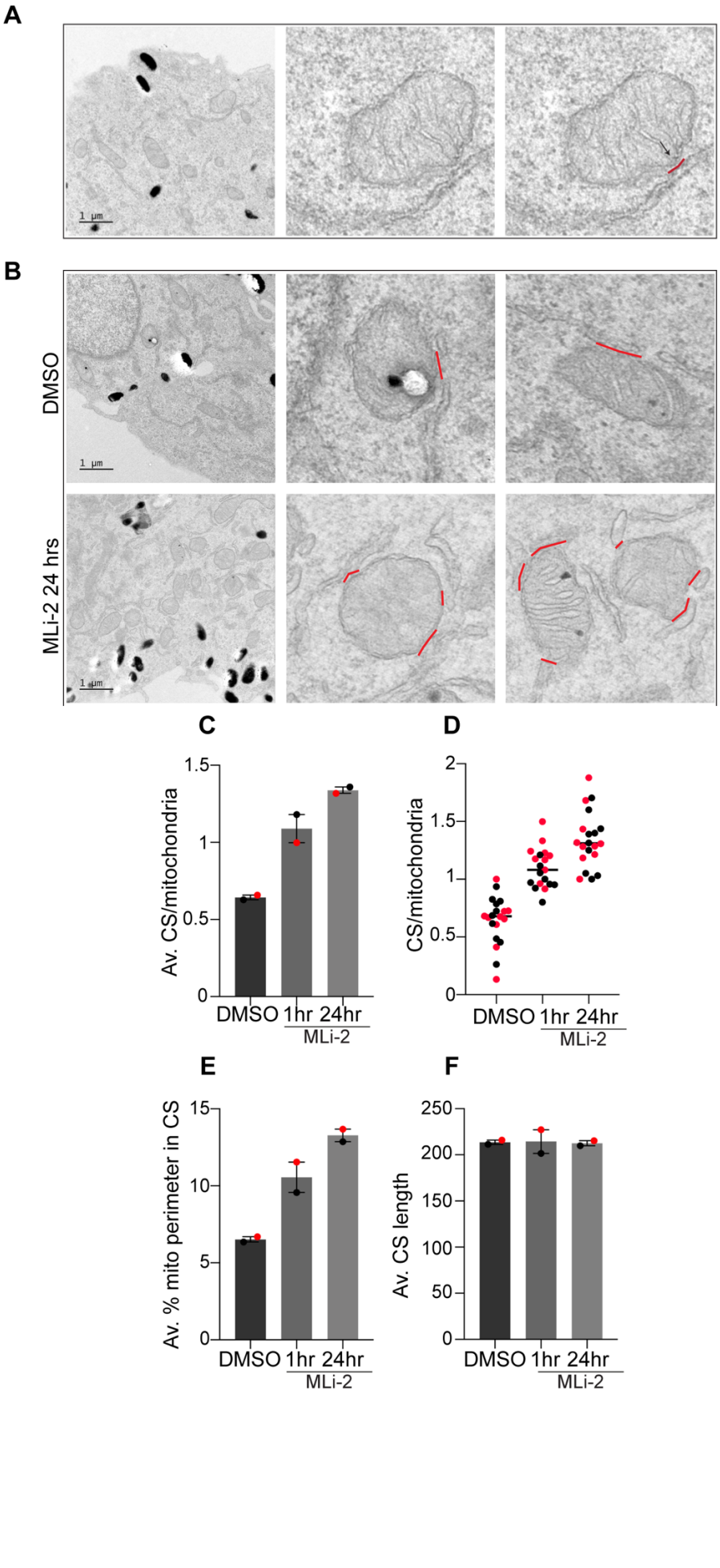
A
B
DMSO
MLi-2 24 hrs
1 µm
C
Av. CS/mitochondria
1.5
1
0.5
0
DMSO
1hr
24hr
MLi-2
D
CS/mitochondria
2
1.5
1
0.5
0
DMSO
1hr
24hr
MLi-2
E
Av. % mito perimeter in CS
15
10
5
0
DMSO
1hr
24hr
MLi-2
F
Av. CS length
250
200
150
100
50
0
DMSO
1hr
24hr
MLi-2

Figure 5.24 Inhibition of LRRK2 increases the number of ER-mitochondria contact sites
A Melan-a cells were treated with MLi-2 (200 nM) for the indicated time points. Cells were fixed and processed for EM. Images were acquired using a TEM microscope. Contact sites were counted if mitochondria and ER were within 30 nm of each other. **B** Representative images of +/- MLi-2 are shown. **C** Average ER-mitochondria contact sites per mitochondria. Individual points represent different experiments. **D** Average number of contact sites per mitochondria. Points represent individual cells. **E** Average percentage of mitochondrial perimeter in a contact site. **F** Average contact site length. Individual points represent different experiments. R1- **DMSO-** 10 cells, 258 mitochondria, 178 contact sites, MLi-2 1hr- 9 cells, 465 mitochondria, 457 contact sites, MLi-2 24 hr- 10 cells, 264 mitochondria, 344 contact sites R2- **DMSO** 10 cells, 370 mitochondria, 238 contact sites, **MLi-2 1 hr-** 10 cells, 441 mitochondria, 506 contact sites, **MLi-2 24 hr-** 10 cells, 446 mitochondria, 606 contact sites. Error bars: Range. n=2 biological replicates.

5.7. Discussion

5.7.1. LRRK2 and melanogenesis

In this chapter I show a novel link between the PD associated protein LRRK2 and melanogenesis. In chapter 4 I showed an inverse relationship between LRRK2 and melanogenesis transcription factor MITF. Collectively the data from brightfield imaging, immunofluorescence and EM all showed that treatment with LRRK2 inhibitor for longer time points, and depletion of LRRK2, induces an increase in pigmentation. Melanosome fractionation experiments revealed a portion of LRRK2 is localised to the melanosome enriched fractions and this pool is enriched with LRRK2 inhibition. The localisation of LRRK2 to this organelle has not been previously reported, however, this is undoubtably due to the lack of studies in this specialised cell type. Rab32 was also enriched in this fraction following LRRK2 inhibition at 24 hours. Rab32 has been shown to recruit LRRK2 to endolysosomal compartments in non-pigmented cells (Waschbüsch et al., 2014). Therefore, in this specialised cell type, where Rab32 plays a role in the trafficking of melanogenesis proteins, LRRK2 may be recruited to the melanosome membrane by Rab32.

To consider how this could relate to the relationship between PD and melanoma, we must remember that in PD, LRRK2 is hyperactivated by pathogenic mutations. You therefore may expect that hyperactivating mutations in LRRK2 would result in a decrease in pigmentation. It is not clear how this would affect susceptibility to melanoma. A decrease in pigmentation would result in a decrease in the nuclear protective caps formed around cells in the skin epidermis which could result in increased vulnerability to DNA damage by UV radiation. It could also be that LRRK2 hyperactivation is key for the progression of melanoma to later stages of disease. Loss of pigmentation is a key marker for the later stages of melanoma coupled with an increase in invasiveness. These hypotheses assume that the hyperactivating mutations of LRRK2 would result in the opposite phenotype to the inhibitor. However, as discussed in chapter 4, this is not always the case.

The EM images revealed a morphology change in melanosomes with 1 hour of LRRK2 inhibition. This “halo” phenotype was characterised by a loose or baggy outer membrane around the main body of the melanosome. The “halo” phenotype was enriched after 1-hour inhibition, but this was resolved by the 24-hour time point. This phenotype followed the same temporal pattern as the LysoTracker and Rab7 phenotypes observed in chapter 4, which would support the idea that these changes relate to melanosomes. I confirmed that the rapid acidification phenotype was not specific to Melan-a cells by looking at MNT1 cells. The finding that LysoTracker labelling and LAMP1 staining were unchanged in WM266.4 cells, which are a non-pigmented cell line, further supports the assumption that the changes we see are related to melanosomes and not lysosomes. Additionally, I did not observe many structures by EM which would resemble a lysosome in any of the samples imaged.

If we assume that the rapid acidification and halo phenotypes are related, one explanation may be that there is a defect in the recycling pathway from melanosomes. In this proposed model, acute inhibition would result in the accumulation of the v-ATPase at melanosomes leading to hyper-acidification.

It has previously been shown that melanosomes shed some of their machinery prior to transfer in a process which is dependent on Myosin VI (Ripoll et al., 2018). It was shown that depletion of Myosin VI resulted in a failure of the neck of the tubules to constrict, leaving wide necked tubules extending from melanosomes which take longer to resolve. In the case of LRRK2 inhibition we do not see anything that resembles a tubule, but instead a more general detachment of the outer membrane which may indicate a failure to properly form tubules. LRRK2 has been linked to lysosomal tubule formation in response to lysosome permeabilization by LLOME (Malik et al., 2020). There may be a related process that occurs in melanosomes which is regulated by LRRK2 activity, where inhibition causes a failure in this process accounting for the morphology change. Previous work has also shown that LRRK2 is able to interact with the v-ATPase a1 subunit, and that selective LRRK2 hyperactivating mutations result in changes in lysosomal pH (Wallings et al., 2019b). The data in this thesis would support previous work indicating a role for LRRK2 in regulating acidification by the v-ATPase. This is consistent with previous studies linking LRRK2 activity to alterations in autophagy, as well as lysosomal defects in other cell types (Baptista et al., 2013; Henry et al., 2015; Hockey et al., 2015; Gómez-Suaga et al., 2014; Tong et al., 2010b; MacLeod et al., 2013). The work in this chapter proposes a novel role for LRRK2 in melanogenesis where acidification by the v-ATPase and recycling of this machinery are disrupted with LRRK2 inhibition.

Rab7 has previously been identified as a melanosome related protein (Jordens et al., 2006; Gomez et al., 2001). Rab7 was enriched at the melanosome enriched fraction following 1-hour and 24-hour inhibition of LRRK2. This is in line with the GST-RILP pulldown data in chapter 4 showing an increase in GTP-bound Rab7 at both time points. One conclusion from this data might be that LRRK2 inhibition results in an increase in GTP-Rab7 which is associated with the melanosome membrane. This could explain the rapid increase in Rab7 positive vesicles with LRRK2 inhibition. What is still not clear, is whether the effects seen at 1 hour and 24 hours are the same process or two separate processes.

From the melanosome fractionation experiments there's an enrichment of Rab32 and Rab27A at the longer 24-hour time point. These are clear markers for the later stages of melanosome formation and transfer (Jordens et al., 2006; Raposo and Marks, 2007; Wasmeier et al., 2006; Wu et al., 2001). However, the acidification phenotype is related to earlier stages of melanogenesis, where melanosomes are not pigmented. This may indicate that there are two separate phenotypes- one which is an acute response and one which is seen with prolonged treatment. The inverse relationship between LRRK2 and MITF may be part of this prolonged response, as the acute phenotypic changes are too quick to be dependent on transcription and translation. Collectively these findings would be consistent with a model in which LRRK2 acts to negatively regulate melanogenesis. The finding that depletion of MITF results in a larger increase in the levels of LRRK2 suggests that MITF acts to suppress LRRK2 expression which may act as a positive feedback mechanism to drive melanogenesis in melanocytes. It would be interesting to consider the significance of melanosome dysfunction in dopaminergic neurons and if there is a role for LRRK2 in the regulation of neuromelanin formation and maintenance.

5.7.2. LRRK2 and ER-mitochondrial contact sites

From the EM images I found that LRRK2 inhibition increases the number of ER-mitochondria contact sites in Melan-a cells, with no increase in contact site length. LRRK2 has been linked to mitophagy dysfunction by a number of studies- a link that is thought to be physiologically relevant to PD (**Section 1.4.11**). ER-mitochondrial contact sites are also thought to be significant to neurodegenerative diseases. Ca^{2+} uptake by the mitochondria is essential for buffering cytosolic Ca^{2+}. Dopaminergic neurons affected by PD are more vulnerable to defects in Ca^{2+} signalling as they are highly dependent on the pace-making regulated by Ca^{2+} handling (Lee et al., 2018). Both PINK1 loss and hyperactivation of LRRK2 have been shown to induce elevation in mitochondrial Ca^{2+}. This indicates that Ca^{2+} homeostasis is generally important in the context of PD. Furthermore, work has shown that PINK1 is

recruited to and promotes ER-mitochondria contact sites (Gelmetti et al., 2017).

A previous paper looked at the effect of hyperactivating [G2019S] mutation, kinase dead [D1994A] mutation and LRRK2 knockout on ER-mitochondria contact sites (Toyofuku et al., 2020). They found that both knockout and [G2019S] mutation resulted in a decrease in the number of contact sites by EM but not the [D1994A] mutation. They also looked by proximity ligation assay (PLA) at ER-mito contact sites and found that the [D1994A] mutation increased the signal whereas [G2019S] mutation and knockout of LRRK2 resulted in a loss of contact sites. The data from Melan-a cells would support a role for LRRK2 in the maintenance/resolution of ER-mitochondria contact sites which is dependent on its kinase activity. ER-mitochondrial contact sites have been reported to be significant to neurodegenerative diseases including PD. Other PD associated genes including Parkin and alpha synuclein have been linked to ER-mitochondria contact sites (Xu et al., 2020; Wilson and Metzakopian, 2021).

5.7.3. LRRK2 and melanoma hallmarks

In this chapter I present data which identify a role for LRRK2 in other cellular processes in melanoma. Unlike the negative correlation between LRRK2 expression and pigmentation, LRRK2 positively correlated with cell invasion markers. Cell tracking experiments which showed that inhibition or depletion of LRRK2 resulted in a decrease in the accumulated distance travelled by cells, would support a role for LRRK2 in promoting cell invasion. Inhibition of LRRK2 also resulted in a change in the morphology of cells, making them more elongated with longer projections. These results could be interpreted as these cells undergoing the EMT, common to later stages of cancer. However, as seen in **Figure 5.11**, these cells have already undergone this switch and express N-cadherin. You would also expect that if inhibition was promoting an EMT phenotype, there would be an increase in invasiveness. In fact, we see the opposite, suggesting that invasive melanoma cells would upregulate

LRRK2 to promote invasion. In normal conditions, melanocytes sit in the base of the skin epidermis and have elongated projections which are able to contact a number of keratinocytes. The change in morphology in WM266.4 cells with LRRK2 inhibition may be re-establishing a more characteristic melanocyte morphology that was lost when cells were transformed.

LRRK2 depletion had no effect on the cell proliferation of WM266.4 cells. High proliferation is important to early-stage tumour formation in melanoma (Li et al., 2015). This would indicate that LRRK2 is specifically important to the later stages of melanoma progression. This would be consistent with the idea that LRRK2 is part of the phenotypic switching model of melanoma progression. Previous work has shown how melanoma cells can be highly dependent on Rab7 in the early stages of the disease, but that this is then rewired as the disease progresses through the later stages (Alonso-Curbelo et al., 2014). The cell proliferation experiments confirmed that depletion of Rab7 decreased cell growth in melanoma cells, which would be consistent with a role in core tumour formation. In melanoma tumours, MITF can act as an oncogene where its expression promotes cell survival and proliferation (Garraway et al., 2005). However, it has also been found to be key to “phenotypic switching” and found to be down regulated in the metastatic populations of cells in melanomas (Goodall et al., 2008; Hoek and Goding, 2010). Expression of MITF is commonly lost across metastatic melanoma immortalised cell lines, which is translated in the loss of pigmentation such as in WM266.4 cells (**Figure 3.2**). The data give evidence that LRRK2 is a previously unidentified marker for the phenotypic switch in melanoma. The inverse relationship between LRRK2 and MITF is consistent with MITF being a driver of the highly proliferative early-stage melanomas and LRRK2 being a driver of the highly invasive later stages of melanoma.

6. Final conclusions

The molecular mechanisms underlying PD remain poorly understood with approximately 85-90% of cases regarded as idiopathic (Bandres-Ciga et al., 2020). What is very clear from studying familial genes involved in PD is the mitophagy and protein homeostasis pathways are key to pathogenesis. Hyperactivating mutations in LRRK2 are the most common cause of familial PD and result in an autosomal dominant inheritance pattern. There is still much debate in the field around the clinically significant substrate(s) of LRRK2. It is important to understand the physiological function, as well as the pathogenic function, as many pharmaceutical companies are pursuing LRRK2 as a therapeutic target. One thing that remains elusive surrounding PD is the mechanism underpinning the higher incidence of melanoma in PD patients compared to the general population. The work carried out in this thesis aimed to gain a deeper understanding of the physiological function of LRRK2 and focused specifically on melanoma cells. It also aimed to build a platform which will enable future studies to better understand cross talk between LRRK2 and other PD related genes such as VPS35.

6.1. LRRK2 and VPS35

In this thesis I have generated supporting data showing that LRRK2 and VPS35 operate in a common pathway. Together with Katy McCarron I generated inducible VPS35 WT and [D620N] mutant RPE1 Flp-In cell lines. These were made to study the pathogenic mutation in VPS35 which causes autosomal dominant forms of PD. We also set up the established GST-RILP assay for studying Rab7 activity. Previous work has shown that VPS35 KO results in a “hyperactivation” of Rab7 (Jimenez‐Orgaz et al., 2018). Additionally, hyperactivating mutations in LRRK2 were found to result in a decrease in GTP-bound Rab7 which would suggest LRRK2 kinase activity negatively regulates Rab7 (Gómez-Suaga et al., 2014). This is consistent with data from this thesis which showed that inhibition of LRRK2 increased the pool of GTP-bound Rab7 (**Figure 4.14**). It is not clear whether the effects of LRRK2

and VPS35 in regulating Rab7 are due to a common or two independent pathways. Previous work found VPS35 [D620N] to lie upstream of LRRK2 and hyperactivate kinase activity (Mir et al., 2018). Therefore, you would predict that induction of VPS35 [D620N] expression would result in an increase in LRRK2 kinase activity and a decrease in GTP-Rab7. This is part of ongoing work in the laboratory and the work carried out in this thesis generated and characterised tools which will be used in future studies to address this question. LRRK2 hyperactivation has been shown to result in a disruption of the TGN which is dependent on its kinase activity (Liu et al., 2018; Purlyte et al., 2018; Beilina et al., 2020). In this thesis I have confirmed that [G2019S] LRRK2 induces disruption of the TGN and found that the VPS35 [D620N] mutation also induces a similar phenotype (**Figure 3.16** and **Figure 4.19**). This is consistent with the VPS35 [D620N] mutation being an upstream activator of LRRK2 kinase activity, as it can phenocopy the hyperactive LRRK2 mutants. In the context of PD, disruption of trafficking from the Golgi would be predicted to effect anterograde and retrograde transport of essential lysosomal proteins. This dysregulation could lead to changes is protein homeostasis due to alterations in lysosomal activity which are predicted to be key factors in PD pathology.

6.2. LRRK2 and melanogenesis

Early work on this project identified a novel relationship between LRRK2 and two related transcription factors, MITF and TFEB. Many papers have previously indicated a role for LRRK2 in the endolysosomal system which is thought to be significant to the pathogenesis of PD (Baptista et al., 2013; Giaime et al., 2017; Henry et al., 2015; Hockey et al., 2015; Tong et al., 2012; Ysselstein et al., 2019). Initial results indicated that loss of LRRK2 caused defects in the later stages of the pathway, with late endosomal and lysosomal markers as well as LysoTracker staining being altered. The initial assumption was that these results were due to changes in late endosomes and or lysosomes and that this was related to the inverse relationship observed between LRRK2 and TFEB. However, the finding that 1 hour inhibition of LRRK2 was sufficient to induce the maximum phenotype showed that the

initial response is independent of TFEB and transcription. I did not initially consider that many markers for the late endosome and lysosomal system, as well as LysoTracker dye, will also label melanosomes. In this thesis I show that loss of LRRK2 kinase activity results in an increase in pigmentation in melanocytes. This is consistent with the finding that LRRK2 expression is inversely related to the levels of pigmentation markers across melanoma cell lines. With all the data in this thesis considered, it is more likely that the phenotypes observed in Melan-a cells are a result of changes in the melanogenesis pathway rather than the endolysosomal pathway. The EM data in Chapter 5 confirmed that there is an increase in the number of melanosomes with LRRK2 inhibition at the longer time point. There was also a lack of structures resembling lysosomes by EM which would support that the changes are in the melanogenesis pathway. Additionally, I was unable to recapitulate the acidification or LAMP1 phenotypes in the non-pigmented WM266.4 melanoma cells, whereas the pigmented MNT1 melanoma cells phenocopied the Melan-a melanocytes. This would further suggest changes are melanosome related.

By EM there is a change in melanosome morphology with acute inhibition of LRRK2 which resolves itself by the 24-hour time point. This is distinct from the classical morphologies described previously for the four stages of melanogenesis (Raposo and Marks, 2007; Ohbayashi and Fukuda, 2020) and different from a previously described defect in melanosome recycling (Ripoll et al., 2018). It appears that LRRK2 affects melanogenesis at two stages (**Figure 6.1**). There is an initial response with acute inhibition resulting in rapid acidification. This could be due to an effect on the formation and pinching off of recycling tubules from melanosomes, or dysregulation of the melanosome v-ATPase. LRRK2 has previously been shown to regulate tubule formation from lysosomes (Bonet-Ponce et al., 2020). A failure to form tubules would explain the halo phenotype observed in **Figure 5.21**, which is resolved by the 24-hour time point. At this longer time point there is an increase in later stage melanosomes which are neutralised and highly pigmented. In principle, the longer response could be related to the inverse relationship between LRRK2

and MITF. However, there is no increase in total melanogenic enzymes evidenced by western blot or qPCR, which would suggest that the phenotypes are the result of changes in trafficking. LRRK2 has previously been shown to be recruited to membranes by Rab32, one of the Rab proteins responsible for the delivery of melanogenesis enzymes (Bonet-Ponce et al., 2020). Fractionation experiments revealed that LRRK2 is recruited to a melanosome enriched fraction in response to inhibition (**Figure 5.22**). This is a previously unreported localisation of LRRK2 which can be attributed to the lack of work in these specialised cells. It is possible that in pigmented cells, Rab32 can recruit LRRK2 to melanosomes. In non-pigmented cells Rab32 is also able to interact with retromer component SNX6, an interaction which was shown to effect trafficking of the CIMPR (Waschbüsch et al., 2019). It is unclear whether LRRK2's interaction with Rab32 plays a role in this trafficking. Rab32 could play similar role in trafficking and recycling of melanosome components, where LRRK2 is recruited to the melanosome membrane. An alternative explanation for the accumulation of these proteins would be that acute inhibition halts the recycling from melanosomes. This would lead to an accumulation of otherwise cycling proteins at the melanosome membrane. Overall, the data shown suggest a novel role for LRRK2 in regulating the melanogenesis pathway, which may explain why LRRK2 is upregulated in later stage melanoma cells where loss of pigmentation is common. It is not clear whether the hyperactivating mutations in LRRK2 would have the opposite effect on melanocytes and result in a decrease in pigmentation.

The data from my placement in Sheffield from iNPC derived dopaminergic neurons, which do not have melanosomes, are consistent with previous studies which have shown that changes in LRRK2 kinase activity result in changes in the endolysosomal system. LAMP1 staining was dramatically increased without a concomitant increase in lysosomal activity. Together this may indicate that LRRK2 has two related physiological functions. Perhaps LRRK2 can regulate the endolysosomal and lysosome biogenesis pathway in cells without pigmentation, and the melanogenesis pathway in specialised cell types.

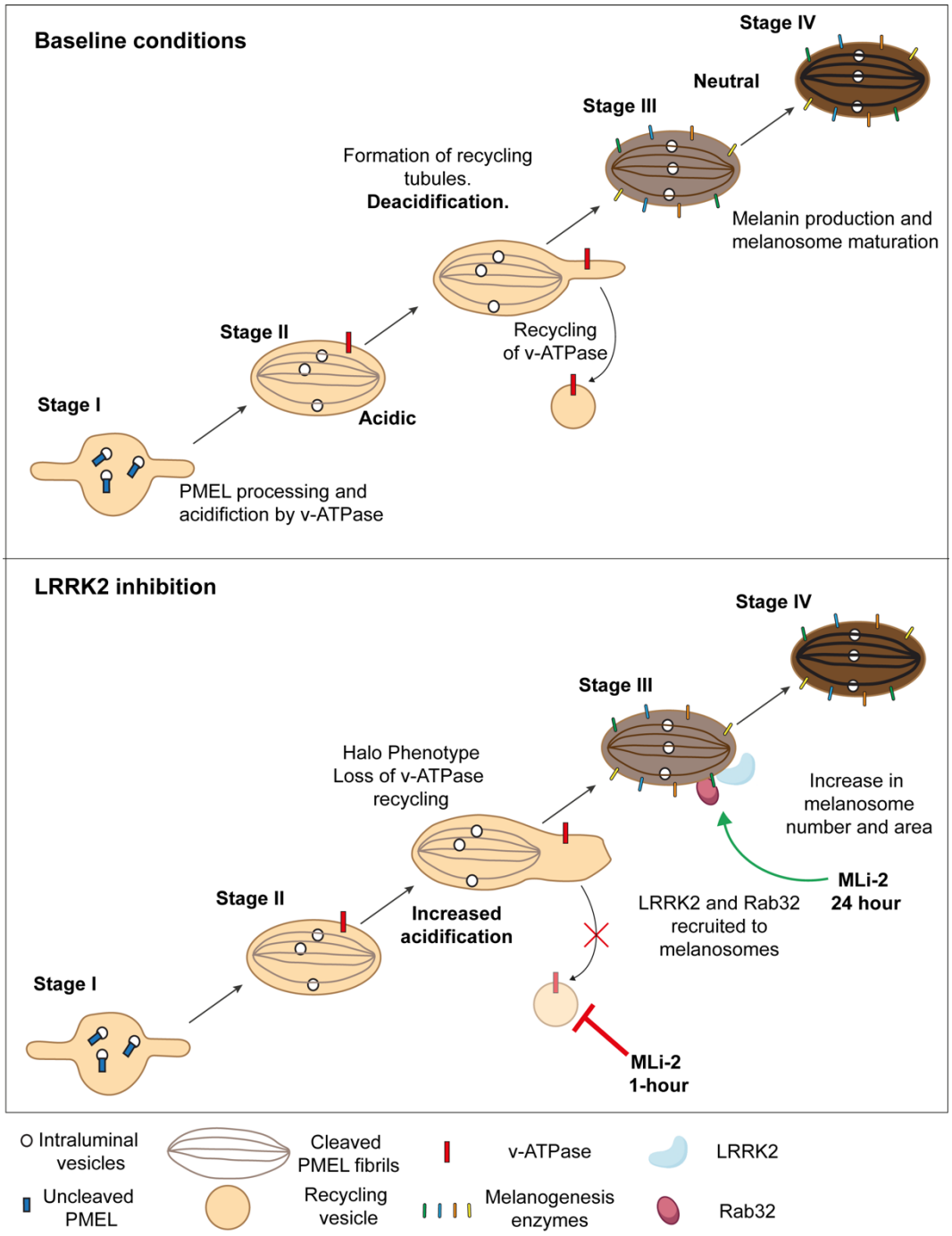

Figure 6.1 LRRK2 inhibition alters the melanogenesis pathway

LRRK2 inhibition in melanocytes alters melanogenesis, potentially at multiple stages. Acute inhibition results in increased acidification. This could be due to a defect in the recycling of the v-ATPase. Longer time points result in an increase in the number of melanosomes per cell, indicating a change in the later stages of melanogenesis.

6.3. LRRK2 and melanoma

LRRK2 has not previously been linked to melanoma. In this project I show that LRRK2 has a characteristic expression pattern where levels are low in melanoma cell lines where pigmentation is high, and invasion is low, and that LRRK2 is upregulated in non-pigmented, invasive melanoma lines. This expression is characteristic of phenotypic switching expression patterns observed in melanoma related proteins, (Li et al., 2015; Hoek and Goding, 2010) and would indicate that LRRK2 activity promotes later stage melanoma phenotypes. Data in this thesis showed that LRRK2 inhibition reduces cell motility, which suggests that LRRK2 kinase activity, and therefore hyperactivating mutations might promote invasion. In contrast to LRRK2, MITF and Rab7 have the opposite expression pattern across melanoma cells, and are upregulated in early-stage melanomas (Alonso-Curbelo et al., 2014; Garraway et al., 2005). Their expression confers advantages such as cell proliferation for bulk tumour formation. Loss of Rab7 was shown to result in an increase in invasive potential, (Alonso-Curbelo et al., 2014) further supporting an upregulation in early-stage melanoma and suppression in late-stage melanoma. I have shown that inhibition of LRRK2 increases the pool of GTP-Rab7 which would in theory reduce cell invasion. Future experiments could investigate whether the effect of LRRK2 on cell invasion is dependent on its ability to effect Rab7 nucleotide binding status. Collectively the data in this thesis propose LRRK2 is a novel marker for the phenotypic switch observed between early and late-stage melanoma.

Appendices

Validation of specificity of GST-RILP assay using GST-beads

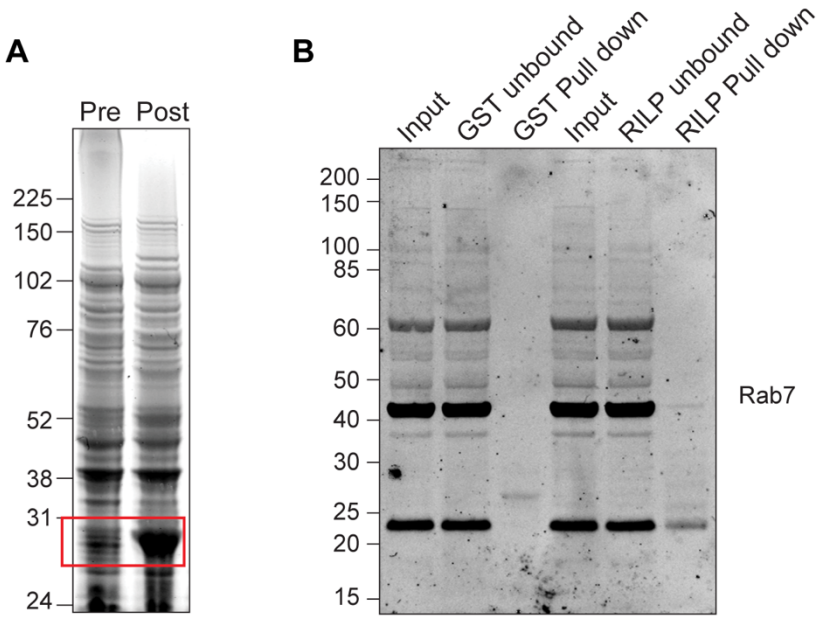

Appendix 1: Validation of GST-RILP assay with GST-beads
A BL21 bacteria were transformed with pGEX-6P-1 plasmid. Positive colonies were picked into a starter culture which was used to inoculate a 1 litre maxi culture. Culture was grown to an OD value of 0.6. Protein expression was induced with IPTG for 4 hours. Pre and post induction samples were taken and resolved by SDS-PAGE. Gel was stained with simply blue stain. GST band indicated by the red box. **B** HEK 293 Flp-In cells were lysed in Rab7 assay lysis buffer and an input sample was taken. 400 µg of protein was loaded onto either GST only or GST-RILP beads and spun on a wheel for 2 hours. Flow through and bound fractions were collected and analysed by western blotting probing for Rab7.

MITF transcriptionally controls Rab27A expression

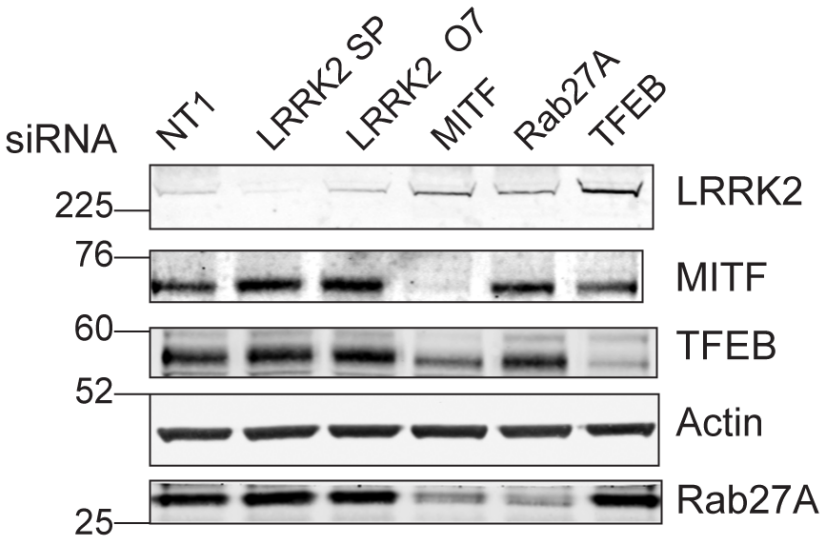

Appendix 2: MITF transcriptionally controls Rab27A levels in Melan-a cells

Melan-a cells were treated with 40 nM siRNA targeting the indicated proteins for 72 hours. Cells were lysed and the lysates were analysed by western blotting, probing for the indicated antibodies.

All repeats of melanosome fractionations in Melan-a cells

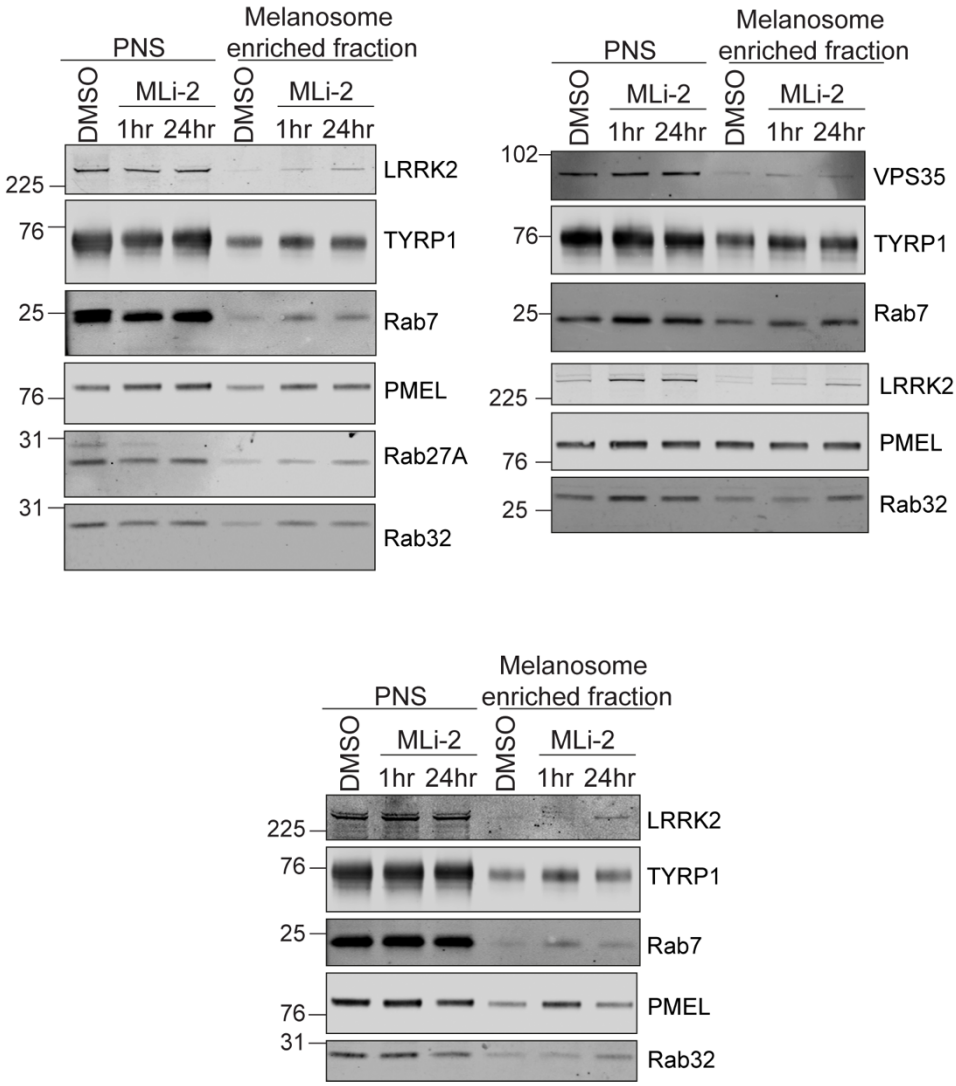

Appendix 3: Melanosome fractionations from Melan-a cells treated with MLi-2 inhibitor

Melan-a cells were treated with MLi-2 (200 nM) for the indicated time points. Cells were homogenised, and then subjected to a series of spins to collect a melanosome enriched fraction. Fractions were analysed by WB probing for the indicated antibodies.

7. References

Aasly, J.O., Vilariño-Güell, C., Dachsel, J.C., et al. (2010) Novel pathogenic LRRK2 p.Asn1437His substitution in familial Parkinson's disease. *Movement Disorders*, 25 (13): 2156–2163. doi:10.1002/mds.23265.

Alexandrov, K., Horiuchi, H., Steele-Mortimer, O., et al. (1994) Rab escort protein-1 is a multifunctional protein that accompanies newly prenylated rab proteins to their target membranes. *The EMBO journal*, 13 (22): 5262–5273.

Alonso-Curbelo, D., Riveiro-Falkenbach, E., Pérez-Guijarro, E., et al. (2014) RAB7 Controls Melanoma Progression by Exploiting a Lineage-Specific Wiring of the Endolysosomal Pathway. *Cancer Cell*, 26 (1): 61–76. doi:10.1016/j.ccr.2014.04.030.

Ancans, J., Tobin, D.J., Hoogduijn, M.J., et al. (2001) Melanosomal pH controls rate of melanogenesis, eumelanin/phaeomelanin ratio and melanosome maturation in melanocytes and melanoma cells. *Experimental Cell Research*, 268 (1): 26–35. doi:10.1006/excr.2001.5251.

Araki, S., Kikuchi, A., Hata, Y., et al. (1990) Regulation of reversible binding of smg p25A, a ras p21-like GTP-binding protein, to synaptic plasma membranes and vesicles by its specific regulatory protein, GDP dissociation inhibitor. *The Journal of biological chemistry*, 265 (22): 13007–15. Available at: http://www.ncbi.nlm.nih.gov/pubmed/2115887 (Accessed: 29 April 2020).

Armstrong, M.J. and Okun, M.S. (2020) Diagnosis and Treatment of Parkinson Disease: A Review. *JAMA - Journal of the American Medical Association*. 323 (6) pp. 548–560. doi:10.1001/jama.2019.22360.

Aroca, P., Solano, F., Garcia-Borron, J.C., et al. (1991) Specificity of dopachrome tautomerase and inhibition by carboxylated indoles. Considerations on the enzyme active site. *Biochemical Journal*, 277 (2): 393–397. doi:10.1042/bj2770393.

Balderhaar, H.J. klein. and Ungermann, C. (2013) CORVET and HOPS tethering complexes - coordinators of endosome and lysosome fusion. *Journal of Cell Science*. 126 (6) pp. 1307–1316. doi:10.1242/jcs.107805.

Bandres-Ciga, S., Diez-Fairen, M., Kim, J.J., et al. (2020) Genetics of Parkinson's disease: An introspection of its journey towards precision

medicine. *Neurobiology of Disease*. 137 p. 104782. doi:10.1016/j.nbd.2020.104782.

Bandres-Ciga, S., Saez-Atienzar, S., Bonet-Ponce, L., et al. (2019) The endocytic membrane trafficking pathway plays a major role in the risk of Parkinson's disease. *Movement Disorders*, 34 (4): 460–468. doi:https://doi.org/10.1002/mds.27614.

Banks, S.M.L., Medeiros, A.T., McQuillan, M., et al. (2020) Hsc70 ameliorates the vesicle recycling defects caused by excess α-synuclein at synapses. *eNeuro*, 7 (1). doi:10.1523/ENEURO.0448-19.2020.

Baptista, M.A.S., Dave, K.D., Frasier, M.A., et al. (2013) Loss of leucine-rich repeat kinase 2 (LRRK2) in rats leads to progressive abnormal phenotypes in peripheral organs. *PLoS ONE*, 8 (11). doi:10.1371/journal.pone.0080705.

Barbeau, A. (1962) The pathogenesis of Parkinson's disease: a new hypothesis. *Canadian Medical Association journal*, 87 (15): 802–807. Available at: https://www.ncbi.nlm.nih.gov/pmc/articles/PMC1849683/ (Accessed: 22 December 2020).

Bardien, S., Lesage, S., Brice, A., et al. (2011) Genetic characteristics of leucine-rich repeat kinase 2 (LRRK2) associated Parkinson's disease. *Parkinsonism and Related Disorders*. 17 (7) pp. 501–508. doi:10.1016/j.parkreldis.2010.11.008.

Barretina, J., Caponigro, G., Stransky, N., et al. (2012) The Cancer Cell Line Encyclopedia enables predictive modelling of anticancer drug sensitivity. *Nature*, 483 (7391): 603–607. doi:10.1038/nature11003.

Behrmann, H., Lürick, A., Kuhlee, A., et al. (2014) Structural identification of the Vps18 β-propeller reveals a critical role in the HOPS complex stability and function. *Journal of Biological Chemistry*, 289 (48): 33503–33512. doi:10.1074/jbc.M114.602714.

Beilina, A., Bonet-Ponce, L., Kumaran, R., et al. (2020) The Parkinson's Disease Protein LRRK2 Interacts with the GARP Complex to Promote Retrograde Transport to the trans-Golgi Network. *Cell Reports*, 31 (5): 107614. doi:10.1016/j.celrep.2020.107614.

Bennett, D.C., Cooper, P.J. and Hart, I.R. (1987) A line of non-tumorigenic mouse melanocytes, syngeneic with the B16 melanoma and requiring a

tumour promoter for growth. *International Journal of Cancer*, 39 (3): 414–418. doi:10.1002/ijc.2910390324.

BERAL, V., EVANS, S., SHAW, H., et al. (1983) Cutaneous factors related to the risk of malignant melanoma. *British Journal of Dermatology*, 109 (2): 165–172. doi:10.1111/j.1365-2133.1983.tb07077.x.

Berson, J.F., Harper, D.C., Tenza, D., et al. (2001) Pmel17 initiates premelanosome morphogenesis within multivesicular bodies. *Molecular Biology of the Cell*, 12 (11): 3451–3464. doi:10.1091/mbc.12.11.3451.

Berson, J.F., Theos, A.C., Harper, D.C., et al. (2003) Proprotein convertase cleavage liberates a fibrillogenic fragment of a resident glycoprotein to initiate melanosome biogenesis. *Journal of Cell Biology*, 161 (3): 521–533. doi:10.1083/jcb.200302072.

Berwick, D.C., Heaton, G.R., Azeggagh, S., et al. (2019) LRRK2 Biology from structure to dysfunction: research progresses, but the themes remain the same. *Molecular Neurodegeneration*, 14 (1): 49. doi:10.1186/s13024-019-0344-2.

Birbeck, M.S.C., Mercer, E.H. and Barnicot, N.A. (1956) The structure and formation of pigment granules in human hair. *Experimental Cell Research*, 10 (2): 505–514. doi:10.1016/0014-4827(56)90022-2.

Blauwendraat, C., Nalls, M.A. and Singleton, A.B. (2020) The genetic architecture of Parkinson's disease. *The Lancet Neurology*. 19 (2) pp. 170–178. doi:10.1016/S1474-4422(19)30287-X.

Bock, J.B., Matern, H.T., Peden, A.A., et al. (2001) A genomic perspective on membrane compartment organization. *Nature*. 409 (6822) pp. 839–841. doi:10.1038/35057024.

Bodnar, A.G., Ouellette, M., Frolkis, M., et al. (1998) Extension of life-span by introduction of telomerase into normal human cells. *Science*, 279 (5349): 349–352. doi:10.1126/science.279.5349.349.

Bonello, F., Hassoun, S.M., Mouton-Liger, F., et al. (2019) LRRK2 impairs PINK1/Parkin-dependent mitophagy via its kinase activity: Pathologic insights into Parkinson's disease. *Human Molecular Genetics*, 28 (10): 1645–1660. doi:10.1093/hmg/ddz004.

Bonet-Ponce, L., Beilina, A., Williamson, C.D., et al. (2020) LRRK2 mediates

tubulation and vesicle sorting from lysosomes. *Science Advances*, 6 (46): eabb2454. doi:10.1126/sciadv.abb2454.

Bonifacino, J.S. and Glick, B.S. (2004) The Mechanisms of Vesicle Budding and Fusion. *Cell*. 116 (2) pp. 153–166. doi:10.1016/S0092-8674(03)01079-1.

Bonifacino, J.S. and Hierro, A. (2011) Transport according to GARP: Receiving retrograde cargo at the trans-Golgi network. *Trends in Cell Biology*. 21 (3) pp. 159–167. doi:10.1016/j.tcb.2010.11.003.

Bos, J.L., Rehmann, H. and Wittinghofer, A. (2007) GEFs and GAPs: Critical Elements in the Control of Small G Proteins. *Cell*. 129 (5) pp. 865–877. doi:10.1016/j.cell.2007.05.018.

Van Den Bossche, K., Naeyaert, J.M. and Lambert, J. (2006) The quest for the mechanism of melanin transfer. *Traffic*. 7 (7) pp. 769–778. doi:10.1111/j.1600-0854.2006.00425.x.

Branza-Nichita, N., Petrescu, A.J., Dwek, R.A., et al. (1999) Tyrosinase folding and copper loading in vivo: A crucial role for calnexin and α-glucosidase II. *Biochemical and Biophysical Research Communications*, 261 (3): 720–725. doi:10.1006/bbrc.1999.1030.

Braschi, E., Goyon, V., Zunino, R., et al. (2010) Vps35 mediates vesicle transport between the mitochondria and peroxisomes. *Current Biology*, 20 (14): 1310–1315. doi:10.1016/j.cub.2010.05.066.

Braulke, T. and Bonifacino, J.S. (2009) Sorting of lysosomal proteins. *Biochimica et Biophysica Acta - Molecular Cell Research*. 1793 (4) pp. 605–614. doi:10.1016/j.bbamcr.2008.10.016.

Bright, N.A., Davis, L.J. and Luzio, J.P. (2016) Endolysosomes Are the Principal Intracellular Sites of Acid Hydrolase Activity. *Current Biology*, 26 (17): 2233–2245. doi:10.1016/j.cub.2016.06.046.

Bröcker, C., Kuhlee, A., Gatsogiannis, C., et al. (2012) Molecular architecture of the multisubunit homotypic fusion and vacuole protein sorting (HOPS) tethering complex. *Proceedings of the National Academy of Sciences of the United States of America*, 109 (6): 1991–1996. doi:10.1073/pnas.1117797109.

Brown, W.J., Goodhouse, J. and Farquhar, M.G. (1986) Mannose-6-phosphate receptors for lysosomal enzymes cycle between the Golgi complex and endosomes. *Journal of Cell Biology*, 103 (4): 1235–1247.

doi:10.1083/jcb.103.4.1235.

Bucci, C., Thomsen, P., Nicoziani, P., et al. (2000) Rab7: A key to lysosome biogenesis. *Molecular Biology of the Cell*, 11 (2): 467–480. doi:10.1091/mbc.11.2.467.

Cantalupo, G., Alifano, P., Roberti, V., et al. (2001) *Rab-interacting lysosomal protein (RILP): the Rab7 effector required for transport to lysosomes.*

Cao, M., Wu, Y., Ashrafi, G., et al. (2017) Parkinson Sac Domain Mutation in Synaptojanin 1 Impairs Clathrin Uncoating at Synapses and Triggers Dystrophic Changes in Dopaminergic Axons. *Neuron*, 93 (4): 882-896.e5. doi:10.1016/j.neuron.2017.01.019.

Carreira, S., Goodall, J., Denat, L., et al. (2006) Mitf regulation of Dia1 controls melanoma proliferation and invasiveness. *Genes and Development*, 20 (24): 3426–3439. doi:10.1101/gad.406406.

Chan, E.Y. and Tooze, S.A. (2009) Evolution of Atg1 function and regulation. *Autophagy*. 5 (6) pp. 758–765. doi:10.4161/auto.8709.

Chang, T.S. (2009) An updated review of tyrosinase inhibitors. *International Journal of Molecular Sciences*. 10 (6) pp. 2440–2475. doi:10.3390/ijms10062440.

Chartier-Harlin, M.C., Kachergus, J., Roumier, C., et al. (2004) α-synuclein locus duplication as a cause of familial Parkinson's disease. *Lancet*, 364 (9440): 1167–1169. doi:10.1016/S0140-6736(04)17103-1.

Chavrier, P., Parton, R.G., Hauri, H.P., et al. (1990) *Localization of Low Molecular Weight GTP Binding Proteins to Exocytic and Endocytic Compartments*.

Chen, H., Salopek, T.G. and Jimbow, K. (2001) The role of phosphoinositide 3-kinase in the sorting and transport of newly synthesized tyrosinase-related protein-1 (TRP-1). *The journal of investigative dermatology. Symposium proceedings*, 6 (1): 105–114. doi:10.1046/j.0022-202x.2001.00012.x.

Chen, Y.A. and Scheller, R.H. (2001) Snare-mediated membrane fusion. *Nature Reviews Molecular Cell Biology*. 2 (2) pp. 98–106. doi:10.1038/35052017.

Chiang, H.L., Terlecky, S.R., Plant, C.P., et al. (1989) A role for a 70-kilodaton heat shock protein in lysosomal degradation of intracellular proteins. *Science*,

246 (4928): 382–385. doi:10.1126/science.2799391.
Chiaverini, C., Beuret, L., Flori, E., et al. (2008) Microphthalmia-associated transcription factor regulates RAB27A gene expression and controls melanosome transport. *Journal of Biological Chemistry*, 283 (18): 12635–12642. doi:10.1074/jbc.M800130200.
Choi, H.G., Zhang, J., Deng, X., et al. (2012) Brain penetrant LRRK2 inhibitor. *ACS Medicinal Chemistry Letters*, 3 (8): 658–662. doi:10.1021/ml300123a.
Christoforidis, S., McBride, H.M., Burgoyne, R.D., et al. (1999) The rab5 effector EEA1 is a core component of endosome docking. *Nature*, 397 (6720): 621–625. doi:10.1038/17618.
Ciechanover, A. (2005) Proteolysis: From the lysosome to ubiquitin and the proteasome. *Nature Reviews Molecular Cell Biology*. 6 (1) pp. 79–86. doi:10.1038/nrm1552.
Clague, M.J. (1998) Molecular aspects of the endocytic pathway. *Biochemical Journal*. 336 (2) pp. 271–282. doi:10.1042/bj3360271.
Clague, M.J. and Rochin, L. (2016) Parkinson's Disease: A Traffic Jam? *Current Biology*. 26 (8) pp. R332–R334. doi:10.1016/j.cub.2016.03.001.
Clague, M.J. and Urbé, S. (2020) Data mining for traffic information. *Traffic*, 21 (1): 162–168. doi:10.1111/tra.12702.
Clark, I.E., Dodson, M.W., Jiang, C., et al. (2006) Drosophila pink1 is required for mitochondrial function and interacts genetically with parkin. *Nature*, 441 (7097): 1162–1166. doi:10.1038/nature04779.
Condon, K.J. and Sabatini, D.M. (2019) Nutrient regulation of mTORC1 at a glance. *Journal of Cell Science*, 132 (21). doi:10.1242/JCS.222570.
Del Conte-Zerial, P., Brusch, L., Rink, J.C., et al. (2008) Membrane identity and GTPase cascades regulated by toggle and cut-out switches. *Molecular Systems Biology*, 4. doi:10.1038/msb.2008.45.
Cookson, M.R. (2010) The role of leucine-rich repeat kinase 2 (LRRK2) in Parkinson's disease. *Nature Reviews Neuroscience*. 11 (12) pp. 791–797. doi:10.1038/nrn2935.
Cooper, A.A., Gitler, A.D., Cashikar, A., et al. (2006) α-synuclein blocks ER-Golgi traffic and Rab1 rescues neuron loss in Parkinson's models. *Science*, 313 (5785): 324–328. doi:10.1126/science.1129462.

Cooper, A.A. and Stevens, T.H. (1996) Vps10p cycles between the late-Golgi and prevacuolar compartments in its function as the sorting receptor for multiple yeast vacuolar hydrolases. *Journal of Cell Biology*, 133 (3): 529–541. doi:10.1083/jcb.133.3.529.

Cremona, O., Di Paolo, G., Wenk, M.R., et al. (1999) Essential role of phosphoinositide metabolism in synaptic vesicle recycling. *Cell*, 99 (2): 179–188. doi:10.1016/S0092-8674(00)81649-9.

Cuervo, A.M., Stafanis, L., Fredenburg, R., et al. (2004) Impaired degradation of mutant α-synuclein by chaperone-mediated autophagy. *Science*, 305 (5688): 1292–1295. doi:10.1126/science.1101738.

Datta, S.R., Brunet, A. and Greenberg, M.E. (1999) Cellular survival: A play in three akts. *Genes and Development*. 13 (22) pp. 2905–2927. doi:10.1101/gad.13.22.2905.

Dauer, W. and Przedborski, S. (2003) Parkinson's disease: Mechanisms and models. *Neuron*. 39 (6) pp. 889–909. doi:10.1016/S0896-6273(03)00568-3.

Delevoye, C., Hurbain, I., Tenza, D., et al. (2009) AP-1 and KIF13A coordinate endosomal sorting and positioning during melanosome biogenesis. *Journal of Cell Biology*, 187 (2): 247–264. doi:10.1083/jcb.200907122.

Dell'Angelica, E.C. (2004) The building BLOC(k)s of lysosomes and related organelles. *Current Opinion in Cell Biology*. 16 (4) pp. 458–464. doi:10.1016/j.ceb.2004.05.001.

Dennis, M.K., Delevoye, C., Acosta-Ruiz, A., et al. (2016) BLOC-1 and BLOC-3 regulate VAMP7 cycling to and from melanosomes via distinct tubular transport carriers. *Journal of Cell Biology*, 214 (3): 293–308. doi:10.1083/jcb.201605090.

Dennis, M.K., Mantegazza, A.R., Snir, O.L., et al. (2015) BLOC-2 targets recycling endosomal tubules to melanosomes for cargo delivery. *Journal of Cell Biology*, 209 (4): 563–577. doi:10.1083/jcb.201410026.

Derivery, E., Sousa, C., Gautier, J.J., et al. (2009) The Arp2/3 Activator WASH Controls the Fission of Endosomes through a Large Multiprotein Complex. *Developmental Cell*, 17 (5): 712–723. doi:10.1016/j.devcel.2009.09.010.

Desnoyers, L., Anant, J.S. and Seabra, M.C. (1996) "Geranylgeranylation of Rab proteins." In *Biochemical Society Transactions*. 1996. Portland Press Ltd.

pp. 699–703. doi:10.1042/bst0240699.
Dickson, D.W., Braak, H., Duda, J.E., et al. (2009) Neuropathological assessment of Parkinson's disease: refining the diagnostic criteria. *The Lancet Neurology*. 8 (12) pp. 1150–1157. doi:10.1016/S1474-4422(09)70238-8.
Dikic, I. and Elazar, Z. (2018) Mechanism and medical implications of mammalian autophagy. *Nature Reviews Molecular Cell Biology*. 19 (6) pp. 349–364. doi:10.1038/s41580-018-0003-4.
Dorszewska, J., Prendecki, M., Lianeri, M., et al. (2014) Molecular Effects of L-dopa Therapy in Parkinson's Disease. *Current Genomics*, 15 (1): 11–17. doi:10.2174/1389202914666131210213042.
De Duve, C., Gianetto, R., Appelmans, F., et al. (1953) Enzymic content of the mitochondria fraction. *Nature*. 172 (4390) pp. 1143–1144. doi:10.1038/1721143a0.
De Duve, C., PRESSMAN, B.C., GIANETTO, R., et al. (1955) Tissue fractionation studies. 6. Intracellular distribution patterns of enzymes in rat-liver tissue. *The Biochemical journal*, 60 (4): 604–617. doi:10.1042/bj0600604.
De Duve, C. and Wattiaux, R. (1966) Functions of Lysosomes. *Annual Review of Physiology*, 28 (1): 435–492. doi:10.1146/annurev.ph.28.030166.002251.
Ebrahimi, A., Keske, E., Mehdipor, A., et al. (2019) Somatic cell reprogramming as a tool for neurodegenerative diseases. *Biomedicine and Pharmacotherapy*. 112 p. 108663. doi:10.1016/j.biopha.2019.108663.
Essner, E. and Novikoff, A.B. (1961) Localization of acid phosphatase activity in hepatic lysosomes by means of electron microscopy. *The Journal of biophysical and biochemical cytology*, 9 (4): 773–784. doi:10.1083/jcb.9.4.773.
Estrada, A.A., Chan, B.K., Baker-Glenn, C., et al. (2014) Discovery of highly potent, selective, and brain-penetrant aminopyrazole Leucine-rich repeat kinase 2 (LRRK2) small molecule inhibitors. *Journal of Medicinal Chemistry*, 57 (3): 921–936. doi:10.1021/jm401654j.
Fasshauer, D., Antonin, W., Subramaniam, V., et al. (2002) SNARE assembly and disassembly exhibit a pronounced hysteresis. *Nature Structural Biology*, 9 (2): 144–151. doi:10.1038/nsb750.
Fasshauer, D., Sutton, R.B., Brunger, A.T., et al. (1998) Conserved structural features of the synaptic fusion complex: SNARE proteins reclassified as Q-

and R-SNAREs. *Proceedings of the National Academy of Sciences of the United States of America*, 95 (26): 15781–15786. doi:10.1073/pnas.95.26.15781.

Fearnley, J.M. and Lees, A.J. (1991) Ageing and parkinson's disease: Substantia nigra regional selectivity. *Brain*, 114 (5): 2283–2301. doi:10.1093/brain/114.5.2283.

Fell, M.J., Mirescu, C., Basu, K., et al. (2015) MLi-2, a potent, selective, and centrally active compound for exploring the therapeutic potential and safety of LRRK2 kinase inhibition. *Journal of Pharmacology and Experimental Therapeutics*, 355 (3): 397–409. doi:10.1124/jpet.115.227587.

Flem-Karlsen, K., Nyakas, M., Farstad, I.N., et al. (2020) Soluble AXL as a marker of disease progression and survival in melanoma. *PloS one*, 15 (1): e0227187–e0227187. doi:10.1371/journal.pone.0227187.

Follett, J., Bugarcic, A., Yang, Z., et al. (2016) Parkinson disease-linked Vps35 R524W mutation impairs the endosomal association of retromer and induces α-synuclein aggregation. *Journal of Biological Chemistry*, 291 (35): 18283–18298. doi:10.1074/jbc.M115.703157.

Di Fonzo, A., Rohé, C.F., Ferreira, J., et al. (2005) A frequent LRRK2 gene mutation associated with autosomal dominant Parkinson's disease. *Lancet (London, England)*, 365 (9457): 412–415. doi:10.1016/S0140-6736(05)17829-5.

Forgac, M. (1998a) Structure, function and regulation of the vacuolar (H+)-ATPases. *FEBS Letters*. 440 (3) pp. 258–263. doi:10.1016/S0014-5793(98)01425-2.

Forgac, M. (1998b) Structure, function and regulation of the vacuolar (H+)-ATPases. *FEBS Letters*. 440 (3) pp. 258–263. doi:10.1016/S0014-5793(98)01425-2.

Forgac, M. (2007) Vacuolar ATPases: Rotary proton pumps in physiology and pathophysiology. *Nature Reviews Molecular Cell Biology*. 8 (11) pp. 917–929. doi:10.1038/nrm2272.

Funayama, M., Hasegawa, K., Ohta, E., et al. (2005) An LRRK2 mutation as a cause for the Parkinsonism in the original PARK8 family. *Annals of Neurology*, 57 (6): 918–921. doi:10.1002/ana.20484.

Futter, C.E., Pearse, A., Hewlett, L.J., et al. (1996) Multivesicular endosomes containing internalized EGF-EGF receptor complexes mature and then fuse directly with lysosomes. *Journal of Cell Biology*, 132 (6): 1011–1023. doi:10.1083/jcb.132.6.1011.

Futter, C.E., Ramalho, J.S., Jaissle, G.B., et al. (2004) The Role of Rab27a in the Regulation of Melanosome Distribution within Retinal Pigment Epithelial Cells. *Molecular Biology of the Cell*, 15 (5): 2264–2275. doi:10.1091/mbc.E03-10-0772.

Ganley, I.G., Lam, D.H., Wang, J., et al. (2009) ULK1·ATG13·FIP200 complex mediates mTOR signaling and is essential for autophagy. *Journal of Biological Chemistry*, 284 (18): 12297–12305. doi:10.1074/jbc.M900573200.

Gao, Y., Wilson, G.R., Stephenson, S.E.M., et al. (2018) The emerging role of Rab GTPases in the pathogenesis of Parkinson's disease. *Movement Disorders*. 33 (2) pp. 196–207. doi:10.1002/mds.27270.

Garraway, L.A., Widlund, H.R., Rubin, M.A., et al. (2005) Integrative genomic analyses identify MITF as a lineage survival oncogene amplified in malignant melanoma. *Nature*, 436 (7047): 117–122. doi:10.1038/nature03664.

Gelmetti, V., De Rosa, P., Torosantucci, L., et al. (2017) PINK1 and BECN1 relocalize at mitochondria-associated membranes during mitophagy and promote ER-mitochondria tethering and autophagosome formation. *Autophagy*, 13 (4): 654–669. doi:10.1080/15548627.2016.1277309.

Gerondopoulos, A., Langemeyer, L., Liang, J.R., et al. (2012) BLOC-3 mutated in Hermansky-Pudlak syndrome is a Rab32/38 guanine nucleotide exchange factor. *Current Biology*, 22 (22): 2135–2139. doi:10.1016/j.cub.2012.09.020.

Ghanem, G. and Fabrice, J. (2011) Tyrosinase related protein 1 (TYRP1/gp75) in human cutaneous melanoma. *Molecular Oncology*. 5 (2) pp. 150–155. doi:10.1016/j.molonc.2011.01.006.

Giaime, E., Tong, Y., Wagner, L.K., et al. (2017) Age-Dependent Dopaminergic Neurodegeneration and Impairment of the Autophagy-Lysosomal Pathway in LRRK-Deficient Mice. *Neuron*, 96 (4): 796-807.e6. doi:10.1016/j.neuron.2017.09.036.

Gieselmann, V., Hasilik, A. and Von Figura, K. (1985) *Processing of Human*

*Cathepsin D in Lysosomes in Vitro**.

Gitler, A.D., Bevis, B.J., Shorter, J., et al. (2008) The Parkinson's disease protein α-synuclein disrupts cellular Rab homeostasis. *Proceedings of the National Academy of Sciences of the United States of America*, 105 (1): 145–150. doi:10.1073/pnas.0710685105.

Glick, D., Barth, S. and Macleod, K.F. (2010) Autophagy: Cellular and molecular mechanisms. *Journal of Pathology*. 221 (1) pp. 3–12. doi:10.1002/path.2697.

Gómez-Suaga, P., Rivero-Ríos, P., Fdez, E., et al. (2014) LRRK2 delays degradative receptor trafficking by impeding late endosomal budding through decreasing Rab7 activity. *Human molecular genetics*, 23 (25): 6779–96. doi:10.1093/hmg/ddu395.

Gomez, P.F., Luo, D., Hirosaki, K., et al. (2001) Identification of rab7 as a melanosome-associated protein involved in the intracellular transport of tyrosinase-related protein 1. *Journal of Investigative Dermatology*, 117 (1): 81–90. doi:10.1046/j.0022-202X.2001.01402.x.

Gomez, T.S. and Billadeau, D.D. (2009) A FAM21-Containing WASH Complex Regulates Retromer-Dependent Sorting. *Developmental Cell*, 17 (5): 699–711. doi:10.1016/j.devcel.2009.09.009.

Goodall, J., Carreira, S., Denat, L., et al. (2008) Brn-2 represses microphthalmia-associated transcription factor expression and marks a distinct subpopulation of microphthalmia-associated transcription factor-negative melanoma cells. *Cancer Research*, 68 (19): 7788–7794. doi:10.1158/0008-5472.CAN-08-1053.

Gorenberg, E.L. and Chandra, S.S. (2017) The role of co-chaperones in synaptic proteostasis and neurodegenerative disease. *Frontiers in Neuroscience*. 11 (MAY). doi:10.3389/fnins.2017.00248.

Greten-Harrison, B., Polydoro, M., Morimoto-Tomita, M., et al. (2010) αβγ-Synuclein triple knockout mice revealage-dependent neuronal dysfunction. *Proceedings of the National Academy of Sciences of the United States of America*, 107 (45): 19573–19578. doi:10.1073/pnas.1005005107.

Guerra, F. and Bucci, C. (2016) Multiple Roles of the Small GTPase Rab7. *Cells*, 5 (3): 34. doi:10.3390/cells5030034.

Haas, A.K., Fuchs, E., Kopajtich, R., et al. (2005) A GTPase-activating protein controls Rab5 function in endocytic trafficking. *Nature Cell Biology*, 7 (9): 887–893. doi:10.1038/ncb1290.

Hah, Y.S., Cho, H.Y., Lim, T.Y., et al. (2012) Induction of melanogenesis by rapamycin in human MNT-1 melanoma cells. *Annals of Dermatology*, 24 (2): 151–157. doi:10.5021/ad.2012.24.2.151.

Haider, M. and Segal, H.L. (1972) Some characteristics of the alanine aminotransferase- and arginase-inactivating system of lysosomes. *Archives of Biochemistry and Biophysics*, 148 (1): 228–237. doi:10.1016/0003-9861(72)90136-1.

Hanson, P.I., Roth, R., Morisaki, H., et al. (1997) Structure and conformational changes in NSF and its membrane receptor complexes visualized by quick-freeze/deep-etch electron microscopy. *Cell*, 90 (3): 523–535. doi:10.1016/S0092-8674(00)80512-7.

Hanss, Z., Larsen, S.B., Antony, P., et al. (2021) Mitochondrial and Clearance Impairment in p.D620N VPS35 Patient-Derived Neurons. *Movement Disorders*, 36 (3): 704–715. doi:10.1002/mds.28365.

Harterink, M., Port, F., Lorenowicz, M.J., et al. (2011) A SNX3-dependent retromer pathway mediates retrograde transport of the Wnt sorting receptor Wntless and is required for Wnt secretion. *Nature Cell Biology*, 13 (8): 914–923. doi:10.1038/ncb2281.

Hartman, M.L. and Czyz, M. (2015) MITF in melanoma: Mechanisms behind its expression and activity. *Cellular and Molecular Life Sciences*. 72 (7) pp. 1249–1260. doi:10.1007/s00018-014-1791-0.

Hasegawa, T., Sugeno, N., Kikuchi, A., et al. (2017) Membrane Trafficking Illuminates a Path to Parkinson's Disease. *The Tohoku journal of experimental medicine*, 242 (1): 63–76. doi:10.1620/tjem.242.63.

Hearing, V.J. (2011) Determination of melanin synthetic pathways. *The Journal of investigative dermatology*. 131 (E1) p. E8. doi:10.1038/skinbio.2011.4.

Helenius, A., Mellman, I., Wall, D., et al. (1983) Endosomes. *Trends in Biochemical Sciences*. 8 (7) pp. 245–250. doi:10.1016/0968-0004(83)90350-X.

Hemesath, T.J., Steingrímsson, E., McGill, G., et al. (1994a) microphthalmia, A critical factor in melanocyte development, defines a discrete transcription factor family. *Genes and Development*, 8 (22): 2770–2780. doi:10.1101/gad.8.22.2770.

Hemesath, T.J., Steingrímsson, E., McGill, G., et al. (1994b) microphthalmia, A critical factor in melanocyte development, defines a discrete transcription factor family. *Genes and Development*, 8 (22): 2770–2780. doi:10.1101/gad.8.22.2770.

Henry, A.G., Aghamohammadzadeh, S., Samaroo, H., et al. (2015) Pathogenic LRRK2 mutations, through increased kinase activity, produce enlarged lysosomes with reduced degradative capacity and increase ATP13A2 expression. *Human Molecular Genetics*, 24 (21): 6013–6028. doi:10.1093/hmg/ddv314.

Hinkle, K.M., Yue, M., Behrouz, B., et al. (2012) LRRK2 knockout mice have an intact dopaminergic system but display alterations in exploratory and motor co-ordination behaviors. *Molecular Neurodegeneration*, 7 (1): 25. doi:10.1186/1750-1326-7-25.

Hirst, J., Futter, C.E. and Hopkins, C.R. (1998) The kinetics of mannose 6-phosphate receptor trafficking in the endocytic pathway in HEp-2 cells: The receptor enters and rapidly leaves multivesicular endosomes without accumulating in a prelysosomal compartment. *Molecular Biology of the Cell*, 9 (4): 809–816. doi:10.1091/mbc.9.4.809.

Ho, P.W.L., Leung, C.T., Liu, H., et al. (2020) Age-dependent accumulation of oligomeric SNCA/α-synuclein from impaired degradation in mutant LRRK2 knockin mouse model of Parkinson disease: role for therapeutic activation of chaperone-mediated autophagy (CMA). *Autophagy*, 16 (2): 347–370. doi:10.1080/15548627.2019.1603545.

Hockey, L.N., Kilpatrick, B.S., Eden, E.R., et al. (2015) Dysregulation of lysosomal morphology by pathogenic LRRK2 is corrected by TPC2 inhibition. *Journal of Cell Science*, 128 (2): 232–238. doi:10.1242/jcs.164152.

Hoek, K.S. and Goding, C.R. (2010) Cancer stem cells versus phenotype-switching in melanoma. *Pigment Cell & Melanoma Research*, 23 (6): 746–759. doi:10.1111/j.1755-148X.2010.00757.x.

Hong, W. (2005) SNAREs and traffic. *Biochimica et biophysica acta*. 1744 (3) pp. 493–517. doi:10.1016/j.bbamcr.2005.03.014.

Höning, S., Sandoval, I. and Von Figura, K. (1998) A di-leucine-based motif in the cytoplasmic tail of LIMP-II and tyrosinase mediates selective binding of AP-3. *EMBO Journal*, 17 (5): 1304–1314. doi:10.1093/emboj/17.5.1304.

Hopkins, C.R., Gibson, A., Shipman, M., et al. (1990) Movement of internalized ligand-receptor complexes along a continuous endosomal reticulum. *Nature*, 346 (6282): 335–339. doi:10.1038/346335a0.

Hornykiewicz, O. (2006) "The discovery of dopamine deficiency in the parkinsonian brain." In *Journal of Neural Transmission, Supplement*. 2006. Springer Wien. pp. 9–15. doi:10.1007/978-3-211-45295-0_3.

Hornykiewicz, O. (2017) L-DOPA. *Journal of Parkinson's Disease*. 7 (s1) pp. S3–S10. doi:10.3233/JPD-179004.

Hough, R., Pratt, G. and Rechsteiner, M. (1986) Ubiquitin-lysozyme conjugates. Identification and characterization of an ATP-dependent protease from rabbit reticulocyte lysates. *Journal of Biological Chemistry*, 261 (5): 2400–2408. Available at: https://www.ncbi.nlm.nih.gov/pubmed/3003114 (Accessed: 18 May 2020).

Hsieh, C.H., Shaltouki, A., Gonzalez, A.E., et al. (2016) Functional Impairment in Miro Degradation and Mitophagy Is a Shared Feature in Familial and Sporadic Parkinson's Disease. *Cell Stem Cell*, 19 (6): 709–724. doi:10.1016/j.stem.2016.08.002.

Hu, Y.B., Dammer, E.B., Ren, R.J., et al. (2015) The endosomal-lysosomal system: From acidification and cargo sorting to neurodegeneration. *Translational Neurodegeneration*. 4 (1) p. 18. doi:10.1186/s40035-015-0041-1.

Huang, P., Yang, X.D., Chen, S. Di, et al. (2015) The association between Parkinson's disease and melanoma: A systematic review and meta-analysis. *Translational Neurodegeneration*. 4 (1). doi:10.1186/s40035-015-0044-y.

Hume, A.N., Collinson, L.M., Rapak, A., et al. (2001) Rab27a regulates the peripheral distribution of melanosomes in melanocytes. *Journal of Cell Biology*, 152 (4): 795–808. doi:10.1083/jcb.152.4.795.

Hume, A.N. and Seabra, M.C. (2011) Melanosomes on the move: A model to

understand organelle dynamics. *Biochemical Society Transactions*. 39 (5) pp. 1191–1196. doi:10.1042/BST0391191.

Hunn, B.H.M., Cragg, S.J., Bolam, J.P., et al. (2015) Impaired intracellular trafficking defines early Parkinson's disease. *Trends in Neurosciences*, 38 (3): 178–188. doi:https://doi.org/10.1016/j.tins.2014.12.009.

Huotari, J. and Helenius, A. (2011) Endosome maturation. *The EMBO Journal*, 30 (17): 3481–3500. doi:10.1038/emboj.2011.286.

Hur, E.M., Jang, E.H., Jeong, G.R., et al. (2019) LRRK2 and membrane trafficking: Nexus of Parkinson's disease. *BMB Reports*. 52 (9) pp. 533–539. doi:10.5483/BMBRep.2019.52.9.186.

Hurbain, I., Geerts, W.J.C., Boudier, T., et al. (2008) Electron tomography of early melanosomes: Implications for melanogenesis and the generation of fibrillar amyloid sheets. *Proceedings of the National Academy of Sciences of the United States of America*, 105 (50): 19726–19731. doi:10.1073/pnas.0803488105.

Ishizu, N., Yui, D., Hebisawa, A., et al. (2016) Impaired striatal dopamine release in homozygous Vps35 D620 N knock-in mice. *Human Molecular Genetics*, 25 (20): 4507–4517. doi:10.1093/hmg/ddw279.

Ito, G., Katsemonova, K., Tonelli, F., et al. (2016) Phos-Tag analysis of Rab10 phosphorylation by LRRK2: A powerful assay for assessing kinase function and inhibitors. *Biochemical Journal*. doi:10.1042/BCJ20160557.

Jackson, I.J., Chambers, D.M., Tsukamoto, K., et al. (1992) A second tyrosinase-related protein, TRP-2, maps to and is mutated at the mouse slaty locus. *EMBO Journal*, 11 (2): 527–535. doi:10.1002/j.1460-2075.1992.tb05083.x.

Jahn, R. and Scheller, R.H. (2006) SNAREs - Engines for membrane fusion. *Nature Reviews Molecular Cell Biology*. 7 (9) pp. 631–643. doi:10.1038/nrm2002.

Jaleel, M., Nichols, R.J., Deak, M., et al. (2007) LRRK2 phosphorylates moesin at threonine-558: characterization of how Parkinson's disease mutants affect kinase activity. *Biochemical Journal*, 405 (2): 307–317. doi:10.1042/BJ20070209.

Jani, R.A., Purushothaman, L.K., Rani, S., et al. (2015) STX13 regulates cargo

delivery from recycling endosomes during melanosome biogenesis. *Journal of Cell Science*, 128 (17): 3263–3276. doi:10.1242/jcs.171165.

Jeong, G.R., Jang, E.-H., Bae, J.R., et al. (2018) Dysregulated phosphorylation of Rab GTPases by LRRK2 induces neurodegeneration. *Molecular neurodegeneration*, 13 (1): 8. doi:10.1186/s13024-018-0240-1.

Jiang, G.M., Tan, Y., Wang, H., et al. (2019) The relationship between autophagy and the immune system and its applications for tumor immunotherapy. *Molecular Cancer*. 18 (1) pp. 1–22. doi:10.1186/s12943-019-0944-z.

Jimbow, K., Gomez, P.F., Toyofuku, K., et al. (1997) Biological role of tyrosinase related protein and its biosynthesis and transport from TGN to stage I melanosome, late endosome, through gene transfection study. *Pigment cell research*, 10 (4): 206–213. doi:10.1111/j.1600-0749.1997.tb00486.x.

Jimenez-Orgaz, A., Kvainickas, A., Nägele, H., et al. (2018) Control of RAB7 activity and localization through the retromer-TBC1D5 complex enables RAB7-dependent mitophagy. *The EMBO journal*, 37 (2): 235–254. doi:10.15252/embj.201797128.

Jimenez-Orgaz, A., Kvainickas, A., Nägele, H., et al. (2018) Control of RAB 7 activity and localization through the retromer-TBC1D5 complex enables RAB 7-dependent mitophagy . *The EMBO Journal*, 37 (2): 235–254. doi:10.15252/embj.201797128.

Jin, S.M., Lazarou, M., Wang, C., et al. (2010) Mitochondrial membrane potential regulates PINK1 import and proteolytic destabilization by PARL. *Journal of Cell Biology*, 191 (5): 933–942. doi:10.1083/jcb.201008084.

Johnson, D.E., Ostrowski, P., Jaumouillé, V., et al. (2016) The position of lysosomes within the cell determines their luminal pH. *Journal of Cell Biology*, 212 (6): 677–692. doi:10.1083/jcb.201507112.

Jordens, I., Fernandez-Borja, M., Marsman, M., et al. (2001) The Rab7 effector protein RILP controls lysosomal transport by inducing the recruitment of dynein-dynactin motors. *Current Biology*, 11 (21): 1680–1685. doi:10.1016/S0960-9822(01)00531-0.

Jordens, I., Westbroek, W., Marsman, M., et al. (2006) Rab7 and Rab27a

control two motor protein activities involved in melanosomal transport. *Pigment Cell Research*, 19 (5): 412–423. doi:10.1111/j.1600-0749.2006.00329.x.

Jovic, M., Sharma, M., Rahajeng, J., et al. (2010) The early endosome: A busy sorting station for proteins at the crossroads. *Histology and Histopathology*. 25 (1) pp. 99–112. doi:10.14670/HH-25.99.

Kamada, Y., Yoshino, K., Kondo, C., et al. (2010) Tor Directly Controls the Atg1 Kinase Complex To Regulate Autophagy. *Molecular and Cellular Biology*, 30 (4): 1049–1058. doi:10.1128/mcb.01344-09.

Kane, L.A., Lazarou, M., Fogel, A.I., et al. (2014) PINK1 phosphorylates ubiquitin to activate parkin E3 ubiquitin ligase activity. *Journal of Cell Biology*, 205 (2): 143–153. doi:10.1083/jcb.201402104.

Kane, P.M. (2006) The Where, When, and How of Organelle Acidification by the Yeast Vacuolar H + -ATPase . *Microbiology and Molecular Biology Reviews*, 70 (1): 177–191. doi:10.1128/mmbr.70.1.177-191.2006.

Kanki, T. and Klionsky, D.J. (2008) Mitophagy in yeast occurs through a selective mechanism. *Journal of Biological Chemistry*, 283 (47): 32386–32393. doi:10.1074/jbc.M802403200.

Van Der Kant, R., Fish, A., Janssen, L., et al. (2013) Late endosomal transport and tethering are coupled processes controlled by RILP and the cholesterol sensor ORP1L. *Journal of Cell Science*, 126 (15): 3462–3474. doi:10.1242/jcs.129270.

Van Der Kant, R., Jonker, C.T.H., Wijdeven, R.H., et al. (2015) Characterization of the mammalian CORVET and HOPS complexes and their modular restructuring for endosome specificity. *Journal of Biological Chemistry*, 290 (51): 30280–30290. doi:10.1074/jbc.M115.688440.

Kaushik, S. and Cuervo, A.M. (2012) Chaperone-mediated autophagy: A unique way to enter the lysosome world. *Trends in Cell Biology*. 22 (8) pp. 407–417. doi:10.1016/j.tcb.2012.05.006.

Khan, N.L., Jain, S., Lynch, J.M., et al. (2005) Mutations in the gene LRRK2 encoding dardarin (PARK8) cause familial Parkinson's disease: clinical, pathological, olfactory and functional imaging and genetic data. *Brain : a journal of neurology*, 128 (Pt 12): 2786–2796. doi:10.1093/brain/awh667.

Khatter, D., Raina, V.B., Dwivedi, D., et al. (2015) The small GTPase Arl8b regulates assembly of the mammalian HOPS complex on lysosomes. *Journal of Cell Science*, 128 (9): 1746–1761. doi:10.1242/jcs.162651.

Kim, J., Efe, J.A., Zhu, S., et al. (2011a) Direct reprogramming of mouse fibroblasts to neural progenitors. *Proceedings of the National Academy of Sciences of the United States of America*, 108 (19): 7838–7843. doi:10.1073/pnas.1103113108.

Kim, J., Kundu, M., Viollet, B., et al. (2011b) AMPK and mTOR regulate autophagy through direct phosphorylation of Ulk1. *Nature Cell Biology*, 13 (2): 132–141. doi:10.1038/ncb2152.

Kirchhausen, T. (2000) Three ways to make a vesicle. *Nature Reviews Molecular Cell Biology*. 1 (3) pp. 187–198. doi:10.1038/35043117.

Klionsky, D.J. (2005) The molecular machinery of autophagy: Unanswered questions. *Journal of Cell Science*, 118 (1): 7–18. doi:10.1242/jcs.01620.

Klionsky, D.J. (2008) Autophagy revisited: A conversation with Christian de Duve. *Autophagy*. 4 (6) pp. 740–743. doi:10.4161/auto.6398.

Kordower, J.H., Olanow, C.W., Dodiya, H.B., et al. (2013) Disease duration and the integrity of the nigrostriatal system in Parkinson's disease. *Brain*, 136 (8): 2419–2431. doi:10.1093/brain/awt192.

Körner, A. and Pawelek, J. (1982) Mammalian tyrosinase catalyzes three reactions in the biosynthesis of melanin. *Science*, 217 (4565): 1163–1165. doi:10.1126/science.6810464.

Kornfeld, S. and Mellman, I. (1989) The biogenesis of lysosomes. *Annual Review of Cell Biology*. 5 pp. 483–525. doi:10.1146/annurev.cb.05.110189.002411.

Koyano, F., Okatsu, K., Kosako, H., et al. (2014) Ubiquitin is phosphorylated by PINK1 to activate parkin. *Nature*, 510 (7503): 162–166. doi:10.1038/nature13392.

Kozar, I., Margue, C., Rothengatter, S., et al. (2019) Many ways to resistance: How melanoma cells evade targeted therapies. *Biochimica et Biophysica Acta - Reviews on Cancer*. 1871 (2) pp. 313–322. doi:10.1016/j.bbcan.2019.02.002.

Kramer, M.L. and Schulz-Schaeffer, W.J. (2007) Presynaptic α-synuclein aggregates, not Lewy bodies, cause neurodegeneration in dementia with lewy

bodies. *Journal of Neuroscience*, 27 (6): 1405–1410. doi:10.1523/JNEUROSCI.4564-06.2007.

Krebs, C.E., Karkheiran, S., Powell, J.C., et al. (2013) The sac1 domain of SYNJ1 identified mutated in a family with early-onset progressive parkinsonism with generalized seizures. *Human Mutation*, 34 (9): 1200–1207. doi:10.1002/humu.22372.

Kuma, A., Hatano, M., Matsui, M., et al. (2004) The role of autophagy during the early neonatal starvation period. *Nature*, 432 (7020): 1032–1036. doi:10.1038/nature03029.

Kuwahara, T., Inoue, K., D'Agati, V.D., et al. (2016) LRRK2 and RAB7L1 coordinately regulate axonal morphology and lysosome integrity in diverse cellular contexts. *Scientific Reports*, 6. doi:10.1038/srep29945.

Kwon, B.S., Haq, A.K., Pomerantz, S.H., et al. (1987) Isolation and sequence of a cDNA clone for human tyrosinase that maps at the mouse c-albino locus. *Proceedings of the National Academy of Sciences of the United States of America*, 84 (21): 7473–7477. doi:10.1073/pnas.84.21.7473.

Lafer, E.M. (2002) Clathrin-Protein Interactions. *Traffic*, 3 (8): 513–520. doi:10.1034/j.1600-0854.2002.30801.x.

Lai, Y., Kondapalli, C., Lehneck, R., et al. (2015a) Phosphoproteomic screening identifies Rab GTP ases as novel downstream targets of PINK 1 . *The EMBO Journal*, 34 (22): 2840–2861. doi:10.15252/embj.201591593.

Lai, Y., Kondapalli, C., Lehneck, R., et al. (2015b) Phosphoproteomic screening identifies Rab <scp>GTP</scp> ases as novel downstream targets of <scp>PINK</scp> 1. *The EMBO Journal*, 34 (22): 2840–2861. doi:10.15252/embj.201591593.

Lamb, C.A., Dooley, H.C. and Tooze, S.A. (2013) Endocytosis and autophagy: Shared machinery for degradation. *BioEssays*, 35 (1): 34–45. doi:10.1002/bies.201200130.

Lee, K.S., Huh, S., Lee, S., et al. (2018) Altered ER-mitochondria contact impacts mitochondria calcium homeostasis and contributes to neurodegeneration in vivo in disease models. *Proceedings of the National Academy of Sciences of the United States of America*, 115 (38): E8844–E8853. doi:10.1073/pnas.1721136115.

Lees, A.J., Hardy, J. and Revesz, T. (2009) Parkinson's disease. *The Lancet*. 373 (9680) pp. 2055–2066. doi:10.1016/S0140-6736(09)60492-X.

Li, C., Wang, D., Wu, W., et al. (2018) DLP1-dependent mitochondrial fragmentation and redistribution mediate prion-associated mitochondrial dysfunction and neuronal death. *Aging cell*, 17 (1): e12693. doi:10.1111/acel.12693.

Li, F.Z., Dhillon, A.S., Anderson, R.L., et al. (2015) Phenotype switching in melanoma: Implications for progression and therapy. *Frontiers in Oncology*. 5 (FEB). doi:10.3389/fonc.2015.00031.

Li, X.D., Ikebe, R. and Ikebei, M. (2005) Activation of myosin Va function by melanophilin, a specific docking partner of myosin Va. *Journal of Biological Chemistry*, 280 (18): 17815–17822. doi:10.1074/jbc.M413295200.

Liang, X.H., Jackson, S., Seaman, M., et al. (1999) Induction of autophagy and inhibition of tumorigenesis by beclin 1 . *Nature*, 402 (6762): 672–676. doi:10.1038/45257.

Liao, Y. and Hung, M.C. (2010) Physiological regulation of Akt activity and stability. *American Journal of Translational Research*. 2 (1) pp. 19–42. Available at: www.ajtr.org/AJTR910005 (Accessed: 8 November 2020).

Lin, R.C. and Scheller, R.H. (1997) Structural organization of the synaptic exocytosis core complex. *Neuron*, 19 (5): 1087–1094. doi:10.1016/S0896-6273(00)80399-2.

Lin, X., Yang, T., Wang, S., et al. (2014) RILP interacts with HOPS complex via VPS41 subunit to regulate endocytic trafficking. *Scientific Reports*, 4. doi:10.1038/srep07282.

Lis, P., Burel, S., Steger, M., et al. (2018) Development of phospho-specific Rab protein antibodies to monitor in vivo activity of the LRRK2 Parkinson's disease kinase. *Biochemical Journal*, 475 (1): 1–22. doi:10.1042/BCJ20170802.

Liu, G.Y. and Sabatini, D.M. (2020) mTOR at the nexus of nutrition, growth, ageing and disease. *Nature Reviews Molecular Cell Biology*. 21 (4) pp. 183–203. doi:10.1038/s41580-019-0199-y.

Liu, J., Liu, W., Li, R., et al. (2019) Mitophagy in Parkinson's Disease: From Pathogenesis to Treatment. *Cells*, 8 (7): 712. doi:10.3390/cells8070712.

Liu, T.F., Kandala, G. and Setaluri, V. (2001a) PDZ domain protein GIPC interacts with the cytoplasmic tail of melanosomal membrane protein gp75 (tyrosinase-related protein-1). *The Journal of biological chemistry*, 276 (38): 35768–35777. doi:10.1074/jbc.M103585200.

Liu, T.F., Kandala, G. and Setaluri, V. (2001b) PDZ Domain Protein GIPC Interacts with the Cytoplasmic Tail of Melanosomal Membrane Protein gp75 (Tyrosinase-related Protein-1). *Journal of Biological Chemistry*, 276 (38): 35768–35777. doi:10.1074/jbc.M103585200.

Liu, Z., Bryant, N., Kumaran, R., et al. (2018) LRRK2 phosphorylates membrane-bound Rabs and is activated by GTP-bound Rab7L1 to promote recruitment to the trans-Golgi network. *Human Molecular Genetics*, 27 (2): 385–395. doi:10.1093/hmg/ddx410.

Loewith, R., Jacinto, E., Wullschleger, S., et al. (2002) Two TOR complexes, only one of which is rapamycin sensitive, have distinct roles in cell growth control. *Molecular Cell*, 10 (3): 457–468. doi:10.1016/S1097-2765(02)00636-6.

Lopes, V.S., Ramalho, J.S., Owen, D.M., et al. (2007a) The ternary Rab27a-Myrip-Myosin VIIa complex regulates melanosome motility in the retinal pigment epithelium. *Traffic*, 8 (5): 486–499. doi:10.1111/j.1600-0854.2007.00548.x.

Lopes, V.S., Ramalho, J.S., Owen, D.M., et al. (2007b) The Ternary Rab27a-Myrip-Myosin VIIa Complex Regulates Melanosome Motility in the Retinal Pigment Epithelium. *Traffic*, 8 (5): 486–499. doi:10.1111/j.1600-0854.2007.00548.x.

Lürick, A., Kuhlee, A., Bröcker, C., et al. (2015) The Habc domain of the SNARE Vam3 interacts with the HOPS tethering complex to facilitate vacuole fusion. *Journal of Biological Chemistry*, 290 (9): 5405–5413. doi:10.1074/jbc.M114.631465.

Ma, S.Y., Röyttä, M., Rinne, J.O., et al. (1997) Correlation between neuromorphometry in the substantia nigra and clinical features in Parkinson's disease using disector counts. *Journal of the Neurological Sciences*, 151 (1): 83–87. doi:10.1016/S0022-510X(97)00100-7.

MacLeod, D.A., Rhinn, H., Kuwahara, T., et al. (2013) RAB7L1 Interacts with

LRRK2 to Modify Intraneuronal Protein Sorting and Parkinson's Disease Risk. *Neuron*, 77 (3): 425–439. doi:10.1016/j.neuron.2012.11.033.

Maday, S., Twelvetrees, A.E., Moughamian, A.J., et al. (2014) Axonal Transport: Cargo-Specific Mechanisms of Motility and Regulation. *Neuron*. 84 (2) pp. 292–309. doi:10.1016/j.neuron.2014.10.019.

Mahanty, S., Ravichandran, K., Chitirala, P., et al. (2016) Rab9A is required for delivery of cargo from recycling endosomes to melanosomes. *Pigment Cell & Melanoma Research*, 29 (1): 43–59. doi:10.1111/pcmr.12434.

Malik, A.U., Karapetsas, A., Nirujogi, R.S., et al. (2020) Deciphering the LRRK code: LRRK1 and LRRK2 phosphorylate distinct Rab proteins and are regulated by diverse mechanisms. *bioRxiv*, p. 2020.11.25.397836. doi:10.1101/2020.11.25.397836.

Malik, B.R., Maddison, D.C., Smith, G.A., et al. (2019) Autophagic and endo-lysosomal dysfunction in neurodegenerative disease. *Molecular Brain*. 12 (1) pp. 1–21. doi:10.1186/s13041-019-0504-x.

Marks, B., Stowell, M.H.B., Vallis, Y., et al. (2001) GTPase activity of dynamin and resulting conformation change are essential for endocytosis. *Nature*, 410 (6825): 231–235. doi:10.1038/35065645.

Del Marmol, V. and Beermann, F. (1996) Tyrosinase and related proteins in mammalian pigmentation. *FEBS Letters*. 381 (3) pp. 165–168. doi:10.1016/0014-5793(96)00109-3.

Martina, J.A., Chen, Y., Gucek, M., et al. (2012) MTORC1 functions as a transcriptional regulator of autophagy by preventing nuclear transport of TFEB. *Autophagy*, 8 (6): 903–914. doi:10.4161/auto.19653.

Mata, I.F., Jang, Y., Kim, C.H., et al. (2015) The RAB39B p.G192R mutation causes X-linked dominant Parkinson's disease. *Molecular Neurodegeneration*, 10 (1): 50. doi:10.1186/s13024-015-0045-4.

Mata, I.F., Kachergus, J.M., Taylor, J.P., et al. (2005) Lrrk2 pathogenic substitutions in Parkinson's disease. *Neurogenetics*, 6 (4): 171–177. doi:10.1007/s10048-005-0005-1.

Matsuda, N., Sato, S., Shiba, K., et al. (2010) PINK1 stabilized by mitochondrial depolarization recruits Parkin to damaged mitochondria and activates latent Parkin for mitophagy. *Journal of Cell Biology*, 189 (2): 211–

221. doi:10.1083/jcb.200910140.
Matta, S., Van Kolen, K., da Cunha, R., et al. (2012) LRRK2 Controls an EndoA Phosphorylation Cycle in Synaptic Endocytosis. *Neuron*, 75 (6): 1008–1021. doi:10.1016/j.neuron.2012.08.022.
Maxfield, F.R. and McGraw, T.E. (2004) Endocytic recycling. *Nature Reviews Molecular Cell Biology*. 5 (2) pp. 121–132. doi:10.1038/nrm1315.
Maxson, M.E. and Grinstein, S. (2014) The vacuolar-type H+-ATPase at a glance – more than a proton pump. *Journal of Cell Science*, 127 (23): 4987–4993. doi:10.1242/jcs.158550.
McGlinchey, R.P., Shewmaker, F., McPhie, P., et al. (2009) The repeat domain of the melanosome fibril protein Pmel17 forms the amyloid core promoting melanin synthesis. *Proceedings of the National Academy of Sciences of the United States of America*, 106 (33): 13731–13736. doi:10.1073/pnas.0906509106.
McGough, I.J., Steinberg, F., Jia, D., et al. (2014) Retromer binding to FAM21 and the WASH complex is perturbed by the Parkinson disease-linked VPS35(D620N) mutation. *Current Biology*, 24 (14): 1670–1676. doi:10.1016/j.cub.2014.06.024.
McGrath, E., Waschbüsch, D., Baker, B.M., et al. (2021) LRRK2 binds to the Rab32 subfamily in a GTP-dependent manner via its armadillo domain. *Small GTPases*, 12 (2): 133–146. doi:10.1080/21541248.2019.1666623.
McMahon, H.T. and Boucrot, E. (2015) Membrane curvature at a glance. *Journal of Cell Science*, 128 (6): 1065–1070. doi:10.1242/jcs.114454.
McPherson, P.S., Garcia, E.P., Slepnev, V.I., et al. (1996) A presynaptic inositol-5-phosphatase. *Nature*, 379 (6563): 353–357. doi:10.1038/379353a0.
Medina, D.L., Di Paola, S., Peluso, I., et al. (2015) Lysosomal calcium signalling regulates autophagy through calcineurin and TFEB. *Nature Cell Biology*, 17 (3): 288–299. doi:10.1038/ncb3114.
Mei, K. and Guo, W. (2018) The exocyst complex. *Current Biology*, 28: R922–R925. doi:10.1016/j.cub.2018.06.042.
Meredith, P. and Sarna, T. (2006) The physical and chemical properties of eumelanin. *Pigment Cell Research*. 19 (6) pp. 572–594. doi:10.1111/j.1600-0749.2006.00345.x.

Meyer, K., Ferraiuolo, L., Miranda, C.J., et al. (2014) Direct conversion of patient fibroblasts demonstrates non-cell autonomous toxicity of astrocytes to motor neurons in familial and sporadic ALS. *Proceedings of the National Academy of Sciences of the United States of America*, 111 (2): 829–832. doi:10.1073/pnas.1314085111.

Mikami, M., Sonoki, T., Ito, M., et al. (2013) Glycosylation of tyrosinase is a determinant of melanin production in cultured melanoma cells. *Molecular Medicine Reports*, 8 (3): 818–822. doi:10.3892/mmr.2013.1602.

Mills, I.G., Jones, A.T. and Clague, M.J. (1999) "Regulation of endosome fusion." In *Molecular Membrane Biology*. 1999. Taylor and Francis Ltd. pp. 73–79. doi:10.1080/096876899294788.

Mills, I.G., Urbé, S. and Clague, M.J. (2001) Relationships between EEA1 binding partners and their role in endosome fusion. *Journal of cell science*, 114 (Pt 10): 1959–1965.

Mir, R., Tonelli, F., Lis, P., et al. (2018) The Parkinson's disease VPS35[D620N] mutation enhances LRRK2-mediated Rab protein phosphorylation in mouse and human. *Biochemical Journal*, 475 (11): 1861–1883. doi:10.1042/BCJ20180248.

Mizushima, N. and Levine, B. (2010) Autophagy in mammalian development and differentiation. *Nature Cell Biology*, 12 (9): 823–830. doi:10.1038/ncb0910-823.

Mizushima, N., Yoshimori, T. and Ohsumi, Y. (2011) The role of atg proteins in autophagosome formation. *Annual Review of Cell and Developmental Biology*, 27: 107–132. doi:10.1146/annurev-cellbio-092910-154005.

Moore, S.F., Hunter, R.W. and Hers, I. (2011) mTORC2 protein-mediated protein kinase B (Akt) serine 473 phosphorylation is not required for Akt1 activity in human platelets. *Journal of Biological Chemistry*, 286 (35): 31062.2-31062. doi:10.1074/jbc.a110.202341.

Moreiras, H., Pereira, F.J.C., Neto, M. V, et al. (2020) The exocyst is required for melanin exocytosis from melanocytes and transfer to keratinocytes. *Pigment cell & melanoma research*, 33 (2): 366–371. doi:10.1111/pcmr.12840.

Morgan, A. and Burgoyne, R.D. (1995) Is NSF a fusion protein? *Trends in Cell Biology*, 5 (9): 335–339. doi:10.1016/S0962-8924(00)89059-5.

Mortiboys, H., Johansen, K.K., Aasly, J.O., et al. (2010) Mitochondrial impairment in patients with Parkinson disease with the G2019S mutation in LRRK2. *Neurology*, 75 (22): 2017–2020. doi:10.1212/WNL.0b013e3181ff9685.

Mukherjee, S., Ghosh, R.N. and Maxfield, F.R. (1997) Endocytosis. *Physiological Reviews*. 77 (3) pp. 759–803. doi:10.1152/physrev.1997.77.3.759.

Nalls, M.A., Pankratz, N., Lill, C.M., et al. (2014) Large-scale meta-analysis of genome-wide association data identifies six new risk loci for Parkinson's disease. *Nature Genetics*, 46 (9): 989–993. doi:10.1038/ng.3043.

Napolitano, G. and Ballabio, A. (2016) TFEB at a glance. *Journal of Cell Science*, 129 (13): 2475–2481. doi:10.1242/jcs.146365.

Narendra, D.P., Jin, S.M., Tanaka, A., et al. (2010) PINK1 is selectively stabilized on impaired mitochondria to activate Parkin. *PLoS Biology*, 8 (1). doi:10.1371/journal.pbio.1000298.

Naslavsky, N. and Caplan, S. (2018) *The enigmatic endosome-sorting the ins and outs of endocytic trafficking*. doi:10.1242/jcs.216499.

Nguyen, M. and Krainc, D. (2018) LRRK2 phosphorylation of auxilin mediates synaptic defects in dopaminergic neurons from patients with Parkinson's disease. *Proceedings of the National Academy of Sciences of the United States of America*, 115 (21): 5576–5581. doi:10.1073/pnas.1717590115.

Nguyen, T. and Wei, M.L. (2007) Hermansky-Pudlak HPS1/pale ear gene regulates epidermal and dermal melanocyte development. *Journal of Investigative Dermatology*, 127 (2): 421–428. doi:10.1038/sj.jid.5700566.

van Niel, G., Bergam, P., Di Cicco, A., et al. (2015) Apolipoprotein E Regulates Amyloid Formation within Endosomes of Pigment Cells. *Cell Reports*, 13 (1): 43–51. doi:10.1016/j.celrep.2015.08.057.

van Niel, G., Charrin, S., Simoes, S., et al. (2011) The Tetraspanin CD63 Regulates ESCRT-Independent and -Dependent Endosomal Sorting during Melanogenesis. *Developmental Cell*, 21 (4): 708–721. doi:10.1016/j.devcel.2011.08.019.

Nixon, R.A. (2013) The role of autophagy in neurodegenerative disease. *Nature Medicine*. 19 (8) pp. 983–997. doi:10.1038/nm.3232.

Van Noorden, C.J.F., Boonacker, E., Bissell, E.R., et al. (1997) Ala-Pro-cresyl violet, a synthetic fluorogenic substrate for the analysis of kinetic parameters of dipeptidyl peptidase IV (CD26) in individual living rat hepatocytes. *Analytical Biochemistry*, 252 (1): 71–77. doi:10.1006/abio.1997.2312.

Novick, P., Field, C. and Schekman, R. (1980) Identification of 23 complementation groups required for post-translational events in the yeast secretory pathway. *Cell*, 21 (1): 205–215. doi:10.1016/0092-8674(80)90128-2.

Ohbayashi, N. and Fukuda, M. (2020) Recent advances in understanding the molecular basis of melanogenesis in melanocytes. *F1000Research*. 9. doi:10.12688/f1000research.24625.1.

Paisán-Ruíz, C., Jain, S., Evans, E.W., et al. (2004) Cloning of the gene containing mutations that cause PARK8-linked Parkinson's disease. *Neuron*, 44 (4): 595–600. doi:10.1016/j.neuron.2004.10.023.

Palmieri, M., Impey, S., Kang, H., et al. (2011) Characterization of the CLEAR network reveals an integrated control of cellular clearance pathways. *Human Molecular Genetics*, 20 (19): 3852–3866. doi:10.1093/hmg/ddr306.

Park, J., Lee, S.B., Lee, S., et al. (2006) Mitochondrial dysfunction in Drosophila PINK1 mutants is complemented by parkin. *Nature*, 441 (7097): 1157–1161. doi:10.1038/nature04788.

Paroutis, P., Touret, N. and Grinstein, S. (2004a) The pH of the secretory pathway: Measurement, determinants, and regulation. *Physiology*. 19 (4) pp. 207–215. doi:10.1152/physiol.00005.2004.

Paroutis, P., Touret, N. and Grinstein, S. (2004b) The pH of the secretory pathway: Measurement, determinants, and regulation. *Physiology*. 19 (4) pp. 207–215. doi:10.1152/physiol.00005.2004.

Patel, D. and Witt, S.N. (2018) Sorting Out the Role of α-Synuclein in Retromer-Mediated Endosomal Protein Sorting. *Journal of Experimental Neuroscience*. 12. doi:10.1177/1179069518796215.

Patwardhan, A., Bardin, S., Miserey-Lenkei, S., et al. (2017) Routing of the RAB6 secretory pathway towards the lysosome related organelle of melanocytes. *Nature Communications*, 8 (1): 1–14. doi:10.1038/ncomms15835.

Perrett, R.M., Alexopoulou, Z. and Tofaris, G.K. (2015) The endosomal pathway in Parkinson's disease. *Molecular and Cellular Neuroscience*. 66 (PA) pp. 21–28. doi:10.1016/j.mcn.2015.02.009.

Petersen, C.M., Nielsent, M.S., Nykjaer, A., et al. (1997) Molecular identification of a novel candidate sorting receptor purified from human brain by receptor-associated protein affinity chromatography. *Journal of Biological Chemistry*, 272 (6): 3599–3605. doi:10.1074/jbc.272.6.3599.

Pfeffer, S.R., Dirac-Svejstrup, A.B. and Soldati, T. (1995) Rab GDP dissociation inhibitor: Putting Rab GTPases in the right place. *Journal of Biological Chemistry*. 270 (29) pp. 17057–17059. doi:10.1074/jbc.270.29.17057.

Plotegher, N. and Duchen, M.R. (2017) Crosstalk between lysosomes and mitochondria in Parkinson's disease. *Frontiers in Cell and Developmental Biology*. 5 (DEC) p. 110. doi:10.3389/fcell.2017.00110.

Poteryaev, D., Datta, S., Ackema, K., et al. (2010) Identification of the switch in early-to-late endosome transition. *Cell*, 141 (3): 497–508. doi:10.1016/j.cell.2010.03.011.

Pu, J., Guardia, C.M., Keren-Kaplan, T., et al. (2016) *Mechanisms and functions of lysosome positioning*. doi:10.1242/jcs.196287.

Pucadyil, T.J. and Schmid, S.L. (2009) Conserved functions of membrane active GTPases in coated vesicle formation. *Science*. 325 (5945) pp. 1217–1220. doi:10.1126/science.1171004.

Purlyte, E., Dhekne, H.S., Sarhan, A.R., et al. (2018) Rab29 activation of the Parkinson's disease-associated LRRK2 kinase. *The EMBO Journal*, 37 (1): 1–18. doi:10.15252/embj.201798099.

Quadri, M., Fang, M., Picillo, M., et al. (2013) Mutation in the SYNJ1 gene associated with autosomal recessive, early-onset parkinsonism. *Human Mutation*, 34 (9): 1208–1215. doi:10.1002/humu.22373.

Raper, H.S. (1927) The Tyrosinase-tyrosine Reaction. *Biochemical Journal*, 21 (1): 89–96. doi:10.1042/bj0210089.

Raposo, G. and Marks, M.S. (2007) Melanosomes - Dark organelles enlighten endosomal membrane transport. *Nature Reviews Molecular Cell Biology*. 8 (10) pp. 786–797. doi:10.1038/nrm2258.

Raposo, G., Tenza, D., Murphy, D.M., et al. (2001) Distinct Protein Sorting and Localization to Premelanosomes, Melanosomes, and Lysosomes in Pigmented Melanocytic Cells✪. *Journal of Cell Biology*, 152 (4): 809–824. doi:10.1083/JCB.152.4.809.

Reeve, A., Simcox, E. and Turnbull, D. (2014) Ageing and Parkinson's disease: Why is advancing age the biggest risk factor? *Ageing Research Reviews*. 14 (1) pp. 19–30. doi:10.1016/j.arr.2014.01.004.

Reith, A.D., Bamborough, P., Jandu, K., et al. (2012) GSK2578215A; A potent and highly selective 2-arylmethyloxy-5-substitutent- N-arylbenzamide LRRK2 kinase inhibitor. *Bioorganic and Medicinal Chemistry Letters*, 22 (17): 5625–5629. doi:10.1016/j.bmcl.2012.06.104.

Réz G; Meldolesi, J. (1980) Freeze-fracture of drug-induced autophagocytosis in the mouse exocrine pancreas - PubMed. *Lab Invest.*, pp. 269–77. Available at: https://pubmed.ncbi.nlm.nih.gov/7401637/ (Accessed: 8 November 2020).

Riboldi, G.M. and Di Fonzo, A.B. (2019) GBA, Gaucher Disease, and Parkinson's Disease: From Genetic to Clinic to New Therapeutic Approaches. *Cells*, 8 (4): 364. doi:10.3390/cells8040364.

Rink, J., Ghigo, E., Kalaidzidis, Y., et al. (2005) Rab conversion as a mechanism of progression from early to late endosomes. *Cell*, 122 (5): 735–749. doi:10.1016/j.cell.2005.06.043.

Ripoll, L., Heiligenstein, X., Hurbain, I., et al. (2018) Myosin VI and branched actin filaments mediate membrane constriction and fission of melanosomal tubule carriers. *Journal of Cell Biology*, 217 (8): 2709–2726. doi:10.1083/jcb.201709055.

Rochin, L., Hurbain, I., Serneels, L., et al. (2013) BACE2 processes PMEL to form the melanosome amyloid matrix in pigment cells. *Proceedings of the National Academy of Sciences of the United States of America*, 110 (26): 10658–10663. doi:10.1073/pnas.1220748110.

Roczniak-Ferguson, A., Petit, C.S., Froehlich, F., et al. (2012) The transcription factor TFEB links mTORC1 signaling to transcriptional control of lysosome homeostasis. *Science Signaling*, 5 (228): ra42–ra42. doi:10.1126/scisignal.2002790.

Rogala, K.B., Gu, X., Kedir, J.F., et al. (2019) Structural basis for the docking

of mTORC1 on the lysosomal surface. *Science*, 366 (6464): 468–475. doi:10.1126/science.aay0166.

Rojas, R., Van Vlijmen, T., Mardones, G.A., et al. (2008) Regulation of retromer recruitment to endosomes by sequential action of Rab5 and Rab7. *Journal of Cell Biology*, 183 (3): 513–526. doi:10.1083/jcb.200804048.

Roth, T.F. and Porter, K.R. (1964) YOLK PROTEIN UPTAKE IN THE OOCYTE OF THE MOSQUITO AEDES AEGYPTI. L. *The Journal of cell biology*, 20: 313–332. doi:10.1083/jcb.20.2.313.

Rothman, J.E. (1994) Mechanisms of intracellular protein transport. *Nature*, 372 (6501): 55–63. doi:10.1038/372055a0.

Rubino, M., Miaczynska, M., Lippé, R., et al. (2000) Selective membrane recruitment of EEA1 suggests a role in directional transport of clathrin-coated vesicles to early endosomes. *Journal of Biological Chemistry*, 275 (6): 3745–3748. doi:10.1074/jbc.275.6.3745.

Rudenko, I.N. and Cookson, M.R. (2014) Heterogeneity of Leucine-Rich Repeat Kinase 2 Mutations: Genetics, Mechanisms and Therapeutic Implications. *Neurotherapeutics*, 11 (4): 738–750. doi:10.1007/s13311-014-0284-z.

Saheki, Y. and De Camilli, P. (2012) Synaptic vesicle endocytosis. *Cold Spring Harbor Perspectives in Biology*, 4 (9). doi:10.1101/cshperspect.a005645.

Salminen, A. and Novick, P.J. (1987) A ras-like protein is required for a post-Golgi event in yeast secretion. *Cell*, 49 (4): 527–538. doi:10.1016/0092-8674(87)90455-7.

Sancak, Y., Bar-Peled, L., Zoncu, R., et al. (2010) Ragulator-rag complex targets mTORC1 to the lysosomal surface and is necessary for its activation by amino acids. *Cell*, 141 (2): 290–303. doi:10.1016/j.cell.2010.02.024.

Sancak, Y., Peterson, T.R., Shaul, Y.D., et al. (2008) The rag GTPases bind raptor and mediate amino acid signaling to mTORC1. *Science*, 320 (5882): 1496–1501. doi:10.1126/science.1157535.

Sancak, Y. and Sabatini, D.M. (2009) Rag proteins regulate amino-acid-induced mTORC1 signalling. *Biochemical Society Transactions*, 37 (1): 289–290. doi:10.1042/BST0370289.

Sardiello, M., Palmieri, M., Ronza, A. Di, et al. (2009) A gene network

regulating lysosomal biogenesis and function. *Science*, 325 (5939): 473–477. doi:10.1126/science.1174447.

Satake, W., Nakabayashi, Y., Mizuta, I., et al. (2009) Genome-wide association study identifies common variants at four loci as genetic risk factors for Parkinson's disease. *Nature Genetics*, 41 (12): 1303–1307. doi:10.1038/ng.485.

Schäfer, I.B., Hesketh, G.G., Bright, N.A., et al. (2012) The binding of Varp to VAMP7 traps VAMP7 in a closed, fusogenically inactive conformation. *Nature Structural and Molecular Biology*, 19 (12): 1300–1309. doi:10.1038/nsmb.2414.

Schmid, S.L., McNiven, M.A. and Camilli, P. De (1998) Dynamin and its partners: A progress report. *Current Opinion in Cell Biology*, 10 (4): 504–512. doi:10.1016/S0955-0674(98)80066-5.

Schmid, S.L., Sorkin, A. and Zerial, M. (2014) Endocytosis: Past, Present, And future. *Cold Spring Harbor Perspectives in Biology*, 6 (12). doi:10.1101/cshperspect.a022509.

Schneider, D.L. (1981) ATP-dependent acidification of intact and disrupted lysosomes. *Journal of Biological Chemistry*, 256 (8): 3858–3864.

Schwab, A.J., Sison, S.L., Meade, M.R., et al. (2017) Decreased Sirtuin Deacetylase Activity in LRRK2 G2019S iPSC-Derived Dopaminergic Neurons. *Stem Cell Reports*, 9 (6): 1839–1852. doi:10.1016/j.stemcr.2017.10.010.

Seabra, M.C. (1996) Nucleotide dependence of rab geranylgeranylation rab escort protein interacts preferentially with GDP-bound Rab. *Journal of Biological Chemistry*, 271 (24): 14398–14404. doi:10.1074/jbc.271.24.14398.

Seaman, M.N.J. (2004) Cargo-selective endosomal sorting for retrieval to the Golgi requires retromer. *Journal of Cell Biology*, 165 (1): 111–122. doi:10.1083/jcb.200312034.

Seaman, M.N.J. (2012) The retromer complex-endosomal protein recycling and beyond. *Journal of Cell Science*. 125 (20) pp. 4693–4702. doi:10.1242/jcs.103440.

Seaman, M.N.J., Harbour, M.E., Tattersall, D., et al. (2009) Membrane recruitment of the cargo-selective retromer subcomplex is catalysed by the small GTPase Rab7 and inhibited by the Rab-GAP TBC1D5. *Journal of Cell*

Science, 122 (14): 2371–2382. doi:10.1242/jcs.048686.

Seaman, M.N.J., Marcusson, E.G., Cereghino, J.L., et al. (1997) Endosome to Golgi retrieval of the vacuolar protein sorting receptor, Vps10p, requires the function of the VPS29, VPS30, and VPS35 gene products. *Journal of Cell Biology*, 137 (1): 79–92. doi:10.1083/jcb.137.1.79.

Seaman, M.N.J., McCaffery, J.M. and Emr, S.D. (1998) A membrane coat complex essential for endosome-to-Golgi retrograde transport in yeast. *Journal of Cell Biology*, 142 (3): 665–681. doi:10.1083/jcb.142.3.665.

Seglen, P.O. and Bohley, P. (1992) Autophagy and other vacuolar protein degradation mechanisms. *Experientia*. 48 (2) pp. 158–172. doi:10.1007/BF01923509.

SEIJI, M., FITZPATRICK, T.B. and BIRBECK, M.S. (1961) The melanosome: a distinctive subcellular particle of mammalian. *The Journal of investigative dermatology*, 36 (4): 243–252. doi:10.1038/jid.1961.42.

SEIJI, M., FITZPATRICK, T.B., SIMPSON, R.T., et al. (1963) Chemical Composition and Terminology Of Specialized Organelles (Melanosomes and Melanin Granules) in Mammalian Melanocytes. *Nature*, 197 (4872): 1082–1084. doi:10.1038/1971082a0.

Settembre, C. and Ballabio, A. (2011) TFEB regulates autophagy: An integrated coordination of cellular degradation and recycling processes. *Autophagy*. 7 (11) pp. 1379–1381. doi:10.4161/auto.7.11.17166.

Settembre, C., Zoncu, R., Medina, D.L., et al. (2012) A lysosome-to-nucleus signalling mechanism senses and regulates the lysosome via mTOR and TFEB. *The EMBO Journal*, 31 (5): 1095–1108. doi:10.1038/emboj.2012.32.

Setty, S.R.G., Tenza, D., Sviderskaya, E. V., et al. (2008) Cell-specific ATP7A transport sustains copper-dependent tyrosinase activity in melanosomes. *Nature*, 454 (7208): 1142–1146. doi:10.1038/nature07163.

Setty, S.R.G., Tenza, D., Truschel, S.T., et al. (2007) BLOC-1 is required for cargo-specific sorting from vacuolar early endosomes toward lysosome-related organelles. *Molecular Biology of the Cell*, 18 (3): 768–780. doi:10.1091/mbc.E06-12-1066.

Shen, K., Choe, A. and Sabatini, D.M. (2017) Intersubunit Crosstalk in the Rag GTPase Heterodimer Enables mTORC1 to Respond Rapidly to Amino Acid

Availability. *Molecular Cell*, 68 (3): 552-565.e8. doi:10.1016/j.molcel.2017.09.026.

Sheng, Z., Zhang, S., Bustos, D., et al. (2012) Ser1292 Autophosphorylation Is an Indicator of LRRK2 Kinase Activity and Contributes to the Cellular Effects of PD Mutations. *Science Translational Medicine*, 4 (164): 164ra161--164ra161. doi:10.1126/scitranslmed.3004485.

Shi, M.M., Shi, C.H. and Xu, Y.M. (2017) Rab GTPases: The key players in the molecular pathway of Parkinson's disease. *Frontiers in Cellular Neuroscience*. 11. doi:10.3389/fncel.2017.00081.

Simmons, J.L., Neuendorf, H.M. and Boyle, G.M. (2020) BRN2 and MITF together impact AXL expression in melanoma. *bioRxiv*, p. 2020.07.27.223982. doi:10.1101/2020.07.27.223982.

Simón-Sánchez, J., Schulte, C., Bras, J.M., et al. (2009) Genome-wide association study reveals genetic risk underlying Parkinson's disease. *Nature Genetics*, 41 (12): 1308–1312. doi:10.1038/ng.487.

Simonsen, A., Lippé, R., Christoforidis, S., et al. (1998) EEA1 links PI(3)K function to Rab5 regulation of endosome fusion. *Nature*, 394 (6692): 494–498. doi:10.1038/28879.

Sitaram, A. and Marks, M.S. (2012) Mechanisms of protein delivery to melanosomes in pigment cells. *Physiology*. 27 (2) pp. 85–99. doi:10.1152/physiol.00043.2011.

Söllner, T., Bennett, M.K., Whiteheart, S.W., et al. (1993) A protein assembly-disassembly pathway in vitro that may correspond to sequential steps of synaptic vesicle docking, activation, and fusion. *Cell*, 75 (3): 409–418. doi:10.1016/0092-8674(93)90376-2.

Song, L., He, Y., Ou, J., et al. (2017) Auxilin Underlies Progressive Locomotor Deficits and Dopaminergic Neuron Loss in a Drosophila Model of Parkinson's Disease. *Cell Reports*, 18 (5): 1132–1143. doi:10.1016/j.celrep.2017.01.005.

Song, Q., Meng, B., Xu, H., et al. (2020) The emerging roles of vacuolar-type ATPase-dependent Lysosomal acidification in neurodegenerative diseases. *Translational Neurodegeneration*. 9 (1) pp. 1–14. doi:10.1186/s40035-020-00196-0.

Soukup, S.F., Kuenen, S., Vanhauwaert, R., et al. (2016) A LRRK2-

Dependent EndophilinA Phosphoswitch Is Critical for Macroautophagy at Presynaptic Terminals. *Neuron*, 92 (4): 829–844. doi:10.1016/j.neuron.2016.09.037.

Spanò, S., Liu, X. and Galán, J.E. (2011) Proteolytic targeting of Rab29 by an effector protein distinguishes the intracellular compartments of human-adapted and broad-host Salmonella. *Proceedings of the National Academy of Sciences of the United States of America*, 108 (45): 18418–18423. doi:10.1073/pnas.1111959108.

Spillantini, M.G., Crowther, R.A., Jakes, R., et al. (1998) α-Synuclein in filamentous inclusions of Lewy bodies from Parkinson's disease and dementia with Lewy bodies. *Proceedings of the National Academy of Sciences of the United States of America*, 95 (11): 6469–6473. doi:10.1073/pnas.95.11.6469.

Spillantini, M.G., Schmidt, M.L., Lee, V.M.Y., et al. (1997) α-synuclein in Lewy bodies [8]. *Nature*. 388 (6645) pp. 839–840. doi:10.1038/42166.

Steger, M., Diez, F., Dhekne, H.S., et al. (2017) Systematic proteomic analysis of LRRK2-mediated rab GTPase phosphorylation establishes a connection to ciliogenesis. *eLife*, 6. doi:10.7554/eLife.31012.

Steger, M., Tonelli, F., Ito, G., et al. (2016) Phosphoproteomics reveals that Parkinson's disease kinase LRRK2 regulates a subset of Rab GTPases. *eLife*, 5 (JANUARY2016). doi:10.7554/eLife.12813.001.

Stenmark, H. (2009) Rab GTPases as coordinators of vesicle traffic. *Nature Reviews Molecular Cell Biology*. 10 (8) pp. 513–525. doi:10.1038/nrm2728.

Stolz, A., Ernst, A. and Dikic, I. (2014) Cargo recognition and trafficking in selective autophagy. *Nature Cell Biology*. 16 (6) pp. 495–501. doi:10.1038/ncb2979.

Sugiura, A., McLelland, G., Fon, E.A., et al. (2014) A new pathway for mitochondrial quality control: mitochondrial-derived vesicles. *The EMBO Journal*, 33 (19): 2142–2156. doi:10.15252/embj.201488104.

Sun, J., Deghmane, A.E., Bucci, C., et al. (2009) Detection of activated rab7 gtpase with an immobilized rilp probe. *Methods in Molecular Biology*, 531: 57–69. doi:10.1007/978-1-59745-396-7_5.

Swarbrick, J.D., Shaw, D.J., Chhabra, S., et al. (2011) VPS29 Is Not an Active Metallo-Phosphatase but Is a Rigid Scaffold Required for Retromer Interaction

with Accessory Proteins Johannes, L. (ed.). *PLoS ONE*, 6 (5): e20420. doi:10.1371/journal.pone.0020420.

Tabata, H., Kawamura, N., Sun-Wada, G.-H., et al. (2008) Vacuolar-type H+-ATPase with the a3 isoform is the proton pump on premature melanosomes. *Cell and Tissue Research*, 332 (3): 447–460. doi:10.1007/s00441-008-0597-5.

Takei, K., McPherson, P.S., Schmid, S.L., et al. (1995) Tubular membrane invaginations coated by dynamin rings are induced by GTP-γS in nerve terminals. *Nature*, 374 (6518): 186–190. doi:10.1038/374186a0.

Tanaka, K., Waxman, L. and Goldberg, A.L. (1983) ATP serves two distinct roles in protein degradation in reticulocytes, one requiring and one independent of ubiquitin. *Journal of Cell Biology*, 96 (6): 1580–1585. doi:10.1083/jcb.96.6.1580.

Tang, F.L., Erion, J.R., Tian, Y., et al. (2015a) VPS35 in dopamine neurons is required for endosome-to- golgi retrieval of Lamp2a, a receptor of chaperone-mediated autophagy that is critical for α-synuclein degradation and prevention of pathogenesis of Parkinson's disease. *Journal of Neuroscience*, 35 (29): 10613–10628. doi:10.1523/JNEUROSCI.0042-15.2015.

Tang, F.L., Liu, W., Hu, J.X., et al. (2015b) VPS35 Deficiency or Mutation Causes Dopaminergic Neuronal Loss by Impairing Mitochondrial Fusion and Function. *Cell Reports*, 12 (10): 1631–1643. doi:10.1016/j.celrep.2015.08.001.

Tarafder, A.K., Bolasco, G., Correia, M.S., et al. (2014) Rab11b mediates melanin transfer between donor melanocytes and acceptor keratinocytes via coupled exo/endocytosis. *Journal of Investigative Dermatology*, 134 (4): 1056–1066. doi:10.1038/jid.2013.432.

Temkin, P., Lauffer, B., Jäger, S., et al. (2011) SNX27 mediates retromer tubule entry and endosome-to-plasma membrane trafficking of signalling receptors. *Nature Cell Biology*, 13 (6): 715–723. doi:10.1038/ncb2252.

Theos, A.C., Tenza, D., Martina, J.A., et al. (2005) Functions of adaptor protein (AP)-3 and AP-1 in tyrosinase sorting from endosomes to melanosomes. *Molecular Biology of the Cell*, 16 (11): 5356–5372. doi:10.1091/mbc.E05-07-0626.

Toei, M., Saum, R. and Forgac, M. (2010) Regulation and isoform function of

the V-ATPases. *Biochemistry*, 49 (23): 4715–4723. doi:10.1021/bi100397s.
Tong, Y., Giaime, E., Yamaguchi, H., et al. (2012) Loss of leucine-rich repeat kinase 2 causes age-dependent bi-phasic alterations of the autophagy pathway. *Molecular Neurodegeneration*, 7 (1): 2. doi:10.1186/1750-1326-7-2.
Tong, Y., Yamaguchi, H., Giaime, E., et al. (2010a) Loss of leucine-rich repeat kinase 2 causes impairment of protein degradation pathways, accumulation of α-synuclein, and apoptotic cell death in aged mice. *Proceedings of the National Academy of Sciences of the United States of America*, 107 (21): 9879–9884. doi:10.1073/pnas.1004676107.
Tong, Y., Yamaguchi, H., Giaime, E., et al. (2010b) Loss of leucine-rich repeat kinase 2 causes impairment of protein degradation pathways, accumulation of α-synuclein, and apoptotic cell death in aged mice. *Proceedings of the National Academy of Sciences of the United States of America*, 107 (21): 9879–9884. doi:10.1073/pnas.1004676107.
Toyofuku, T., Okamoto, Y., Ishikawa, T., et al. (2020) <scp>LRRK</scp> 2 regulates endoplasmic reticulum–mitochondrial tethering through the <scp>PERK</scp> -mediated ubiquitination pathway. *The EMBO Journal*, 39 (2). doi:10.15252/embj.2018100875.
Tsukada, M. and Ohsumi, Y. (1993) Isolation and characterization of autophagy-defective mutants of Saccharomyces cerevisiae. *FEBS Letters*, 333 (1–2): 169–174. doi:10.1016/0014-5793(93)80398-E.
Tucci, A., Nalls, M.A., Houlden, H., et al. (2010) Genetic variability at the PARK16 locus. *European Journal of Human Genetics*, 18 (12): 1356–1359. doi:10.1038/ejhg.2010.125.
Tysnes, O.B. and Storstein, A. (2017) Epidemiology of Parkinson's disease. *Journal of Neural Transmission*. 124 (8) pp. 901–905. doi:10.1007/s00702-017-1686-y.
Ungewickell, E., Ungewickell, H., Holstein, S.E.H., et al. (1995) Role of auxilin in uncoating clathrin-coated vesicles. *Nature*, 378 (6557): 632–635. doi:10.1038/378632a0.
Unternaehrer, J.J. and Daley, G.Q. (2011) Induced pluripotent stem cells for modelling human diseases. *Philosophical transactions of the Royal Society of London. Series B, Biological sciences*, 366 (1575): 2274–2285.

doi:10.1098/rstb.2011.0017.

Vandamme, N. and Berx, G. (2014) Melanoma cells revive an embryonic transcriptional network to dictate phenotypic heterogeneity. *Frontiers in Oncology*. 4 (NOV). doi:10.3389/fonc.2014.00352.

Vanhauwaert, R., Kuenen, S., Masius, R., et al. (2017) The SAC1 domain in synaptojanin is required for autophagosome maturation at presynaptic terminals. *The EMBO Journal*, 36 (10): 1392–1411. doi:10.15252/embj.201695773.

Vargas, K.J., Makani, S., Davis, T., et al. (2014) Synucleins regulate the kinetics of synaptic vesicle endocytosis. *Journal of Neuroscience*, 34 (28): 9364–9376. doi:10.1523/JNEUROSCI.4787-13.2014.

Vidyadhara, D.J., Lee, J.E. and Chandra, S.S. (2019) Role of the endolysosomal system in Parkinson's disease. *Journal of Neurochemistry*. 150 (5) pp. 487–506. doi:10.1111/jnc.14820.

Vilariño-Güell, C., Wider, C., Ross, O.A., et al. (2011) VPS35 mutations in parkinson disease. *American Journal of Human Genetics*, 89 (1): 162–167. doi:10.1016/j.ajhg.2011.06.001.

Wakamatsu, K. and Ito, S. (2002) Advanced chemical methods in melanin determination. *Pigment Cell Research*. 15 (3) pp. 174–183. doi:10.1034/j.1600-0749.2002.02017.x.

Wallings, R., Connor-Robson, N. and Wade-Martins, R. (2019a) LRRK2 interacts with the vacuolar-type H+-ATPase pump a1 subunit to regulate lysosomal function. *Human Molecular Genetics*, 28 (16): 2696–2710. doi:10.1093/hmg/ddz088.

Wallings, R., Connor-Robson, N. and Wade-Martins, R. (2019b) LRRK2 interacts with the vacuolar-type H+-ATPase pump a1 subunit to regulate lysosomal function. *Human Molecular Genetics*, 28 (16): 2696–2710. doi:10.1093/hmg/ddz088.

Walter, J., Bolognin, S., Antony, P.M.A., et al. (2019) Neural Stem Cells of Parkinson's Disease Patients Exhibit Aberrant Mitochondrial Morphology and Functionality. *Stem Cell Reports*, 12 (5): 878–889. doi:10.1016/j.stemcr.2019.03.004.

Wang, C.W. and Klionsky, D.J. (2003) The molecular mechanism of

autophagy. *Molecular Medicine*. 9 (3–4) pp. 65–76. doi:10.1007/bf03402040.

Wang, N. and Hebert, D.N. (2006) Tyrosinase maturation through the mammalian secretory pathway: bringing color to life. *Pigment Cell Research*, 19 (1): 3–18. doi:10.1111/j.1600-0749.2005.00288.x.

Wang, W., #1, W., Fujioka, H., et al. (2016) Parkinson's disease-associated mutant VPS35 causes mitochondrial dysfunction by recycling DLP1 complexes Europe PMC Funders Group. *Nat Med*, 22 (1): 54–63. doi:10.1038/nm.3983.

Wang, X. (2017) Destructive cellular paths underlying familial and sporadic Parkinson disease converge on mitophagy. *Autophagy*. 13 (11) pp. 1998–1999. doi:10.1080/15548627.2017.1327511.

Waschbüsch, D., Hübel, N., Ossendorf, E., et al. (2019) Rab32 interacts with SNX6 and affects retromer-dependent Golgi trafficking. *PLOS ONE*, 14 (1): e0208889. Available at: https://doi.org/10.1371/journal.pone.0208889.

Waschbüsch, D., Michels, H., Strassheim, S., et al. (2014) LRRK2 transport is regulated by its novel interacting partner Rab32. *PLoS ONE*, 9 (10). doi:10.1371/journal.pone.0111632.

Wasmeier, C., Romao, M., Plowright, L., et al. (2006) Rab38 and Rab32 control post-Golgi trafficking of melanogenic enzymes. *Journal of Cell Biology*, 175 (2): 271–281. doi:10.1083/jcb.200606050.

Wassmer, T., Attar, N., Bujny, M. V., et al. (2007) A loss-of-function screen reveals SNX5 and SNX6 as potential components of the mammalian retromer. *Journal of Cell Science*, 120 (1): 45–54. doi:10.1242/jcs.03302.

Wassmer, T., Attar, N., Harterink, M., et al. (2009) The Retromer Coat Complex Coordinates Endosomal Sorting and Dynein-Mediated Transport, with Carrier Recognition by the trans-Golgi Network. *Developmental Cell*, 17 (1): 110–122. doi:10.1016/j.devcel.2009.04.016.

Watanabe, S., Mamer, L.E., Raychaudhuri, S., et al. (2018) Synaptojanin and Endophilin Mediate Neck Formation during Ultrafast Endocytosis. *Neuron*, 98 (6): 1184-1197.e6. doi:10.1016/j.neuron.2018.06.005.

Watt, B., Van Niel, G., Raposo, G., et al. (2013) PMEL: A pigment cell-specific model for functional amyloid formation. *Pigment Cell and Melanoma Research*, 26 (3): 300–315. doi:10.1111/pcmr.12067.

Wauters, F., Cornelissen, T., Imberechts, D., et al. (2020) LRRK2 mutations impair depolarization-induced mitophagy through inhibition of mitochondrial accumulation of RAB10. *Autophagy*, 16 (2): 203–222. doi:10.1080/15548627.2019.1603548.

West, A.B., Moore, D.J., Biskup, S., et al. (2005) Parkinson's disease-associated mutations in leucine-rich repeat kinase 2 augment kinase activity. *Proceedings of the National Academy of Sciences of the United States of America*, 102 (46): 16842–16847. doi:10.1073/pnas.0507360102.

Westphal, C.H. and Chandra, S.S. (2013) Monomeric synucleins generate membrane curvature. *Journal of Biological Chemistry*, 288 (3): 1829–1840. doi:10.1074/jbc.M112.418871.

White, M.F. (1998) The IRS-signalling system: A network of docking proteins that mediate insulin action. *Molecular and Cellular Biochemistry*, 182 (1–2): 3–11. doi:10.1023/A:1006806722619.

Williams, E.T., Chen, X. and Moore, D.J. (2017) VPS35, the retromer complex and Parkinson's disease. *Journal of Parkinson's Disease*. 7 (2) pp. 219–233. doi:10.3233/JPD-161020.

Wilson, E.L. and Metzakopian, E. (2021) ER-mitochondria contact sites in neurodegeneration: genetic screening approaches to investigate novel disease mechanisms. *Cell Death & Differentiation*, 28 (6): 1804–1821. doi:10.1038/s41418-020-00705-8.

Wilson, G.R., Sim, J.C.H., McLean, C., et al. (2014) Mutations in RAB39B cause X-linked intellectual disability and early-onset parkinson disease with α-synuclein pathology. *American Journal of Human Genetics*, 95 (6): 729–735. doi:10.1016/j.ajhg.2014.10.015.

Wong, Y.C., Ysselstein, D. and Krainc, D. (2018) Mitochondria-lysosome contacts regulate mitochondrial fission via RAB7 GTP hydrolysis. *Nature*, 554 (7692): 382–386. doi:10.1038/nature25486.

Wu, X., Rao, K., Bowers, M.B., et al. (2001) Rab27a enables myosin Va-dependent melanosome capture by recruiting the myosin to the organelle. *Journal of Cell Science*, 114 (6): 1091 LP – 1100. Available at: http://jcs.biologists.org/content/114/6/1091.abstract.

Wu, X.S., Tsan, G.L. and Hammer 3rd, J.A. (2005) Melanophilin and myosin

Va track the microtubule plus end on EB1. *The Journal of cell biology*, 171 (2): 201–207. doi:10.1083/jcb.200503028.

Wu, Y.W., Tan, K.T., Waldmann, H., et al. (2007) Interaction analysis of prenylated Rab GTPase with Rab escort protein and GDP dissociation inhibitor explains the need for both regulators. *Proceedings of the National Academy of Sciences of the United States of America*, 104 (30): 12294–12299. doi:10.1073/pnas.0701817104.

Wyant, G.A., Abu-Remaileh, M., Wolfson, R.L., et al. (2017) mTORC1 Activator SLC38A9 Is Required to Efflux Essential Amino Acids from Lysosomes and Use Protein as a Nutrient. *Cell*, 171 (3): 642-654.e12. doi:10.1016/j.cell.2017.09.046.

Xie, Z. and Klionsky, D.J. (2007) Autophagosome formation: Core machinery and adaptations. *Nature Cell Biology*. 9 (10) pp. 1102–1109. doi:10.1038/ncb1007-1102.

Xu, L., Wang, X. and Tong, C. (2020) Endoplasmic Reticulum-Mitochondria Contact Sites and Neurodegeneration. *Frontiers in cell and developmental biology*, 8: 428. doi:10.3389/fcell.2020.00428.

Yamano, K., Fogel, A.I., Wang, C., et al. (2014) Mitochondrial Rab GAPs govern autophagosome biogenesis during mitophagy. *eLife*, 3: e01612–e01612. doi:10.7554/eLife.01612.

Yamano, K., Wang, C., Sarraf, S.A., et al. (2018) Endosomal rab cycles regulate parkin-mediated mitophagy. *eLife*, 7. doi:10.7554/eLife.31326.

Yamano, K. and Youle, R.J. (2013) PINK1 is degraded through the N-end rule pathway. *Autophagy*, 9 (11): 1758–1769. doi:10.4161/auto.24633.

Yang, Q., Inoki, K., Kim, E., et al. (2006) TSC1/TSC2 and Rheb have different effects on TORC1 and TORC2 activity. *Proceedings of the National Academy of Sciences of the United States of America*, 103 (18): 6811–6816. doi:10.1073/pnas.0602282103.

Yang, Y., Coleman, M., Zhang, L., et al. (2013) Autophagy in axonal and dendritic degeneration. *Trends in Neurosciences*. 36 (7) pp. 418–428. doi:10.1016/j.tins.2013.04.001.

Yao, C., Johnson, W.M., Gao, Y., et al. (2013) Kinase inhibitors arrest neurodegeneration in cell and C. elegans models of LRRK2 toxicity. *Human*

Molecular Genetics, 22 (2): 328–344. doi:10.1093/hmg/dds431.

Yim, W.W.Y. and Mizushima, N. (2020) Lysosome biology in autophagy. *Cell Discovery*. 6 (1) p. 6. doi:10.1038/s41421-020-0141-7.

Yim, Y.I., Sun, T., Wu, L.G., et al. (2010) Endocytosis and clathrin-uncoating defects at synapses of auxilin knockout mice. *Proceedings of the National Academy of Sciences of the United States of America*, 107 (9): 4412–4417. doi:10.1073/pnas.1000738107.

Yoon, T.Y. and Munson, M. (2018) SNARE complex assembly and disassembly. *Current Biology*. 28 (8) pp. R397–R401. doi:10.1016/j.cub.2018.01.005.

Yorimitsu, T. and Klionsky, D.J. (2005) Autophagy: Molecular machinery for self-eating. *Cell Death and Differentiation*. 12 (Suppl 2) pp. 1542–1552. doi:10.1038/sj.cdd.4401765.

Ysselstein, D., Nguyen, M., Young, T.J., et al. (2019) LRRK2 kinase activity regulates lysosomal glucocerebrosidase in neurons derived from Parkinson's disease patients. *Nature Communications*, 10 (1): 5570. doi:10.1038/s41467-019-13413-w.

Zahraouis, A., Touchott, N., Chardin, P., et al. (1989) *THE JOURNAL OF BIOLOGICAL CHEMISTRY The Human Rub Genes Encode a Family of GTP-binding Proteins Related to Yeast YPTl and SEC4 Products Involved in Secretion**.

Zerial, M. and McBride, H. (2001) Rab proteins as membrane organizers. *Nature Reviews Molecular Cell Biology*. 2 (2) pp. 107–117. doi:10.1038/35052055.

Zerial, M. and Stenmark, H. (1993) Rab GTPases in vesicular transport. *Current Opinion in Cell Biology*, 5 (4): 613–620. doi:10.1016/0955-0674(93)90130-I.

Zhou, B.K., Boissy, R.E., Pifko-Hirst, S., et al. (1993) Lysosome-associated membrane protein-1 (LAMP-1) is the melanocyte vesicular membrane glycoprotein band II. *Journal of Investigative Dermatology*, 100 (2): 110–114. doi:10.1111/1523-1747.ep12462775.

Zimprich, A., Benet-Pagès, A., Struhal, W., et al. (2011) A mutation in VPS35, encoding a subunit of the retromer complex, causes late-onset parkinson

disease. *American Journal of Human Genetics*, 89 (1): 168–175. doi:10.1016/j.ajhg.2011.06.008.

Zimprich, A., Biskup, S., Leitner, P., et al. (2004) Mutations in LRRK2 cause autosomal-dominant parkinsonism with pleomorphic pathology. *Neuron*, 44 (4): 601–607. doi:10.1016/j.neuron.2004.11.005.

Zoncu, R., Bar-Peled, L., Efeyan, A., et al. (2011a) mTORC1 senses lysosomal amino acids through an inside-out mechanism that requires the vacuolar H+-ATPase. *Science*, 334 (6056): 678–683. doi:10.1126/science.1207056.

Zoncu, R., Efeyan, A. and Sabatini, D.M. (2011b) MTOR: From growth signal integration to cancer, diabetes and ageing. *Nature Reviews Molecular Cell Biology*. 12 (1) pp. 21–35. doi:10.1038/nrm3025.